ROMA TRE
UNIVERSITÀ DEGLI STUDI

linQ
laboratorio idrogeologia numerica e quantitativa

"Study of seawater intrusion in the coastal areas of Circeo National Park and Litorale Romano Natural Reserve, for the implementation of numerical modeling methods"

Phd Student: Fabio Manca

Supervisor: Prof. Giuseppe Capelli

ROMA TRE
UNIVERSITÀ DEGLI STUDI

Scuola Dottorale in Geologia dell'Ambiente e Delle Risorse

XXVI Ciclo

"Study of seawater intrusion in the coastal areas of Circeo National Park and Litorale Romano Natural Reserve, for the implementation of numerical modeling methods"

Dottorando: Fabio Manca

Tutor: Prof. Giuseppe Capelli

Coordinatore: Prof.ssa Sveva Corrado

Direttore della Scuola Dottorale: Prof. Claudio Faccenna

Grazie alle Maestre Mascarucci, Pisani e Scifo,
che mi hanno insegnato ad imparare.

Grazie ai bambini della Scuola Popolare Piero Bruno,
per avermi insegnato che un maestro
non smette mai di imparare.

Index

FIGURE INDEX

TABLE INDEX

RIASSUNTO

Le piane costiere rappresentano le aree maggiormente abitate del pianeta poiché favoriscono un rapido sviluppo sia dal punto di vista urbano, agricolo che industriale. La principale risorsa delle piane costiere è rappresentata dalle acque sotterranee, che ben si prestano a soddisfare le esigenze idriche per queste attività. Gli acquiferi costieri rappresentano il punto di incontro tra le acque dolci di natura continentale e le acque salate di origine marina. Le acque dolci tendono a sovrastare le acque salate a causa della loro minor densità, dando vita ad un delicato equilibrio. Alcuni processi, sia naturali che antropici, possono tuttavia turbare questo equilibrio, determinando un incremento di salinità nelle acque sotterranee. La principale attività umana in grado di determinare la salinizzazione degli acquiferi costieri è la risalita della zona di interfaccia dovuta ai pompaggi (*upconing*). Fattori naturali sono invece l'intrusione laterale, la dissoluzione di evaporiti, la contaminazione da acque salate fossili, gli aerosol marini e l'intrusione del cuneo salino lungo i fiumi. Proprio questi ultimi due processi sono stati approfonditi nel presente lavoro, poiché poco studiati in ricerche di carattere regionale.

L'obiettivo di questa tesi è stato lo studio della salinizzazione delle falde costiere indotta da fiumi o canali antropici, determinata dall'azione dei venti o dalla variazione del deflusso fluviale nel tempo, in zone dove coesistono aree protette ed aree fortemente antropizzate: il Delta del Tevere e La Piana Pontina. Le due aree sono state scelte poiché presentano numerose analogie: entrambe sono composte da sistemi acquiferi sedimentari multistrato e presentano una morfologia costiera fortemente condizionata da opere di bonifica dei secoli scorsi. La maggiore differenza consiste nella presenza di diversi corpi idrologici: nel Delta del Tevere è presente un grande fiume che condiziona i meccanismi di salinizzazione dell'area, mentre nella Piana Pontina sono i laghi costieri ed i canali di bonifica a determinare la distribuzione ed il movimento delle acque salate.

Questo studio è stato eseguito con numerosi metodi come i rilevamenti idrologici ed idrogeologici, rilevamenti multitemporali dei parametri chimico-fisici delle acque di falda lungo le aree costiere, rilevamenti idrochimici, utilizzo di tecniche di monitoraggio remoto, analisi statistiche per l'interpretazione dei dati metereologici e l'utilizzo delle più innovative tecniche di modellazione numerica. Nell'area del Delta del Tevere si è riconosciuta l'importanza dell'effetto dei venti sui processi di salinizzazione, osservando che i venti possono causare sia la messa in posto del cuneo salino nella foce del Tevere, sia la deposizione dello *spray* marino sulle chiome degli alberi della Riserva Naturale del Litorale Romano. Il cuneo salino nel Tevere, osservato fino ad 8.8 km dalla foce, è ritenuta la causa più probabile di salinizzazione nell'area alluvionale di Ostia Antica. Inoltre i rilevamenti idrogeochimici regionali svolti in quest'area, hanno consentito l'identificazione di processi di *freshening* legati a scambio ionico, dovuti alla presenza di saline attive nell'area nei secoli scorsi.

Nell'area Pontina, in corrispondenza della fascia costiera che ospita il Parco Nazionale del Circeo, la salinizzazione è risultata legata alla presenza di acqua marina nei canali di bonifica e nei laghi costieri.

Come suggerito dal titolo della tesi, lo scopo finale del lavoro è stato l'implementazione di un modello numerico per analizzare i processi di salinizzazione. La modellazione numerica consente infatti di investigare ed analizzare pù approfonditamente ciò che avviene in un sistema idrogeologico complesso. La modellazione è stata realizzata usando il *software* FEFLOW per tentare di comprendere le relazioni tra la salinizzazione delle acque sotterranee e quelle di un canale di bonifica. Il modello in 2D, implementato in regime di trasporto di flusso e massa transitorio, è stato sviluppato alla foce del Canale Moscarello (Pianura Pontina), dove si è rilevata la presenza del cuneo salino. Il canale è risultato soggetto a significative variazioni di flusso, capaci di determinare un gradiente idraulico con conseguente trasporto di massa nell'adiacente acquifero. Questo trasporto di acqua attraverso il fondo alveo è risultato in grado di determinare il movimento di un *plume* salino presente nell'acquifero, condizionando quindi i valori di salinità raccolti in un piezometro.

ABSTRACT

Coastal plains represent the most populated areas of the world because they allow an industrial, urban and agricultural development. Groundwater is the main resource in coastal plains and it can satisfy the water demand for these activities. Coastal aquifers represent the place where continental freshwater and seawater meet. Freshwater tends to overly seawater because of its lower density, creating a fragile balance. Nevertheless some processes, both natural and anthropic, can perturb this balance determining groundwater salinization. The main human induced salinization process is the upconing. Natural processes can be the lateral intrusion, evaporite dissolution, fossil water contamination, sea spray aerosol deposition and salt-wedge intrusion in river mouths. Last two processes were deepened in the present study because they are usually not so diffused in regional researches. The aim of this thesis was the study of groundwater salinization induced by rivers or anthropic canals, determined by the wind action or the variation of fluvial discharge rate in time, in areas where protected and anthropic areas coexist: the Tiber Delta and the Pontina Plain. The areas were chosen because they exhibit analogies: both are composed by multi-layered sedimentary aquifers and coastal morphology is strongly affected by reclamation works of the past centuries. The major difference is represented by the presence of different hydrological bodies: in the Tiber Delta area a great river is present and it influences salinization mechanisms in the hydrogeological system, whereas in the Pontina Plain lakes and reclamation canals determine the distribution and movement of seawater.

This study was developed with several methods, such as hydrological and hydrogeological surveys, multi-temporal chemo-physical surveys of groundwater, hydrochemical surveys, remote sensing techniques, statistical analyses about meteorological data and the use of the most innovative techniques of numerical modeling.

In the Tiber Delta area the importance of the westerly winds for the salinization processes was investigated. In fact the winds determine both a salt-wedge emplacement in the Tiber mouth during the falls, and a groundwater salinization in the Litorale Romano Natural Reserve pine forest because of sea spray aerosols deposition.

The salt-wedge presence in the Tiber River, noticed up to 8.8 km from the Tiber mouth, is supposed to be the more likely reason of the seawater intrusion processes identified in the alluvial area of Ostia Antica. Furthermore regional hydrochemical analyses permitted to identify freshening processes ascribable to ion-exchange, related to the presence of historical solar salt works in the Ostia Antica area.

In the Pontina Plain, along the coastal area which hosts the Circeo National Park, salinization resulted linked to the presence of seawater in reclamation canals and lakes.

As suggested by the dissertation title, the final aim of the work was the implementation of a numerical model, to detect salinization processes. The use of numerical modeling is a further investigation tool to analyze and quantify what happens in a complex hydrogeological system. The implementation of numerical modeling was performed using the software FEFLOW 6.0, to understand the relationships between groundwater and a reclamation canal salinization. The 2D model, implemented in a transient flow-mass transport state, was located at the Moscarello Canal mouth (Pontina Plain), where a salt-wedge intrusion was noticed. The canal resulted to be subject to a strong discharge modification, which is able to determine a hydraulic gradient and a consequent mass transport in the adjacent aquifer. This transport through the canal bottom resulted able to induce the movement of a saline plume present in the aquifer, determining hence an enhancement of salinity values collected in a piezometer.

GENERAL INTRODUCTION

Coastal plains usually represent preferential areas regarding the anthropic, industrial and agricultural settlements (Capaccioni et al. 2005). Coastal aquifers are the subsurface equivalents of coastal areas where continental fresh groundwater and seawater meet (Post 2005). The effects of increasing groundwater extraction determine an increasing salinity in coastal aquifers. Salinity is an indication of the concentration of dissolved salts in surficial waters or groundwater. The ions responsible for salinity include the major cations (Ca^{2+}, Mg^{2+}, Na^{+} and K^{+}) and major anions (CO_3^{2-}, HCO_3^{-}, SO_4^{2-} and Cl^{-}) but the most significant are Na^{+} and Cl^{-} because they are the main components of seawater (Sverdrup et al. 1942).

Usually freshwater and seawater are in a dynamic balance in a coastal aquifer. This balance was described for the first time by Drabbe and Badon Ghyben (1889) and Herzberg (1901) and it is also known as the Ghyben-Herzberg relation:

$$z = \frac{\rho_f}{\rho_s - \rho_f} h \qquad \text{Eq.1}$$

Eq.1 relates the elevation of the water table (h) to the depth of the boundary of the interface between freshwater and the underlying saltwater zones of an aquifer (z) and it is based on the balance of the height of two columns of fluids of differing density. Freshwater (ρ_f) has a density of about 1.000 g/cm^3 at 20°C, whereas that of seawater (ρ_s) is about 1.025 g/cm^3. Although the difference between the density of freshwater and seawater is small, Eq. 2 indicates that this density contrast results in 40 m of freshwater below sea level for every 1 m of freshwater above sea level, that is:

$$z = 40h \qquad \text{Eq.2}$$

As stated above, the Ghyben-Herzberg relation describes the dynamic balance between freshwater and seawater in a coastal aquifer. Actually other processes can determine an aquifer salinization, either naturally or resulting from human activities (NRM 2014).

Natural salinity, as known as primary salinity, can occur for several processes including:

- sea salt aerosol (SSA) deposition: it consists in the dry deposition of sea spray particles transported by the wind from the sea surface to the land, where they accumulate on the coastal tree foliage (Lewis and Schwartz 2004);
- lateral intrusion: it is the movement of seawater from sea to the bottom of an aquifer as a consequence of a recharge reduction (Ward et al. 2009);
- salt-wedge intrusion: it happens when a water course carrying freshwater, reaches a basin with saline water (sea, ocean or inland sea) and the saline water tends to propagate into the river mouth, affecting the quality of water (UNESCO 1991);
- evaporite dissolution: it takes place when a dissolution of evaporite deposits occurs, with a consequent increase of salt content (Panno et al. 2006)
- fossil seawater contamination: this salinization is due to the mixing between groundwater and paleo-saline waters. Paleo-saline waters are defined as groundwater formed under previous climatic conditions and hydrogeological settings (Edmunds 2001).

Human activity as well can determine salinization processes, known as secondary salinity. The main process are:

- upconing: it occurs when a pumping of freshwater causes a cone of the freshwater head around the well (Bear et al. 1999). This cone, in turn, determines an upward movement of seawater for the Ghyben-Herzberg Principle;
- reclamation activities: they can determine a reduction of the dune systems and consequently facilitate the movement of saline waters inland (Antonellini et al. 2008); furthermore the dug of a drainage network can increase the potentiality of seawater to penetrate coastal areas;

- irrigation: especially in arid and semi-arid zones, high water table levels can determine a mobilization of salts accumulated near the soil surface (Smedema and Shiati 2002).

An easy and diffused method to detect the salinity presence in groundwater and surficial waters is the Electrical Conductivity. In fact it can represent an indirect salinity marker because a linear relationship exists between EC and Cl^- content (Cruz et al. 2011; Kelly 2005). The main method to identify the salinity presence in this PhD thesis was the Electrical Conductivity, measured in coastal wells, piezometers, lakes, rivers and drainage canals. This work developed with the help of the research group of the "*Laboratorio di Idrogeologia Numerica e Quantitativa* (LINQ)" of the Roma Tre University. Field investigations covered a time range from the beginning of 2011 to the end of 2013. They were carried out in two areas located in two coastal plains along the Tyrrhenian coast line of the Latium Region. They were chosen because in the last decades the LINQ carried out several researches in these areas, which allowed to have a great stratigraphic and well data availability. Furthermore the areas show very similar geological characteristics because they consist in sedimentary multi-lyered coastal aquifers and they were interested by reclamation activities in the past centuries. The surveyed areas include the Litorale Romano Natural Reserve (near Rome) and the Circeo National Park (nearby Latina City). Both the study areas show a dense hydrografical network deriving from the reclamation activities and the presence of natural rivers, which drive the salinization processes.

Study areas include also the coastal plain of the Tiber River, lying on the hydrographical left of the Tiber River and the whole Pontina Plain sector, delimited by the coast line and the Sisto River (Fig.0.1). In Pontina Plain a further area was investigated. It is located on the hydrographical right of the Moscarello Canal mouth, occupied by an ex-industrial area belonging to "*Società per la Gestione degli Impianti Nucleari* (SOGIN)" (Fig.0.1). At the end of the surveys an overall surface of about 300 km^2 was investigated, 260 km^2 and 40 km^2 for Pontina Plain and the Tiber Delta respectively. Studies were conducted using 2500 € of research founds. The economic support was provided by the University of Roma Tre. Money was spent for the data collection, to participate to national and international congresses and to move to the University of Queensland, (Brisbane, Australia), to implement a numerical model.

STRUCTURE OF THE THESIS AND AIMS

The present work is divided in five chapters and it is structured as a series of scientific papers, due to the several salinization processes identified during the experimental surveys. This work organization, suggested by the most recent guidelines coming from Cambridge University (Gustavii 2013), gives a lot of advantages such as a major probability to be read by others and a quicker and wider possibility to spread the papers through electronic journals. Furthermore a paper structure is well defined, established and universal and every chapter can be separated from the overall work. At the moment of writing, chapter 1, titled "Wind-induced salt-wedge intrusion in the Tiber River mouth (Rome-Central Italy)" has already been published on the Environmental earth Sciences international journal (see appendix 1).

The thesis is divided in two sections: chapters 1-3 belong to the Section A, which describes salinization processes about the Tiber River Delta area; chapters 4-5 are part of the Section B, which includes the topics faced in the Pontina Plain area.

The two study areas were contextualized by means of regional surveys, to analyze groundwater patterns and their evolution in time. Furthermore Multi-temporal chemo-physical surveys along the coastal areas and remote sensing techniques allowed to identify the main salinization processes, discerning the anthropic and natural salt contamination sources. Statistical analisys were developed for the meteorological data interpretation.

Despite of several hydrogeological salinization processes, the dissertation holds a main guideline: it focused on groundwater salinization induced by rivers and anthropic canals, due to wind effect and river discharge modification in time, in areas where anthropic and protected areas coexist. The study of the effect of the river discharge on coastal aquifer salinization was performed with the help of the most innovative techniques of numerical modeling, improved at the Department of Civil Engineering of the University of Queensland, Brisbane, Australia.

Chapters 1-2 describe the importance of the westerly winds for the salinization processes in the Tiber River Delta area. In fact the winds determine both a salt-wedge emplacement in the Tiber mouth during the falls, and a groundwater salinization in the Litorale Romano Natural Reserve pine forest because of SSA deposition.

The Tiber River Delta regional surveys described in the chapter 3 were combined with hydrogeochemical analyses and allowed to relate the salinity sources to the above mentioned salinization processes: the salt-wedge presence in the Tiber River, noticed up to 8.8 km from the Tiber mouth, is the more likely reason of the seawater intrusion processes identified in the alluvial area of Ostia Antica. SSA deposition is the main vehicle of salinization in the Castel Fusano Natural Reserve pine forest, located along the coast line. Hydrogeochemical analyses permitted further to identify freshening processes ascribable to ion-exchange, related to the presence of historical solar salt works in the Ostia Antica area.

Chapter 4 focused on groundwater salinization related to the presence of seawater in the anthropic canal network and in the coastal lakes of the Pontina Plain, in the area of the Circeo National Park. In that area a strict connection between surface and groundwater salinization was identified, also because of the great reclamation activities of the past century.

As suggested by the dissertation title, the final aim of the work was the use of numerical modeling, to detect salinization processes. The use of numerical modeling is a further investigation tool to analyze and quantify what happens in a complex groundwater system. Chapter 5 is about the implementation of numerical modeling using FEFLOW 6.0 (Diersch 2009), to understand the relationships between groundwater and river salinization. The model was implemented at the Moscarello Canal mouth (SOGIN area), in which a salt-wedge intrusion was noticed. The canal, anthropic and dug in the past century, resulted to be subject to a strong discharge modification, which is able to determine inflows of water in the adjacent aquifer. The inflows of water from the canal bottom resulted to be able to push a saline plume present in the aquifer.

REGIONAL GEOLOGICAL AND HYDROGEOLOGICAL SETTING

Geological setting about the Italian peninsula comes from the convergence between the African and the European Plates, that determined the Apennine orogenesis and the Tyrrhenian basin opening (Vai and Martini 2001). The subduction of the African plate under the European plate had a climax in the Miocene and Medium Pliocene (Selvaggi and Chiarabba 1995; Piromallo and Morelli 2003), when the convergence and subduction determined the Apennines formation. Tectonic units were composed mainly by carbonate rocks about the Mesozoic and Cenozoic, that constitute several mounts of the Latium Region [i.e. Lepini Mounts, and the isolated Circeo Mount (Parotto and Praturlon 1975)].

In the Miocene, tectonic convergent processes migrated toward the Adriatic Sea and extensional tectonics developed on the Tyrrhenian side, which created normal faults with a NW-SE trend (Mattei et al. 2008). These faults bordered sedimentary basins, lying in unconformity on the previous orogenic structures (Bossio et al. 1998). Along the crustal discontinuities the volcanism developed from the Medium Pleistocene along the Latium Tyrrhenian margin (De Rita et al. 1994; Peccerillo 2005).

In the Pliocene and Lower Pleistocene, the Tyrrhenian edge was subject to several transgressive and regressive phases, that created thick sedimentary deposits (Barberi et al. 1994; Cosentino et al. 2006). At the base of the sedimentary succession, thick clayey deposits developed. They represent the regional aquiclude of the two study areas. The morphology of the impermeable basement was described by Barberi et al. (1994) and results strongly affected both by tectonics and the presence of the volcanic complexes (i.e. Colli Albani Volcanic Complex).

In the Tiber Delta Area, the impermeable basement is overlaid by the Tiber Depositional Sequence (Milli et al. 2013). In the Pontina Plain the regional aquiclude is overlaid by clastic sediment of marine, alluvial, marsh, lagoon and beach ridge environment (Barbieri et al. 1999; Kamermans 1991).

From a historical point of view, the two macro areas show several similarities: both of them were interested by strong reclamation activities in the past centuries, that changed the morphological and hydrological pattern substantially (Amenduni 1884; Brunamonte and Serangeli 1996; Serva and Brunamonte 2007). The human activities, along with the geological characteristics, determine complex groundwater patterns, whose morphology changes in time.

Boni et al. (1988) and Capelli et al. (2012) gather together the outcropping deposits located in the studied areas, categorizing them according to the hydraulic potentiality (Fig.0.2). The most represented hydrogeological complex is called “Coastal dune complex” and includes dune sands, beach sands and fluvial sands, with thickness up to tens of

meters. In the study areas swamp-fluvial-lacustrine deposits outcrop as well, provided of low hydraulic potentiality. They are mainly composed by silts and clays, with local intercalations of gravels and travertine and the thickness can reach tens of meters. In the Tiber Delta area the recent alluvial hydrogeological complex outcrops, formed by fluvial sands, clays, gravels and silts from the Tiber River. The hydraulic potentiality ranges between low to medium-high and the thickness is up to one hundred meters. Both the study areas are characterized in general by low hydraulic gradients and are recharged both by zenithal recharge and from the surrounding mounts that are: Colli Albani Mounts in the Tiber area and Lepini Mounts in the Pontina area.

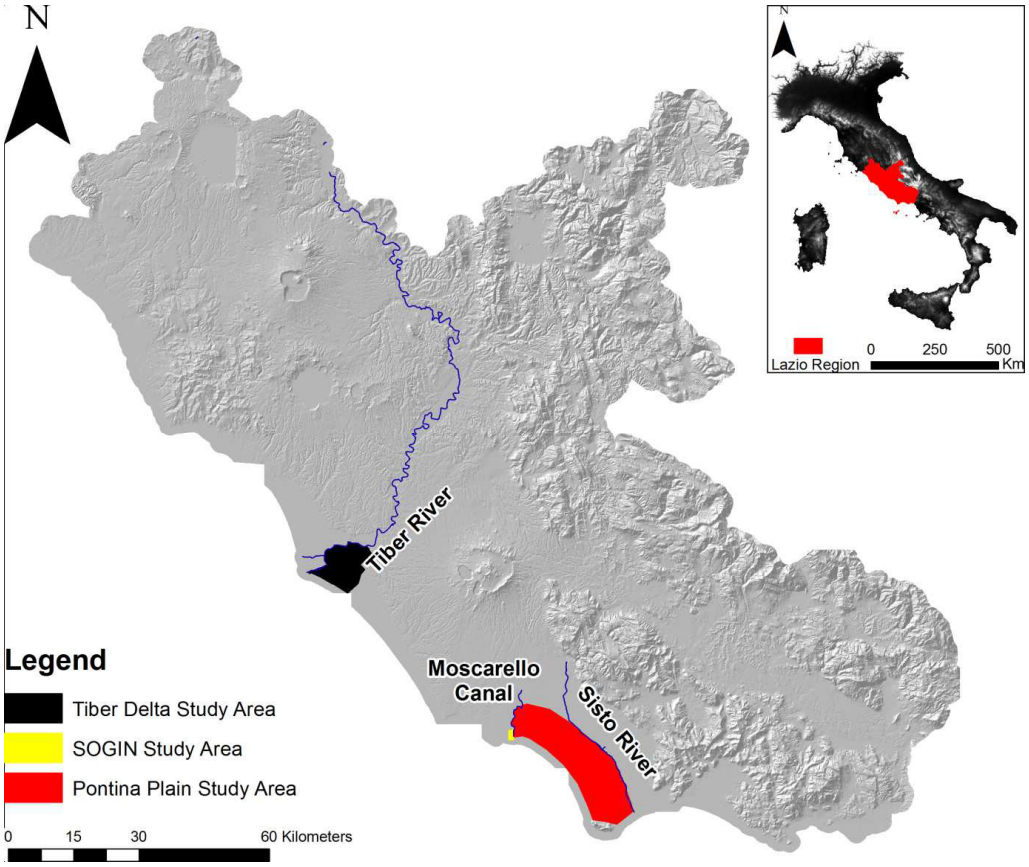

Fig. 0.1: the study areas located along the Latium region

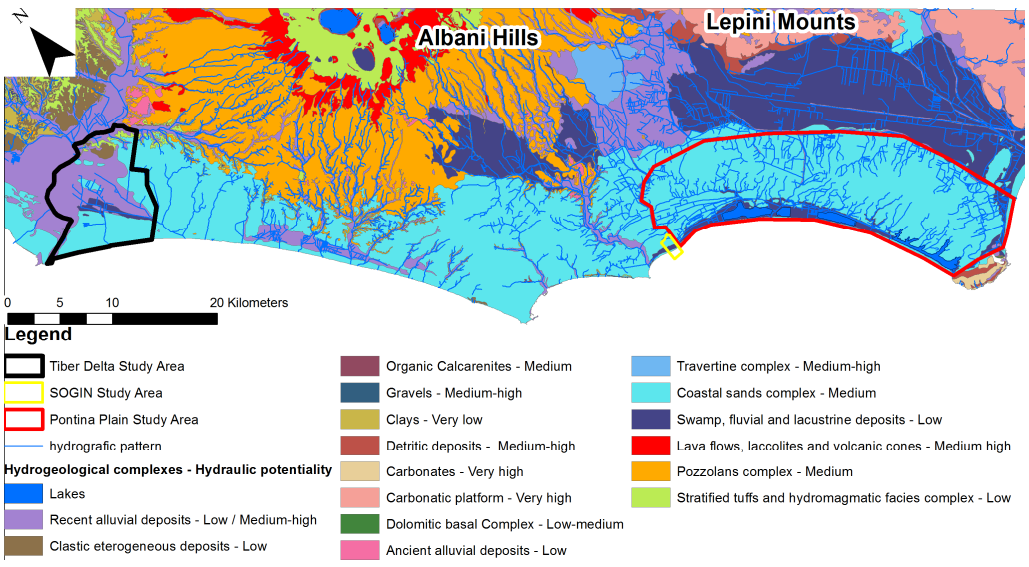

Fig. 0.2: hydrogeological complexes outcropping along the Latium coast line (After Capelli et al. 2012)

REFERENCES

Amenduni G (1884) Sulle opere di bonificazione della plaga litoranea dell'Agro Romano che comprende le paludi e gli stagni di Ostia, Porto, Maccarese e delle terre vallive di Stracciacappa, Baccano, Pantano e Lago dei Tartari. Relazione del progetto generale 15/7/1880. Ministero Lavori Pubblici,

Antonellini M, Mollema P, Giambastiani B, Bishop K, Caruso L, Minchio A, Pellegrini L, Sabia M, Ulazzi E, Gabbianelli G (2008) Salt water intrusion in the coastal aquifer of the southern Po Plain, Italy. Hydrogeology Journal 16 (8):1541-1556. doi:10.1007/s10040-008-0319-9

Barberi F, Buonasorte G, Cioni R, Fiordelisi A, Foresi L, Iaccarino S, Laurenzi MA, Sbrana A, Vernia L, Villa IM (1994) Plio-Pleistocene geological evolution of the geothermal area of Tuscany and Latium. Memorie Descrittive della Carta Geologica Italiana 49:77-134

Barbieri A, Carrara C, Castorina F, Dai Pra G, Esu D, Gliozzi E, Paganin G, Sadori L (1999) Multidisciplinary study of Middle-Upper Pleistocene deposits in a core from the Piana Pontina (central Italy). Giornale di geologia 61:47-73

Bear J, Cheng AH-D, Sorek S, Ouzer D, Herrera I (1999) Geophysical investigations. In: Jacob Bear AHDCSSDO, Ismael H (eds) Seawater Intrusion in Coastal Aquifers - Concepts, Methods and Practises. Kluwer Academic Publishers, Dordrecht, The Nederlands, pp 9-50

Boni C, Bono P, Capelli G (1988) Carta Idrogeologica del territorio della Regione Lazio. Scala 1:250.000. Pubblicazione Speciale Regione Lazio Vol. Unico. Studio Marinelli, Roma

Bossio A, Costantini A, Foresi LM, Lazzarotto A, Mazzanti R, Mazzei R, Pascucci V, Salvatorini G, Sandrelli F, Terzuoli A (1998) Neogene-Quaternary sedimentary evolution in the western side of the Northern Apennines (Italy). Memorie della Società Geologica Italiana 52:513-525

Brunamonte F, Serangeli S (1996) Evoluzione naturale ed intervento antropico nello sviluppo dei fenomeni di subsidenza nella Pianura Pontina. Memorie della Società Geologica Italiana 51:823-836

Capaccioni B, Didero M, Paletta C, Didero L (2005) Saline intrusion and refreshening in a multilayer coastal aquifer in the Catania Plain (Sicily, Southern Italy): dynamics of degradation processes according to the hydrochemical characteristics of groundwaters. Journal of Hydrology 307 (1-4):1-16. doi:10.1016/j.jhydrol.2004.08.037

Capelli G, Mastrorillo L, Mazza R, Petitta M, Baldoni T, Banzato F, Cascone D, Di Salvo C, La Vigna F, Taviani S, Teoli P (2012) Carta Idrogeologica del Territorio della Regione Lazio. Scala 1:100.000 (4 Fogli). S.EL.CA., Firenze - Italy

Cosentino D, Federici I, Cipollari P, Gliozzi E (2006) Environments and tectonic instability in central Italy (Garigliano Basin) during the late Messinian Lago-Mare episode: new data from the onshore Mondragone 1 well (Garigliano plain, central Italy). Sedimentary Geology 188-189:297-317

Cruz JV, Coutinho R, Pacheco D, Cymbron R, Antunes P, Freire P, Mendes S (2011) Groundwater salinization in the Azores archipelago (Portugal). Environmental Earth Sciences 62 (6):1273-1285. doi:10.1007/s12665-010-0615-2

De Rita D, Bertagnini A, Carboni G, Ciccacci S, Filippo M, Faccenna C, Fredi P, Funiciello R, Landi P, Sciacca P, Vannucci N, Zarlenga F (1994) Geological-petrological evolution of the Cerini Mountains area (Latium, Central Italy). Memorie Descrittive della Società Geologica Italiana 49:291-322

Diersch HJG (2009) FEFLOW Reference Manual. DHI-WASY GmbH, Berlin

Drabbe J, Badon Ghyben W (1889) Nota in verband met de voorgenomen puboring nabij Amsterdam. Amsterdam

Edmunds WM (2001) Paleowater in European coastal aquifers – the goals and main conclusions of the PALAEAUX project. In: Edmunds WM, Milne CJ (eds) Paleowaters in Coastal Europe, vol 189. vol Geological Society Special Publication. The Geological Society, Bath, pp 1-16

Gustavii B (2013) How to Prepare a Scientific Doctoral Dissertation Based on Research Articles. Cambridge University Press, New York

Herzberg B (1901) Die wasserversorgundeinigerNordseebâder. Journal gasbeleuchtung und Wasserversorgung 44:815-819, 824-844

Kamermans H (1991) Faulted land: the geology of the Agro Pontino. In: A. Voorrips SHLHK (ed) The Agro Pontino survey project, methods and preliminary results. Amsterdam, p 131

Kelly D (2005) Seawater intrusion Topic Paper. vol 6. WRIA, Island County

Lewis ER, Schwartz S (2004). In: Board AB (ed) Sea Salt Aerosols Production; Mechanism, Methods, Measurement and Models. Washington DC, USA, pp 1-5

Mattei M, Funiciello R, Parotto M (2008) Roma e contesto geodinamico dell'Italia Centrale. In: Funiciello R, Praturlon A, Giordano G (eds) La Geologia di Roma dal cetro storico alla periferia, vol 1. vol Memorie Descrittive della Carta Geologica d'Italia. S.EL.C.A., Firenze, pp 13-24

Milli S, D'Ambrogi C, Bellotti P, Calderoni G, Carboni MG, Celant A, Di Bella L, Di Rita F, Frezza V, Magri D, Pichezzi RM, Ricci V (2013) The transition from wave-dominated estuary to wave-dominated delta: The Late Quaternary stratigraphic architecture of Tiber River deltaic succession (Italy). Sedimentary Geology 284:159-180. doi:10.1016/j.sedgeo.2012.12.003

NRM (2014) Department of Natural Resources and Mines. Government of Queensland. www.nrm.qld.gov.au.

Panno SV, Hackley KC, Hwang HH, Greenberg SE, Kaprac IG, Landsberger S, O'Kelly DJ (2006) Characterization and identification of Na-Cl sources in ground water (vol 44, pg 176, 2006). Ground Water 44 (2):129-129. doi:10.1111/j.1745-6584.2006.00200.x

Parotto M, Praturlon A (1975) Geological summary of the Central Appennines. Quaderni della Ricerca Scientifica 90:257-311

Peccerillo A (2005) Plio-Quaternary volcanism in Italy Petrology, Geochemistry, Geodynamics

Piromallo C, Morelli A (2003) P wave tomography of the mantle under the Alpine-Mediterranean area. Journal of Geophysical Research: Solid Earth 108 (B2). doi:10.1029/2002JB001757

Post VEA (2005) Fresh and saline groundwater interaction in coastal aquifers: Is our technology ready for the problems ahead? Hydrogeology Journal 13 (1):120-123. doi:10.1077/s10040-004-0417-2

Selvaggi G, Chiarabba C (1995) Seismicity and P-wave velocity image of the Southern Tyrrhenian subduction zone. Geophysical Journal International 121:818-826. doi:10.1111/j.1365-246X.1995.tb06441.x

Serva L, Brunamonte F (2007) Subsidence in the Pontina Plain, Italy. Bulletin of Engineering Geology and the Environment 66 (2):125-134. doi:10.1007/s10064-006-0057-y

Smedema LK, Shiati K (2002) Irrigation and salinity: a perspecive review of the salinity hazards of irrigation development in the arid zone. Irrigation and Drainage Systems 16:161-174

Sverdrup HU, Johnson MW, Fleming RH (1942) Chemistry of Seawater. In: Inc. P-H (ed) The Oceans - Their Physics, Chemistry and General Biology. New York, pp 165-227

UNESCO (1991) Guidelines on the study of seawater intrusion into rivers. United Nations Educational, Scientific and Cultural Organization, Paris

Vai GB, Martini I (2001) Anatomy of an orogen: The Appennines and adjacent Mediterranean basin. Bodmin Kluwer Academic, Dodrecht

Ward J, Werner AD, Howe B (2009) Saltwater intrusion in Southern Eyre Peninsula. Eyre Peninsula Groundwater, Allocation and Planning Project,

COLLABORATIONS

The research activity was conducted in collaboration with many state and local authorities.
In the Tiber Delta they were:

- the office of "*Servizio di Polizia Provinciale e Protezione Civile*" led by Alessio Argentieri, which offered the means to realize the navigation along the Tiber River; the surveys were supported by Dr. Sara Taviani and Dr. Stefano Viaroli
- the surveys inside the Litorale Romano Natural Reserve were conducted with the authorization of the "*Dipartimento X - Tutela Ambientale e del Verde and Protezione Civile - Ufficio Gestione Riserva Naturale Statale Litorale Romano*", of the "*Roma Capitale*" municipal bureau. This departement was led before by Romano Maria Delli Santi and after by Tommaso Profeta and under the supervision of the "*Corpo Forestale dello Stato*";
- the surveys in the archeological area of Ostia Antica were possible thanks to the "*Soprintendenza Speciale per i Beni Archeologici*" of the "*Ministero dei Beni e delle Attività Culturali e del Turismo*", under the authorization of Maria Rosaria Barbera;
- some surveys were possible also thanks to local authorities as "*FIDAL Lazio*" and the "*Consorzio di Casal Palocco*";
- a special thanks for the logistical support about the surveys goes to Claudio Papiccio, an agent of the "*Polizia Municipale di Roma Capitale*" corps;
- the chemical analytical laboratory to evaluate the water types of the samples collected in the roman area, was offered by the Prof. Paola Tuccimei of the University of Roma Tre;

In the Pontina plain they were:

- the surveys in Pontina Plain were possible thanks to the "*Ufficio Territoriale per la Biodiversità di Fogliano*", led by Sergio Zerunian. The personnel of the "*Corpo Forestale dello Stato*" and especially Alessandra Noal, offered assistance during the data collection and for the logistic base in the Circeo National Park guestrooms;
- some aspects of the Pontina Plain studies were carried out with the precious help of Vinicio Gragnanini;
- in the ex-industrial area of Borgo Sabotino the collaboration was carried out with the "*Società per la Gestione degli Impianti Nucleari*" (SOGIN) staff, under the supervision of Giancarlo Ventura and the precious help of Michele Rosati;
- the numerical model about the data collected in the SOGIN area was implemented at the University of Queensland, Brisbane, Australia, under the supervision of the Prof. Ling Li and Dr. Pei Xin;

Finally the help of many students was important for the data collection. Three Master's degrees were supervised and the students Emanuele Ruta, Barbara Zaccaria and Marco Fantini worked hard to obtain good scientific results.
A Bachelor's degree as well was supervised, achieved by Valerio Ricci.

SECTION A: THE TIBER RIVER DELTA

1. WIND-INDUCED SALT-WEDGE INTRUSION IN THE TIBER RIVER MOUTH (ROME-CENTRAL ITALY)

ABSTRACT

The wind effect on river water quality was illustrated by means of thermohaline measurements carried out in the Tiber River in May 2012. The survey was carried out using a boat, in stations located in the two Tiber branches: Fiumara Grande and Traiano Canal. Thermohaline variables (salinity and temperature) were used to describe the water-type patterns and to define the salt-wedge position. Although the river flow rate was rather high, saltwater intrusion happened. Wind data suggested that the more probable cause of salt-wedge intrusion was the wind action. Especially wind speeds higher than 4 m/s are able to dominate the sea current at surface layers, determining an increase in the sea level. Therefore westerly winds determined a seawater inflow in the river mouths.

1.1 INTRODUCTION

Coastal areas are the most important environments for the human development due to the great water resources availability and climatic quality. The increasing urbanization, industrialization and agricultural requirements lead to various problems such as depletion of groundwater, deterioration of water quality, land subsidence and salinization (Capaccioni et al. 2005; Park et al. 2012). Really salinization became a very important issue in water management problems all over the world (Barlow and Reichard 2010; Trabelsi et al. 2012) and it is mainly caused by:

- evaporite dissolution (Ahmed et al. 2013);
- fossil seawater (Farid et al. 2013);
- seawater intrusion (Tran et al. 2012).

Seawater intrusion is defined as the mass transport of saline waters into zones previously occupied by fresher waters (Bear et al. 1999). In coastal areas, rivers are preferential way to lead seawater inland, through salt-wedge intrusion (Custodio and Llamas 2005). Salt-wedge intrusion happens when a water course carrying fresh-water, reaches a basin with saline water (sea, ocean or inland sea) and the saline water tends to propagate into the river mouth, affecting the quality of water (UNESCO 1991). Whereby the salt's front position moves upstream in close proximity to pumping areas, the direction of flow between the aquifer system and the river can be reversed, determining seawater intrusion in groundwater (Barlow 2003). In the last decades several authors (Eagling et al. 2012; Pezzetta et al. 2011; Teien et al. 2006; Wong 1994; Wong et al. 2013) are pointing attention on estuarine environments to understand the problem of mobilization of metals and trace elements, connected to seawater intrusion. For this reason, understanding how the salt-wedge intrusion occurs, can help researchers to understand water chemistry modifications. Several authors (Fagerburg and Alexander 1994; Sierra et al. 2004; Zhou et al. 2012) have focused attention on salt-wedge intrusion in several world rivers, emphasizing the importance of freshwater river discharge, because it can represent a hydraulic barrier to the salt-wedge progress inland. Other authors (Lenkopane et al. 2009; Robinson et al. 2007a; Robinson et al. 2007b) concentrated their studies on tidal effect and how it can strongly affect the salinization of a river, and consequently groundwater salinization. The implications of river morphology on salt-wedge propagation were investigated both by laboratory experiments (Fujiwara et al. 1997) and by experimental surveys (Qian and Ishikawa 2003), demonstrating for example, the importance of shallow bathymetries in the river bottom morphology, on the intensity and frequency of a saltwater wedge intrusion effect. River discharge and morphology can therefore influence the salt-wedge shape. Pritchard (1955) classified the river estuaries on the basis of vertical structure of salinity. This classification considers the competition between buoyancy forcing from river discharge and mixing from tidal forcing. Mixing from tidal forcing is proportional to the volume of oceanic water entering the estuary during every tidal cycle (Valle-Levinson 2010). Fig.1.1 shows salinity patterns with respect to different equilibrium cases, between river discharge and tide intensity. Halocline configuration can be very different, starting from "salt-wedge" pattern, with very sharp haloclines, to a "well mixed" pattern, with vertical haloclines.

In this context several studies have been conducted to understand the relationships between the winds and the wind induced flows, in gulfs (Murray and Johns 1997) or straits (Valle-Levinson and Blanco 2004) and how wind can even strongly influence wind-forced upwelling dynamics (Macias et al. 2012; Roegner et al. 2011). deCastro et al. (2000) focused attention on wind and tidal influence on water circulation in an estuary, finding close connections between wind direction and the current developing at the sea surface layer. This assumption is based on the quadratic stress law of Large and Pond (1981): $U_w = \sqrt{\rho_a / \rho_w}\, W$, where, U_w is water velocity, ρ_a and ρ_w are air and water densities respectively and W is wind speed. This provides a wind induced water velocity of about 3% of the wind velocity. In particular deCastro et al. (2000) noticed that winds with speed higher than 4 m/s are able to induce a sea current speed, bigger than the one induced by tide.

In this study data collected in the Tiber River were analyzed. The aim of the study is to detect the connections between the wind-induced sea-flows movement and the related salt-wedge emplacement, based on the temperature pattern detected at the river mouth.

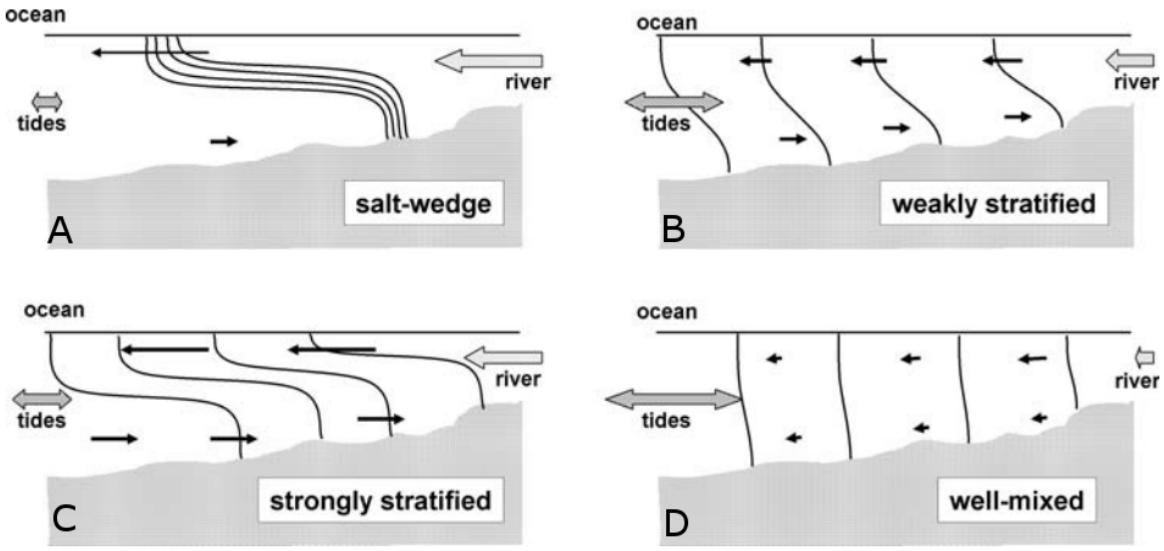

Fig. 1.1: haloacline patterns (after Valle-Levinson, 2010): A) large river discharge and weak tidal forcing result in salt-wedge estuaries; B) weakly stratified or partially mixed estuaries result from moderate to strong tidal forcing and weak to moderate river discharge; C) moderate to large river discharge and weak to moderate tidal forcing result in strongly stratified estuaries; D) strong tidal forcing and weak river discharge result in vertically mixed estuaries

1.2 STUDY AREA

Tiber River is 405 km in length and it rises in Tuscany at about 1268 m a.s.l.. Its basin comprises $1.7*10^4$ km^2 and it crosses the regions of Tuscany, Emilia Romagna, Umbria and Latium. After crossing the urban area of Rome (La Vigna et al. 2010; La Vigna et al. 2013) it flows into the Tyrrhenian Sea forming an estuary with two branches, the northernmost Traiano Canal (TC) and the southernmost Fiumara Grande (FG), divided by a small island (Fig.1.2). The Tiber River at its mouth flows in the alluvial sediments about the High Stand System Tract of the Tiber Depositional Sequence, developed from 6000 to 5000 years BP. This sequence is mainly composed by clay, silt, sand and organic matter lenses (Milli et al. 2013, for a further description see chapter 3.2). These deposits allow a hydraulic communication between groundwater and the river. In general flow paths are directed toward the river, except in the area of Ostia Antica (Fig.1.2), where the ground level is below the river level and water table is below the mean sea level (see chapter 3.6).

Tiber River shows variable discharge, increasing in the October-June period and decreasing from July to September. Data collected from the Ripetta water gauge during the decade 2002-2011 (IdrograficoLazio 2012a), show an average monthly value of discharge of about 162 m^3/s with maximum and minimum values of about 478 m^3/s and 73 m^3/s, in December 2005 and August 2007 respectively. TC receive about the 20% of the Tiber flow rate (Mikhailova et al. 1999). The Tiber River mouth is considered an arched estuary (Ricci Lucchi 1980) of the wave dominated type (Wright

1977). In the mouth area the astronomical tidal range has an average value of 0.4-0.6 m, whereas the meteorological tides can amount to 4.0 m (Bellotti et al. 1995). The Tiber mouth conditions determine seawater intrusion especially during the low-flow period (Capelli et al. 2007; Mikhailova et al. 1999).

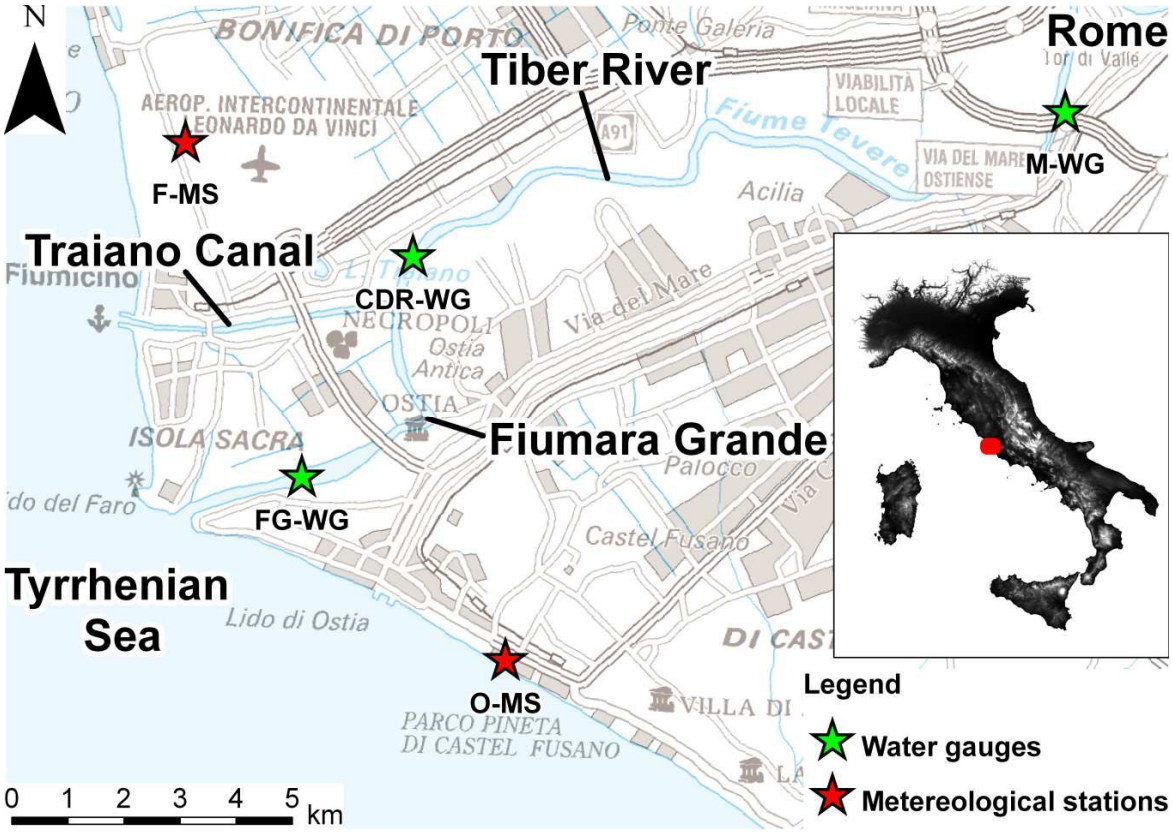

Fig. 1.2: Study area: the two river branches divided by the Sacra Island; location of water gauges and metereological stations; F-MS: Fiumicino MS; O-MS: Ostia MS; M-WG: Mezzocammino WG; CDR-WG: Capo Due Rami WG; FG: Fiumara Grande WG

1.3 AVAILABLE DATA AND METHODS

Hydrologic survey was performed by means of a boat in two days, the 16th and 24th May 2012, for TC and FG respectively. Thermohaline measurements were carried out using a 20.0 m cable length conductivity-meter which collected data about electrical conductivity (EC ± 0.5% µS/cm, normalized at 25.0 °C), salinity (Sal ± 0.1 g/l, accuracy) and temperature (T ± 0.1 °C) and they were collected for 37 stations: 24 for FG (Fig.1.3) and 13 for TC (Fig.1.4). Sal values were automatically converted from the EC values, by the conductivity-meter according to UNESCO (1983) directives. The points from FG16 to FG1 were in reality collected in the Tiber River, but they were named with FG acronym for simplicity's sake. The choice of the measurement points location was realized using the positions illustrated in Capelli et al. (2007), to better compare the results of data collection. Chemo-physical parameterization was realized during the countercurrent navigation, stopping the boat and maintaining the position by means of a GPS. Vertical measurements were realized every 0.5 m for all the points with the exception of the points from FG1 to FG13, where a distance of 1 m was maintained. They were realized from river surface to river bottom. The EC range detected was 1.1-57.0 mS/cm, Sal range was 0.4-37.5 g/l and T range was 16.2-19.4 °C. The navigation was about 23.1 km in length (19.2 km for FG and 3.9 km for TC). A bathymetric survey was conducted during the current navigation, with an echo sounder installed on the boat for 209 stations, at a distance of about every 100 m (164 points for FG and 45 for TC), without stopping the boat. Maximum river bottom depths were 12.0 and 5.8 for FG and TC respectively. Minimum river bottom depths were 1.7 and 2.8 for FG and TC respectively. Average river bottom depths were from 6.0 to 4.6 m for FG and TC respectively.

River level data were collected from three water gauges (WG, Fig.1.2) with a time step of 15 min (IdrograficoLazio 2012b). The period of data collection was from 1st January to 15thMay 2012.

Seawater level and temperature data were collected from the Anzio tidal gauge (TG) because its proximity to the study area. It is located about 45 km south of FG mouth, along the Tyrrhenian coast line, with data collected every 10 min (ISPRA 2012). Surface wind data were collected from two meteorological stations (MS), located in Fiumicino (Wunderground 2012a) and Ostia (Wunderground 2012b), nearby the FG and TC mouths (Fig.1.2). They were chosen because subject to the same dominant wind pattern and better representing wind conditions in the estuary. Ostia MS provided February-May wind data, recorded every 5 min. The Fiumicino MS provided the missing wind data of January, recorded every 2 min.

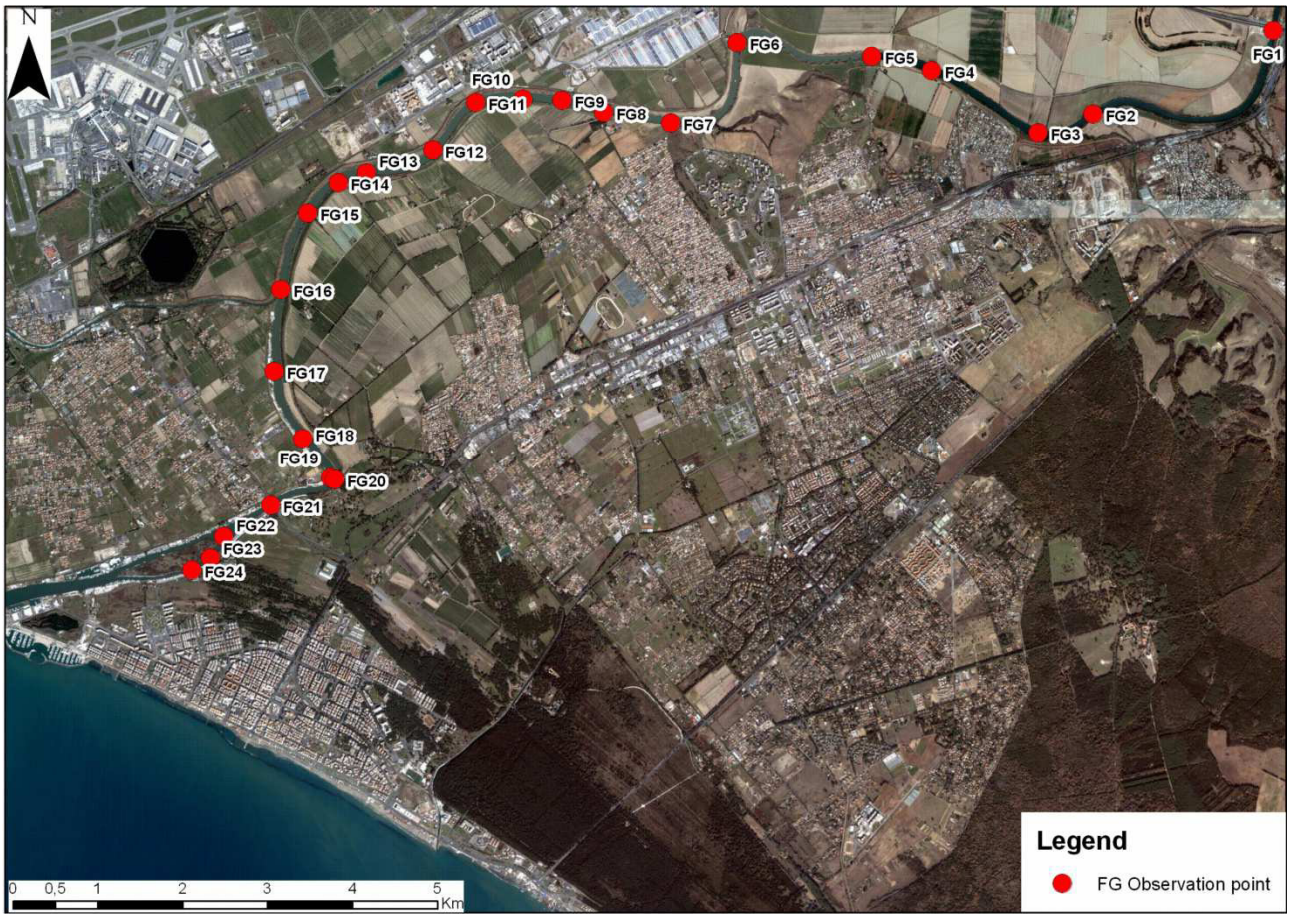

Fig. 1.3: Fiumara Grande measuerements points

Fig. 1.4: Traiano Canal measuerements points

1.3.1 FG AND TC DATA ANALYSIS

Graphs of Fig.1.5 show thermohalines of FG branch. From FG1 to FG13 the trend between Sal and T parameters is almost parallel whereas from FG14, the two lines start converging. It means that Sal values start increasing as moving toward the FG mouth. From FG17 onward, the lines intersect, revealing that the decrease of Sal values corresponds to an increase in T values. Only the point FG22 doesn't show the same trend, due to a bathymetric elevation nearby a small island.

The FG crossed section in Fig.1.6 summarizes the previous graphs, showing the salt-wedge position. Sal range division was realized according to the Freeze and Cherry (1979) classification, which considers waters with Sal≤1 g/l as freshwater; 1.1<Sal≤30 as brackish water; Sal >30 g/l as seawater.

Both the mixing zone (brackish) and the seawater zone reached a maximum thickness of 3 m at the point FG21. The anomalous morphology of the mixing zone at the point FG19 is probably due to a freshwater inflow of a drainage pump, located on the ideographical right of FG branch. The salt-wedge was noticed up to 8.8 km from the FG mouth. This datum is in agreement with previous works (Capelli et al. 2007; Mikhailova et al. 1999).

Thermohaline graphs about TC are shown in Fig.1.7. The convergent trend of the T and Sal parameters in all the graphics indicates the presence of brackish water along the whole river branch, with presence of seawater at TC bottom. Fig.1.8 shows the seawater distribution along TC. A very important role is performed by FG, which represents a natural barrier to salt-wedge propagation along TC, due to its higher discharge rate.

The eco sounder highlighted a lot of bathymetric depressions along both of the river branches.

According to Cameron and Pritchard (1963) and Pritchard (1955), FG and TC sharp haloclines can be classified as salt-wedge stratified estuary and a strongly stratified estuary respectively.

FG is characterized by high river discharge and weak inflow of seawater in the near-bottom layer, whereas TC is characterized by moderate river discharge and weak tidal forcing (Dyer 1997).

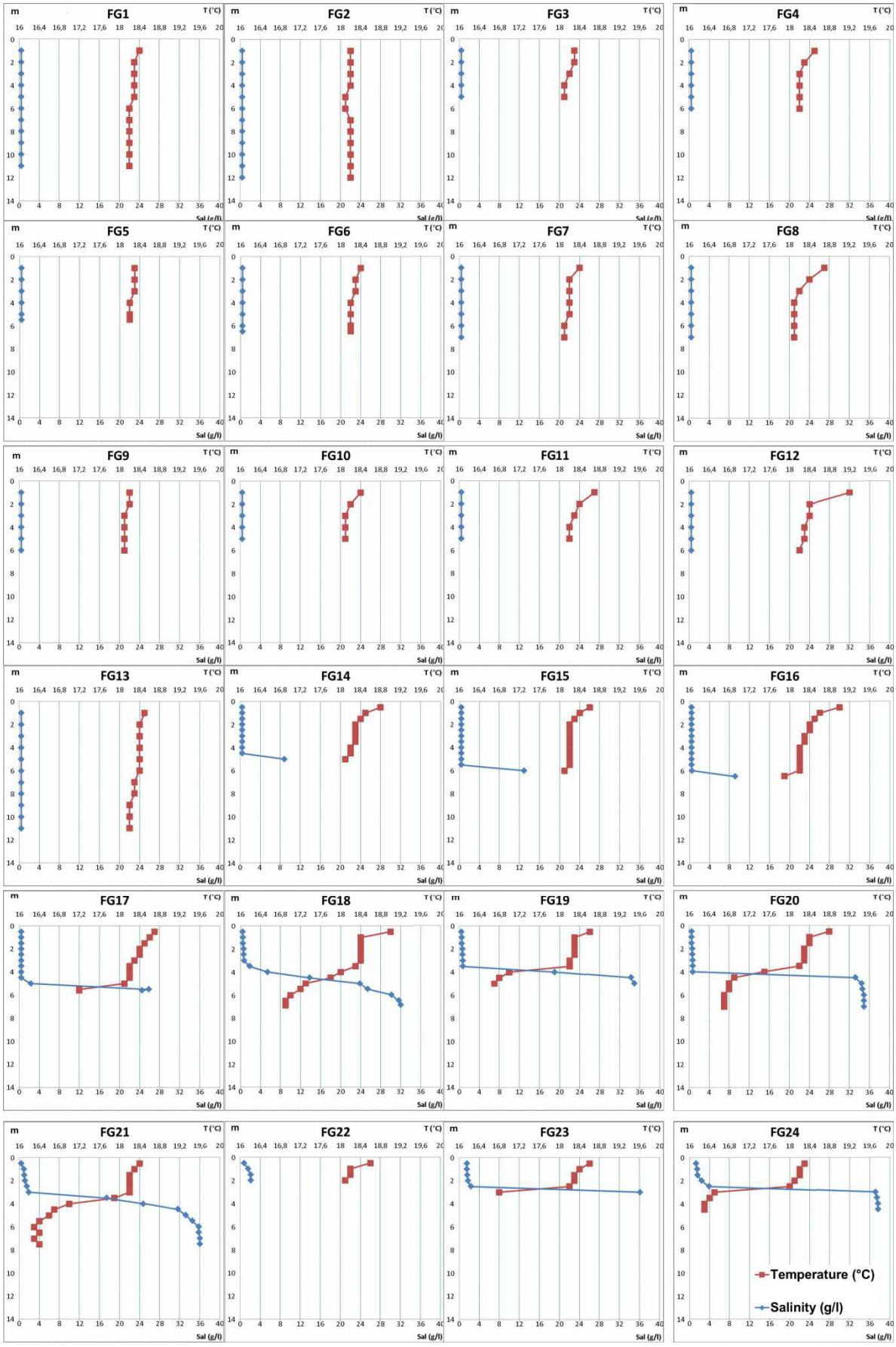

Fig. 1.5: thermohalines about of Fiumara Grande branch; salinity is indicated in blue whereas temperature is in red. Three types of trend between the two parameters can occur: parallel, when Sal and T are constant along the vertical; converging, when water starts to be brackish; intersecting, when salt-water with a T lower than freshwater lies on river bottom. The location of the measurement points is indicated in Fig.1.3

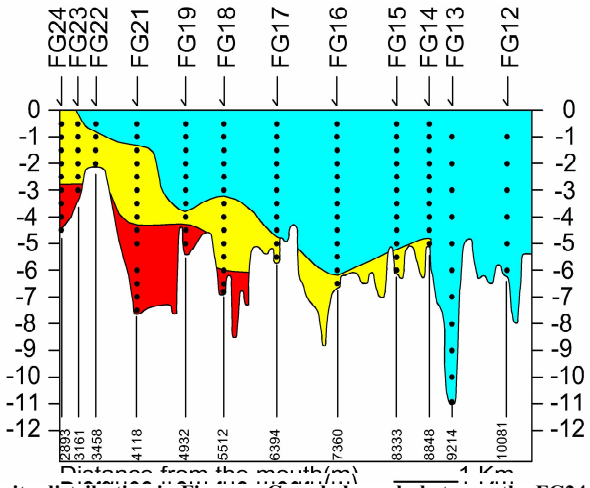

Fig. 1.6: crossed section about the salinity distribution in Fiumara Grande branch, between the FG24 and FG12 measurement stations. The data before FG12 are not represented because of the same salinity of water column. FG mouth is leftward. Salt-wedge position was noticed up to 8,8 km form the mouth. Seawater is represented red, brackish water in yellow and freshwater in ciano. Both the mixing zone (brackish) and the seawater zone reached a maximum thickness of 3.0 m at the point FG21. The anomalous morphology of the mixing zone at the point FG19 is probably due to a freshwater inflow of a drainage pump, located on the hydrographical right of Fimara Grande branch; black points indicate the vertical measurement locations. The location of the measurement points is indicated in Fig.1.3

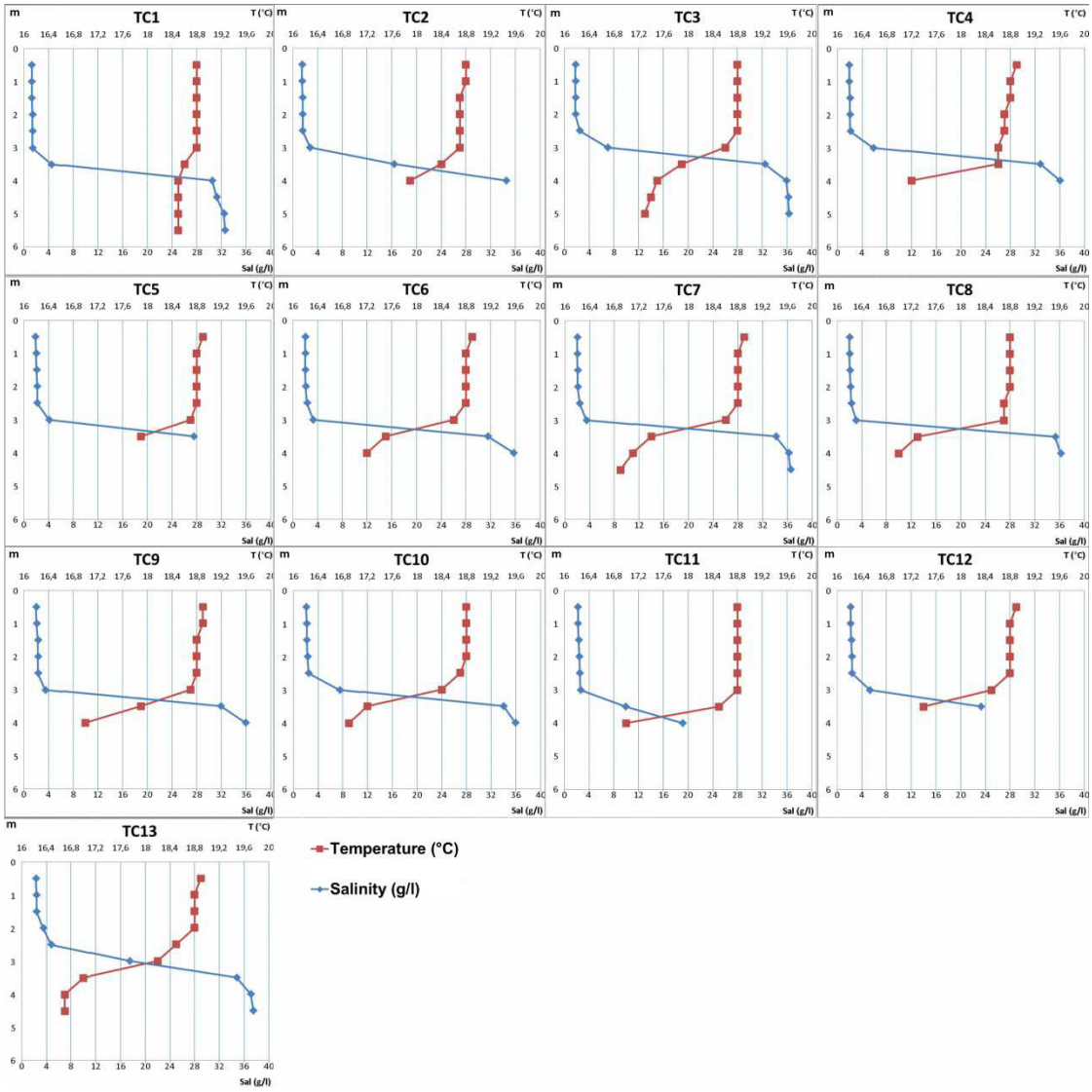

Fig. 1.7: thermohalines about of Traiano Canal; branch salinity is indicated in blue whereas temperature is in red. Three types of trend between the two parameters can occur: parallel, when Sal and T are constant along the vertical; converging, when water starts to be brackish; intersecting, when salt-water with a T lower than freshwater lies on the river bottom. The location of the measurement points is indicated in Fig.1.4

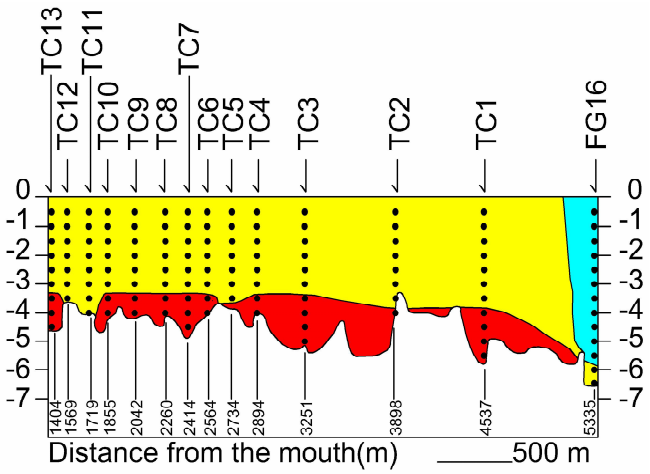

Fig. 1.8: crossed section of salinity distribution in TC branch. TC mouth is leftward while FG is rightward. Salt-wedge position was noticed along the whole TC bottom. Seawater is represented in red, brackish water in yellow and freshwater in ciano; black points indicate the vertical measurement locations. The location of the measurement points is indicated in Fig.1.4

1.3.2 River and sea levels

Levels about the three water gauges and Anzio tidal gauge are shown in Fig.1.9. Since water gauges and the tidal gauge held a different time frequency, they were filtered every 30 minutes (min) to fit each other. Data collected were subject to Fourier analysis using the fast Fourier transform (FFT) function in MATLAB, to analyze the connections between river and sea levels. The FFT method can be applied to analyze the dominant periods of the tide variations.

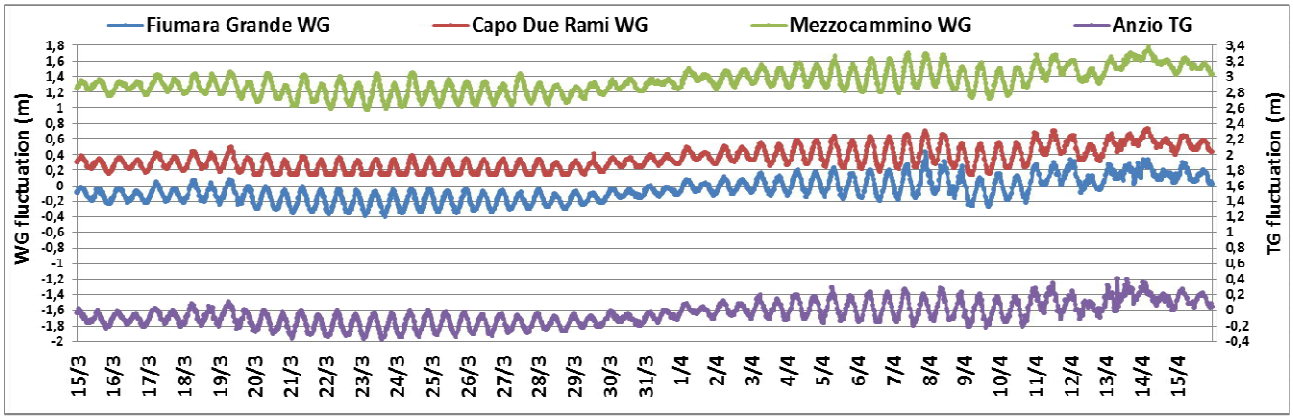

Fig. 1.9 levels about the three Water gauges (WG) and Anzio tidal gauge (TG), with a 30 minutes frequency. As it can be observed graphically, there is a strict relationship between the river-water and tidal fluctuations. The time series is from the 15th March to the 15th of April. The left Y axis is about the WGs level fluctuation, while the left Y axis is about the Anzio TG fluctuation

The results in Fig.1.10 show that the dominant frequencies for the level data are 1.0 d^{-1}, 1.94 d^{-1} and 2.0 d^{-1} and they represent the lunar diurnal, lunar semi-diurnal and solar semi-diurnal constituent respectively (Mao et al. 2006). Hydrometric levels are affected by sea level fluctuation even up to Mezzocammino water gauge, located about 22 km from the river branches mouth.

Cross-correlation (CC) was used to quantify the delay among the tide-induced river fluctuations at the WGs with respect to the tidal fluctuation at the tidal gauge. CC measures the similarity of two waveforms as a function of a time-lag applied to one of them. The dataset was sub-divided in daily time-series and a moving average (MA) was applied to obtain the removal of the noise from the wave-form signal.

CC was computed among the Anzio tidal gauge daily time-series and each water gauge daily time-series, for the whole period from the 1st January to 15th of May. The computed daily lag was the maximizer of the absolute values of the CC values. CC allowed to evaluate the standard deviation about the time-lags of the three water gauges.

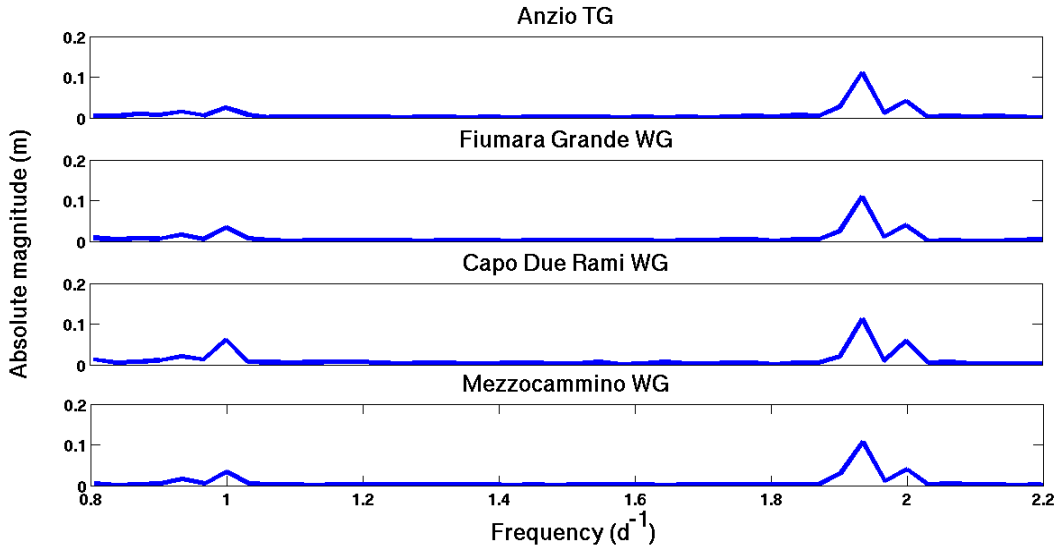

Fig. 1.10: dominant frequencies for the level data about the Anzio tidal gauge and the three water gauges. dominant frequencies are 1.0 d^{-1}, 1.94 d^{-1} and 2.0 d^{-1} and they represent the lunar diurnal, lunar semi-diurnal and solar semi-diurnal constituent

Fig.1.11 shows the average of the daily time-lags and the corresponding standard deviation computed over the whole period of registration, for each of the water gauges with respect to Anzio tide gauge.

Mezzocammino water gauge showed the highest values of standard deviation. It means that far from the river mouth, other factors affect the river fluctuation more than the tide fluctuation (i.e. the freshwater flow discharge). The lower values of standard deviation about the other two coastward water gauges, showed how they are more influenced by the sea fluctuation, which can determine salt-wedge intrusion processes nearby the mouth. The estimated tide-induced delay of the river fluctuation was about 48.53, 61.32 and 110.51 min respectively for Fiumara Grande, Capo Due Rami and Mezzocammino water gauges. Both the average delay time and the standard deviation increased moving away from the river mouths.

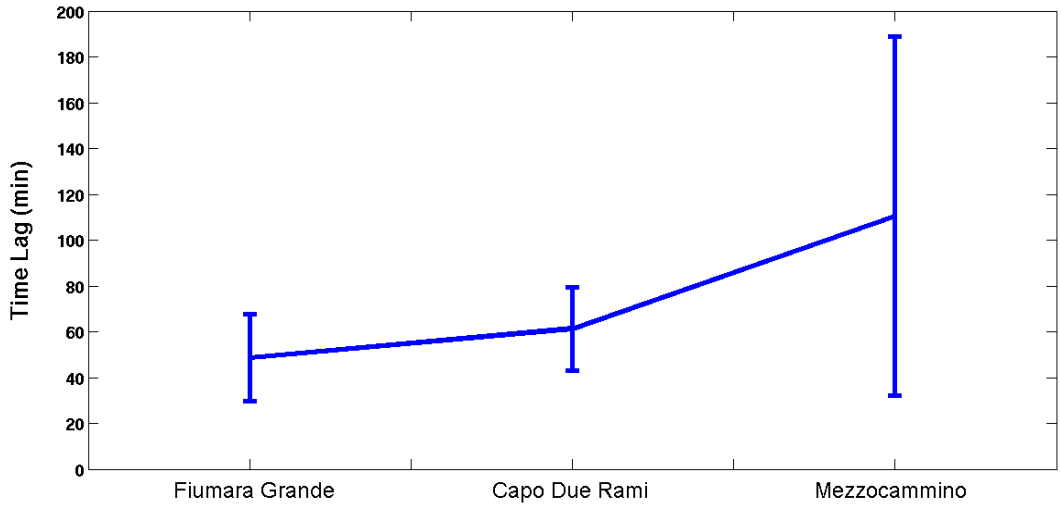

Fig. 1.11: average of the daily time-lags and the corresponding standard deviation about the tree water gauges, with respect to Anzio tidal gauge

1.3.3 SEAWATER TEMPERATURES

Seawater temperature values about Anzio TG were collected to analyze the relationships with the temperature of seawater observed at the mouths of the river branches.

In fact also seawater temperature can be used as a marker of salt-wedge intrusion because it holds a different distribution in the water column, depending on the different stages of the year. During the Autumn, the Tiber River seawater at the bottom is warmer than freshwater because it conserves the heat accumulated during the year (Mikhailova et al. 1999). Vice versa seawater at the river bottom is cooler than freshwater during the Spring, as observed in Fig.1.5 and Fig.1.7.

Seawater temperatures about the Anzio TG are shown in Tab.1 and represent the monthly average temperatures, derived from data registered every 1 hour (ISPRA 2012). Average temperatures of May are about the 1st -15th of May because the first survey on TC branch, was carried out the 16th of May. The minimum value occurred in February with an increasing trend afterward.

January	February	March	April	May
12,45	10,94	14,93	16,63	18,45

Table 1.1: monthly average temperatures registered every 1 hour

1.3.4 WIND DATA

Wind data analysis was realized to analyze the relationships between the wind pattern and the sea level fluctuation. Fiumicino and Ostia meteorological stations provided data with different time steps, 2 min and 5 min respectively. 5 min frequency is the most accurate and continuous, because it represents the average values of wind intensity and direction of the wind vector, recorded every two min (Civano et al. 2004). Therefore Fiumicino station data were filtered and averaged to obtain a wind database with a 5 min frequency. Lacking time series of Ostia station were integrated with the Fiumicino data, applying the same 5 min time frequency. May wind data are about 1st-15th of May, for the above indicated reasons. Datasets were subject to frequency analysis, through the creation of wind intensity histograms, essential to create compass roses. These representations show predominant wind provenances. The statistical analysis was effectuated on wind data with speed higher than 4 m/s. In fact winds with a speed higher than 4 m/s are able to induce a current at the sea surface bigger than the one induced by tide (deCastro et al. 2000). This current can generate a sea level setup and an inflow of seawater in an estuary can occur (Wong 1994). Percentages of data with these characteristics were 27.03%, 41.00%, 29.17%, 51.31% and 42,65%, respectively for the months from January to May. The top wind speed was 20.5 m/s during April.

Compass roses (Fig.1.12) show predominant winds: they were northeasterly during the months of January and February, southeasterly in March and westerly in April and May.

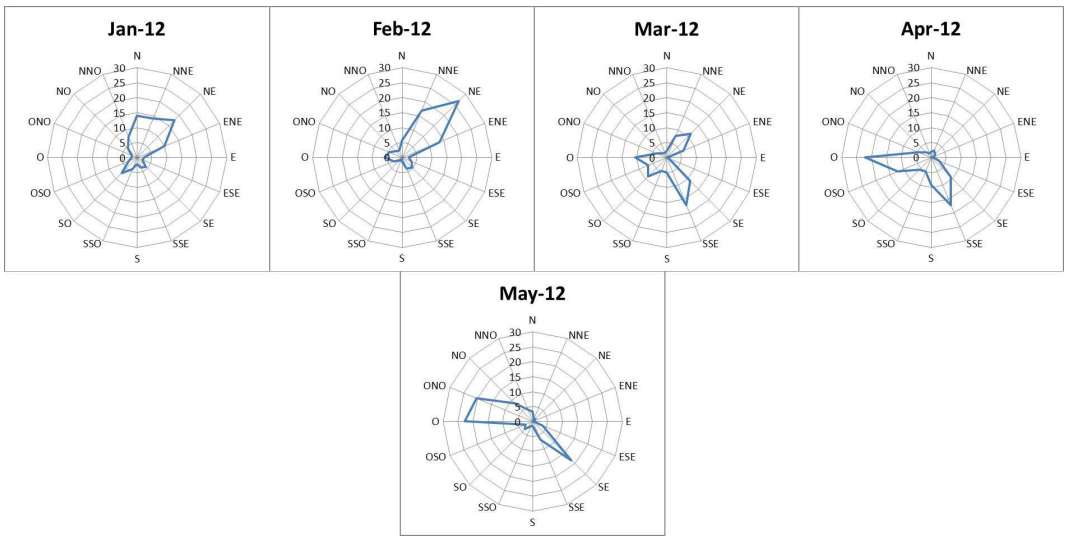

Fig. 1.12: compass roses about the wind with a speed higher than 4 m/s, showing the wind direction provenances. They were northeasterly during the months of January and February, southeasterly in March and westerly in April and May

1.4 DISCUSSION

To better understand the salt-wedge dynamics in a river mouth, it is important to evaluate all the natural events occurring together, as the river discharge, wind intensity, wind direction and the related wave induced sea level variation. In the case of Tiber River mouth, the contemporary occurrence of all these events can determine salt-water wedge intrusion. Usually the most significant variable in salt-wedge migration is the river discharge. Consequently the greater volume of seawater intrusion is expected during the summer. In this season the rainfall rate and therefore the river flow decrease strongly.

During the survey of Tiber River branches a different type of salt-wedge intrusion was noticed, depending primarily on wind influence. The first step to understand this phenomenon came from thermal analysis of seawater, discovered at FG branch bottom (Fig.1.13). FG average thermal value about the near-bottom seawater was 16.68°C. If a non-thermal exchange is supposed between seawater and freshwater of the FG branch, this value is assumed to be the one of seawater at the moment of intrusion. If this value is compared to the average thermic values recorded at Anzio tidal gauge (Tab.1), it is possible to see a great similarity to the April thermic value of seawater (16.63 °C). Exactly in this month the main wind-provenance changed, determining a pattern from northwesterly to westerly winds. The frequency of winds with a speed major than 4 m/s changed from 29.17% of March to the 51.31% of April. It means that the wind effect was higher during April. As a consequence a sea-level raise induced by wind was noticed, as demonstrated by the tidal data about March and April (Fig.1.9). In fact the maximum average high-tide levels were 0.01 m and 0.23 m respectively for March and April. This datum is in accord with (Wong 1994), who noticed that an inflow of seawater in an estuary, can occur with a coastal sea level setup. In general, under similar meteorological conditions, when the wind has a westerly component, a sea surface water layer tends to move against the estuary. At this stage seawater is forced to sink near the entrance of the estuary (Fraga and Prego 1989; Tilstone et al. 1994) due to its higher density, developing a salt-wedge.

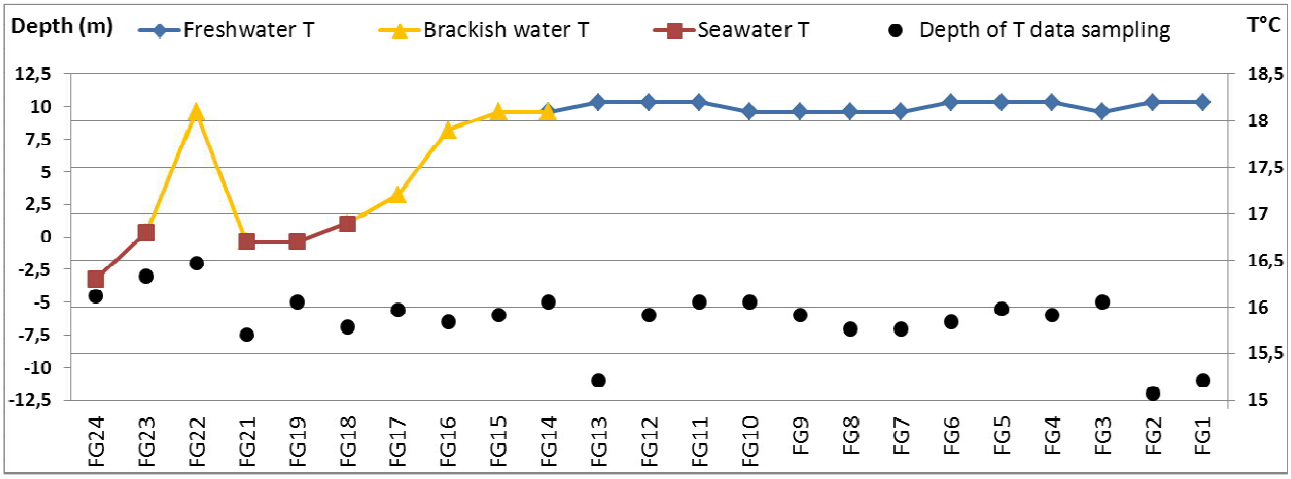

Fig. 1.13: thermal values about Fiumara Grande branch bottom. The brench mouth is located leftward. Measurement points are represented in black. Blue points and lines represent T values about freshwater; Yellow points and lines represent T values about brackish water; red points and lines represent T values about seawater

In the case of TC branch (Fig.1.14) thermal values for seawater can be divided in two groups: the first includes the points TC3-TC13 with an average seawater T of 17.03°C, whereas the second group is composed by TC1 and TC2 with average seawater T of 18.20°C. The first group is close to the mouth and the salinization processes for this branch part is thought to be the same of FG branch, due to the similar seawater T. The second part, with a higher average thermic value, is likely due to an older salt-wedge intrusion.

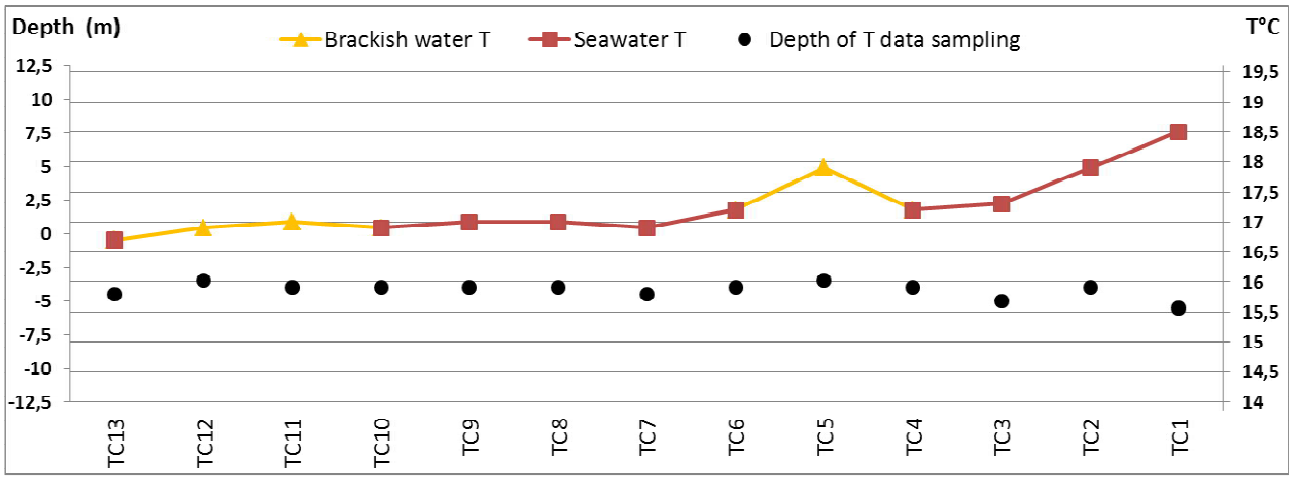

Fig. 1.14: thermal values about TC branch bottom. The brench mouth is located leftward, while FG rightward. Measurement points are represented in black. Yellow points and lines represent T values about brackish water; red points and lines represent T values about seawater

Further evidence on the salt-wedge intrusion due to wind effect, is the discharge analysis about the Tiber River. Fig.1.15 shows March and April average daily flow rate recorded at Ripetta WG, in the center of Roma (IdrograficoLazio 2012c), with monthly average values of 92.67 m^3/s and 108.00 m^3/s respectively. Despite the average flow rate increased from March to April, the salt-wedge penetrated in the river branches, and it was not removed by the high discharge rate.

Furthermore the values of the standard deviation about the time-lags coming from the

CC of the three water gauges (Fig.1.10), confirm that the water gauges located near the mouth are less influenced by the discharge rate and are more affected by the tide fluctuation. Therefore the influence of sea level fluctuation at the mouth is stronger and it can determine salt-wedge intrusion independently from the discharge rate.

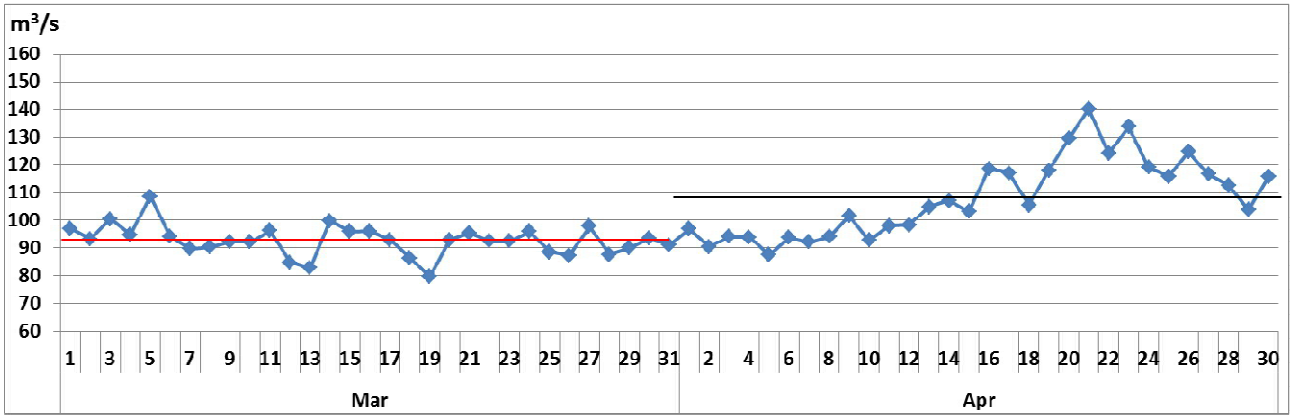

Fig. 1.15: discharge rate at Ripetta water gauge during March and April 2012. The average discharge rate about March and April are 92.67 m^3/s (red line) and 108 m^3/s (black line) respectively

1.5 CONCLUSIONS

Chemo-physical characteristics of the Tiber River mouth were investigated in May 2012 during two navigations. It was used a conductivity-meter and the surveyed points were reached using a GPS. Also a bathymetric survey was conducted and it showed very irregular river bottom morphology.

Salinity pattern showed a salt-wedge intrusion affecting the whole Traiano Canal branch, while in the Fiumara Grande one, it penetrated up to 8.8 km from the mouth. This datum agrees with previous studies (Capelli et al. 2007; Mikhailova et al. 1999). According to Cameron and Pritchard (1963) and Pritchard (1955) FG and TC can be classified as salt-wedge stratified estuary and a strongly stratified estuary respectively. A FFT analysis was realized on the

Fiumara Grande, Capo Due Rami and Mezzocammino water gauges and the Anzio tidal gauge data. It exhibited that the river level fluctuation in all the water gauges station has close connections with the tide, as demonstrated by the same dominant frequencies of fluctuation, that are 1.0 d^{-1}, 1.94 d^{-1} and 2.0 d^{-1}. They represent the lunar diurnal, lunar semi-diurnal and solar semi-diurnal constituent respectively (Mao et al. 2006). The cross correlation showed that the tide-induced river level fluctuation exhibits a delay moving away from the mouth. The delay was quantified in 48.53, 61.32 and 110.51 min respectively for Fiumara Grande, Capo Due Rami and Mezzocammino water gauges.

The wind statistical analysis was developed using the criterion of deCastro et al. (2000), which presumes that winds with a speed above 4 m/s able to develop a current at the surface. The statistical analysis showed a very high wind intensity in April (51.31% of the wind data held a wind speed higher than 4 m/s), when the wind pattern turned to westerly.

Wind action affected sea level, determining a raising effect (Wong 1994). It is proved by the maximum average high-tide levels, that passed from the 0.01 m of March to the 0.23 m of April.

Consequently seawater was forced to sink near the entrance of the river branches mouth (Fraga and Prego 1989; Tilstone et al. 1994) due to its higher density, with the development of a salt-wedge. Salt-wedge intrusion noticed in May, probably emplaced during April, as demonstrated by the similarity between the thermal seawater data of April (16.63 °C, ISPRA 2012) and the surveyed ones (16.68 °C and 17.03 °C for FG and TC respectively). Finally, the high discharge rate seemed to not obstacle the salt-wedge emplacement. In fact the different dispersion of the standard deviation values about the average daily time-lags of the three water gauges, indicates that Mezzocammino water gauge is more influenced by the discharge flow, while Capo due Rami and Fiumara Grande water gauges are more influenced by the sea level fluctuation. Therefore the influence of sea level fluctuation at the mouth is stronger and it can determine salt-wedge intrusion independently from the discharge rate.

Although several authors noticed that salt-wedge intrusion happens during the low-flow period (Fagerburg and Alexander 1994; Sierra et al. 2004; Zhou et al. 2012; Mikhailova et al. 1999; Capelli et al. 2007), this paper showed how salt-wedge intrusion can occur also during the high discharge rate, mainly due to the wind effect.

1.6 REFERENCES

Ahmed MA, Samie SGA, Badawy HA (2013) Factors controlling mechanisms of groundwater salinization and hydrogeochemical processes in the Quaternary aquifer of the Eastern Nile Delta, Egypt. Environmental Earth Sciences 68 (2):369-394. doi:10.1007/s12665-012-1744-6

Barlow PM (2003) Salwater Intrusion from the Delaware River During Drought-Implications for the Effect of Sea-Level Rise on Coastal Aquifers. In: Ground Water in Freshwater-Saltwater Environments of the Atlantic Coast. U.S. Geological Survey, Reston, Virginia, USA, pp 46-48

Barlow PM, Reichard EG (2010) Saltwater intrusion in coastal regions of North America. Hydrogeology Journal 18 (1):247-260. doi:10.1007/s10040-009-0514-3

Bear J, Cheng AH-D, Sorek S, Ouzer D, Herrera I (1999) Geophysical investigations. In: Jacob Bear AHDCSSDO, Ismael H (eds) Seawater Intrusion in Coastal Aquifers - Concepts, Methods and Practises. Kluwer Academic Publishers, Dordrecht, The Nederlands, pp 9-50

Bellotti P, Milli S, Tortora P, Valeri P (1995) Physical stratigraphy and sedimentology of the Late Pleistocene-Holocene Tiber Delta depositional sequence. Sedimentology 42 (4):617-634. doi:10.1111/j.1365-3091.1995.tb00396.x

Cameron WM, Pritchard DW (1963) Estuaries. In: The Sea, vol 2. Wiley, New York, USA, pp 306-324

Capaccioni B, Didero M, Paletta C, Didero L (2005) Saline intrusion and refreshening in a multilayer coastal aquifer in the Catania Plain (Sicily, Southern Italy): dynamics of degradation processes according to the hydrochemical characteristics of groundwaters. Journal of Hydrology 307 (1-4):1-16. doi:10.1016/j.jhydrol.2004.08.037

Capelli G, Mazza R, Papiccio C (2007) Saline intrusion in the Tiber Delta. Geology, hydrology and hydrogeology of the coastal plain of the roman sector. Giornale di Geologa Applicata 5:13-28

Civano A, Morini M, Sodi R (2004) Caratteristiche del vento all'aeroporto di Genova in base all'analisi dei dati anemometrici raccolti su due punti. ENAV,

Custodio E, Llamas MR (2005) Rapporti tra le acque dolci e salate nelle regioni costiere. In: Flaccovio D (ed) Idrologia sotterranea, vol 2. Palermo, pp 1248-1274

deCastro M, Gomez-Gesteira M, Prego R, Taboada JJ, Montero P, Herbello P, Perez-Villar V (2000) Wind and tidal influence on water circulation in a Galician ria (NW Spain). Estuarine Coastal and Shelf Science 51 (2):161-176. doi:10.1006/ecss.2000.0619

Dyer KR (1997) Estuaries-a physical introduction 2nd Edition. Chichester

Eagling J, Worsfold PJ, Blake WH, Keith-Roach MJ (2012) Mobilization of Technetium from Reduced Sediments under Seawater Inundation and Intrusion Scenarios. Environmental Science & Technology 46 (21):11798-11803. doi:10.1021/es3025935

Fagerburg TL, Alexander MP (1994) Underwater Sill Construction for Mitigating Salt-wedge Migration on the Lower Mississipi River.

Farid I, Trabelsi R, Zouari K, Abid K, Ayachi M (2013) Hydrogeochemical processes affecting groundwater in an irrigated land in Central Tunisia. Environmental Earth Sciences 68 (5):1215-1231. doi:10.1007/s12665-012-1788-7

Fraga F, Prego R (1989) Condiciones hidrograficas previas a la purga de mar. Cuadernos da Area de Ciencias Marinas:21-44

Freeze RA, Cherry JA (1979) Groundwater. Englewood Cliffs, New Jersey

Fujiwara H, Sawamoto M, Tanaka H (1997) Comparison of Mixing Characteristics of Density Current Between in Compound Channel and in Single Section Channel. vol 41. Annual Journal of Hydraulic Engineering,

IdrograficoLazio (2012) Bollettino delle portate medie mensili dell'idrometro di Ripetta dal gennaio 2002 al dicembre 2011. http://www.idrografico.roma.it/std_page.aspx?Page=bollettini.

IdrograficoLazio (2012) Dati degli idrometri di Fiumara Grande, Capo Due Rami e Mezzocammino, nel periodo gennaio-Maggio 2012. Regione Lazio,

IdrograficoLazio (2012) Bollettino delle portate giornaliere dell'idrometro di Ripetta di marzo ed aprile 2012. http://www.idrografico.roma.it/std_page.aspx?Page=ripetta&Anno=2012.

ISPRA (2012) Dati idrometrici e termici del mareografo di Anzio del periodo gennaio-maggio 2012http://www.mareografico.it/?session=0S40109837687072L74877081O&syslng=ita&sysmen=-1&sysind=-1&syssub=-1&sysfnt=0&code=STAZ&idst=2C.

La Vigna F, Ciadamidaro S, Mazza R, Mancini L (2010) Water quality and relationship between superficial and ground water in Rome (Aniene River basin, central Italy). Environmental Earth Sciences 60 (6):1267-1279. doi:10.1007/s12665-009-0267-2La Vigna F, Demiray Z, Mazza R (2013) Exploring the use of alternative groundwater models to understand hydrogeological flow processes in an alluvial context (Tiber River, Rome, Italy). Environmental Earth Sciences. doi:10.1007/s12665-013-2515-8

Large WG, Pond S (1981) Open Ocean Momentum Flux Measurements in Moderate to Strong Winds. Journal of Physical Oceanography 11:324-336

Lenkopane M, Werner AD, Lockington DA, Li L (2009) Influence of variable salinity conditions in a tidal creek on riparian groundwater flow and salinity dynamics. Journal of Hydrology 375 (3-4):536-545. doi:10.1016/j.jhydrol.2009.07.004

Macias D, Landry MR, Gershunov A, Miller AJ, Franks PJS (2012) Climatic Control of Upwelling Variability along the Western North-American Coast. Plos One 7 (1). doi:10.1371/journal.pone.0030436

Mao X, Enot P, Barry DA, Li L, Binley A, Jeng DS (2006) Tidal influence on behaviour of a coastal aquifer adjacent to a low-relief estuary. Journal of Hydrology 327 (1-2):110-127. doi:10.1016/j.jhydrol.2005.11.030

Mikhailova MV, Bellotti P, Valeri P, Tortora P (1999) Intrusion of seawater into the River Part of the Tiber Mouth. Water Resources 26 (6):679-686

Milli S, D'Ambrogi C, Bellotti P, Calderoni G, Carboni MG, Celant A, Di Bella L, Di Rita F, Frezza V, Magri D, Pichezzi RM, Ricci V (2013) The transition from wave-dominated estuary to wave-dominated delta: The Late Quaternary stratigraphic architecture of Tiber River deltaic succession (Italy). Sedimentary Geology 284:159-180. doi:10.1016/j.sedgeo.2012.12.003

Murray SP, Johns W (1997) Direct observations of seasonal exchange through the Bab el Mandab Strait. Geophysical Research Letters 24 (21):2557-2560. doi:10.1029/97gl02741

Park Y, Lee J-Y, Kim J-H, Song S-H (2012) National scale evaluation of groundwater chemistry in Korea coastal aquifers: evidences of seawater intrusion. Environmental Earth Sciences 66 (3):707-718. doi:10.1007/s12665-011-1278-3

Pezzetta E, Lutman A, Martinuzzi I, Viola C, Bernardis G, Fuccaro V (2011) Iron concentrations in selected groundwater samples from the lower Friulian Plain, northeast Italy: importance of salinity. Environmental Earth Sciences 62 (2):377-391. doi:10.1007/s12665-010-0533-3

Pritchard DW Estuarine circulation patterns. In: American Society of Civil Engineers, 1955. pp 1-11

Qian X, Ishikawa T (2003) Influence of shallows on salt-wedge intrusion in takase river. Paper presented at the International Conference on Estuaries and Coasts, Hangzhou, China,

Ricci Lucchi F (1980) Sedimentologia - Ambienti sedimentari e facies. In, vol 3. Bologna, pp 119-172

Robinson C, Gibbes B, Carey H, Li L (2007a) Salt-freshwater dynamics in a subterranean estuary over a spring-neap tidal cycle. Journal of Geophysical Research-Oceans 112 (C9). doi:10.1029/2006jc003888

Robinson C, Li L, Barry DA (2007b) Effect of tidal forcing on a subterranean estuary. Advances in Water Resources 30 (4):851-865. doi:10.1016/j.advwatres.2006.07.006

Roegner GC, Needoba JA, Baptista AM (2011) Coastal Upwelling Supplies Oxygen-Depleted Water to the Columbia River Estuary. Plos One 6 (4). doi:10.1371/journal.pone.0018672

Sierra JP, Sanchez-Arcilla A, Figueras PA, Del Rio JG, Rassmussen EK, Mosso C (2004) Effects of discharge reductions on salt-wedge dynamics of the Ebro River. River Research and Applications 20 (1):61-77. doi:10.1002/rra.721
Teien HC, Standring WJF, Salbu B (2006) Mobilization of river transported colloidal aluminium upon mixing with seawater and subsequent deposition in fish gills. Science of the Total Environment 364 (1-3):149-164. doi:10.1016/j.scitotenv.2006.01.005
Tilstone GH, Figueiras FG, Fraga F (1994) Upwelling-downwelling sequences in the generation of red tides in a coastal upwelling system. Marine Ecology Progress Series 112 (3):241-253. doi:10.3354/meps112241
Trabelsi R, Abid K, Zouari K, Yahyaoui H (2012) Groundwater salinization processes in shallow coastal aquifer of Djeffara plain of Medenine, Southeastern Tunisia. Environmental Earth Sciences 66 (2):641-653. doi:10.1007/s12665-011-1273-8
Tran LT, Larsen F, Pham NQ, Christiansen AV, Nghi T, Vu HV, Tran LV, Hoang HV, Hinsby K (2012) Origin and extent of fresh groundwater, salty paleowaters and recent saltwater intrusions in Red River flood plain aquifers, Vietnam. Hydrogeology Journal 20 (7):1295-1313. doi:10.1007/s10040-012-0874-y
UNESCO (1983) Algorithms for computation of fundamental properties of seawater.
UNESCO (1991) Guidelines on the study of seawater intrusion into rivers. H. van der Tuin,
Valle-Levinson A (2010) Contemporary issues in Estuarine Physics. Cambridge University Press, Cambridge
Valle-Levinson A, Blanco JL (2004) Observations of wind influence on exchange flows in a strait of the Chilean Inland Sea. Journal of Marine Research 62 (5):721-741
Wong KC (1994) On the nature of transverse variability in a coastal-plain estuary. Journal of Geophysical Research-Oceans 99 (C7):14209-14222. doi:10.1029/94jc00861
Wong VNL, Johnston SG, Burton ED, Bush RT, Sullivan LA, Slavich PG (2013) Seawater-induced mobilization of trace metals from mackinawite-rich estuarine sediments. Water Research 47 (2):821-832. doi:10.1016/j.watres.2012.11.009
Wright LD (1977) Sediment transport and deposition at river mouths: a synthesis. GeolSocAmBull 88:857-868
Wunderground (2012) Dati anemometrici della stazione di Fiumicino relativi al periodo gennaio-maggio 2012. http://www.wunderground.com/cgi-bin/findweather/getForecast?query=zmw:00000.1.16242.
Wunderground (2012) Dati anemometrici della stazione della Lega Navale di Ostia relativi al periodo gennaio-maggio 2012. http://www.wunderground.com/cgi-bin/findweather/getForecast?query=41.71937561,12.30211830&sp=IROMELID3.
Zhou W, Luo L, Xu H, Wang D (2012) Saltwater intrusion in the Pearl River Estuary during winter. Aquatic Ecosystem Health & Management 15 (1):70-80. doi:10.1080/14634988.2012.649238

2. SEA SALT AEROSOL SALINIZATION OF GROUNDWATER IN THE LITORALE ROMANO NATURAL RESERVE (ROME – CENTRAL ITALY)

ABSTRACT

A yearly survey in a piezometric network was realized in the Litorale Romano Natural Reserve, collecting water table and chemo-physical data. Monthly chemo-physical surveys highlighted a groundwater salinity variability in the coastal aquifer. The aquifer is mostly composed by aeolian sands of a still preserved dune ridge environment, on which a pine forest develops. The groundwater salinity variability resulted connected to the wind pattern and rainfalls. In fact wind speed higher than 4 m/s is responsible of generating sea salt aerosols (SSA) from sea surface. A statistical analysis was performed for wind with a speed higher than 4 m/s, to detect wind orientation. The dry deposition of SSA on the tree foliage appeared correlated to the westerly winds, blowing in the springtime. When the rainy seasons occur, the SSA is washed out from the trees and it is directed to groundwater, where an enhancement of the Electrical Condctivity (EC) values is noticed. Whenever rain events occur and winds are not westerly, a dilution of groundwater salinity takes place and consequently a reduction of EC. Chemical analyses were realized as well. They confirmed that groundwater of piezometers located close to the coast line is enriched of SSA elements.

2.1 INTRODUCTION

Soil salinization is one of the most widespread soil degradation processes on earth (Toth et al. 2008) and it is the process by which water-soluble salts accumulate in the soil. Solute accumulation can be due to a variety of natural (primary salinization) and anthropogenic (secondary salinization) factors operating at a range of temporal and spatial scales (Schofield et al. 2001). Marine aerosol production is a natural process deriving from the interaction of wind stress at the ocean surface. This interaction forms waves, some of which break spreading sea spray bubbles into the atmosphere (Lewis and Schwartz 2004). Winds blowing landward, determine an accumulation of sea spray aerosols (SSA) along the coastal areas, especially whereby coastal forests develop. Coastal forests create a barrier effect and a dry deposition can occur on the foliage of the trees (Gustafsson and Franzen 2000; Hasselrot and Grennfelt 1987). The precipitations wash out the accumulated SSA, which can reach groundwater determining hence an increase of salinization. Several studies have been conducted to quantify the volumes (Erickson and Duce 1988; Gong et al. 2002) and the size of aerosol particles depending on wind velocity, in laboratory experiments (Martensson et al. 2003; Fuentes et al. 2010). O'Dowd and De Leeuw (2007) recognized that a speed higher than 4 m/s is an adequate threshold to generate SSA from the sea surface. Tuccimei (2010) noticed that in the area of the Litorale Romano Natural Reserve (LRNR) there is a strict connection among the winds, the rains and the salinization of groundwater. The aim of this study was to understand how the salinization of groundwater, surveyed yearly in a piezometric network in the LRNR changed in time, in relation with the precipitation rate and the action of the winds.

2.2 GEOLOGICAL AND HYDROGEOLOGICAL SETTING

The study area is located along the Tyrrhenian coast line near the town of Ostia, 25 km southwestward with respect to the center of Rome. It spreads in the LRNR, a 9.5 km^2 protected area (Fig.2.1). The vegetation is mainly composed by a pine forest, but in July 2000 a fire burnt down almost one quarter of the forested area. The area spreads on the aeolian dune sandy deposits, that in turn overly sands and silty sands of beach ridge environment, which can reach up to 20 meters of thickness (Bellotti et al. 1989). These deposits developed in the last 6000 years and belong to a Highstand System Tract depositional sequence of the Tiber Depositional Sequence (Milli et al. 2013; Bellotti et al. 2007). They form the main aquifer, whose aquiclude is composed by the clayey basement of the Monte Mario Sequence, on which lie the gravelly deposits of the Ponte Galeria Formation (Milli 1997; Milli and Palombo 2011) (Fig.2.2). In general the

sandy deposits hold a medium to high hydraulic potentiality (Capelli et al. 2012). The LRNR is delimited northeastward and northwestward by anthropic canals: the Collettore Primario di Levante Canal and the Pescatori Canal respectively; southeastward by the Castel Porziano Natural Reserve and southwestward by the Tyrrhenian Sea. It can be considered an isolated hydrogeological system recharged only by rainfalls (Capelli and Salvati 2003), with a shallow water table set about three meters below ground level (Capelli et al. 2007). The LRNR represents one of the few pristine areas (Capelli et al. 2005), unaffected by the reclamation activities of the 19th century (Amenduni 1884). In the LRNR the dune ridges system is still preserved and it determines the hydrogeological pattern: in fact the water table traces the morphology and flow paths are directed to the sea, and to the drainage canals.

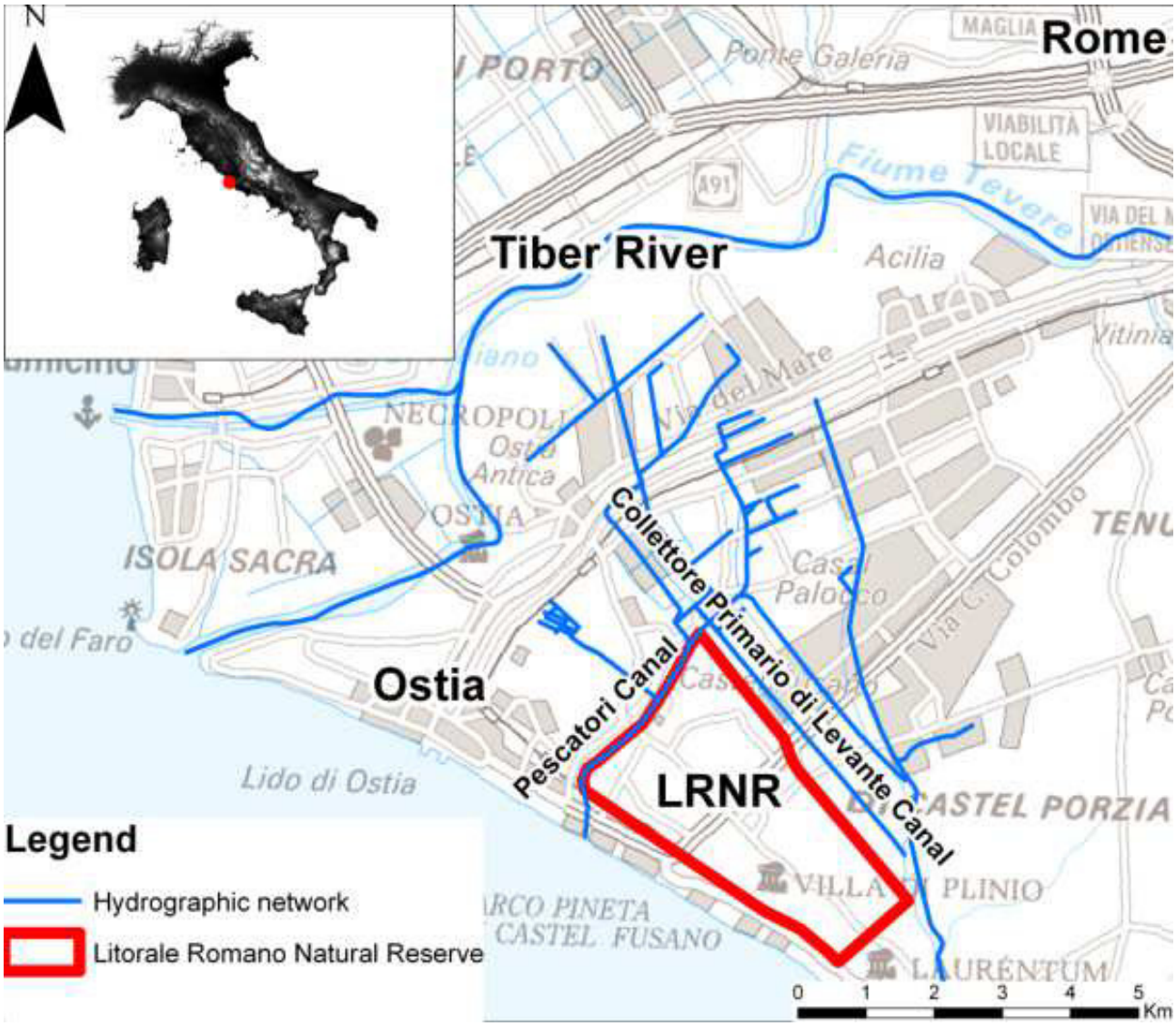

Fig. 2.1: the area of the Litorale Romano Natural Reserve

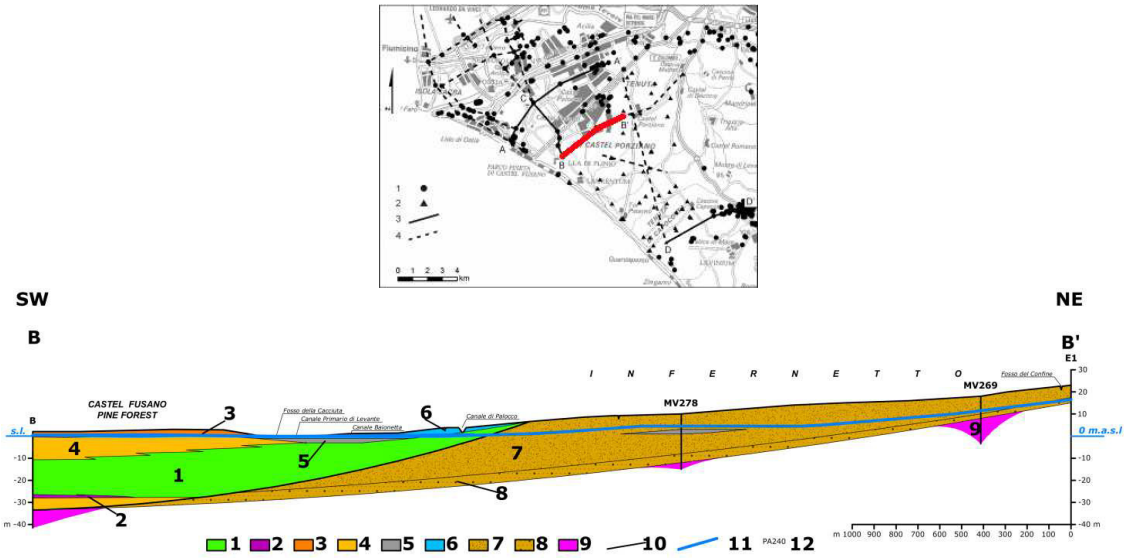

Fig. 2.2: B-B' Geological cross-section. Legend: 1 - Heterometric grey-yellow sands, with gravel lenses. The thickness ranges till 20m. Represent fluvial deposits. (litofacies 1/a in Bellotti et al., 1989); 2 - Sandy pelites, frequently interbedded with bioclastic levels and vegetal reminders, in the lower part clayey silt and green clay, fossil-rich, are present. The highest thickness has not yet been defined. Represent a transition-platform complex (litofacies 3 in Bellotti et al., 1989); 3 - Grey or grey-blue pelites, interbedded with thin sandy levels, peat levels and sandy lenses. Thickness of some meters. Constitute an haff complex (litofacies 3 in Bellotti et al., 1989); 4 - Thin or medium thin grey-red sands, femic-rich, with vegetal remainders. Represent the existing dune bar. Thickness ranges from 3 m to 15 m (litofacies 4/a in Bellotti et al., 1989); 5 - Heterometric grey sandys, femic-rich, fossil-rich and vegetal remainders. Constitute a costal barrier. Thickness ranges from some meters to 10 m (litofacies 4/b in Bellotti et al., 1989); 6 - Grey-yellow pelites with thin gravels, drying structures, travertine concretions, altered volcanic deposits, peat and fossil levels (alluvial deposits latu sensu). Thickness of 7-8 meters (litofacies 2 in Bellotti et al., 1989); 7 - Bedded peats, black organic clays, black sands. Thickness ranges from some decimeters to some meters; 8 - Heterometric sands and brown-red silty sands, terraced. Thickness ranges from some meters to 20-25 m ("Duna Antica" auct.) Upper Pleistocene; 9 - Grey silty clays ("Formazione di Ponte Galeria" auct. p.p.) lower-middle Pleistocene; 10 - Incoherent gravels or in sandy-silty matrix, rarely heterometric sands or silty sands. Thickness ranges from some meters to 10 meters (Formazione di Ponte Galeria auct. P.p., litofacies 6 in Bellotti et al. 1989) lower-middle Pleistocene; 11 - Grey-blue clays and silty clays, interbedded with grey sandy silts. Upper Pliocene- Peistocene p.p.; 12 - Grey clays and marls. Pliocene (from Carta Geologica, F° 149 "Cerveteri", 1967); 13 - Surface of the shallow aquifer- year 2004; 14 - Surface of the shallow aquifer- year 2002; 15 - Geognostic borehole and database code. (After Capelli et al. (2007))

Since after the fire, studies were conducted in the area, to evaluate the chemistry of groundwater (Tuccimei et al. 2010; Tuccimei et al. 2003). Tuccimei et al. (2010) noticed that groundwater chemistry had a strong relationship with the SSA transported inland by western winds and it was enriched in chloride and sodium (contained in the SSA). The process can be resumed by Fig.2.3 and can be divided in two main moments:

1) an accumulation phase, in which a dry deposition of SSA occurs (Fig.2.3A);
2) a mobilization phase, acted by the rains, in which a salty solution is released in the groundwater system (Fig.2.3B).

This assumption was based on the similar behavior showed by chemical analysis about water coming from stemflows and throughfalls, compared to groundwater chemical analysis.

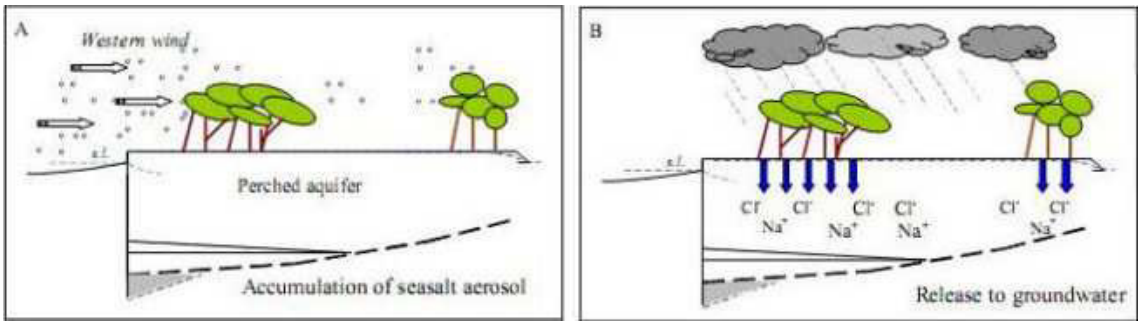

Fig. 2.3: depositional mechanism of SSA accumulation and mobilization; A) when westerly winds occur, SSA is transported landward and accumulate on the tree foliage; B) when rains fall, the SSA is solubilized and is transported into the groundwater, determining an increase of Cl^- and Na^+ content (After Tuccimei et al. (2010))

Furthermore Tuccimei et al. (2010) noticed that SSA deposition on the tree foliage decreases inversely to the distance from the coastline (Fig.2.4), as a consequence of the barrier effect acted by the pine forest.

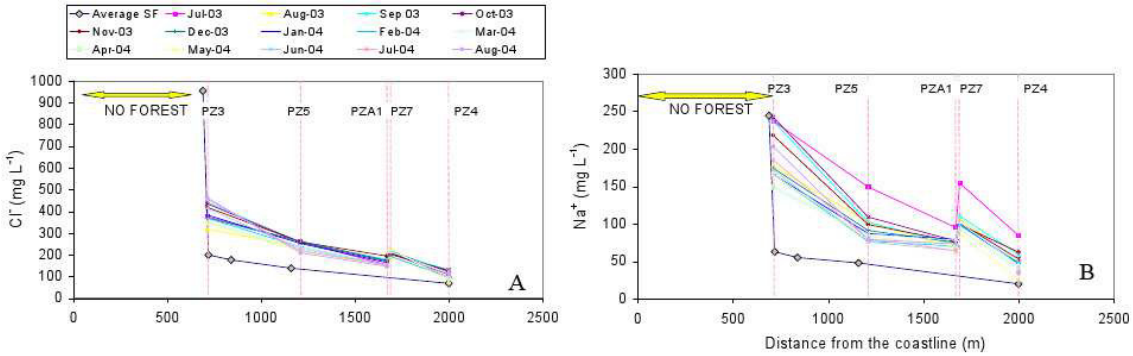

Fig. 2.4: content of Cl^- (A) and Na^+ (B) about water samples coming from stemflows throughfalls and groundwater. Chemical analysis showed how higher content of the two ions were measured near the coast line, as a consequence of the barrier effect acted by the pine forest (After Tuccimei et al. (2010))

2.3 MATERIALS AND METHODS

The study area was investigated by means of 13 monthly water table measurements and chemico-physical parameterization, started in May 2011 and ran out in May 2012. The water table was evaluated using a 10 m cable length electric contact meter in 14 piezometers with a depth ranging from 8 to 8.5 meters and screened for the last 1.5 meters, with a 2,5 inches diameter.

Chemo-physical data about Electrical Conductivity (EC, in µS/cm ± 0.5%, normalized at 25°C), and Temperature (Temp ± 0.1, in °C) were collected using a 20 m cable length portable conductivity-meter. The measurements were performed at the screened part of the piezometers.

Furthermore a water level sensor was installed in the Pz3 to analyze hourly the water table fluctuation (Fig.2.5).

In October 2012 water samples about 4 piezometers were collected to identify the geochemical water type: Pz6, Pz10, Pz12 and Pz14 (Fig.2.5). Pz10 and Pz12 were chosen because of their position next to the borders of the LRNR; Pz14 and Pz6 were selected because of their proximity to the pine forest edge. Water sampling was effectuated collecting waters with a 0.5 l groundwater sampler. Water samples were collected at the third drop in the well, to avoid the contamination due to the previous water samplings.

Laboratory analyses about major ions were conducted and for every sampling station two water samples were taken. One of the samples was acidified using a 1 ml nitric acid (HNO_3), to lower the pH <2, to avoid the cations precipitation. Samples were filled completely and capped tightly in a double cap 0.5 l polyethylene bottle, before transporting them into the laboratory where they were stored dark and refrigerated at a temperature of about 4°C. Once in the laboratory, samples of groundwater were filtered through a 0.45µm cellulose filter. Ca^{2+} and Mg^{2+} cations were determined using complexometric titration with 0.01 M EDTA. Na^+ and K^+ were determined using the flame emission photometric method (Corning Flame Photometer 410). Cl^- content was evaluated using a potentiometric method (Mettler Toledo Seven Multi) with an ion-selective electrode (Orion 9716 BN). HCO_3^-, SO_4^{2-} and NO_3^- content was performed using a multi-parameter colorimeter (Orbeco Hellige MC 500).

Surface wind data were collected from two meteorological stations (MS), located in Fiumicino (Wunderground 2012b) and Ostia (Wunderground 2012a), nearby LRNR (Fig.2.5). Two wind data stations were chosen because some wind data series about the Ostia MS were lacking and they were integrated with those of Fiumicino MS. The two stations were chosen because subject to the same dominant wind pattern and better representing wind conditions in the RNLR. Ostia MS provided the majority of wind data, recorded every 5 min. The Fiumicino MS provided the missing wind data, recorded every 2 min.

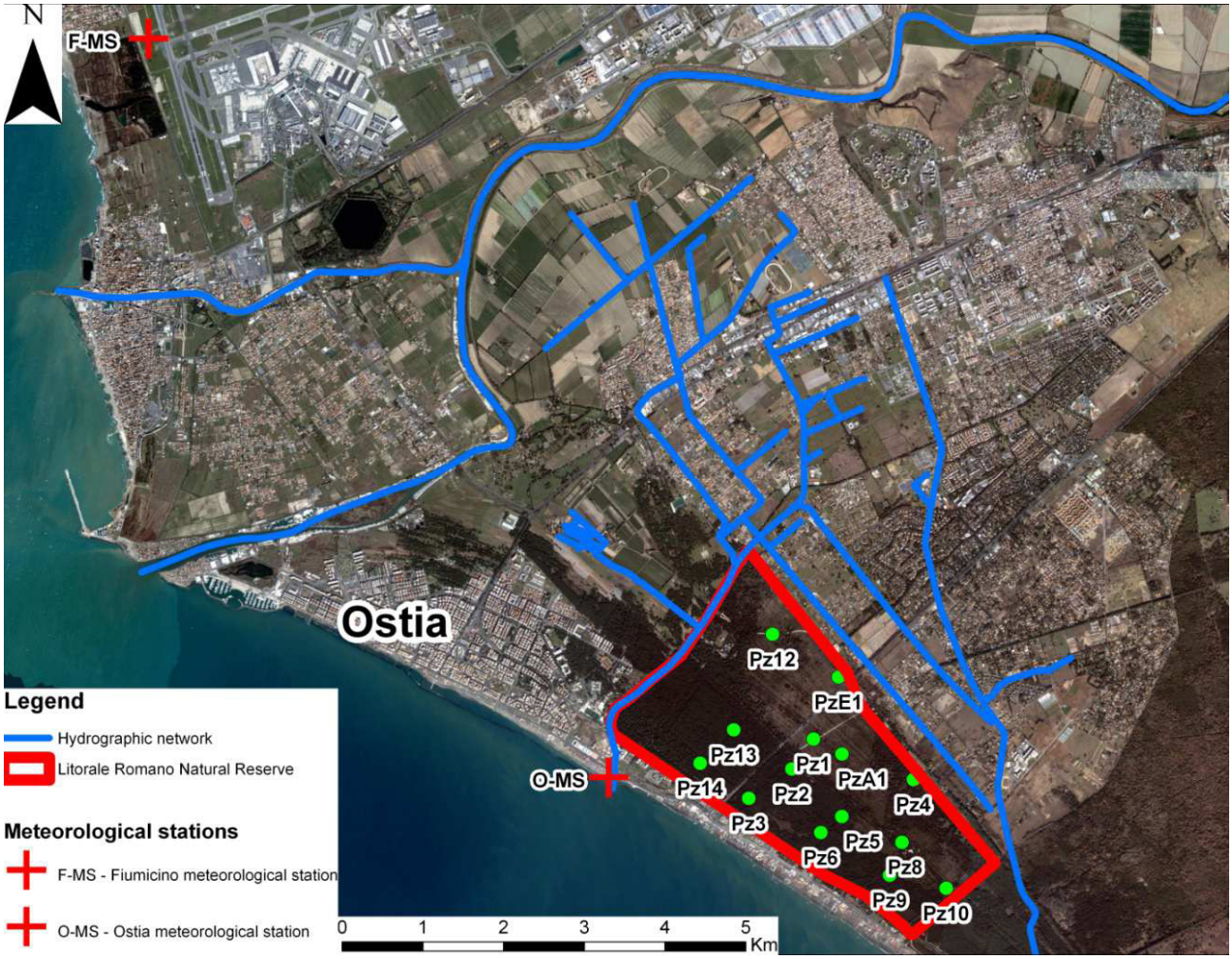

Fig. 2.5: the location of the piezometric network and the Fiumicino and Ostia metreological stations

2.4 RESULTS

Data about water level sensor in Fig.2.6 show how the maximum water table level about Pz3 was in May 2011(1.47 m a.s.l.) and the minimum in October 2011 (0.78 m a.s.l.). At the beginning of the autumn (October 2011), the rains (Wunderground 2012c) started to recharge groundwater, with a following maximum in March 2012 (1.29 m a.s.l.), after which a new decreasing trend started. For this reason the two groundwater patterns about May 2011 and October 2011 were represented in Fig.2.7a and Fig.2.7b respectively. They were drawn with an equidistance of 0.2 m and they were realized using the inverse data weight (IDW) function in ArcGis (ESRI 2008). Both the groundwater patterns show the maximum hydraulic head (2 m and 1 m a.s.l. respectively for May and October) located next to Pz9 and Pz10 because of their major altitude. The groundwater investigation in the LRNR, confirmed that the groundwater pattern traces the morphology, with a centrifuge flow path pattern with respect to the dune ridge.
After the summer 2011 the seaward hydraulic gradient reduced substantially, passing from 1.8‰ of May 2011 to 0.9‰ of October 2011.

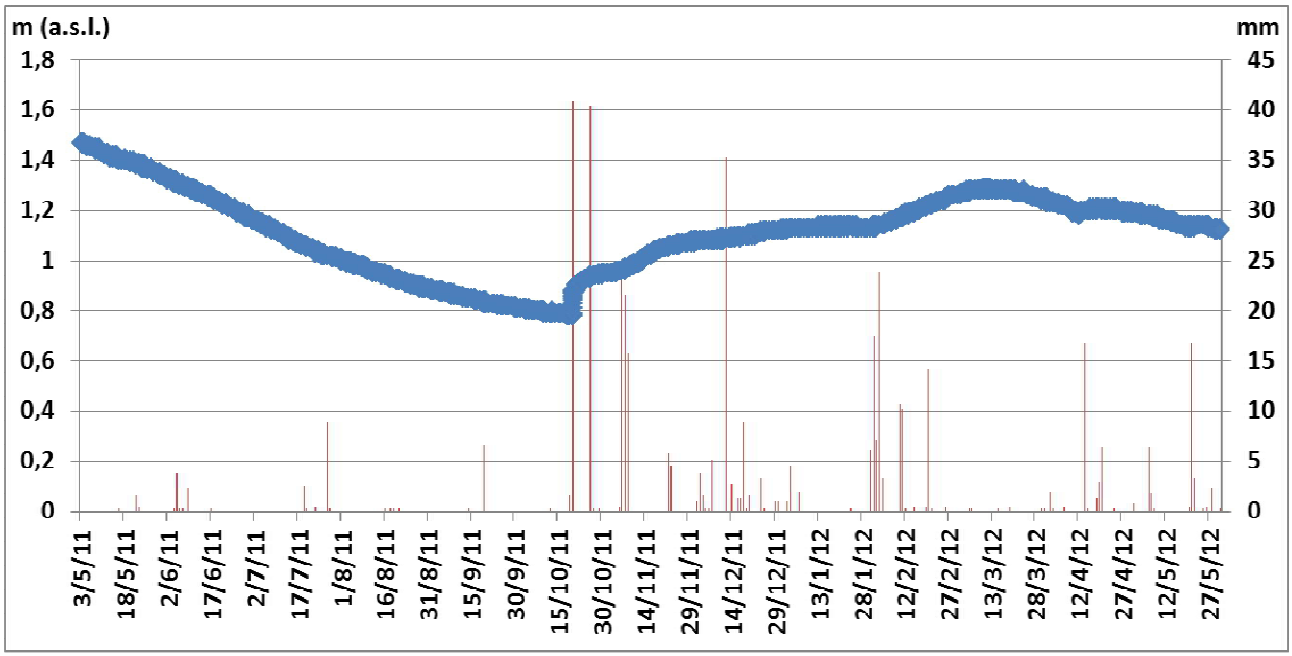

Fig. 2.6: water table fluctuation about the Pz3. The maximum water table level was in May 2011(1.47 m a.s.l.) and the minimum in October 2011 (0.78 m a.s.l.). It can be observed how the water table level increases very quickly when rains occur

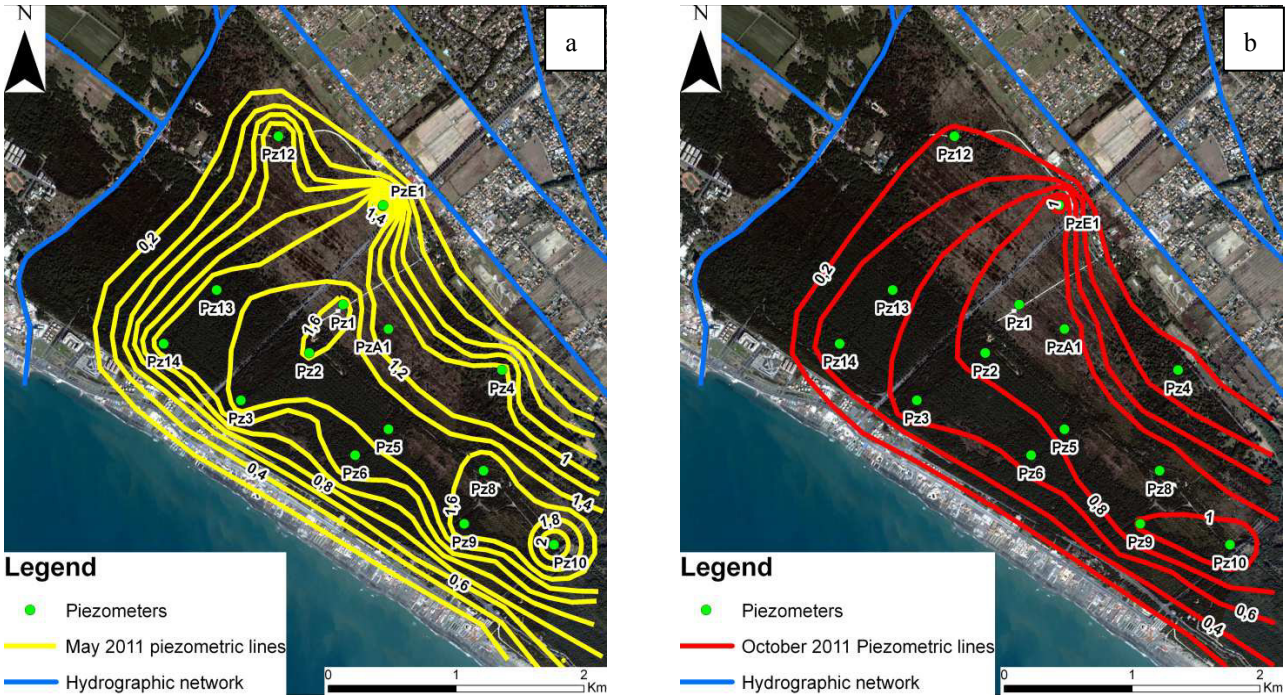

Fig. 2.7: water table about the maximum and minimum levels (May 2011(a) and October 2011(b) respectively). In the observation time a reduction from 1.8‰ to 0.9‰ of the hydraulic gradient was quantified

Chemo-physical data about EC of all the investigated piezometers are resumed in the boxplot in Fig.2.8. The depth of data collection is indicated in parenthesis and was 1 meter from the piezometer bottom. The EC values represent the chemo-physical characteristics of the most surficial part of the aquifer (lithology 4, in Fig2.2), in which the contribution of SSA salinization can be identified. They show how the EC values changed in the time of investigation. In general the EC values ranged between 610 and 3150 µS/cm, with an average value of 1350 µS/cm.

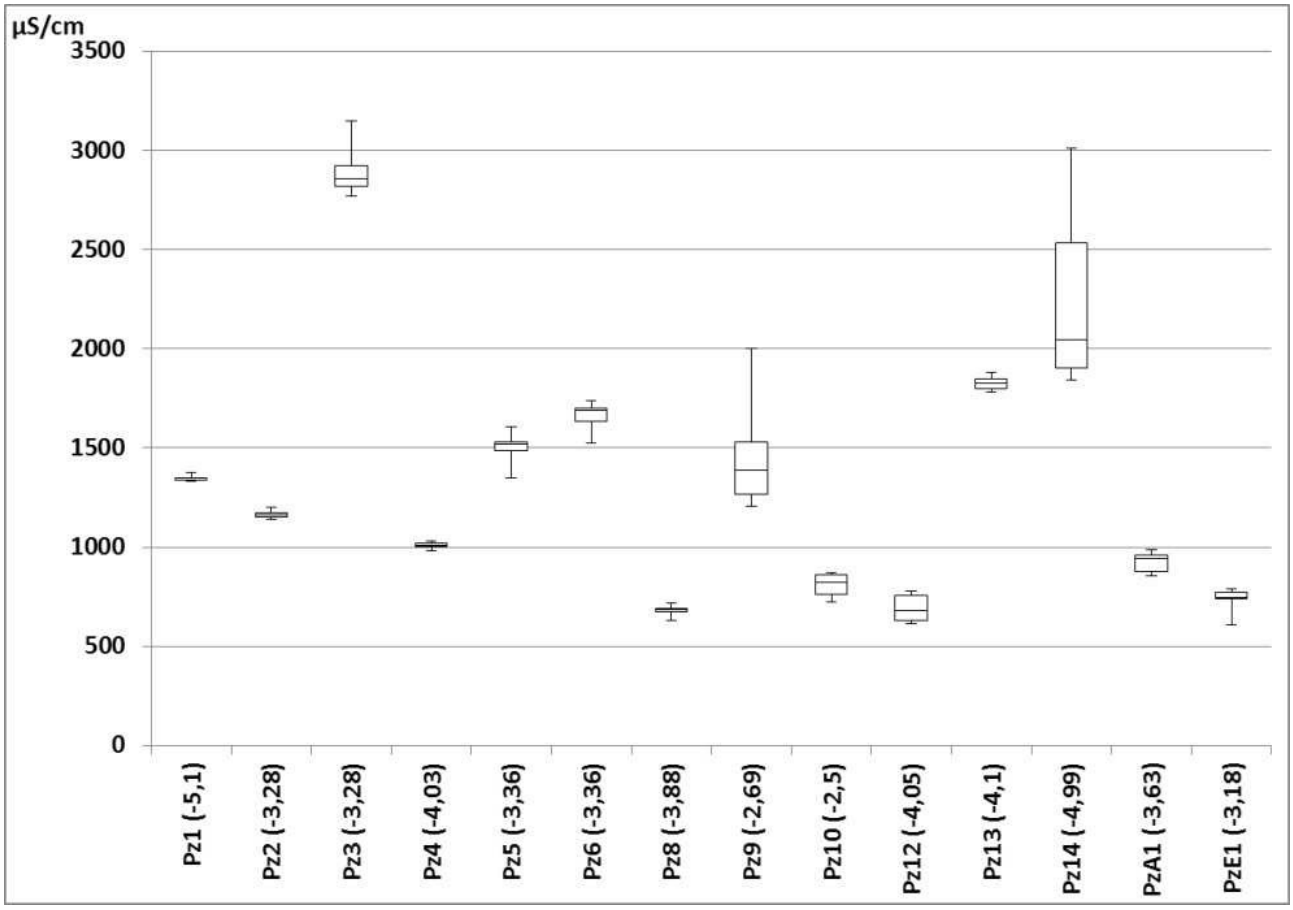

Fig. 2.8: EC values about the piezometers network surveyed between May 2011 and May 2012. It can be observed how Pz3, Pz9 and Pz14 were the most variable and they reached high values of EC. All of them are located nearby the coast line

The results of the chemical analysis are shown in Table.2.1 and the water type is figured in the Piper Diagram in Fig.2.9. Pz10 and Pz12 resulted to be about the $Ca(HCO_3)_2$ water type; Pz6 landed in the transition zone between $Ca(HCO_3)_2$ and $CaCl_2$ water types, while Pz12 landed in the transition zone between $CaCl_2$ and NaCl water types.

Sample	Cl^- meq/l	Na^+ meq/l	K^+ meq/l	HCO_3^- meq/l	SO_4^{2-} meq/l	NO_3^- meq/l	Ca^{2+} meq/l	Mg^{2+} meq/l	EC (µS/cm)	T(°C)	Sampling date
PZ 6	8,12	3,87	0,3	6,4	0,45	0	8,64	2,47	1654	15,6	October 2012
PZ 10	1,47	1,52	0,22	12,6	0,21	0	12,37	0,6	772	15,7	October 2012
PZ 12	0,82	0,91	0,07	6	0,15	0	4,31	1,33	559	15,7	October 2012
PZ 14	23,79	15,27	0,77	9,8	0,62	0	15,16	4,27	3340	16	October 2012

Table 2.1: Chemical analysis of the major elements expressed in meq/l, about October 2012

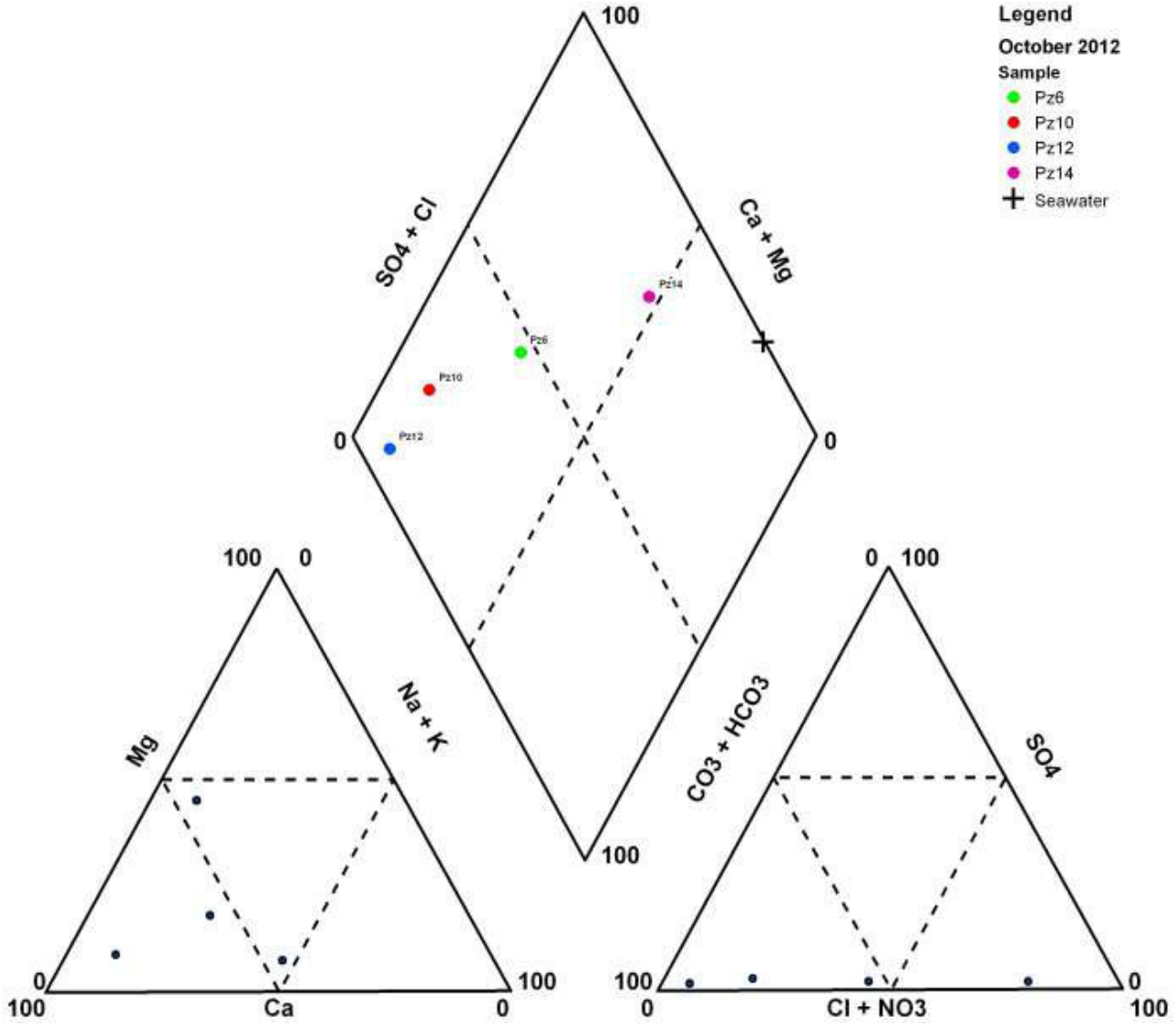

Fig. 2.9: Piper Diagram representing the main water types. it can be observed how Pz10 and Pz12 resulted to be about the $CaHCO_3$ water type; Pz6 landed in the transition zone between $CaHCO_3$ and $CaCl_2$ water types, while Pz12 landed in the transition zone between $CaCl_2$ and NaCl water types

Wind data collected from Fiumicino MS and Ostia MS provided data with different time steps, 2 min and 5 min respectively. 5 min frequency is the most accurate and continuous, because it represents the average values of wind intensity and direction of the wind vector, recorded every two minutes (Civano et al. 2004). Therefore Fiumicino MS data were filtered and averaged to obtain a wind database with a 5 min frequency. Lacking time series of Ostia station were integrated with the Fiumicino data, applying the same 5 minutes time frequency.

Datasets were subject to frequency analysis, through the creation of wind intensity histograms, essential to create compass roses. These representations show predominant wind provenances. Following the criterion of O'Dowd and De Leeuw (2007), the statistical analysis was effectuated on wind data with wind speed higher than 4 m/s. Compass roses (Fig.2.10) show predominant winds: they were westerly during the months from May to September 2011; from October 2011 to March 2012 they had a variable provenance, from northeasterly to southeasterly; from April to May 2012, they returned to be westerly.

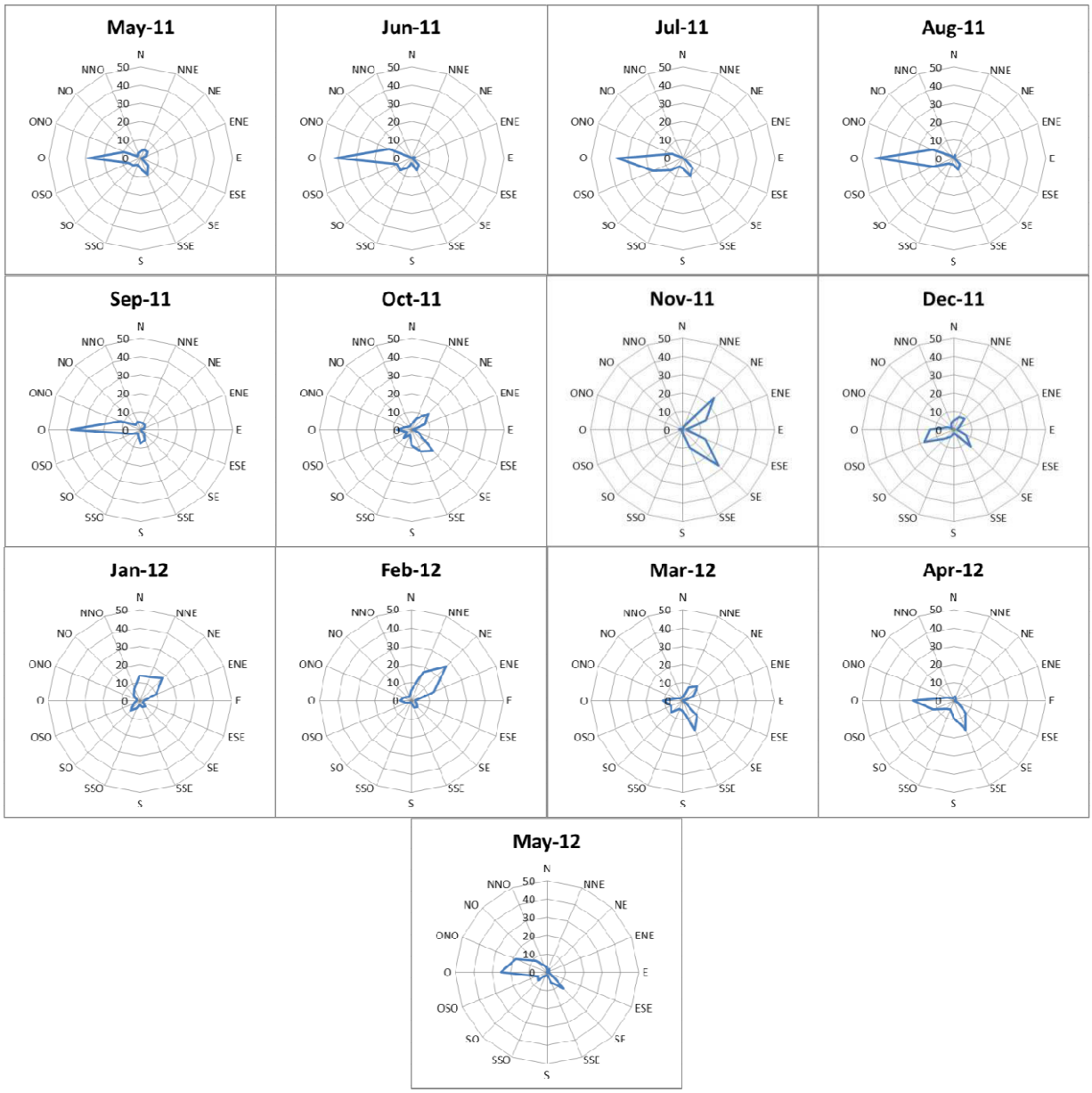

Fig. 2.10: compass roses derived from a statistical analysis of the wind speed higher than 4 m/s (O'Dowd and De Leeuw, 2007). In the period from May to September 2011 the winds were westerly; from October 2011 to March 2012 the wind pattern was variable with winds from northeasterly to southeasterly; from April to May 2012, they started again to be westerly.

2.5 DISCUSSION

Pz3, Pz9 and Pz14 piezometers, located closer to the coastline, showed high EC values and a great variability during the yearly measurements (Fig.2.8), according to Tuccimei et al. (2010).

Since the dominant mass fraction of SSA is inorganic sea salt (O'Dowd and De Leeuw 2007) and the main component of sea salt is Cl^-, EC was used as an indirect marker to evaluate the SSA accumulation, because a linear relationship exists between EC and Cl^- content (Cruz et al. 2011; Kelly 2005). In this way it was possible to explain the variability about the EC values of the piezometers and in particular the Pz3 EC values.

EC data about Pz3 were compared to the rainfalls and to the wind provenance and connections among the three parameters were found. Fig.2.11 summarizes these relationships, representing the cumulate rains (blue line), the EC values (red bars) and the wind provenance. In the period between May and September 2011 the wind pattern was mainly westerly. In this case winds blowing from the sea determined a dry deposition on the foliage of the pine trees. The low rain rate occurred in August and September 2011 determined a mobilization of the SSA toward the ground. The salty solution reached groundwater determining a slight increase of EC values. In October 2011 the Autumnal rains

started and a great quantity of rain fell down (about 100 mm). It determined a complete washout of the tree foliage and the maximum value of 2740 µS/cm occurred in November 2011. From the beginning of December, freshwater rain started to dilute groundwater salinity. In this period SSA dry deposition didn't take place because of the wind pattern was not from the sea. In April 2012 groundwater EC values started to increase again, due to the rains and a newly westerly wind pattern, which determined again a SSA dry deposition.

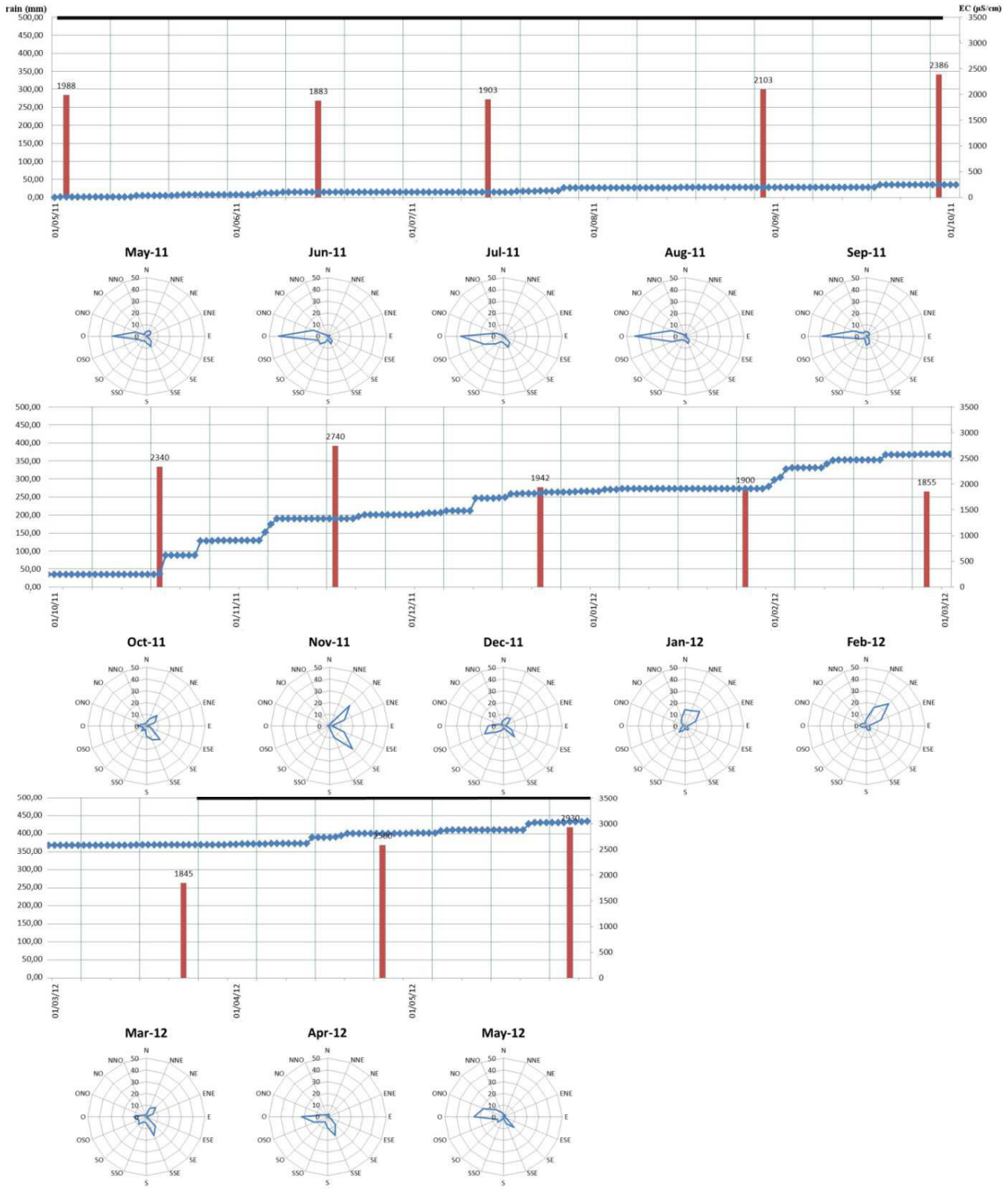

Fig. 2.11: relationships among wind provenance (compass roses), rains (cumulate in blue line) and EC about the Pz3 (red bars). It can be observed how in the period from May to September 2011a SSA accumulation occurred on the tree foliage. In October 2011, with the beginning of the rainy season, a great quantity of rains fell down, increasing the EC values. Once the SSA was wash out a dilution acted by the rain water took place and EC values decreased. They started to increase again in April 2012, due to a new accumulation cycle determined by a newly westerly wind pattern. The black line indicates the periods of SSA dry deposition on the tree foliage

Chemical analysis confirmed that the SSA accumulation decreases inland, according to Tuccimei et al. (2010). Observing Fig.2.12 it is possible to see that Pz14 has a high concentration of Cl^- and Na^+ and it is a mixture between the NaCl and $CaCl_2$ water types. Going toward the Pz6, that shows a mix between $CaCl_2$ and $CaHCO_3$ water types, it is possible to notice a strong reduction of the two main seawater elements. Last two samples, Pz10 and Pz12, showed a drastic reduction of Cl^- and Na^+, but they were enriched in Ca^{2+} and HCO_3^-, the main ions of their $CaHCO_3$ water type. Therefore the water types occurring in the LRNR groundwater show a decreasing salinization pattern from the costal line to the inner part, passing from a NaCl, to a $CaHCO_3$ water type.

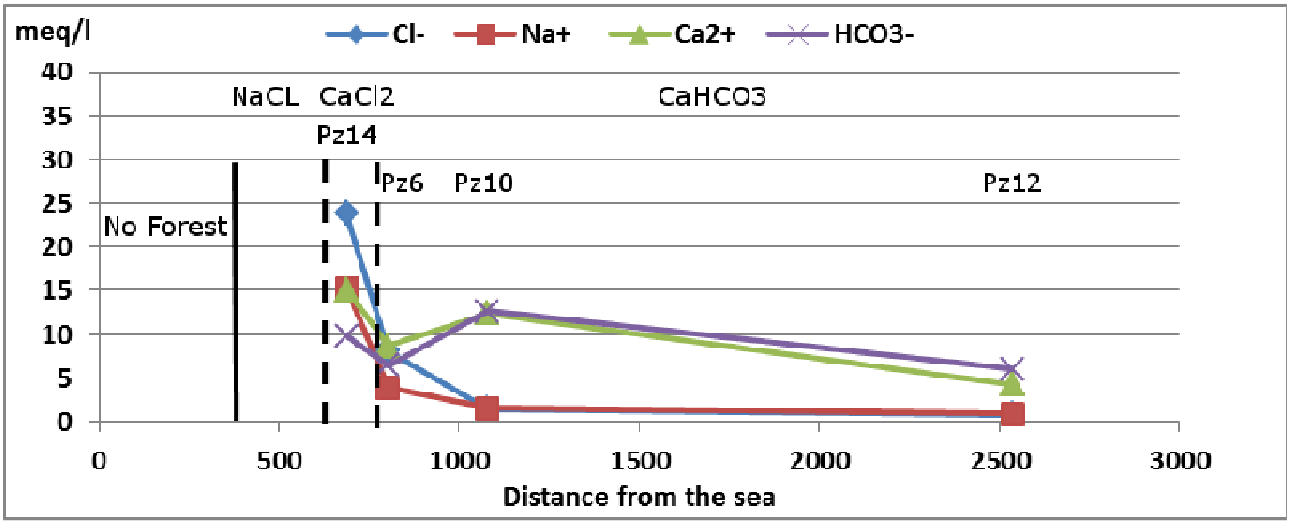

Fig. 2.12: Transect of groundwater chemistry about the four piezometers. It can be seen how the richest in Cl^- and Na^+ are those located nearby the coast line. They show mix water types, ranging from NaCl to Ca_2Cl. Last two piezometers are enriched in Ca^{2+} and HCO_3^-, because of their freshwater composition

2.6 CONCLUSIONS

This study allowed to relate the SSA aerosol salinization to the groundwater salinity pattern. It was possible collecting data about EC values of groundwater in the LRNR monthly. A wind statistical analysis, based on the O'Dowd and De Leeuw (2007) assumption that a wind speed higher than 4 m/s is an adequate threshold to generate SSA from the sea surface, permitted to identify the periods of dry deposition of SSA on the foliage of the pine forest. This deposition occurred during Spring and Summertime, when westerly winds blow. During the rainy seasons, a SSA dissolution from the tree foliage and a transport to groundwater occurred, as shown by the EC values modification in time. In fact EC is a good marker to identify salinization, because a linear relationship exists between EC and Cl^- content (Cruz et al. 2011; Kelly 2005). The salinization pattern decreases from the coast line moving inland. It is demonstrated by the high values of EC of the coastal piezometers (Pz3, Pz9 and Pz14), according to Tuccimei et al. (2010). Also the chemical analysis, confirmed this assumption, showing that Pz14 shows a NaCl-$CaCl_2$ mix water types, Pz6 shows a CaCl2-$CaHCO_3$ mix water type and Pz10 and Pz12 belong to the $CaHCO_3$ water type. This chemical distribution in groundwater allowed to prove further that the water type in the LRNR, is strictly related to the distance from the sea and therefore strictly dependent on the SSA salinity contribution coming from the dry deposition on the tree foliage.

2.7 REFERENCES

Amenduni G (1884) Sulle opere di bonificazione della plaga litoranea dell'Agro Romano che comprende le paludi e gli stagni di Ostia, Porto, Maccarese e delle terre vallive di Stracciacappa, Baccano, Pantano e Lago dei Tartari. Relazione del progetto generale 15/7/1880. Ministero Lavori Pubblici,

Bellotti P, Calderoni G, Carboni MG, Di Bella L, Tortora P, Valeri P, Zernitskaya V (2007) Late Quaternary landscape evolution of the Tiber River delta plain (Central Italy): new evidence from pollen data, biostratigraphy and C-14 dating. Zeitschrift Fur Geomorphologie 51 (4):505-534. doi:10.1127/0372-8854/2007/0051-0505

Bellotti P, Tortora P, Valeri P (1989) Sedimentological and morphological features of the Tiber Delta Sedimentology 36 (5)

Capelli G, Mastrorillo L, Mazza R, Petitta M, Baldoni T, Banzato F, Cascone D, Di Salvo C, La Vigna F, Taviani S, Teoli P (2012) Carta Idrogeologica del Territorio della Regione Lazio. Scala 1:100.000 (4 Fogli). S.EL.CA., Firenze - Italy

Capelli G, Mazza R, Gazzetti C (2005) Strumenti e strategie per la tutel e l'uso compatibile della risorsa idrica nel Lazio, vol 78. Quaderni di Tecniche di Protezione Ambientale. Bologna

Capelli G, Mazza R, Papiccio C (2007) Saline intrusion in the Tiber Delta. Geology, hydrology and hydrogeology of the coastal plain of the roman sector. Giornale di Geologa Applicata 5:13-28

Capelli G, Salvati R (2003) Studi per la riforestazione della Pineta di Castelfusano. Comune di Roma, Dipartimento X-Politiche Ambientali e Agricole & Università di Roma Tre, Dipartimento di Scienze Geologiche,

Civano A, Morini M, Sodi R (2004) Caratteristiche del vento all'aeroporto di Genova in base all'analisi dei dati anemometrici raccolti su due punti. ENAV,

Cruz JV, Coutinho R, Pacheco D, Cymbron R, Antunes P, Freire P, Mendes S (2011) Groundwater salinization in the Azores archipelago (Portugal). Environmental Earth Sciences 62 (6):1273-1285. doi:10.1007/s12665-010-0615-2

Erickson DJ, Duce RA (1988) On the global flux of the armospheric sea salt. Journal of Geophysical Research-Oceans 93 (C11):14079-14088. doi:10.1029/JC093iC11p14079

ESRI (2008) ArcGIS – A Complete Integrated System. http://www.esri.com/software/arcgis.

Fuentes E, Coe H, Green D, de Leeuw G, McFiggans G (2010) Laboratory-generated primary marine aerosol via bubble-bursting and atomization. Atmospheric Measurement Techniques 3 (1):141-162. doi:10.5194/amt-3-141-2010

Gong SL, Barrie LA, Lazare M (2002) Canadian Aerosol Module (CAM): A size-segregated simulation of atmospheric aerosol processes for climate and air quality models - 2. Global sea-salt aerosol and its budgets. Journal of Geophysical Research-Atmospheres 107 (D24). doi:10.1029/2001jd002004

Gustafsson MER, Franzen LG (2000) Inland transport of marine aerosols in southern Sweden. Atmospheric Environment 34 (2):313-325. doi:10.1016/s1352-2310(99)00198-3

Hasselrot B, Grennfelt P (1987) Deposition of air-pollutants in a wind-exposed forest edge. Water Air and Soil Pollution 34 (2):135-143. doi:10.1007/bf00184756

Kelly D (2005) Seawater intrusion Topic Paper. vol 6. WRIA, Island County

Lewis ER, Schwartz S (2004). In: Board AB (ed) Sea Salt Aerosols Production; Mechanism, Methods, Measurement and Models. Washington DC, USA, pp 1-5

Martensson EM, Nilsson ED, de Leeuw G, Cohen LH, Hansson HC (2003) Laboratory simulations and parameterization of the primary marine aerosol production. Journal of Geophysical Research-Atmospheres 108 (D9). doi:10.1029/2002jd002263

Milli S (1997) Depositional setting and high-frequency sequence stratigraphy of the middle-upper Pleistocene to Holocene deposits of the Roman basin. Geologica Romana 33:99-136

Milli S, D'Ambrogi C, Bellotti P, Calderoni G, Carboni MG, Celant A, Di Bella L, Di Rita F, Frezza V, Magri D, Pichezzi RM, Ricci V (2013) The transition from wave-dominated estuary to wave-dominated delta: The Late Quaternary stratigraphic architecture of Tiber River deltaic succession (Italy). Sedimentary Geology 284:159-180. doi:10.1016/j.sedgeo.2012.12.003

Milli S, Palombo MR (2011) Stratigrafia fisica e assetto deposizionale della successione del tardo Pleistocene inferiore/Olocene del Bacino Romano - I depositi pleistocenici di Ponte Galeria e la Polledrara di Cecanibbio. Paper presented at the Congresso Aiqua - Il Quaternario Italiano - Conoscenze e prospettive, Roma, 24-25 febbraio 2011

O'Dowd CD, De Leeuw G (2007) Marine aerosol production: a review of the current knowledge. Philosophical Transactions of the Royal Society a-Mathematical Physical and Engineering Sciences 365 (1856):1753-1774. doi:10.1098/rsta.2007.2043

Schofield R, Thomas DSG, Kirkby MJ (2001) Causal processes of soil salinization in Tunisia, Spain and Hungary. Land Degradation and Development 12:163-181. doi:10.1002/ldr.446

Toth G, Adhikari K, Varallyay GY, Toth T, Bodis K, Stolbovoy V (2008) Updated Map Of Salt Affected Soils In The European Union. In: Gergely Tóth LMaER (ed) Threats To Soil Quality In Europe. European Commission, Joint Research Centre, Institute for Environment and Sustainability Luxemburg, pp 65-78. doi:DOI 10.2788/8647

Tuccimei P, D'Angelantonio M, Manetti MC, Cutini A, Amorini E, Capelli G (2010) The chemistry of precipitation and groundwater in a coastal Pinus Pinea forest (Castel Fusano area, Central Italy) and its relation to stand and canopy structure. In: Szigethy BVaJ (ed) Horizons in Earth Science Research, vol 4. Nova Science Publishers, Inc., pp 1-17

Tuccimei P, Salvati R, Delitala MC, Capelli G, Amorini E, Cutini A, Manetti MC (2003) Studi sulle relazioni tra assetto idro-geochimico e copertura forestale nella pineta costiera di Castelfusano (Roma). Paper presented at the FIST - Geoitalia, Bellaria, 16-18 Settembre 2003

Wunderground (2012a) Dati anemometrici della stazione della Lega Navale di Ostia relativi al periodo maggio 2011-maggio 2012. http://www.wunderground.com/cgi-bin/findweather/getForecast?query=41.71937561,12.30211830&sp=IROMELID3.

Wunderground (2012b) Dati anemometrici della stazione di Fiumicino relativi al periodo maggio 2011-maggio 2012. http://www.wunderground.com/cgi-bin/findweather/getForecast?query=zmw:00000.1.16242.

Wunderground (2012c) Piogge relative al pluviometro di Ostia nel periodo 1/05/2011-31/05/2012. http://www.wunderground.com/weatherstation/WXDailyHistory.asp?ID=IROMELID3&day=23&month=07&year=2013.

3. GEOCHEMICAL INVESTIGATION OF THE TIBER RIVER DELTA (ROME – CENTRAL ITALY), FOR THE ASSESSMENT OF THE SALINIZATION SOURCES

ABSTRACT

Tiber River Delta is a densely populated area, reclaimed at the end of the 19th century. Hydrogeological and hydrochemical surveys were carried out in a post-summer period and after the falls. Hydrogeological surveys allowed to update the knowledge of the groundwater morphology and to analyze the water table modification in time. Hydrochemical analyses allowed to identify the main water types and their distribution in the area and the occurrence of processes of ion exchange. Salinization processes resulted to be located mostly along the coast line and in a depressed area along the river course. The calculation of the Base Exchange Indexes (BEX) allowed to discriminate the salinization sources: nearby the river banks seawater intrusion processes were identified, related to groundwater pumping of Tiber water, were a salt-wedge intrusion develops; freshening processes were observed in areas were solar salt works were present until the reclamation works; along the coast line, the processes of salinization were related to sea spray aerosol deposition on the foliage of the coastal forest

3.1 INTRODUCTION

The Tiber River delta area is a very complex system in which topography, morphology and land use coexist with rivers, canals, urban, industrial, agricultural and tourist establishments areas. For its position nearby the coast, it is strategic for the development of the Capital City of Italy, Rome. The anthropic pressure determines an increasing exploitation of groundwater, mainly for agricultural and industrial use. Withdrawals can determine the aquifer salinization, a problem detected in many low-lying deltas around the world (Mollema and Antonellini 2013; Barlow and Reichard 2010; Custodio 2010; Post 2005; Simmons 2005; Werner 2010) and this problem worsens due to rising sea levels and changing weather patterns (Maas 2007; Essink et al. 2010; Vandenbohede et al. 2011; Bobba 2002). Salinization consists in seawater intrusion, defined as the mass transport of saline waters into zones previously occupied by fresher waters (Bear et al. 1999) and it can contaminate a freshwater aquifer through several pathways, including lateral intrusion from the ocean; by upward intrusion from deeper, more saline zones of the groundwater system (upconing); by downward intrusion from coastal waters (Barlow 2003); by evaporite dissolution (Farid et al. 2013); by fossil seawater mobilization (Tran et al. 2012).

Salinization is the most widespread phenomenon of water contamination. It determines an increase in the content of certain dissolved chemical species such as sodium and chloride, changing the overall chemical water composition (Barker et al. 1998; Cruz et al. 2011; Gimenez and Morell 1997; Kim et al. 2006) and deteriorating water quality for human use. In reclaimed areas the process of seawater intrusion can be strongly amplified. For example the dune removal can facilitate the salinization processes due to the disappearance of a natural barrier, suitable to store freshwater lenses (Bakker 1990; Antonellini et al. 2008) and consequently capable of delimiting seawater intrusion; drainage canals or rivers mouths can increase greatly the potentiality of salt-wedge intrusion to penetrate inland, because they are a preferential way of intrusion, both during low discharge (Giambastiani et al. 2007; UNESCO 1983; Xue et al. 2009) and high discharge periods (Manca et al. 2014).

The studies about seawater intrusion in the Tiber River Delta started at the beginning of the last decade (Capelli et al. 2007; Capelli and Mazza 2005) and focused mainly on the connection between the hydrographical pattern and water pumping. The aim of this study is to update the knowledge about groundwater morphology ten years after last studies, also in the light of the latest knowledge on the sedimentary structure of the delta (Milli et al. 2013). For this reason two hydrogeological surveys were conducted in October 2012 and February 2013, to evaluate the water table evolution and the chemical-physics characteristics of groundwater. Furthermore chemical analyses were carried out on water samples collected both on October and February to try to identify the salinization pattern and sources in the area.

3.2 GEOLOGICAL AND HYDROGEOLOGICAL SETTING

The study area is located on the left bank of the Tiber River and it holds an extension of 89 km^2 (Fig.3.1). It is delimited Northeastward by the Malafede Trench, Southward by the Castel Porziano Natural Reserve, Westward by the Tyrrhenian Sea and Northward by the Tiber River. The morphology of the area is almost entirely composed by a coastal plain with the exception of the Acilia and Vitinia areas, where a hill landscape develops. Furthermore in the area of the Litorale Romano Natural Reserve (LRNR) a coastal dune morphology develops. Ostia Antica and Infernetto areas are located below the mean sea level and they were reclaimed in the 19th century from swamp and pond areas respectively.

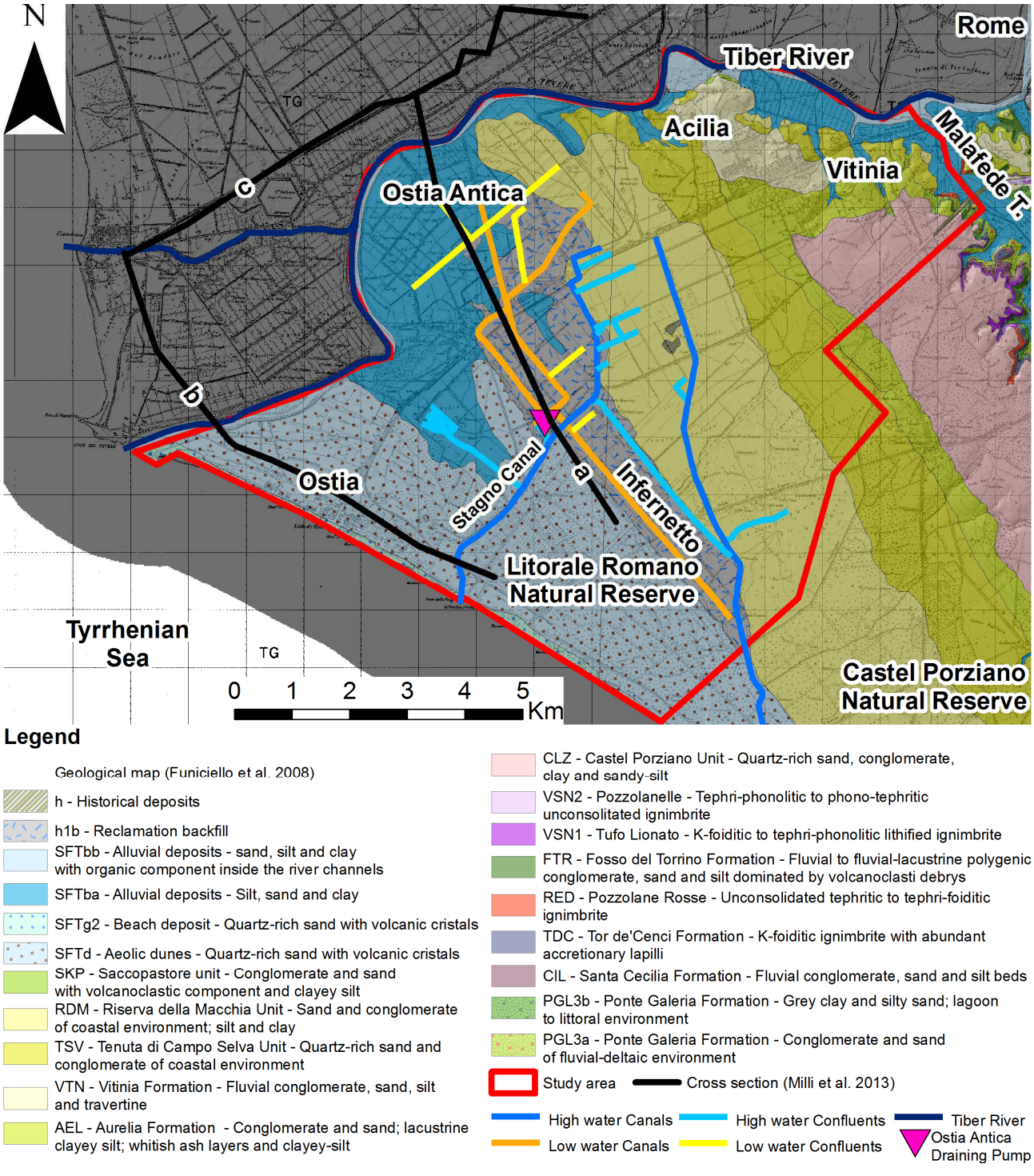

Fig. 3.1: the study area location; the geologic map is after Funiciello et al. (2008), the cross sections are after Milli et al. (2013)

In the Ostia Antica area drainage canals digging and draining pumps installation determined a strong hydrographic pattern modification. In the Infernetto area filling activities and drainage canals digging dried out the Stagno di Ostia Pond (Amenduni 1884). Several authors (Giordano et al. 2003; Funiciello et al. 2008; Funiciello and Giordano 2008) studied the geological setting of the area, focusing attention on the surface geology. The inner part of the study area is characterized by a surface geology composed mainly by deposits about the Middle-Upper Pleistocene. It includes both sedimentary deposits and Alban Hills volcanic units. In the external sector, the coastal plain is characterized by the outcrop of sand deposits about aeolic dunes environment, whereas in the area of Ostia Antica the main deposits are made up of silt, sand and clay about alluvial deposits. Filling reclamation deposits outcrop as well in the Infernetto area, behind the coastal dunes of the LRNR. Other authors focused attention on the subsurface geology and the evolution of the deltaic area (Bellotti et al. 1987; Bellotti et al. 2007; Bellotti et al. 1989a; Bellotti et al. 1994; Bellotti et al. 1995; Bellotti et al. 1989b; Amorosi and Milli 2001). Milli et al. (2013) reviewed the previous literature and, with the help of new stratigraphic data, accurately described the Late Quaternary stratigraphic architecture of Tiber River deltaic succession within the Roman Basin.

The Roman Basin is the result of a continuous regional tectonic uplift started in the Late Pliocene (Bordoni and Valensise 1998; Giordano et al. 2003; Milli 1997; Conato et al. 1980; Malatesta and Zarlenga 1986) and of the intense volcanic activity, which reached a climax in the Middle-Upper Pleistocene, when the volcanic complexes of the Roman Magmatic Province developed (Locardi et al. 1976; Cioni et al. 1993; De Rita et al. 1993; Karner et al. 2001).The sedimentary deposition was strongly influenced by the glacioeustatic sea-level fluctuations, related to the Quaternary climatic changes (De Rita et al. 1994; De Rita et al. 2002; Milli 1994, 1997; Marra et al. 1998; Giordano et al. 2003; Milli et al. 2008).

The stratigraphic succession is composed by several depositional units, which represent high-frequency depositional sequences of the 4th order with a variable duration (from 30to 120 kyr). They constitute in turn, two composite 3rd order sequences (Mitchum and Vanwagoner 1991): the Monte Mario Sequence (MMS, Lower Pleistocene) and the Ponte Galeria Sequence (PGS, LateLower Pleistocene-Holocene) (Milli 1997; Milli and Palombo 2011). Milli et al. (2013) suggested a chronostratigraphic and sequence-stratigraphic scheme about the Pleistocene deposits of the Roman Basin (Fig.3.2): MMS deposits are represented by coastal and transition-shelf depositional systems, developing during the Late Low-stand and Transgressive Systems tracts of MMS. These deposits consist of clays and silty clays with local intercalations of sandy levels, aged 1.5-1.2 Ma (Carboni 1993). The PGS contains fluvial, fluvio-lacustrine, barrier island-lagoon, and transition shelf depositional systems, organized to constitute the low-stand (LST), the transgressive (TST) and the high-stand (HST) system tracts of the PGS. PGS is constituted by gravels and sandy gravels with pebbles of carbonate rocks from the Apennines and rare volcanic clasts derived from the volcanic complexes of the Roman Comagmatic Province. The last sequence of the PGS, also known as PG9, is about the Tiber Depositional sequence (TDS), developed entirely during the last HST and it constitutes an incomplete fourth-order depositional sequence, which is still evolving.

The TDS is illustrated in the cross sections in Fig.3.3. The lower boundary of this sequence is an erosional surface (S1 in Fig.3.3) that cuts the underlying Lower and Middle Pleistocene deposits, originated in correspondence of the last glacial maximum expansion (LGM, between 19 and 17 ky BP). LMG determined a sea level set between the 120 and 140 m below the present level and it concluded 19 kyr ago (Lambeck et al. 2002; Peltier and Fairbanks 2006). The TDS consists almost entirely of a transgressive–regressive wedge formed during the last 14 kyr.

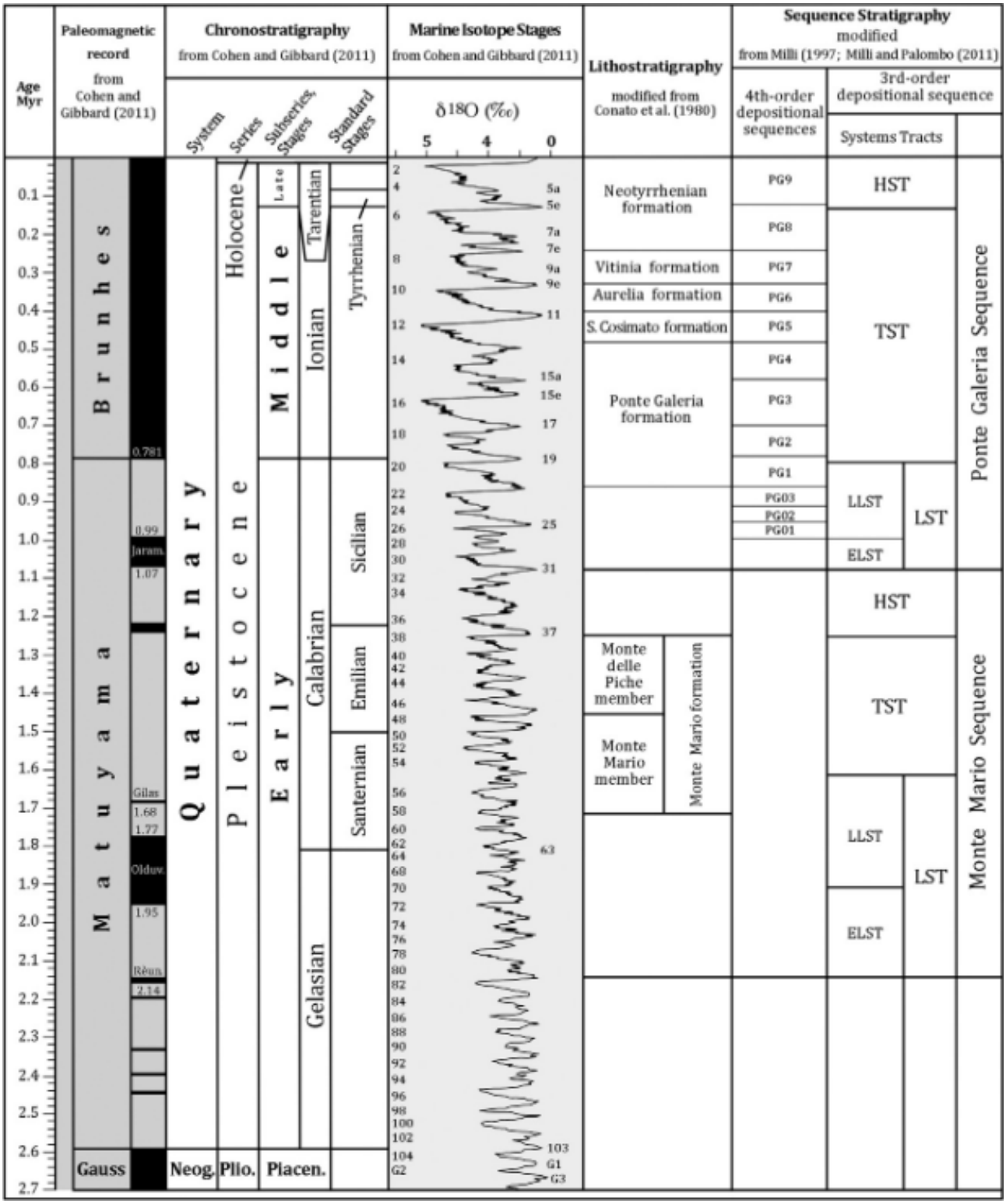

Fig. 3.2: chronostratigraphic and sequence-stratigraphic scheme of the Pleistocene deposits of the Roman Basin (after Milli, 1997; Milli and Palombo, 2011). HST: High-stand Systems Tract; TST: Transgressive Systems Tract; LST: Low-stand Systems Tract; ELST: Early Low-stand Systems Tract; LLST: Late Low-stand Systems Tract (Milli et al. 2013)

Fig. 3.3: cross sections about the TDS (after Milli et al. 2013)

3.2.1 Low-stand System Tracts deposits

These deposits can be divided in two main sequences: the Early LST (ELST) formed during the sea level fall and the Late LST (LLST) formed during the stillstand and the sea level rise. The ELST deposits (120 and 30-26 kyr BP) occur in the northernmost and southernmost part of the delta area and they are mainly composed by fluvial (sands, gravels, muds and travertine), beach (gravels and sandy gravels) and lagoon deposits (organic-rich muds with frequent intercalations of thin sandy layers, often associated to shell debris). At the top they are cut by an unconformity surface. The LLST deposits formed 30-26 and 14 kyr BP (Fig.3.4a). They occupy the most depressed area of the Tiber river incised valley and they are constituted by fluvial sands and sandy gravels passing laterally and vertically to floodplain muddy deposits with peat layers.

3.2.2 Transgressive System Tract deposits

These deposits (14 and 6-5 kyr BP) present a retro-gradational stacking pattern deposition and lie directly above another unconformity surface (ts in Fig.3.3), formed during a submergence phase (Penland et al. 1988). They are mainly constituted by deposits of fluvial-bay-head deltaic system (sands and silty sands), coastal barrier-lagoon system (silty clays and clays) and finally a transition to shelf system (coastal barrier deposits, sands and silty sands). The depositional architecture within the TST of TDS can be subdivided into a series of steps, recording the sedimentary evolution of the study area.

During the early phase of TST (between 14 and 13 kyr BP) the deltaic body was transformed into an "erosional headland with flanking barriers" (Penland et al. 1988), at the back of which open lagoons occurred (Fig. 3.4b). Fluvial channels and floodplain sands and silty-clays are the main lithologies deposited in this period. During this phase the Tiber River migrated its course toward SE of about 2.5 km with respect to the previous position.

Between 13 and 5 kyr BP a lagoon basin formed, bordered by barrier islands. In this time-frame three deltas developed in sequence during a progressive movement of the coastal barrier landward, due to the sea-level rise: T1 (13-9 kyr BP) with a maximum thickness of 20–21 m and lateral extension of about 3 km, formed during a slowdown in sea level rise, due to the cold period of Younger Dryas (Fig.3.4c);

T2 (9-8.5 kyr BP) extends laterally for about 5.6 km (Fig.3.4d) and holds a maximum thickness of 17–18 m;

T3 (8.5-6 kyr BP), represents the smallest deltaic body and reaches a thickness of 5–10 m (Fig.3.4e).

The bay-head delta T3 prograded very rapidly within this lagoon due to the increase of sediment supply and the decrease of the rate at which new accommodation space was created. The lagoon was transformed into two marshy coastal ponds (Stagno di Maccarese to the north and Stagno di Ostia to the south), poorly and intermittently connected to the sea, which remained active up to the 1884 reclamation (Amenduni 1884).

The final sedimentation phase of TST is marked into the lagoon by the presence of a thick and continuous peat layer, dated between 6 and 5 kyr BP.

3.2.3 High-stand System Tract deposits

The final stage of the Tiber delta deposition is represented by the high-stand system tract, developed from 6 to 5 kyr BP. In this period the TST lagoon was filled and cuspate delta started to develop. The delta depositions can be divided in three main phases: at the beginning of the first phase, dated about 6-5.7 kyr (Fig.3.4f), the Tiber acquired a marine mouth and started to migrate seaward. This progradation lasted about 3 kyr at a rate of at least 1 m/year (Bellotti et al. 2011) and a cuspate delta with several beach ridges developed.

In the second phase (Fig.3.4g) between 2.7 and 1.9 kyr BP, an abrupt southward migration of the river mouth occurred, probably as a result of a strong flood event. The mouth progradation rate was estimated to be about 5–6 m/year (Bellotti et al. 2011). At the beginning of the third phase, between 1.9 kyr to present (Fig.3.4h), the last progradation of the Tiber Delta occurred and it has been quite intense for the last 500 yr.

One can conclude that the Delta evolution had a strong correlation with the Tiber flood events and consequently with its solid transport. In fact the erosion of beach ridges occurred in low sediment supply phases (Bellotti et al. 1994; Bellotti et al. 2011; Giraudi 2011) related to warm climatic phases. Otherwise the shoreline progradation happened between the 15th and 20th centuries is connected to Little Ice Age, when more frequent and intense floods are historically documented in the city of Rome. During this period the Tiber delta prograded for about 3 km, at a rate of about 9 m/year (Giraudi 2011; Bellotti et al. 1994). Nowadays the Tiber Delta can be classified as a wave-dominated arcuate delta, with lateral transition to strand plains fed by long shore drift.

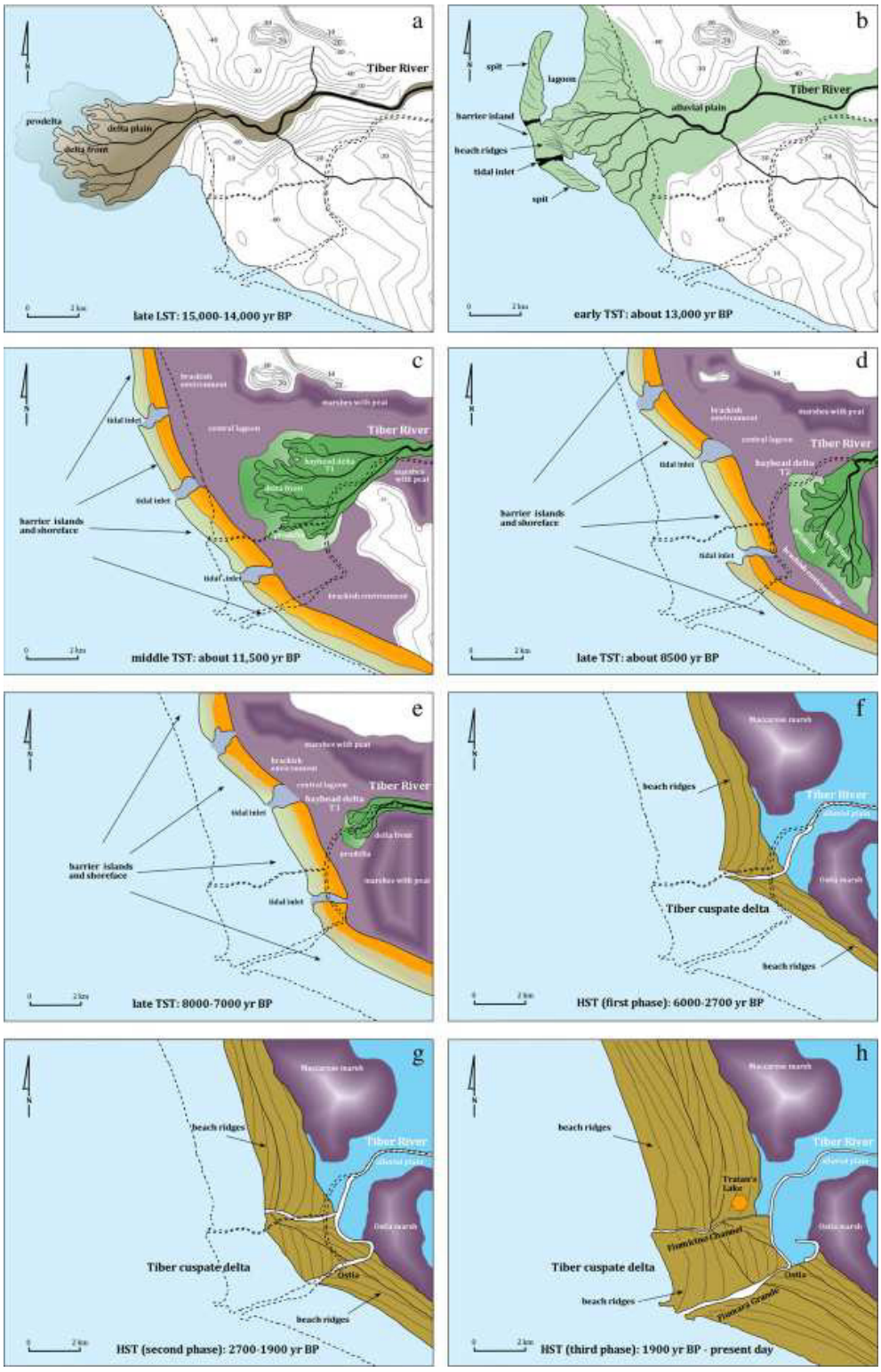

Fig. 3.4: evolution of the Tiber River Basin: depositional phases according to the sea-level changes (Milli et al. 2013)

3.3 HYDROGEOLOGICAL SETTING

Hydrogeological pattern of the Tiber delta is strictly related to the geological setting of the area. It includes confined and semi-confined aquifers, supported by the low permeability Plio-Pleistocene clayey basement of the MMS (Capelli et al. 2007). The MMS appears strongly affected by tectonics and the flow paths direction depends strictly on the areas characterized by a high topographic position of the basement.

The groundwater pattern of the area (Fig.3.5) (Capelli and Mazza 2005) traces the topography and the hydraulic head is located in correspondence of the morpho-structural ridge of Acilia-Pomezia (APR, Capelli et al. 2007). It consists in a high stand of the clayey basement, underlying the PGS gravel units and volcanic units from Alban Hills (Bucci and Grillini 2001; Ventriglia 1990). It runs in parallel to the coast line passing through Castel Porziano Natural Reserve and it is bordered Northeastward by the Malafede Trench. The water table is located at variable depths along the APR, which determines the main directions of the flow paths, representing the physical and hydrogeological watershed between the TDS deposits and the volcanic units of the Alban Hills (Capelli et al. 2007). In the shallower sandy deposits of the APR a small discontinuous aquifer is present, recharged directly by rainfalls (Capelli et al. 2007). From APR, groundwater flows Northeastward to the Malafede Trench, where groundwater coming from the Alban Hills flows as well. APR determines also flow paths directed Northwestward to the Tiber River and Southwestward to the coastal plain. In the area of Acilia, Axa and Castel Porziano the main aquifer is represented by the gravels of PGS, directly overlaying the MMS units (Capelli et al. 2007; Anselmi et al. 1995). Moving away from the APR, the thickness of the aquifer increases due to a greater depth of the MMS low permeability basement (Mastrorillo and Petitta 2009). Also the hydraulic gradient changes, decreasing from the 10 ‰ e to the 3 ‰ (Bucci and Grillini 2001), probably due to the major thickening of the APR lithologies with respect to the recent dune deposits (Mastrorillo and Petitta 2009).

In the coastal plain the water table is shallow and represents the main hydrogeological resources of the Latium Region (Boni et al. 1988), soaking the most permeable lithologies of the TDS, determining unconfined and semi-confined aquifers (Capelli et al. 2007). In the study area the different deposits can be divided into hydrogeological complexes characterized by different hydraulic potentialities (Capelli et al. 2012):

- alluvial deposits, with a hydraulic potentiality from low to very high;
- dune complexes, characterized by a medium-high hydraulic potentiality;
- lagoon complexes provided of a low hydraulic potentiality.

The great variability of the lithologies connected to the geological history, determines different aquiferous units in the different sectors of the study area. In the area of Ostia Antica the aquifer units are mainly constituted by the sand deposits about the T2 bay delta (Fig.3.3a), underlying the low permeability peaty-lagoon deposits about the TST and the multi-layered aquifer of the alluvial deposits of the Tiber River, formed during the HST. Moving Southeastward to the Ostia Town area, the hydrogeological setting changes, due to the presence of the sands and silty sands about beach ridge and dune deposits of the HST, provided of a great thickness (up to 20 m, Fig.3.3b) and overlying low permeability deposits (clay and silty clays shelfal deposits about the TST/HST) and in the more distal areas, the deposits about the early LST, characterized by different permeabilities.

Ostia Antica and Ostia areas show a water table level which can reach up to -5 m b.s.l., mostly due to the withdrawals and the ground level below the mean sea level (Capelli et al. 2005). In the coastal area of the LRNR, a slight hydraulic head is present (up to 1 m a.s.l.; see chapter 2). Its existence is allowed by the pristine coastal dune environment, completely demolished in the other coastal areas (Capelli et al. 2007). Chemo-physical characterization of groundwater in the study area, realized in 2004 (Capelli et al. 2007), showed a presence of salinity in the coastal zones and in the most depressed topographic areas.

3.4 HYDROLOGICAL SETTING

The reclamation activities have affected the study area since the 1884 and the hydrological network changed substantially. Drainage canals can be divided in two groups: “High Waters” canals and “Low Water” canals (Fig.3.1).

"High waters" canals were obtained by the natural hydrographical network to make the water, coming from relatively high topographic areas (4-5 m a.s.l.), flow directly into the sea.

"Low Waters" canals are the drainages whose bottom is below sea level and they collect waters from areas located below the mean sea level (Ostia Antica and Infernetto, Fig.3.1). Their purpose is to direct the waters to a drainage pump (Ostia Antica Draining Pump, Fig.3.1), which lifts the water up into the Stagno Canal, which in turn, flows into the sea. The two canal systems were realized to avoid the water stagnation and to dry out the Stagno di Ostia Pond, located in the Infernetto area.

Capelli et al. (2007) investigated the salinization about the hydrographical network. Anomalies about electrical conductivity values were discovered in some points of the "Low Waters" canals and were ascribed to local events of pollution, due to the pumping for agricultural use. Data about the Tiber River showed salty and brackish waters located at the river bottom up to 8.8 km from the mouth (Manca et al. 2014; Capelli et al. 2007; Mikhailova et al. 1999).

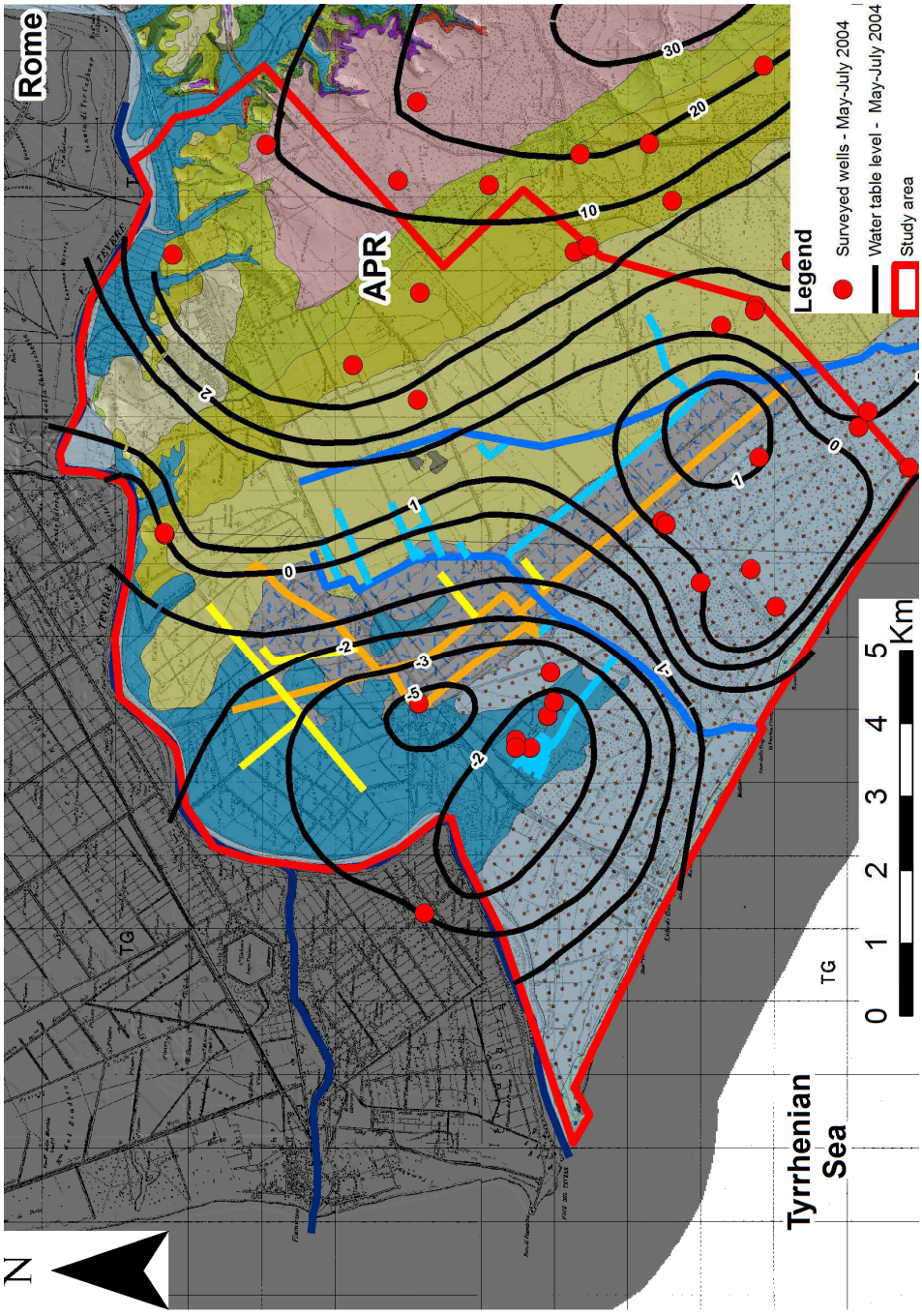

Fig. 3.5: the groundwater pattern of the Tiber River Delta traces the topography and the hydraulic head is located in correspondence of the morpho-structural ridge of Acilia-Pomezia (APR). For the legend see Fig.3.1

3.5 MATERIAL AND METHODS

The study area was investigated by means of water table measurements, chemo-physical parameterization of groundwater and groundwater sampling for chemical analysis. Two surveys were carried out: a post summer survey (October 2012) and a winter survey (February 2013). The water table depth was evaluated using a 50 m cable length electric contact meter and two water table maps were realized by hand, using the interpolation method (Custodio and Llamas 2005c). 64 and 63wells were measured respectively in October 2012 and February 2013surveys, maintaining the same well network during the two surveys. Whereby it was impossible, nearby wells were chosen, to maintain the measurements network as uniform as possible. Depth range about the well was between 3.5 and 50.45 m.
The chemo-physical data about pH (pH, ± 0.01), Electrical Conductivity (EC, in µS/cm ± 0.5%, normalized at 25°C), and Temperature (Temp ± 0.1, in °C) were collected using a portable pH-conductivity-meter. Water sampling was effectuated collecting waters from the well pumps, after leaving waters flow for 5-10 minutes. Whereby the water pumps were absent, 0.5 or 1 liter water samplers were used. Water samples were collected at the third drop in the well, to avoid the contamination due to the previous water samples.
Laboratory analyses about major ions were conducted and for every sampling station two water samples were taken. One of the samples was acidified using a 1 ml nitric acid (HNO_3), to lower the pH <2 and to avoid the cations precipitation. Samples were filled completely and capped tightly in a double cap 0.5 l polyethylene bottle, before transporting them into the laboratory where they were stored dark and refrigerated at a temperature of about 4°C. 35 samples were collected in October 2012. 6 more water samples were collected in February 2013 whereby salinization processes were expected.
Once in the laboratory, samples of groundwater were filtered through a 0.45µm cellulose filter. Ca^{2+} and Mg^{2+} cations were determined using complexometric titration with 0.01 M EDTA. Na^{+} and K^{+} were determined using the flame emission photometric method (Corning Flame Photometer 410). Cl^{-} content was evaluated using a potentiometric method (Mettler Toledo Seven Multi) with an ion-selective electrode (Orion 9716 BN). HCO_3^{-}, SO_4^{2-} and NO_3^{-} content was performed using a multi-parameter colorimeter (Orbeco Hellige MC 500). In February 2013 Chemical analysis about NO_3^{-} were not carried out because of the low concentrations detected in the previous analysis.

3.6 RESULTS

3.6.1 HYDROGEOLOGY

The general hydrogeological pattern did not change substantially from previous representations about the May-July 2004 survey depicted in Fig.3.5 (Capelli and Mazza 2005), but some differences were noticed. In fact the position of the general hydraulic head, identified within the APR, showed a higher elevation of about 5 meters (Fig.3.6 and Fig.3.7). In the Infernetto area a general increase of the water table level was recognized and a more regular Southwestward flow paths trend was identified in the 2012-13 period. This is probably due to the different water management practiced by the local water authority, which forbade the use of groundwater for domestic use. In the area of Ostia Antica and Ostia, water table level was localized below the mean sea level. However the groundwater withdrawals rather decreased, as demonstrated by the reduction of water table depressions, which reached in 2004 a depth up to 5 meters below sea level (Fig.3.5). On the other hand, the differences between the two seasonal surveys didn't show a strong variability of the groundwater scenario. In fact the recharge caused by rainwaters, determined a widening of the coastal hydraulic head of the Castel Fusano Natural Reserve and a reduction of the water table depression of the Ostia and Ostia Antica areas. Furthermore the hydrographic network influences the water table, determining a drop whereby the canal bottom is located below the sea level. The exception is represented by the "High Waters" canals, which hold a concrete riverbed that isolates groundwater from surficial waters.

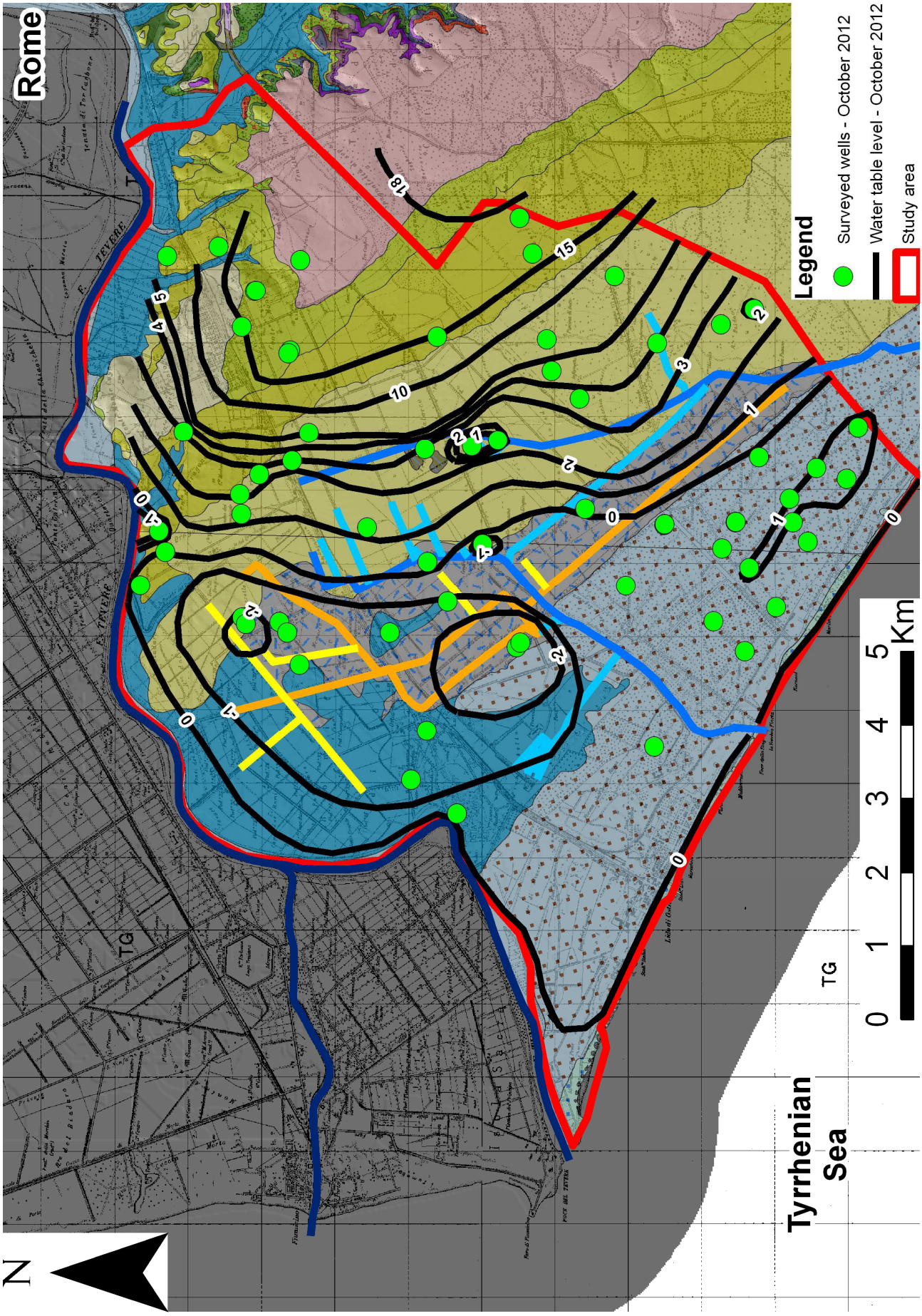

Fig. 3.6:groundwater pattern about October 2012. For the legend see Fig.3.1

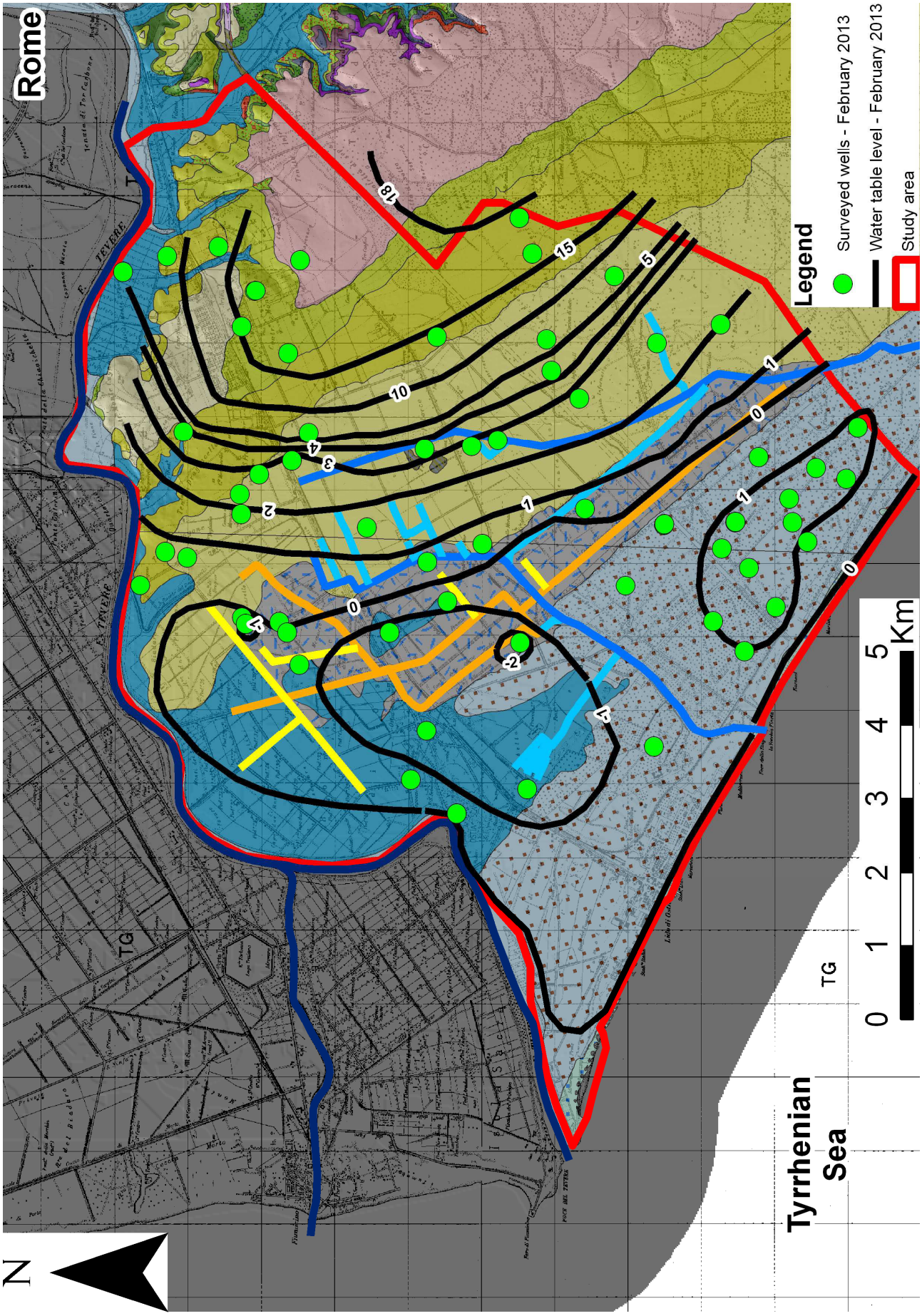

Fig. 3.7: groundwater pattern about February 2012. For the legend see Fig.3.1

3.6.2 GROUNDWATER CHEMISTRY

The results of the chemical analyses of the water samples collected during the surveys are shown in Table 1.1. Data showed a highly variable mineralization, reflected by the EC measurements, which ranged from 559 to 10850 µS/cm, with an average value of 2797 µS/cm. The highest EC values were concentrated along the coastal area and the Tiber River. Waters are mainly slightly acidic to slightly alkaline, with a pH ranging between 5.63 and 8.08, with an average of 6.75.

Sample	Cl^-	Na^+	K^+	HCO_3^-	SO_4^{2-}	NO_3^-	Ca^{2+}	Mg^{2+}	EC (µS/cm)	pH	T(°C)	Sampling date
P1	2.31	3	0.05	9.4	4.06	0.21	11.35	2.67	1054	7.06	19.3	October 2012
P2	2.86	3.44	0.04	9.3	0.75	0.23	9.8	1.07	1102	7.18	18.1	October 2012
P3	1.89	2.32	0.05	9.2	0.49	0.37	9.27	1.07	975	6.92	23	October 2012
P4	7.05	2.55	0.09	9.5	2.45	0.4	15.67	2.67	1551	6.85	18.5	October 2012
P5	1.3	1.43	0.06	7.5	0.39	1.02	8.11	1.6	802	7.27	20.4	October 2012
P6	0.56	0.76	0.03	7.2	0.31	0.13	6.47	1.6	637	6.75	20.7	October 2012
P7	33.09	27.46	0.24	9.5	0.6	0.08	14.57	3.47	4390	7	19.4	October 2012
P8	59.52	41.37	0.26	9.7	0.68	0.18	32.27	2.67	5110	6.35	18.8	October 2012
P9	65.28	55.87	0.32	11.4	1.25	0.26	14.34	11.73	5810	6.3	19	October 2012
P10	8.86	4.34	0.08	6.5	0.39	1.08	8.18	2.67	1434	6.76	20.6	October 2012
P11	27.65	22.3	0.1	11	0.52	0.61	10.24	11.07	3800	6.5	19.7	October 2012
P12	4.09	3.79	1.02	8.7	0.99	1.13	6.75	2.4	1332	6.9	20.2	October 2012
P13	8.58	16.74	0.12	9.5	1.09	0.27	0.8	0.8	1733	7.11	18.5	October 2012
P14	6.32	1.55	0.06	8	0.83	0.31	10.11	3.47	1583	6.46	18.7	October 2012
P15	12.98	10.31	0.82	8.3	0.43	0.08	10.5	0.27	2260	6.48	20.1	October 2012
P16	5.75	3.52	0.14	9.3	0.81	0.31	11.7	0.8	1425	6.41	19.8	October 2012
P17	1.3	3.22	0.55	9.2	0.75	0.34	8.11	0.13	1002	6.29	19.8	October 2012
P18	42.28	38.83	1.58	5.6	0.99	0.08	3.99	1.23	5220	6.12	18	October 2012
P19	2.2	2.57	0.24	7.9	0.39	0.15	7.98	0	954	6.64	20.4	October 2012
P20	5.09	7.09	0.14	9.4	0.44	0.32	7.71	0.27	1355	6.63	19.9	October 2012
P21	3.58	2.31	0.1	7.1	0.29	0.61	7.84	2.27	1172	6.59	19.1	October 2012
P22	15.85	13.53	0.18	9.9	1.14	0.34	13.43	2	2810	6.6	19.1	October 2012
P23	5.36	4.48	0.05	8	1.07	1.74	11.43	1.73	1537	6.61	19.5	October 2012
P24	3.81	4.48	0.12	10.3	0.39	0.6	8.51	1.33	1335	6.48	18	October 2012
P25	1.18	1.96	0.04	9.7	0.65	0.24	7.58	2.53	1099	6.59	19.7	October 2012
P26	2.65	2.48	0.05	11.4	0.78	0.18	11.43	2.4	1467	6.51	19.5	October 2012
P45	0.68	1.22	0.02	6.9	0.88	0	5.57	2.4	814	6.67	19	October 2012
P46	5.22	9.66	1.91	13	0.68	0.06	2.13	3.73	1611	7.64	15.9	October 2012
P47	1.89	3.48	1.96	5.8	4	0	3.86	1.47	1053	8.08	15.3	October 2012
Pz10	1.47	1.52	0.22	12.6	0.21	0	12.37	0.6	772	-	15.7	October 2012
Pz12	0.82	0.91	0.07	6	0.15	0	4.31	1.33	559	-	15.7	October 2012
Pz14	23.79	15.27	0.77	9.8	0.62	0	15.16	4.27	3340	-	16	October 2012
Pz6	8.12	3.87	0.3	6.4	0.45	0	8.64	2.47	1654	-	15.6	October 2012
PzA	2.2	2.26	0.77	8.4	4	0	9.57	2.8	780	-	15.6	October 2012
PzE	91.82	80.17	0.72	5.6	1.66	0.06	4.12	13.07	10850	-	16.3	October 2012
P33	6.09	3.12	0.08	7.8	2.19	-	9.33	4.69	1463	5.61	14.3	February 2013
P38	1.52	1	0.03	4	0.42	-	3.84	0.66	751	7.06	12.8	February 2013
P43	1.3	4.96	0.59	6.8	0.46	-	1.45	1.32	933	7.17	15.4	February 2013
P48	9.82	4.35	0.08	4.39	1.46	-	6.93	2.8	1854	6.88	18.1	February 2013
49	3.75	9.61	0.72	11.39	0.1	-	3.34	3.05	1336	5.95	15.6	February 2013
50	4.74	1.96	1.59	5.39	1.87	-	8.03	1.56	1315	5.88	18.2	February 2013

Table 3.1: Chemical analysis about the 41 wells, collected between October 2012 and February 2013. Concentrations are expressed in meq/l

Groundwater in the study area can be divided in two groups: freshwater (EC<2500 µS/cm) and brackish water (2500 ≤ EC <46700 µS/cm) according to the classification of Freeze and Cherry (1979). Based on this classification the 19.5% of the water samples analyzed can be classified as brackish water type. Box plots in Fig.3.8. show the ionic composition of the fresh and brackish waters and it can be observed how brackish waters are enriched firstly in Na^+ and Cl^- and secondly in Ca^{2+} and Mg^{2+} (Park et al. 2012).

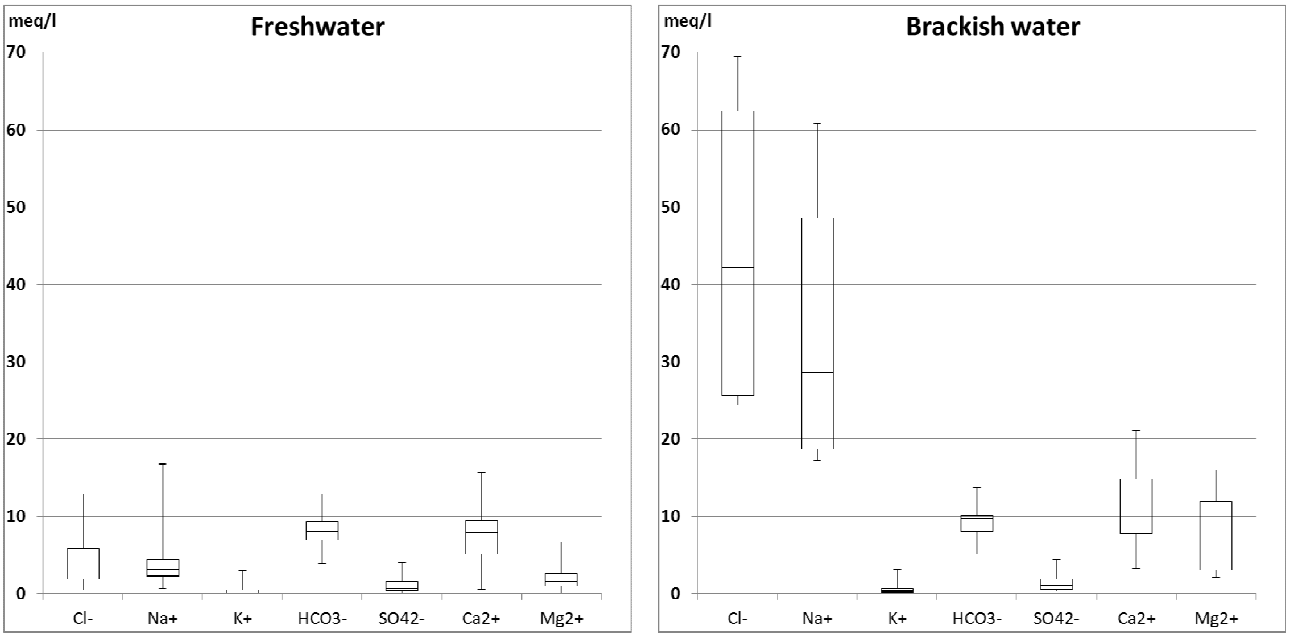

Fig. 3.8: water types according to the classification of Freeze and Cherry (1979). The ionic composition of the water samples shows how brackish water is enriched firstly in Na^+ and Cl^- and secondly in Ca^{2+} and Mg^{2+}

Therefore water mineralization is mainly controlled by Na^+ and Cl^-, positively correlated (R^2 = 0.965 in Fig.3.9) (Park et al. 2012; Duriez et al. 2008; Giambastiani et al. 2012; Pulido-Leboeuf 2004) and their contribution to the overall chemical composition of the groundwater can be shown by the correlation between Cl^- and EC (R^2 = 0.9553 in Fig.3.10) (Cruz et al. 2011; Kelly 2005).

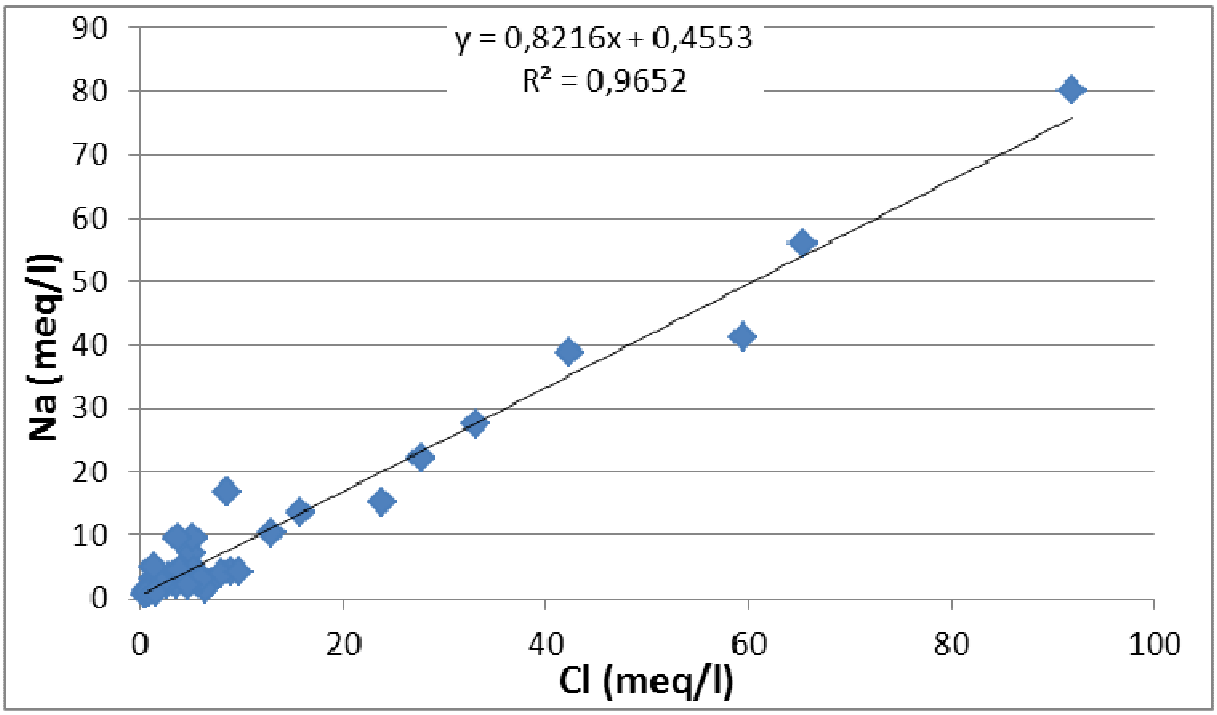

Fig. 3.9: linear correlation between Na^+ and Cl^-

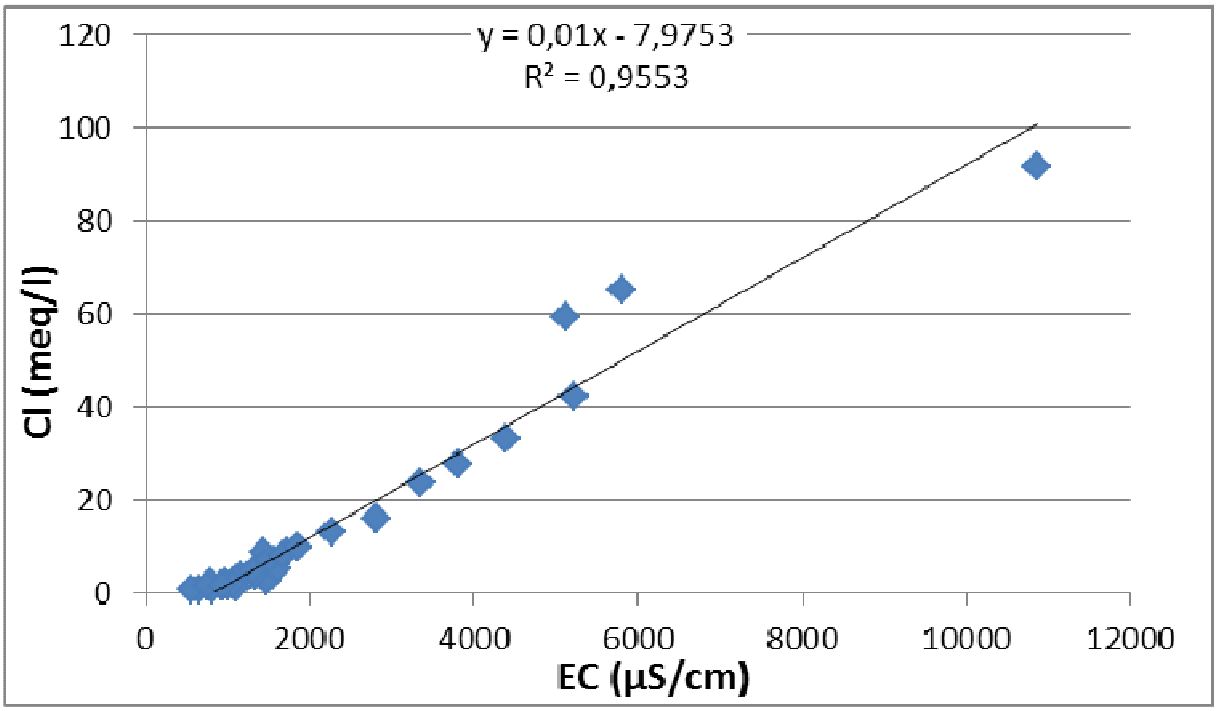

Fig. 3.10: linear correlation between Cl^- and EC

The most represented water type in the study area is $Ca(HCO_3)_2$. In fact, usually the hydrogeochemical composition of coastal groundwater unaffected by seawater intrusion is dominated by Ca^{2+} and HCO_3^- ions (Sung-Wook et al. 2001; Kim et al. 2006; Appelo and Postma 1999).

In the study the area this water type derives from the outcrop of clastic deposits. They derive mostly from the alteration of volcanic deposits erupted by the Alban Hills and the Sabatini Volcanic Complex. The mineralogical composition of these products can be observed in the TAS diagram (Total Alkali Silica) in Fig.3.11 (Le Bas et al. 1986), which represents the main source rocks in terms of volcanism type. Most of the rocks land in basic-intermediate area, characterized by Tephri-Basanites and Phonolites, whose major minerals are Leucite and Clinopiroxene (Diopside and Hedenbergite). A geochemical system can be considered as a dynamic system, in which groundwater and crustal elements interact. In this case the interactions between groundwater and clastic deposits lead to the dissolution of the inorganic phases of the system and/or to the precipitation of new phases. These processes determine the enrichment of new chemical species in the groundwater solution. $CaHCO_3$ water type originates from an incongruent dissolution of the above cited minerals, catalyzed by a slight acidic pH (average pH = 6.75), which indicates the presence of CO_2 in groundwater:

Leucite $2KAlSi_2O_6 + 2H_2CO_3 + H_2O \rightarrow 2K^+ + 2HCO_3^- + 2SiO_2 + Al_2Si_2O_5(OH)_4$ Eq.1

Diopside $CaMgSi_2O_6 + 4CO_2 + 6H_2O \rightarrow Ca^{2+} + Mg^{2+} + 2H_4SiO_4 + 4HCO_3^-$ Eq.2

Incongruent reactions in Eq.1 and Eq.2 can justify the enrichment of Ca^{2+} e HCO_3^- for the $CaHCO_3$ water type. This water type is generally characterized by low TDS content (EC range 600-1500 µS/cm). It consequently infers that a short contact time between minerals and groundwater takes place.

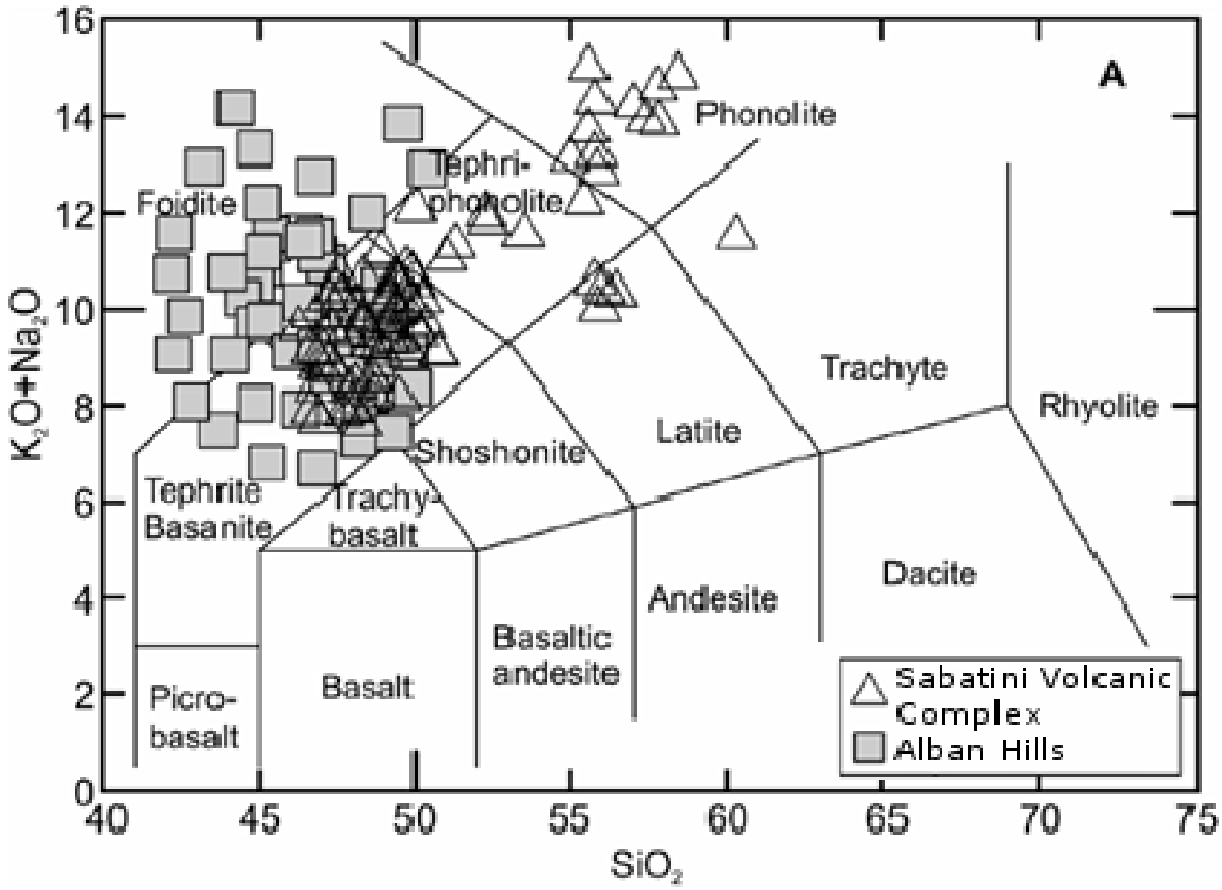

Fig. 3.11: TAS shows the mineralogical composition of the main volcanic products of the Sabatini volcanic Complex and the Alban Hills (after Le Bas et al. 1986). Most of the rocks land in basic-intermediate area, characterized by Tephri-Basanites and Phonolites, whose major minerals are Leucite and Clinopiroxene (Diopside and Hedenbergite)

Therefore the compositional end members in the coastal areas are $Ca(HCO_3)_2$ (freshwater) and the NaCl (seawater-derived) water types. If there is a conservative mixing with pure seawater (without any ionic exchange), the chemical composition of groundwater should plot along a straight line (red line in Fig.3.12). In case the points are located above or below the straight red line, it means that a process of cation exchange may occur. It takes place when an aquifer is subject to seawater contamination (Appelo and Postma 1999; Cruz and Silva 2000; Park et al. 2012; Kim et al. 2006; Capaccioni et al. 2005) and a cation exchanger, composed by clayey levels (Custodio and Llamas 2005b; Schoeller 1965), acts mainly on Ca^{2+} and Mg^{2+} or Na^{+} (Custodio and Llamas 2005a).

Appelo and Postma (1999) described the cation exchange with two equations:

$$Na^{+} + ½\ Ca\text{-}X_2 \rightarrow Na\text{-}X + ½\ Ca^{2+} \qquad \text{Eq.(3)}$$

$$½\ Ca^{2+} + Na\text{-}X \rightarrow ½Ca\text{-}X_2 + Na^{+} \qquad \text{Eq.(4)}$$

where X indicates the soil exchanger (site).

By the Eq.3, Na^{+} is taken up by the exchanger and Ca^{2+} is consequently released into the water phase. This happens when seawater, richer in Na^{+} content, intrudes a fresh coastal aquifer. The result will be a $CaCl_2$ water type. The reverse process, known as freshening and described by Eq.4, happens when freshwater goes to occupy again an aquifer in which seawater previously intruded; in this case a $NaHCO_3$ water type forms, enriched in Na^{+}, released by the cation exchanger which adsorbs the Ca^{2+} of freshwater.

Plotting the data in a Piper Diagram, based on the relative proportion of major ions, it was possible to determine the main water types of the study area, surveyed in October 2012 and February 2013 (Fig.3.12).

The Piper Diagram shows the presence of all the water types, proving that processes of ion exchange occur in the study area.

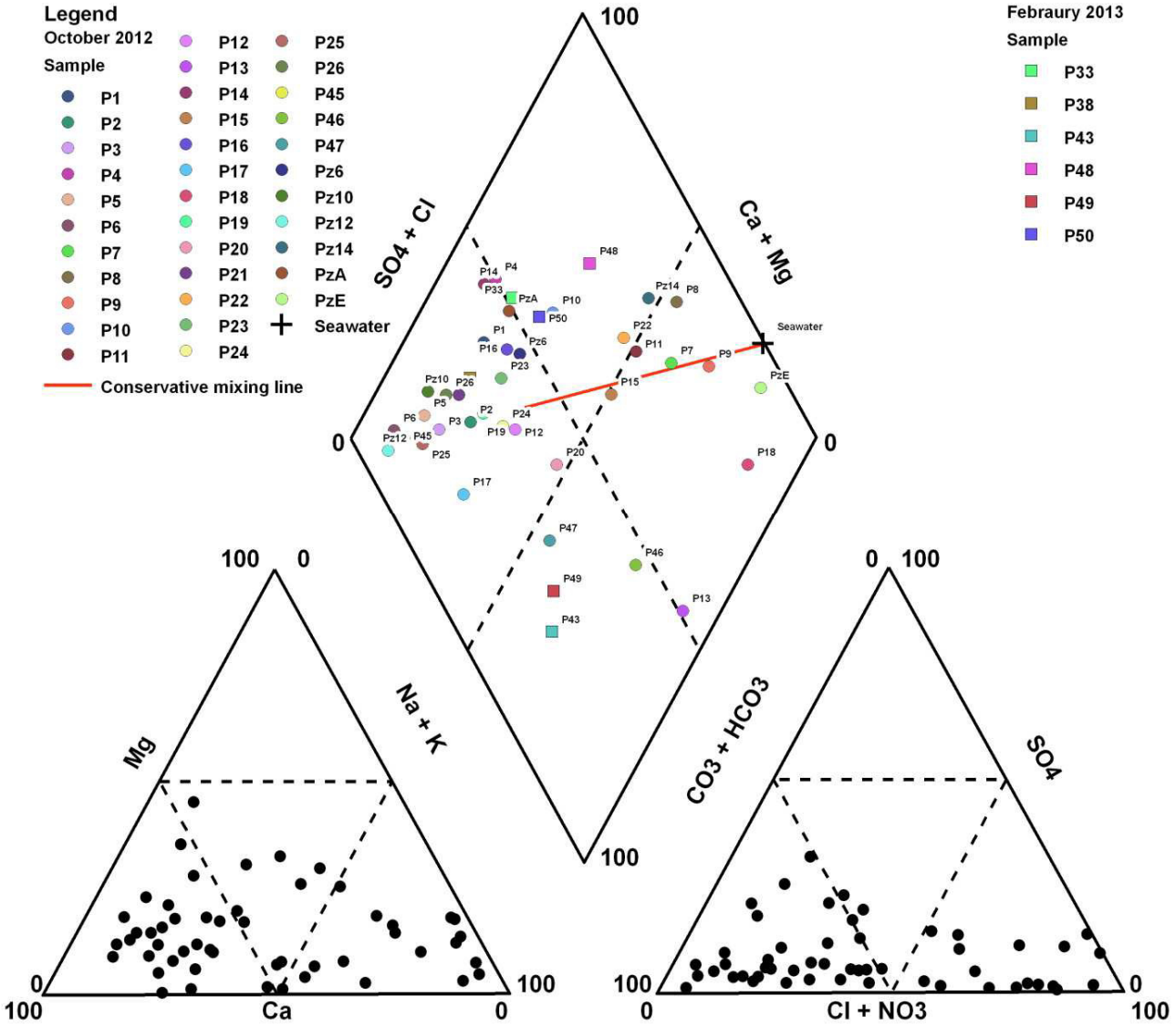

Fig. 3.12: data samples about the October 2012 and February 2013 plotted in the Piper Diagram. It shows how all the water types are represented in the study area. If there is a conservative mixing with pure seawater, the chemical composition of groundwater should plot along the straight red line (red line). In case the points are located above or below the straight red line, it means that a process of cation exchange is occurring. It takes place when an aquifer is subject to seawater contamination and a cation exchanger, composed by clayey levels, acts mainly on Ca^{2+} and Mg^{2+} or Na^{+}

3.7 DISCUSSION

Fig.3.13 shows the main hydrochemical families and their distribution in the study area. All the water families are represented and it indicates that different processes affect groundwater chemistry.

$Ca(HCO_3)_2$ resulted to be the most represented water family for the above mentioned processes. It is mostly located in the central part of the area, where the sandy and gravelly deposits that form the APR outcrop. Other water families are present along the borders of the study area. Each of them is located in one peculiar sector and is related to different types of seawater-freshwater interaction.

NaCl water type is well represented in the area of Ostia Antica, which is characterized by groundwater and ground levels below the mean sea level. The reason of the salinization sources could be different:

- Capelli et al. (2007) observed that in summertime, draining pumps located along the Tiber course, input occasionally river waters for agricultural use in the "High Waters" canals. Given that in the Tiber River a salt-

wedge intrusion was noticed mouth (Manca et al. 2014; Capelli et al. 2007; Mikhailova et al. 1999), the salinization could be induced by an anthropic inflow of Tiber seawater;

- seawater of the Tiber River could be caught by the well pumping for agricultural use occurring in the alluvial plain (Barlow 2003);
- the different hydraulic head between the Tiber River level in correspondence of the alluvial plain (above the mean sea level) and groundwater level in Ostia Antica area (below the mean sea level), could determine a lateral inflow of Tiber seawater to groundwater system, through the multi-layered alluvial deposits of the HST (in ciano, cross section "a" in Fig.3.3).

An anomaly is represented by PzE, located in the LRNR, nearby the filled Stagno di Ostia Pond. Highest EC values (10850 µS/cm) and consequently Cl^- content (91.82 meq/l) were noticed in this piezometer. It is about 30 m deep and it is located nearby another 35 m deep well (PzA), that showed a low EC (780 µS/cm) and a $Ca(HCO_3)_2$ water type. The high salinity could come from a conservative mixing between freshwater and paleo-salty waters. In fact Tran et al. (2012) noticed that paleo-salty waters can be trapped in the sediments of alluvial plains. According to the geological cross section "a" in Fig.3.3, the paleo-salty aquifer should be composed by the sand and silty sands of the coastal barrier deposits of the Early LST of the TDS. These deposits are confined upward by the silty clays and lagoon clays of the TST (Milli et al. 2013). Historical EC values of groundwater about PzE in the 2003-2012 time frame (Fig.3.14) show a decrease of the EC of about 15000 µS/cm. It likely means that the well drilling connected the previous isolated deep aquifer with the shallower one, causing a freshwater dilution.

As stated above $CaCl_2$ and $NaHCO_3$ water types can derive from ion exchange due to seawater intrusion/freshening processes. Nevertheless not all the water samples were subject to ion exchange processes. To detect where these processes occurred, the Base Exchange Indexes (BEX) were calculated (Schoeller 1962; Cruz et al. 2011). BEX are frequently used in regional hydrochemical surveys, for indicating whether an aquifer is salinizing or freshening, or has been freshened or salinized in the past (Stuyfzand 2008). BEX are defined as (Custodio and Llamas 2005a):

$$BEX = \frac{rCl - r(Na+K)}{rCl} \qquad \text{Eq.(5)}$$

where *r* is the meq/l concentration of the relative ion.

When a positive exchange index is present, it indicates that Na^+ and K^+ have changed Ca^{2+} and Mg^{2+}, as a consequence of seawater intrusion; when the value is negative it means that a freshening occurred. Fig.3.15 shows the BEX about all the water samples except those about the $Ca(HCO_3)_2$ water type.

Negative BEX values are related to the $NaHCO_3$ water type, that was noticed in wells (P13, P43, P46 and P47) located in the Ostia Antica area, where the Tiber River alluvial deposits outcrop. These deposits constitute a multilayered aquifer, which contains more clayey levels and therefore more ionic exchanger. This water type probably represents the partly flushed remains of anciently entrapped saline water bodies (Mercado 1985). As stated above, Ostia Antica was completely reclaimed starting from 1884 (Amenduni 1884). Before that period the area of the Ostia Antica Town was used as solar salt works. Solar salt works, with a rectangular shape, were linked to the Stagno di Ostia Pond (reclaimed in the 1880's), which in turn, was linked to the sea through the Stagno Canal (Fig.3.15). Contamination of soil and groundwater could be determined either by the infiltration of a part of seawater from salt works through the soil and consequently into phreatic aquifers (Angelopoulos and Nicolaou 2002; Cheng and Ouzar 2004), or could come from salty deposits buried in the alluvial plain (Capelli et al. 2007). A different hypothesis must be made for P49: in fact it is located far from the salt works area, near the Tiber River course. It could represent the remnants of salt-groundwater deriving from an older salt-wedge intrusion occurred along the river bottom and freshened by the action of the fresh river waters and rains.

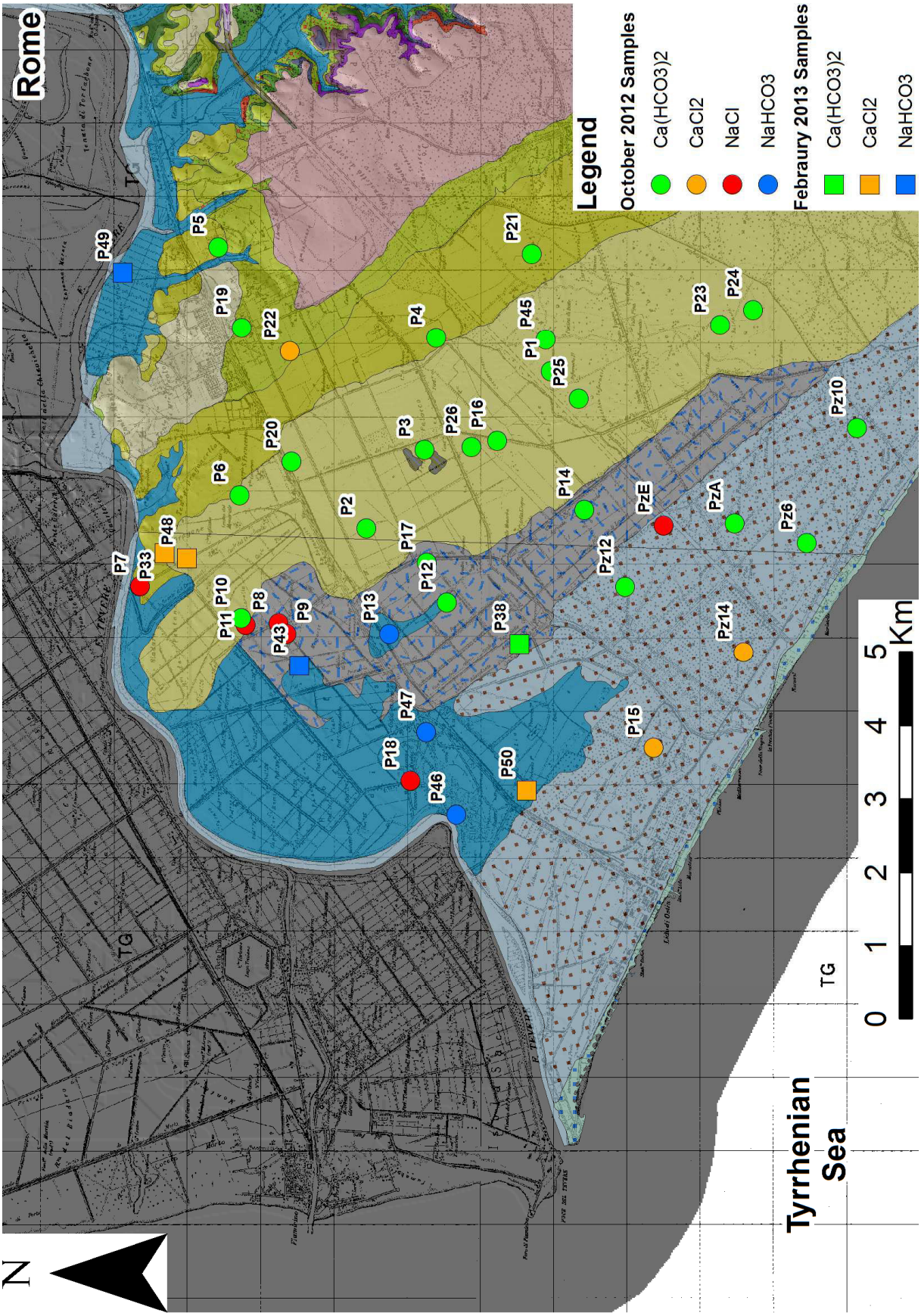

Fig. 3.13: localization of the water types in the study area. The largest group of water samples is composed by $Ca(HCO_3)_2$.They are mainly located in the central part of the study area, where the sandy and gravelly deposits that form the APR outcrop. The $CaCl_2$ water type is disposed along the borders of the study area, near the sea and Tiber River. this water type is typical of areas subject to salinization of groundwater. It can be produced by two main processes in the study area: mixing deriving by an intrusion of seawater and SSA contamination. The last the $NaHCO_3$ water type was noticed in wells located in the Tiber River alluvial deposits, containing more clayey levels and therefore more ionic exchanger. They probably represent the partly flushed remains of an anciently entrapped saline water body

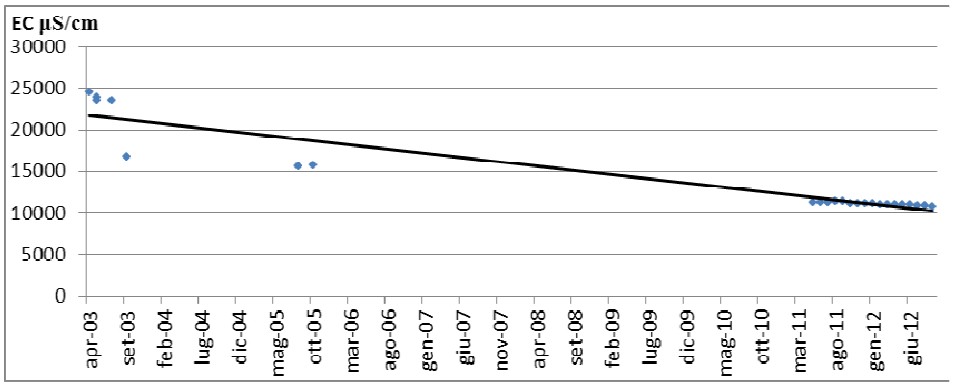

Fig. 3.14: EC values about PzE from April 2003 to September 2012. Its salinity could be due to the presence of connate paleo-salty water, reached by the well bottom. The decreasing EC trend could be connected to a a freshwater dilution of the paleo-salty deep waters caused by the fresher surficial groundwater

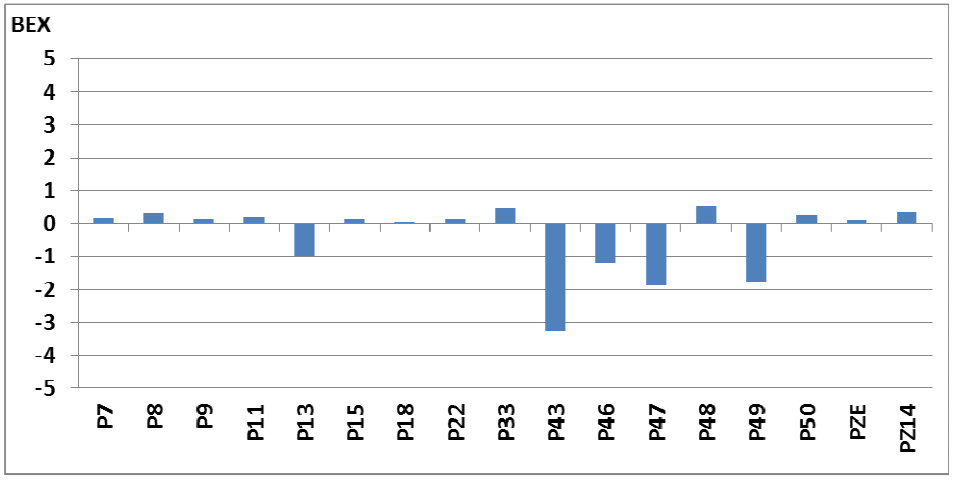

Fig. 3.15: BEX are useful to evaluate the salinization of a coastal aquifer. When a positive BEX is present, it indicates that Na^+ and K^+ have changed Ca^{2+} and Mg^{2+}, determined by seawater intrusion; when the value is negative it means that a freshening occurred and Ca^{2+} and Mg^{2+} have changed Na^+ and K^+

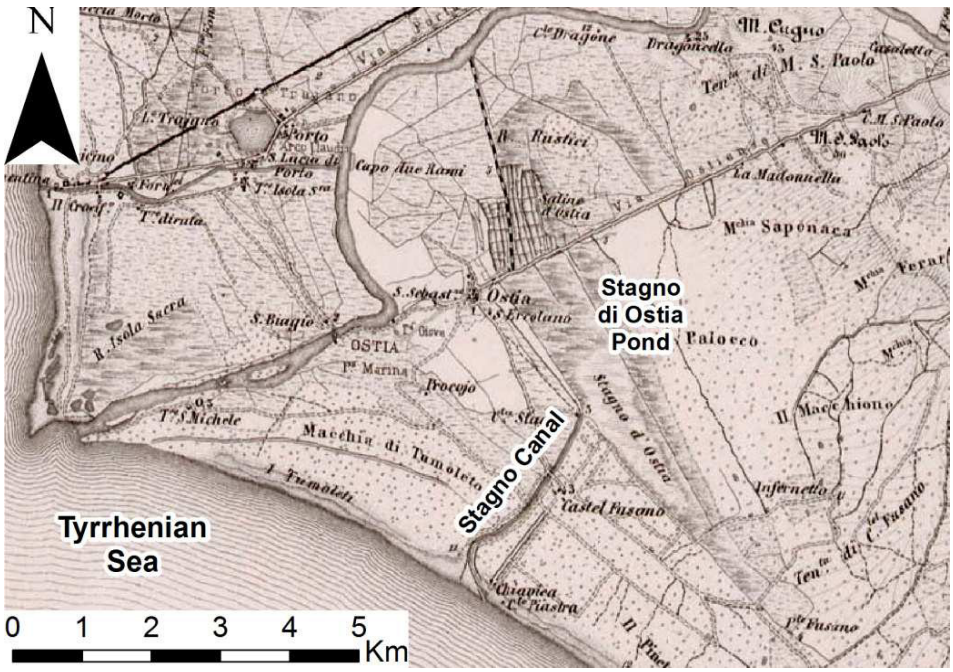

Fig. 3.16: historical map of the Tiber Delta area (IGM 1880). The solar salt works were linked to the Stagno di Ostia Pond via a canal. Stagno di Ostia Pond, in turn, was linked to the sea through the Stagno Canal

$CaCl_2$ water type is disposed along the borders of the study area, near the sea and Tiber River (except P22) and it is characterized by high Cl^- content. The slightly positive BEX values depicted in Fig.3.14 suggest that ion exchange processes related to seawater intrusion processes can be supposed for P33 and P48, located nearby a well (P7) where seawater intrusion was noticed. Along the coast line it is likely related to the presence of pine forests and the seawater spraying. In fact seawater spraying is a mechanism that can contribute along the rain action to determine groundwater evolution and mineralization (Berner and Berner 2012; Carreira et al. 2010; Tuccimei et al. 2010). Tall trees presence represents a barrier for the sea spray aerosols (SSA), mostly composed by particles of Na^+ and Cl^-. In fact, SSA is transported by western winds and accumulate on the pine forest foliage. Once a rainy event occurs, the water flushes the salts from the tree foliage and moves them to groundwater, increasing the salinity. The wells located along the coast line (P15, P50 and Pz14) show Values of BEX close to zero and they are hence related to sea spray aerosol deposition. The diagram in Fig.3.17 shows the water samples chemistry of the piezometers located in the LRNR, in which a decreasing salinity was noticed moving away from the coast line (see chapter 2). The diagram represents the evolution from $CaCl_2$ to NaCl water type by means of the ratio among HCO_3^-/Cl^- (main anions) and Ca^{2+}/Na^+ (main cations). In absence of cation exchange, an addiction of Na+ and Cl- coming from SSA occurs. This contributions determines a reduction of the HCO_3^-/Cl^- and Ca^{2+}/Na^+ ratios and a consequent migration to the NaCl sector of the diagram, passing through the $CaCl_2$ sector. In this case the $NaHCO_3$ water type will not develop, because the concentration of Ca^{2+} and HCO_3^- keeps constant in groundwater.

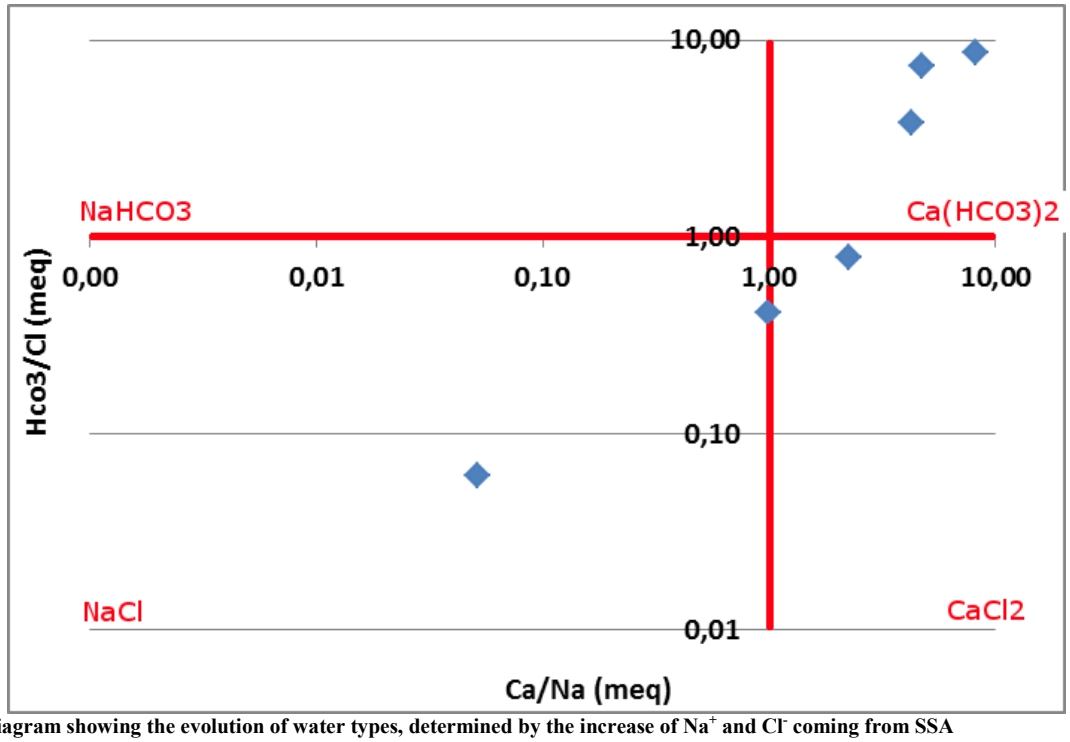

Fig. 3.17: diagram showing the evolution of water types, determined by the increase of Na^+ and Cl^- coming from SSA

3.8 CONCLUSIONS

This study allowed to evaluate the modification of the water table morphology occurring between October 2012 and February 2013. In general in the rainy period the coastal hydraulic head of the Castel Fusano Natural Reserve enlarged, while the groundwater depression of the Ostia and Ostia Antica area reduced. The water table patterns resulted to be strictly related to the morpholgy of the area and the hydraulic head which governates groundwater flows is located in correspondence of the APR. The seasonal variation didn't affect substantially the morphology of the APR hydraulic head.

Furthermore groundwater morphology showed strict connections with the artificial hydrographical network. Water table exhibited a drop in correspondence of "Low Waters" canals. A significant modification of the groundwater pattern was recognized with respect to previous works (Capelli and Mazza 2005). It is probably due to the different water management applied in the Infernetto area, where the local water authority prohibited groundwater pumping.

From the APR flow paths direct toward the sea and toward the Tiber River, except for the alluvial area of Ostia and Ostia Antica. In fact the water level of the Tiber in correspondence of the alluvial plain results to be higher than water table level and, as a consequence, a lateral inflow from the river may occur.

The hydraulic gradient toward the alluvial plain could be the source of salinization due to the presence of seawater about a salt-wedge intrusion in the Tiber River bottom mouth (Manca et al. 2014; Capelli et al. 2007; Mikhailova et al. 1999). The sandy deposits of the alluvial multi-layered aquifer may be the vehicle to move the salinization inland. Furthermore the process could be accelerated by agricultural withdrawals in the alluvial plain (Barlow 2003). Also the occasional inflow of water from the Tiber in the drainage canal system, acted by the draining pumps located along the Tiber course, may input seawater in the hydrogeological system (Capelli et al. 2007).

Chemical analysis were effectuated for 41 water samples. The distribution in the Piper diagram showed that all the water types are present in the area and that ion-exchange processes took place.

The salinization pattern was proved by the NaCl water type. It is located mostly in the alluvial plain, while in the surrounding area, the most represented water type was the $Ca(HCO_3)_2$. The presence of a high salinity well far from the alluvial plain is probably related to paleo-salty waters included in the early deposits of the TDS.

$CaCl_2$ water type was identified as well and it is probably due to two main processes:

1. in the alluvial plain it likely represents the salinization process of fresher water due to ion-exchange induced by pumping (Appelo and Postma 1999). It is demonstrated by positive values of BEX;
2. along the coast line the salinization is determined by SSA deposition on the tree foliage (see chapter 2; Tuccimei et al 2010). $CaCl_2$ originates from the Na^+ and Cl^- supply acted by SSA, that determinates an evolution of the $Ca(HCO_3)_2$ water type.

$NaHCO_3$ was the last water type recognized in the study area and it is located in the alluvial plain as well. $NaHCO_3$ water type is usual in ion exchange processes deriving from freshening. This water type probably represents the partly flushed remains of anciently entrapped saline water bodies (Mercado 1985).

The ancient saline water bodies could have been originated by the solar salt works, existing in the Ostia Antica town until the 1890's. Salt works could have determined groundwater salt pollution as a consequence of soil contamination (Angelopoulos and Nicolaou 2002; Cheng and Ouzar 2004). The reclamation activities as well could be responsible of the salinization because they could have produced a burial of salty deposits in the alluvial plain (Capelli et al. 2007).

Although several hypothesis about the salinization processes affecting the study area have been advanced, further chemical analyses should be improved to discriminate the salinization sources, using for example the Br/Cl ratio (Panno et al. 2006; Sung-Wook et al. 2001). In fact the Br/Cl ratio can be an important tool to discriminate salinization sources due to the different values it assumes for seawater intrusion, sea spray aerosols and halite dissolution processes (Davis et al. 1998; Winchester and Duce 1967)

In this way a more accurate understanding about the salinization processes occurring in the Tiber Delta area could be reached.

3.9 REFERENCES

Amenduni G (1884) Sulle opere di bonificazione della plaga litoranea dell'Agro Romano che comprende le paludi e gli stagni di Ostia, Porto, Maccarese e delle terre vallive di Stracciacappa, Baccano, Pantano e Lago dei Tartari. Relazione del progetto generale 15/7/1880. Ministero Lavori Pubblici,

Amorosi A, Milli S (2001) Late Quaternary depositional architecture of Po and Tevere river deltas (Italy) and worldwide comparison with coeval deltaic succession. Sedimentary Geology 144:357-375

Angelopoulos C, Nicolaou E (2002) Salt works and their impact on soil and groundwater. The case study of Angelohori and Kristos, Greece. Studia Universitatis Babes-Bolyai, Geologia 48 (2):3-12

Anselmi B, Blasi L, Brandimarte U, Brondi M, Bucci M, Caprioli R, Cautilli F, Collepiccolo R, Crovato C, Farneti G, Ghiara E, Girolimetti G, Grillini M, Milli M, Vincenzi D (1995) Monitoraggio idrogeologico – Studi idrogeologici e monitoraggio delle falde. Paper presented at the Progetto di Monitoraggio ambientale della Tenuta di Castelporziano, Creazione di un Sistema Informativo Territoriale Ambientale Castelporziano (SITAC), Castelporziano, Roma, 12 maggio 1995

Antonellini M, Mollema P, Giambastiani B, Bishop K, Caruso L, Minchio A, Pellegrini L, Sabia M, Ulazzi E, Gabbianelli G (2008) Salt water intrusion in the coastal aquifer of the southern Po Plain, Italy. Hydrogeology Journal 16 (8):1541-1556. doi:10.1007/s10040-008-0319-9

Appelo CAJ, Postma D (1999) Ion exchange and sorption. In: Geochemistry, Groundwater and Pollution. 4th edn. A.A. Balkema, Rotterdam, Netherlands, pp 142-198

Bakker TWM (1990) The geohydrology of coastal dunes. In: Th.W. Bakker PDJ, amp, Klijn JA (eds) Dunes of the European Coasts. vol 18. Catena Supplement, Destedt-Cremlingen, pp 109-119

Barker AP, Newton RJ, Bottrell SH, Tellam JH (1998) Processes affecting groundwater chemistry in a zone of saline intrusion into an urban sandstone aquifer. Applied Geochemistry 13 (6):735-749. doi:10.1016/s0883-2927(98)00006-7

Barlow PM (2003) Salwater Intrusion from the Delaware River During Drought-Implications for the Effect of Sea-Level Rise on Coastal Aquifers. In: Ground Water in Freshwater-Saltwater Environments of the Atlantic Coast. U.S. Geological Survey, Reston, Virginia, USA, pp 46-48

Barlow PM, Reichard EG (2010) Saltwater intrusion in coastal regions of North America. Hydrogeology Journal 18 (1):247-260. doi:10.1007/s10040-009-0514-3

Bear J, Cheng AH-D, Sorek S, Ouzer D, Herrera I (1999) Geophysical investigations. In: Jacob Bear AHDCSSDO, Ismael H (eds) Seawater Intrusion in Coastal Aquifers - Concepts, Methods and Practises. Kluwer Academic Publishers, Dordrecht, The Nederlands, pp 9-50

Bellotti P, Biagi PF, Tortora P, Valeri P (1987) Il delta del Tevere: caratteri morfologici e sedimentologici della piana deltizia. Giornale di Geologia 49 (1):89-99

Bellotti P, Calderoni G, Carboni MG, Di Bella L, Tortora P, Valeri P, Zernitskaya V (2007) Late Quaternary landscape evolution of the Tiber River delta plain (Central Italy): new evidence from pollen data, biostratigraphy and C-14 dating. Zeitschrift Fur Geomorphologie 51 (4):505-534. doi:10.1127/0372-8854/2007/0051-0505

Bellotti P, Calderoni G, Di Rita F, D'Orefice M, D'Amico C, Esu D, Magri D, Martinez MP, Tortora P, Valeri P (2011) The Tiber river delta plain (central Italy): Coastal evolution and implications for the ancient Ostia Roman settlement. Holocene 21 (7):1105-1116. doi:10.1177/0959683611400464

Bellotti P, Carboni MG, Milli S, Tortora P, Valeri P (1989a) La piana deltizia del Fiume Tevere: analisi di facies e ipotesi evolutiva dall'ultimo lowstand glaciale all'attuale. Giornale di Geologia 51 (1):71-91

Bellotti P, Chiocci FL, Milli S, Tortora P, Valeri P (1994) Sequence stratigraphy and depositional setting of the Tiber Delta - integration of high-resolution seismic, well logs and archaeological data. Journal of Sedimentary Research Section B-Stratigraphy and Global Studies 64 (3):416-432

Bellotti P, Milli S, Tortora P, Valeri P (1995) Physical stratigraphy and sedimentology of the Late Pleistocene-Holocene Tiber Delta depositional sequence. Sedimentology 42 (4):617-634. doi:10.1111/j.1365-3091.1995.tb00396.x

Bellotti P, Tortora P, Valeri P (1989b) Sedimentological and morphological features of the Tiber Delta Sedimentology 36 (5)

Berner EK, Berner RA (eds) (2012) The global water cycle, geochemistry and environment. 2nd edn. Princeton University Press, Woodstock, UK

Bobba AG (2002) Numerical modelling of salt-water intrusion due to human activities and sea-level change in the Godavari Delta, India. Hydrological Sciences Journal-Journal Des Sciences Hydrologiques 47:S67-S80

Boni C, Bono P, Capelli G (1988) Carta Idrogeologica del territorio della Regione Lazio. Scala 1:250.000. Pubblicazione Speciale Regione Lazio Vol. Unico. Studio Marinelli, Roma

Bordoni P, Valensise G (1998) Deformation of the 125 ka Marine Terrace in Italy: Tectonic Implications, vol Special Pubblication. Coastal Tectonics, vol 146. Geological Society London, London

Bucci M, Grillini M (2001) Studi geologici, geomorfologici e idrogeologici sulla Tenuta Presidenziale di Castelporziano. Geologia Tecnica & Ambientale 4:21-32

Capaccioni B, Didero M, Paletta C, Didero L (2005) Saline intrusion and refreshening in a multilayer coastal aquifer in the Catania Plain (Sicily, Southern Italy): dynamics of degradation processes according to the hydrochemical characteristics of groundwaters. Journal of Hydrology 307 (1-4):1-16. doi:10.1016/j.jhydrol.2004.08.037

Capelli G, Mastrorillo L, Mazza R, Petitta M, Baldoni T, Banzato F, Cascone D, Di Salvo C, La Vigna F, Taviani S, Teoli P (2012) Carta Idrogeologica del Territorio della Regione Lazio. Scala 1:100.000 (4 Fogli). S.EL.CA., Firenze - Italy

Capelli G, Mazza R (2005) Schema idrogeologico della Città di Roma. Gestione della risorsa idrica e del rischio idrogeologico. Geologia dell'Ambiente 4 (supplemento):47-58

Capelli G, Mazza R, Gazzetti C (2005) Strumenti e strategie per la tutel e l'uso compatibile della risorsa idrica nel Lazio, vol 78. Quaderni di Tecniche di Protezione Ambientale. Bologna

Capelli G, Mazza R, Papiccio C (2007) Saline intrusion in the Tiber Delta. Geology, hydrology and hydrogeology of the coastal plain of the roman sector. Giornale di Geologa Applicata 5:13-28

Carboni MG (1993) Contributo alla stratigrafia del Quaternario laziale. Il Quaternario 6:27-37

Carreira PM, Marques JM, Pina A, Mota Gomes A, Galego Fernandes PA, Monteiro Santos F (2010) Groundwater Assessment at Santiago Island (Cabo Verde): A Multidisciplinary Approach to a Recurring Source of Water Supply. Water Resources Management 24:1139–1159. doi:10.1007/s11269-009-9489-z

Cheng AH-D, Ouzar D (2004) Coastal aquifer management - monitoring, modeling, and case study. CRC Press,

Cioni R, Laurenzi MA, Sbrana A, Villa IM (1993) 40Ar/39Ar chronostratigraphy of the initial activity in the Sabatini Volcanic Complex (Italy). Bollettino della Societa Geologica Italiana 112:251-263

Conato V, Esu D, Malatesta A, Zarlenga F (1980) New data on the Pleistocene of Rome. Quaternaria 22:131-176

Cruz JV, Coutinho R, Pacheco D, Cymbron R, Antunes P, Freire P, Mendes S (2011) Groundwater salinization in the Azores archipelago (Portugal). Environmental Earth Sciences 62 (6):1273-1285. doi:10.1007/s12665-010-0615-2

Cruz JV, Silva MO (2000) Groundwater salinization in Pico Island (Azores, Portugal): origin and mechanisms. Environmental Geology 39 (10):1181-1189

Custodio E (2010) Coastal aquifers of Europe: an overview. Hydrogeology Journal 18 (1):269-280. doi:10.1007/s10040-009-0496-1

Custodio E, Llamas MR (2005a) Apporto di sali e fenomeni modificatori. In: Flaccovio D (ed) Idrologia sotterranea, vol 1. Palermo, pp 958-968

Custodio E, Llamas MR (2005b) Elementi di chimica delle acque. In: Flaccovio D (ed) Idrologia sotterranea, vol 1. Palermo, pp 171-189
Custodio E, Llamas MR (2005c) Superfici piezometriche. In: Flaccovio D (ed) Idrologia sotterranea, vol 1. Palermo, pp 511-528
Davis SN, Whittemore DO, Fabryka-Martin J (1998) Uses of chloride/bromide ratios in studies of potable water. Ground Water 36 (2):338-350. doi:10.1111/j.1745-6584.1998.tb01099.x
De Rita D, Fabbri M, Mazzini I, Paccara P, Sposato A, Trigari A (2002) Volcanoclastic sedimentation in coastal environments: the interplay between volcanism and Quaternary sea level changes (central Italy). Quaternary International 95-6:141-154. doi:10.1016/s1040-6182(02)00035-6
De Rita D, Funiciello R, Corda L, Sposato A, Rossi U (1993) Volcanic Unit. In: Di Filippo M (ed) Sabatini Volcanic Complex, vol 11. Progetto Finalizzato " Geodinamica " Monografie Finali. Consiglio Nazionale Delle Ricerche, Roma, pp 33-79
De Rita D, Milli S, Rosa C, Zarlenga F, Cavinato GP (1994) Catastrophic eruptions and eustatyc cycles: example of Lazio volcanoes. Paper presented at the Atti dei Convegni Lincei, Roma,
Duriez A, Marlin C, Dotsika E, Massault M, Noret A, Morel JL (2008) Geochemical evidence of seawater intrusion into a coastal geothermal field of central Greece: example of the Thermopylae system. Environmental Geology 54 (3):551-564. doi:10.1007/s00254-007-0857-9
Essink GHPO, van Baaren ES, de Louw PGB (2010) Effects of climate change on coastal groundwater systems: A modeling study in the Netherlands. Water Resources Research 46. doi:10.1029/2009wr008719
Farid I, Trabelsi R, Zouari K, Abid K, Ayachi M (2013) Hydrogeochemical processes affecting groundwater in an irrigated land in Central Tunisia. Environmental Earth Sciences 68 (5):1215-1231. doi:10.1007/s12665-012-1788-7
Freeze RA, Cherry JA (1979) Groundwater. Englewood Cliffs, New Jersey
Funiciello R, Giordano G (2008) Note illustrative della Carta Geologica d'Italia alla scala 1:50000, Foglio 374 Roma.
Funiciello R, Giordano G, Mattei M (2008) Carta Geologica del Comune di Roma 1:50000. Firenze
Giambastiani B, Mastrocicco M, Colombani N, Severi P (2012) Salinization and Freshening Processes in Coastal Aquifer of Ferrara (Italy) Paper presented at the BALWOIS 2012 - International Scientific Conference on Water, Climate and Environment, Ohrid, Republic of Macedonia, 28 May - 2 June 2012
Giambastiani BMS, Antonellini M, Essink GHPO, Stuurman RJ (2007) Saltwater intrusion in the unconfined coastal aquifer of Ravenna (Italy): A numerical model. Journal of Hydrology 340 (1-2):91-104. doi:10.1016/j.jhydrol.2007.04.001
Gimenez E, Morell I (1997) Hydrogeochemical analysis of salinization processes in the coastal aquifer of Oropesa (Castellon, Spain). Environmental Geology 29 (1-2):118-131
Giordano G, Esposito A, De Rita D, Fabbri M, Mazzini I, Trigari A, Rosa C, Funiciello R (2003) he sedimentation along the roman coast between middle and upper Pleistocene: the interplay of eustatism, tectonics and volcanism – new data and review. Il Quaternario 16 (1bis):121-129
Giraudi C (2011) The sediments of the 'Stagno di Maccarese' marsh (Tiber river delta, central Italy): A late-Holocene record of natural and human-induced environmental changes. Holocene 21 (8):1233-1243. doi:10.1177/0959683611405235
IGM (1880) Cerveteri, Foglio 149. Carta Topografica d'Italia scala 1:100.000. Roma
Karner DB, Marra F, Renne PR (2001) The history of the Monti Sabatini and Alban Hills volcanoes: groundwork for assessing volcanic-tectonic hazards for Rome. Journal of Volcanology and Geothermal Research 107 (1-3):185-219. doi:10.1016/s0377-0273(00)00258-4
Kelly D (2005) Seawater intrusion Topic Paper. vol 6. WRIA, Island County
Kim RH, Kim JH, Ryu JS, Chang HW (2006) Salinization properties of a shallow groundwater in a coastal reclaimed area, Yeonggwang, Korea. Environmental Geology 49 (8):1180-1194. doi:10.1007/s00254-005-0163-3
Lambeck K, Yokoyama Y, Purcell T (2002) Into and out of the Last Glacial Maximum: sea-level change during Oxygen Isotope Stages 3 and 2. Quaternary Science Reviews 21 (1-3):343-360. doi:10.1016/s0277-3791(01)00071-3
Le Bas MJ, Le Maitre RW, Streckeisen A, Zanettin (1986) A chemical classification of volcanic rocks based on the total alkali - silica diagram. . Journal of Petrology 27:745-750
Locardi E, Lombardi G, Funiciello R, Parotto M (1976) The main volcanic group of Lazio (Italy): relations between structural evolution and petrogenesis. Geologica Romana 15:279-300
Maas K (2007) Influence of climate change on a Ghijben-Herzberg lens. Journal of Hydrology 347 (1-2):223-228. doi:10.1016/j.jhydrol.2007.09.020
Malatesta A, Zarlenga F (1986) Evoluzione paleogeografico-strutturale plio-pleistocenica del basso Bacino Romano a Nord e a Sud del Tevere. Memorie della Società Geologica Italiana 35:75-85
Manca F, Capelli G, La Vigna F, Mazza R, Pascarella A (2014) Wind-induced salt-wedge intrusion in the Tiber river mouth (Rome–Central Italy). Environmental Earth Sciences January 2014. doi:10.1007/s12665-013-3024-5
Marra F, Rosa C, De Rita D, Funiciello R (1998) Stratigraphic and tectonic features of the Middle Pleistocene sedimentary and volcanic deposits in the area of Rome (Italy). Quaternary International 47-8:51-63. doi:10.1016/s1040-6182(97)00070-0
Mastrorillo L, Petitta M (2009) La rete di monitoraggio idrogeologico della tenuta presidenziale di Castelporziano (Roma). Engineering Hydro Environmental Geology 12:187-198. doi:10.1474/EHEGeology.2009-12.0-16.0273
Mercado A (1985) The use of hydrogeochemical patterns in carbonate sand and sandstone aquifers to identify intrusion and flushing of saline waters. Ground Water 23 (5):635-645. doi:10.1111/j.1745-6584.1985.tb01512.x
Mikhailova MV, Bellotti P, Valeri P, Tortora P (1999) Intrusion of seawater into the River Part of the Tiber Mouth. Water Resources 26 (6):679-686
Milli S (1994) High-frequency sequence stratigraphy of themiddle-late Pleistocene to Holocene deposits of the Roman Basin (Rome, Italy): relationships among high-frequency eustatic cycles, tectonics and volcanism. Paper presented at the Second High-Resolution Sequence Stratigraphy Conference, Tremp, Spain,, 20-27 June 1994
Milli S (1997) Depositional setting and high-frequency sequence stratigraphy of the middle-upper Pleistocene to Holocene deposits of the Roman basin. Geologica Romana 33:99-136
Milli S, D'Ambrogi C, Bellotti P, Calderoni G, Carboni MG, Celant A, Di Bella L, Di Rita F, Frezza V, Magri D, Pichezzi RM, Ricci V (2013) The transition from wave-dominated estuary to wave-dominated delta: The Late Quaternary stratigraphic architecture of Tiber River deltaic succession (Italy). Sedimentary Geology 284:159-180. doi:10.1016/j.sedgeo.2012.12.003
Milli S, Moscatelli M, Palombo MR, Parlagreco L, Paciucci M (2008) Incised valleys, their filling andmammal fossil record: a case study fromMiddle-Upper Pleistocene deposits of the Roman Basin (Latium, Italy). GeoActa Special Publication Special Pubblication (1):67-87
Milli S, Palombo MR (2011) Stratigrafia fisica e assetto deposizionale della successione del tardo Pleistocene inferiore/Olocene del Bacino Romano - I depositi pleistocenici di Ponte Galeria e la Polledrara di Cecanibbio. Paper presented at the Congresso Aiqua - Il Quaternario Italiano - Conoscenze e prospettive, Roma, 24-25 febbraio 2011
Mitchum RM, Vanwagoner JC (1991) High-frequency sequences and their stacking patterns - sequence-stratigraphic evidence of high-frequency eustatic cycles. Sedimentary Geology 70 (2-4):131-160. doi:10.1016/0037-0738(91)90139-5
Mollema PN, Antonellini M (2013) Seasonal variation in natural recharge of coastal aquifers. Hydrogeology Journal 21 (4):787-797. doi:10.1007/s10040-013-0960-9
Panno SV, Hackley KC, Hwang HH, Greenberg SE, Kaprac IG, Landsberger S, O'Kelly DJ (2006) Characterization and identification of Na-Cl sources in ground water (vol 44, pg 176, 2006). Ground Water 44 (2):129-129. doi:10.1111/j.1745-6584.2006.00200.x
Park Y, Lee J-Y, Kim J-H, Song S-H (2012) National scale evaluation of groundwater chemistry in Korea coastal aquifers: evidences of seawater intrusion. Environmental Earth Sciences 66 (3):707-718. doi:10.1007/s12665-011-1278-3
Peltier WR, Fairbanks RG (2006) Global glacial ice volume and Last Glacial Maximum duration from an extended Barbados sea level record. Quaternary Science Reviews 25 (23-24):3322-3337. doi:10.1016/j.quascirev.2006.04.010

Penland S, Boyd R, Suter JR (1988) Transgressive depositional system of the Mississippi delta plain: a model for barrier shoreline and shelf sand development. Journal of Sedimentary Petrology 58 (6):932-949
Post VEA (2005) Fresh and saline groundwater interaction in coastal aquifers: Is our technology ready for the problems ahead? Hydrogeology Journal 13 (1):120-123. doi:10.1077/s10040-004-0417-2
Pulido-Leboeuf P (2004) Seawater intrusion and associated processes in a small coastal complex aquifer (Castell de Ferro, Spain). Applied Geochemistry 19 (10):1517-1527. doi:10.1016/j.apgeochem.2004.02.004
Schoeller H (1962) Les Eaux Souterraines. Paris
Schoeller H (1965) Hydrodynamique dans le karst. Paper presented at the Colloque de Dubrovnik, Dubrovnik, Octobre 1965
Simmons CT (2005) Variable density groundwater flow: From current challenges to future possibilities. Hydrogeology Journal 13 (1):116-119. doi:10.1007/s10040-004-0408-3
Stuyfzand PJ (2008) Base Exchange Indices as Indicators of Salinization or Freshening of (Coastal) Aquifers Paper presented at the 20th Salt Water Intrusion Meeting, Naples, Florida, USA, 23-27 June 2008
Sung-Wook J, Jun-Mo K, Kyung-Seok K, Byungwoo Y, Ho-Wan C (2001) Hydrogeochemical characteristics of groundwater in a mid-western coastal aquifer system, Korea. Geosciences Journal 5 (4):339-348. doi:10.1007/BF02912705
Tran LT, Larsen F, Pham NQ, Christiansen AV, Nghi T, Vu HV, Tran LV, Hoang HV, Hinsby K (2012) Origin and extent of fresh groundwater, salty paleowaters and recent saltwater intrusions in Red River flood plain aquifers, Vietnam. Hydrogeology Journal 20 (7):1295-1313. doi:10.1007/s10040-012-0874-y
Tuccimei P, D'Angelantonio M, Manetti MC, Cutini A, Amorini E, Capelli G (2010) The chemistry of precipitation and groundwater in a coastal Pinus Pinea forest (Castel Fusano area, Central Italy) and its relation to stand and canopy structure. In: Szigethy BVaJ (ed) Horizons in Earth Science Research, vol 4. Nova Science Publishers, Inc., pp 1-17
UNESCO (1983) Algorithms for computation of fundamental properties of seawater.
Vandenbohede A, Hinsby K, Courtens C, Lebbe L (2011) Flow and transport model of a polder area in the Belgian coastal plain: example of data integration. Hydrogeology Journal 19 (8):1599-1615. doi:10.1007/s10040-011-0781-7
Ventriglia U (1990) Circolazione delle acque sotterranee. In: Idrogeologia della Provincia di Roma, vol Regione vulcanica dei Colli Albani - 3. Amministrazione Provinciale di Roma, Assessorato Lavori Pubblici, Viabilità e Trasporti, Roma, pp 183-187
Werner AD (2010) A review of seawater intrusion and its management in Australia. Hydrogeology Journal 18 (1):281-285. doi:10.1007/s10040-009-0465-8
Winchester JW, Duce RA (1967) The Global Distribution of Iodine, Bromine and Chlorine in MArine Aerosols. Naturwissenschaften 54 (5):110-113
Xue P, Chen C, Ding P, Beardsley RC, Lin H, Ge J, Kong Y (2009) Saltwater intrusion into the Changjiang River: A model-guided mechanism study. Journal of Geophysical Research-Oceans 114. doi:10.1029/2008jc004831

SECTION B: THE PONTINA PLAIN

4. SEAWATER INTRUSION ASSESSMENT IN THE CIRCEO NATIONAL PARK AREA (LATINA – CENTRAL ITALY), RELATED TO THE LANDSCAPE MODIFICATION INDUCED BY RECLAMATION ACTIVITIES

ABSTRACT

Pontina Plain is one of the largest coastal plains in Central Italy and agricultural activities have particular importance from a social and economic point of view. The natural landscape changed a lot after the works of land reclamation during the thirties of the past century, due to the coastal dune removal, the anthropic drainage system digging and the embankment of the lakes. Data about chemo-physical parameters as Temperature, Electric conductance (EC), Salinity (Sal) of groundwater, lakes, river and anthropic canal waters were collected along nine months of hydrogeological surveys. Saltwater intrusion was monitored in ten wells located between two coastal lakes, in the Circeo National Park. Piezometric maps regarding three regional surveys and six detailed hydrogeological sections were realized. A quantitative analysis of dune removal was made in a GIS system, through the comparison between two 1:5000 scale maps of pre and post-reclamation topographies. The piezometric patterns showed a reduction of groundwater supply. The innermost parts of the area are not affected by particular anomalies of EC and Sal. Sal concentration in the hydrographic network was noticed with high values. Areas where a great volume of coastal dune disappeared resulted the most affected by seawater intrusion. Despite the anthropic canal digging lead salt-wedge intrusion, salinization in coastal aquifers didn't increase during the time of observations. The presence of the Circeo National Park is helpful for the hydrogeological system: along the coast it prevents intensive agricultural activities from a groundwater overexploitation; inland, it permits to preserve the morphological height of the Circeo National Park Forest (on the paleo-dune reliefs), as an uncontaminated recharge area. Nevertheless the absence of regional water governance and uncontrolled withdrawals endanger the natural system.

4.1 INTRODUCTION

The constant world demographic growth induces an increasing water demand for drinking water, agricultural and industrial use. Coastal regions, for their great water resources availability, are greatly affected by groundwater overexploitation. In these areas land reclamation is a common approach to satisfy the growing needs for land use (Jiao et al. 2006) and it can affect oceans, rivers, lakes and dune systems. Despite reclamation activities provide valuable land for many coastal areas in the world, they also create various environmental and ecological problems (Jiao et al. 2001). These issues have been studied by some authors all over the world. For example Stuyfzand (1995) studied the interactions between water and reclaimed lakes in the Netherlands. Gowda (1996) discussed the impact of reclamation on the environment of a Hong Kong harbour. Song and Zemansky (2012) noticed that salinization of groundwater in reclaimed areas of Korea is greater than in the natural areas. Antonellini et al. (2008) studied the groundwater salinization in reclaimed areas of North Italy and observed how groundwater salinization increases where the demolition of dune ridges is greater.

The first reclamation activities in Pontina Plain started about 2000 years ago and finished in the late 30's of the past century (Brunamonte and Serangeli 1996; Serva and Brunamonte 2007). During the works the hydrographical and the morphological pattern changed substantially. The pre-reclamation hydrographical pattern was composed of swamp areas in the nearby of coastal lakes and it was modified completely by means of drainage canal digging, rectification of lake shores and filling of polders, whose topographic level was below the mean sea level. The filling activities, in turn, modified strongly the morphological aspect because dune ridges were leveled to obtain filling materials.

The consequences of the reclamation re-arrangement on the environment determined the modification of regional groundwater flow system and the alteration of the dynamic interaction between groundwater and seawater. As a consequence water quality deteriorated because of seawater intrusion. Seawater intrusion is defined as the mass transport of saline waters into zones previously occupied by fresher waters (Bear et al. 1999) and it can contaminate a

freshwater aquifer through several pathways, including lateral intrusion from the ocean; by upward intrusion from deeper, more saline zones of the groundwater system (upconing); and by downward intrusion from coastal waters (Barlow 2003). Seawater and freshwater balance is described through the Ghyben-Herzberg principle (Drabbe and Badon Ghyben 1889; Herzberg 1901), which considers the steady state balance between seawater and freshwater in a coastal aquifer. The depth below sea level to a point on the interface would be (Hubbert 1940):
$Z = (\rho_f / \rho_s - \rho_f) \cdot h$ where ρ_f is the freshwater density, ρ_s is the seawater density and h is the head of freshwater above sea level at the point of interface. The stratification of freshwater on seawater produces a zone of diffusion (interface), due to the perpetual cyclic movement of seawater from the sea floor into the aquifer and back to the sea (Cooper 1959).
Another way of contamination of coastal aquifers is the salt-wedge intrusion. It happens when a water course carrying freshwater, reaches a basin with saline water (sea, ocean or inland sea) and the saline water tends to propagate into the river mouth, affecting the quality of water (UNESCO 1991). In a reclamation area the presence of artificial canal mouths increases greatly the potentiality of salt-wedge intrusion to penetrate inland, because they are preferential ways of intrusion, especially during the low discharge periods (Giambastiani et al. 2007; UNESCO 1983; Xue et al. 2009). Furthermore the digging of the artificial canal network determined the demolition of coastal dunes, producing the disappearance of a natural barrier, suitable to store freshwater lenses (Bakker 1990) and consequently capable of delimiting seawater intrusion.
Seawater intrusion can be strongly amplified in intensive agricultural contexts, where there is the presence of uncontrolled withdrawals. Pontina Plain is an area with a strong agricultural propensity and groundwater pumping is the unique water supply for this activity.
This paper wants to focus attention on morphological changes acted during the land reclamation and the possible implication on the seawater intrusion in the coastal areas. For this reason water-table levels were monitored in three surveys, to identify the coastal areas affected by seawater intrusion. Around the coastal lakes a monitoring network was identified and a one-year survey activity was conducted, to analyze the evolution of seawater intrusion. Furthermore a survey about the drainage system was performed to understand the possible connection between groundwater and superficial water bodies salinization.
A morphological analysis about the dune removal along the coast line was effectuated in a GIS system, to define the areas most affected by reclamation works. Six detailed cross sections were realized to understand the aquifer structure and the hydrogeological potentiality. Finally hydrological, hydrogeological, stratigraphic and morphological data were cross-checked to examine the possible connections between water salinization and reclamation works.

4.2 GEOLOGICAL, HYDROGEOLOGICAL AND HYDROLOGICAL SETTING

The study area is located in Central Italy, along the Tyrrhenian coast line, about 70 km southeast of Rome. It spreads between the Sisto River, Moscarello Canal and the Tyrrhenian Sea and it hosts the Circeo National Park (CNP) (Fig.4.1). Pontina Plain is one of the largest coastal plains in Central Italy, in which farming has particular importance from a social and economic point of view (Casa et al. 2009). Pontina Plain is made up of clastic sediments, aged from the Medium Pleistocene to Holocene, of marine, alluvial, marsh, lagoon and beach ridge environment. The central part of the plain hosts a paleo-dune ridge named *Duna Antica* (Conforto et al. 1962), mainly composed by aeolian deposits. The main lithologies are: gravels, sands, silts, clays, travertine lenses connected to the tectonics activity (Boni et al. 1980) and in northern part, volcanic deposits from the Colli Albani Volcanic Complex (Funiciello and Parotto 1978). The Pleistocene-Holocene deposits overlie a low permeability Plio-Pleistocene clayey basement. This *aquiclude*, in turn, covers Cretaceous-Jurassic carbonate rocks and was affected by normal faulting during the Pliocene and Pleistocene (Cavinato et al. 1992). There are two main aquifer: the first one deep and confined in the carbonate rocks, with a variable permeability from low to very high (Mouton 1977); the second one, aim of this study, located in the superficial clastic aquifer, unconfined, with a medium-high permeability (Capelli et al. 2012).
Hydrogeological studies about the superficial unconfined clastic aquifer of the Pontina Plain were conducted for the first time in the 60's and 70's (Conforto et al. 1962; Gisotti and Scarpelli 1977; Mouton 1977). The purpose of these

surveys was to investigate the water availability for industrial use and to plan the drawing for the protection of the CNP. It spreads over the coastal area of Pontina Plain and a small part of the "*Duna Antica"* dune ridge. During the 80's the studies about Pontina Plain groundwater reduced considerably and just one regional study was conducted (Boni et al. 1988). At the beginning of the last decade new studies were conducted, to better understand the problem of groundwater management of Pontina Plain aquifer (Alimonti et al. 2005; Capelli et al. 2012; Sappa et al. 2005; Sappa and Rossi 2007).

Groundwater patterns derived from the previous works showed that groundwater pattern traces the morphology: higher water table levels are located next to the topographic reliefs of the "*Duna Antica*" in the CNP forest, and in the piedmont plain of the Circeo Mount. Groundwater flows eastward to the Sisto River, southward and westward to the sea and, in the northern part, westward to the Moscarello Canal. The recharge of the clastic aquifer mainly consists in the rainfalls and minimally in the discharge of the carbonate aquifer (RegioneLazio 2007). Seawater intrusion was investigated in the southern part of the plain by Sappa and Coviello (2011) through vertical electrical surveys. The results derived from the comparison with a previous work (CMP 1968) showed a generalized raising of the mixing zone towards the surface, demonstrating that in the last 50 years, the volume of fresh groundwater reduced significantly. Data about coastal lakes are available from different studies (Bono et al. 1985; Hydrodata and DHI-Italia 2012) and show a complete salinization of the lakes due to the direct communication with the sea acted by artificial canals, dug during the reclamation works. Drainage system is composed of a dense network, which allows waters to flow into the sea. Whereby the drainage canal bottoms are below the sea level, the freshwater discharge into the sea is acted by drainage pumps (Fig.4.1).

4.3 MATERIALS AND METHODS

4.3.1 GEOLOGICAL CROSS SECTIONS

All the hydrogeological papers presented in the above section, tried to illustrate the aquifer structure of the area. Six detailed cross sections were realized to summarize the information about works at different scales, integrating the existing datasets with other geological databases, coming from public research institutes (ISPRA 2012b; LINQ 2012) , freelance geologists (Gonios 2012) and data capture from historical hydrogeological works (Aquater 1988). Gravimetric available data (ISPRA 2013; Mouton 1977) were cross-checked with stratigraphic data to better understand the morphology of the clayey low permeability basement, whose morphology appeared strongly affected by tectonics. The reference cartography was a geological map of Fubelli et al. (2001), derived from previous works (Kamermans 1991; Sevink et al. 1991). All the data were managed in a GIS system using a Microsoft Office Access Database. Stratigraphic data were selected in function of the depth and reliability. The geological sections focused mainly on the central and northern part of the study area, due to higher data availability (Fig.4.2).

Fig. 4.1: hydrographical pattern of the study area about rivers, canals and lakes. The territory of the Circeo National Park is shown as well

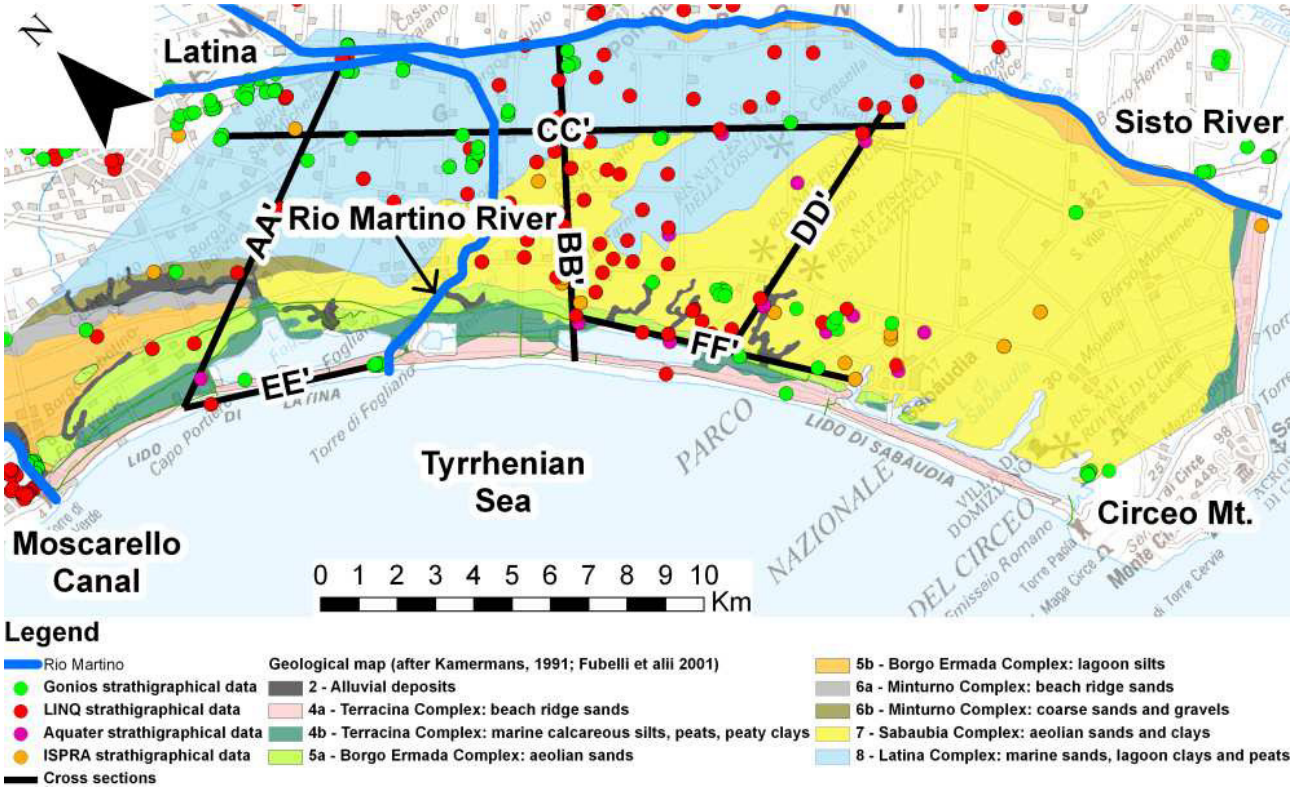

Fig. 4.2: tracks of the geological sections about the study area. They were mainly located in the northern part because of a major data availability

4.3.2 HYDROGEOLOGICAL AND HYDROLOGICAL SURVEYS

Hydrogeological surveys were carried out during three measurement campaigns in wells for agricultural, domestic and livestock use. Measurements were executed always in the same wells to better evaluate the modification of groundwater pattern during the time. Whereby it was impossible, nearby wells were chosen, to maintain the measurement network as uniform as possible. 238 well data level were collected: 85 in May-June 2011, 81in October-November 2011 and 72 in February-March. The decreasing value of measurements is due to the gradual exclusion of too close and shallow wells. The depth range about the investigated wells was between 1 and 70 meters.

Chemo-physical groundwater data about Electrical Conductivity (EC, in µS/cm ± 0.5%, normalized at 25°C), Salinity (Sal ± 0.1, in g/l) and Temperature (Temp ± 0.1, in °C) were collected using a 20 m cable length conductivity-meter, sampling waters extracted from the pumps or logging the parameters directly inside the well. Sal values were automatically converted from the EC values by the conductivity-meter, in accordance with UNESCO (1983) directives.

The yearly survey activity concentrated in a monitoring network of 9 wells along the coast line, between Fogliano, Monaci and Caprolace Lakes. The surrounding area of the Sabaudia Lake was excluded by the research because it was not affected considerably by the reclamation activities (De Pippo et al. 2001). Data were collected once a month, always at the same time to avoid anomalies about the possible tide effect, to analyze salinization change in the different seasons, effectuating log measurements every 0.5 meters. Their finding resulted very difficult because of the diffidence of the resident people, frequently due to a non-notification about the wells. The monitored 9 wells held a depth range between 2.5-20 meters (Fig.4.3). In a 20 m deep well (P2) a multi-parameter sensor about water level, Temp and EC was installed to collect data hourly. For this aim the well was equipped inserting a piezometric tube with 0.05 m of diameter, between the iron coating of the well and the pipe of the pump because it forbade reaching the well bottom, located about 19 meters below the ground level.

The measured ranges about chemo-physical data were: 614-45700 µS/cm for EC, 0-29.2 g/l for Sal and 10.5-23.8 °C for Temp.

Hydrological survey was carried out in January 2012 to evaluate the salinity condition about the hydrographical network in a rainless period, to avoid the freshening effect of rainfalls, in 123 measurement stations. It was conducted by means of boat navigations and bridge measurements. Depth data about the hydrological bodies were collected plumbing the river-canal bottoms. All the data were collected with the aim of a GPS system, necessary especially during the boat navigations to maintain a known distance between the measurement stations. The 20 m cable length conductivity-meter was used to collect data from the surface to the river/canal bottom, using a variable distance of collection, depending on the river-canal depth. The range of the chemico-physical parameters was: 615-58700 µS/cm for EC, 0-37.9 g/l for Sal and 1.9-14.9°C for Temp.

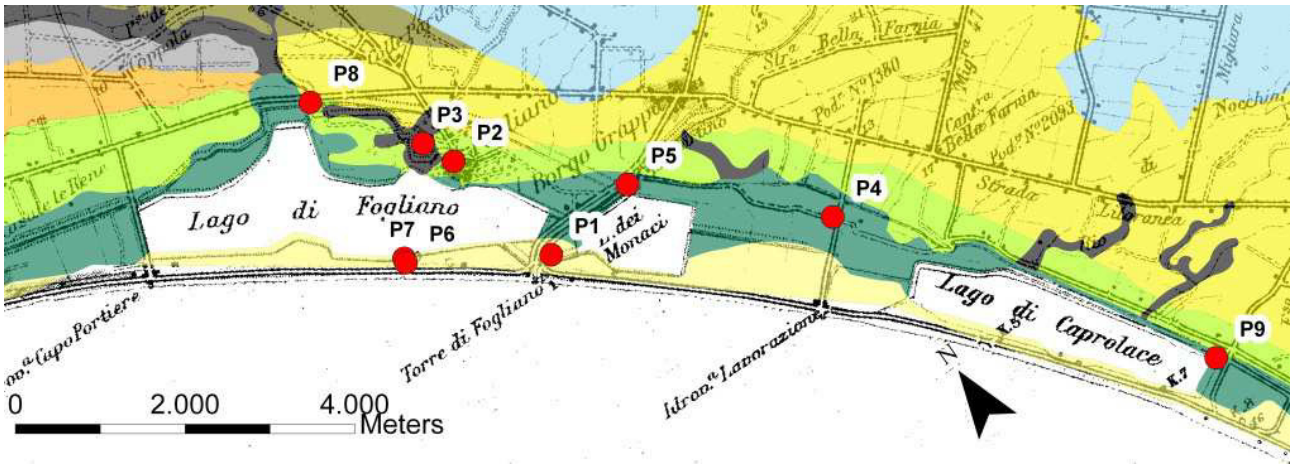

Fig. 4.3: location of the monitoring network to investigate seawater intrusion nearby the coastal lakes. For the legend of the geologic map see Fig.4.2

4.3.3 MORPHOLOGICAL ANALYSIS

A 13 km length and about 200 meters thick coast line was investigated for the morphological analysis, between the Moscarello Canal and Lavorazione draining pump, to quantify the earth moving acted by the land reclamation activities (Gragnanini 2009). It was performed using two 1:5000 topographic maps: a 1927 pre-reclamation map (IGM 1927) with an equidistance of 0.5 meters and a 2006 post reclamation map with an equidistance of 0.5 meters (RegioneLazio 2006), realized in 2003. They were geo-referenced and then digitalized using an Autodesk Map 3D® (Autodesk 2004), for the 13 km length coastal segment. The Autodesk Map 3D® polylines were imported as shape-file in the Esri Arcgis® v.9.3 (ESRI 2008) system and a Triangulated Irregular Network (TIN) was created. A TIN represents a surface using a series of triangles, whose vertexes constitute the input data for the interpolation (Michael et al. 2000). The Digital terrain models (DTMs) were obtained in the GRID format from the TINs, with a 0.5 x 0.5 meters cell. Finally the Hillshades were generated from the DTMs and the morphological analysis was effectuated using the cut/fill function of Esri Arcgis® 9.3. The function bases on the function Vol = A * ΔZ, where "A" is the single cell area, ΔZ is the topographic height difference that is $\Delta Z = Z_{1927} - Z_{2006}$. In this way it was possible to create a layer composed by 3 dominant colors: red for the loss, grey for the unchanged and blue for the gained areas.

4.4 RESULTS

4.4.1 CROSS SECTIONS

Cross sections (Fig.4.4) show the general configuration of the regional aquifer and it can be divided in two main sectors, the coastal one and the inner one. They are characterized by different complexes, related to the different tectonic history, which affected the area: in fact the coastal area is subject to uplift while the central part is subject to subsidence (Barbieri et al. 1999).

In the inner sector the top of the stratigraphic sequence is represented by the Sabaudia Complex, composed by aeolian sands and clays. It represents a low productivity aquifer because of its scant thickness. The Latina Complex, divided in sandy and clayey component (respectively 8a and 8b in Fig.4.4) underlies the previous one and it is mainly composed by an alternation of sandy marine deposits, lagoon clays and peats. The clayey component in the study area increases moving from North-west to South-east (Fig.4.4, cross section CC'), determining a multi-layered aquifer.

The clayey Plio-Pleistocene basement is not detected in deep stratigraphic data because it was strongly influenced by the action of normal tectonics. Therefore the thickness of the multi-layered aquifer in the central sector is more than 80 meters. Travertine lenses, whose presence is documented in several stratigraphic data within the whole study area, can rich a maximum thickness of 10 meters (Fig.4.4 cross sections AA'). Underground data confirmed also the presence of volcanic deposits, whose presence decreases moving toward the Circeo Mount.

The coastal sector is very different due to the outcrop of terraced deposits (Terracina, Borgo Ermada and Minturno Complexes) composed of an alternation of sands about dune and beach ridge environment and low permeability clays about lagoon environment, determining a low productivity multi-layered aquifer.

Downward the main aquifer is formed by gravel lenses, in heteropia with the Latina Complex. Gravels thickness can reach 30 meters and their location is in agreement with the position of paleo-riverbeds about the Wurmian hydrographical network, detected on the sea bottom by La Monica and Raffi (1996). Along the coastal line the clayey basement is shallower than the inner sector and can even lie 10 meters beneath the ground level (Fig.4.4, cross section EE').

4.4.2 HYDROGEOLOGICAL PATTERN

Groundwater pattern maps were realized by hand, using the interpolation method (Custodio and Llamas 2005) and they represent the hydrogeological pattern of the multi-layered high productivity aquifer. Some data of shallow wells about the inner part of the study area were excluded for the groundwater maps realization, according to the methodology of Sappa and Coviello (2011), because they collected groundwater from low productivity suspended aquifers. Fig.4.5 shows the results about the three regional surveys. Hydrogeological patterns confirm the position of the hydraulic heads and show how they are located nearby the morphological rise of the *Duna Antica*. The ridge morphology determines a high hydraulic gradient area, which governs groundwater flow paths. Given the great presence of groundwater depressions surveyed during the three periods, hydrogeological pattern appears very different from the previous works. Flow paths changed considerably during the time depending on the position and the magnitude of withdrawals. In general the highest hydraulic head is located around the piedmont zone of Mount Circeo and it is mainly due to a local setup of the clayey basement. Water table decreases gradually north-westward, moving to Latina City. The area that showed a minor variability, in terms of modification of hydraulic head, is the area in correspondence of the CNP forest. The other areas showed a constant presence of groundwater depressions located mainly in the central part of the study area. The coastal area is characterized by a low hydraulic gradient and flow paths can be strongly modified especially when withdrawals are concentrated behind the coastal lakes, where an inversion of the hydraulic gradient may occur.

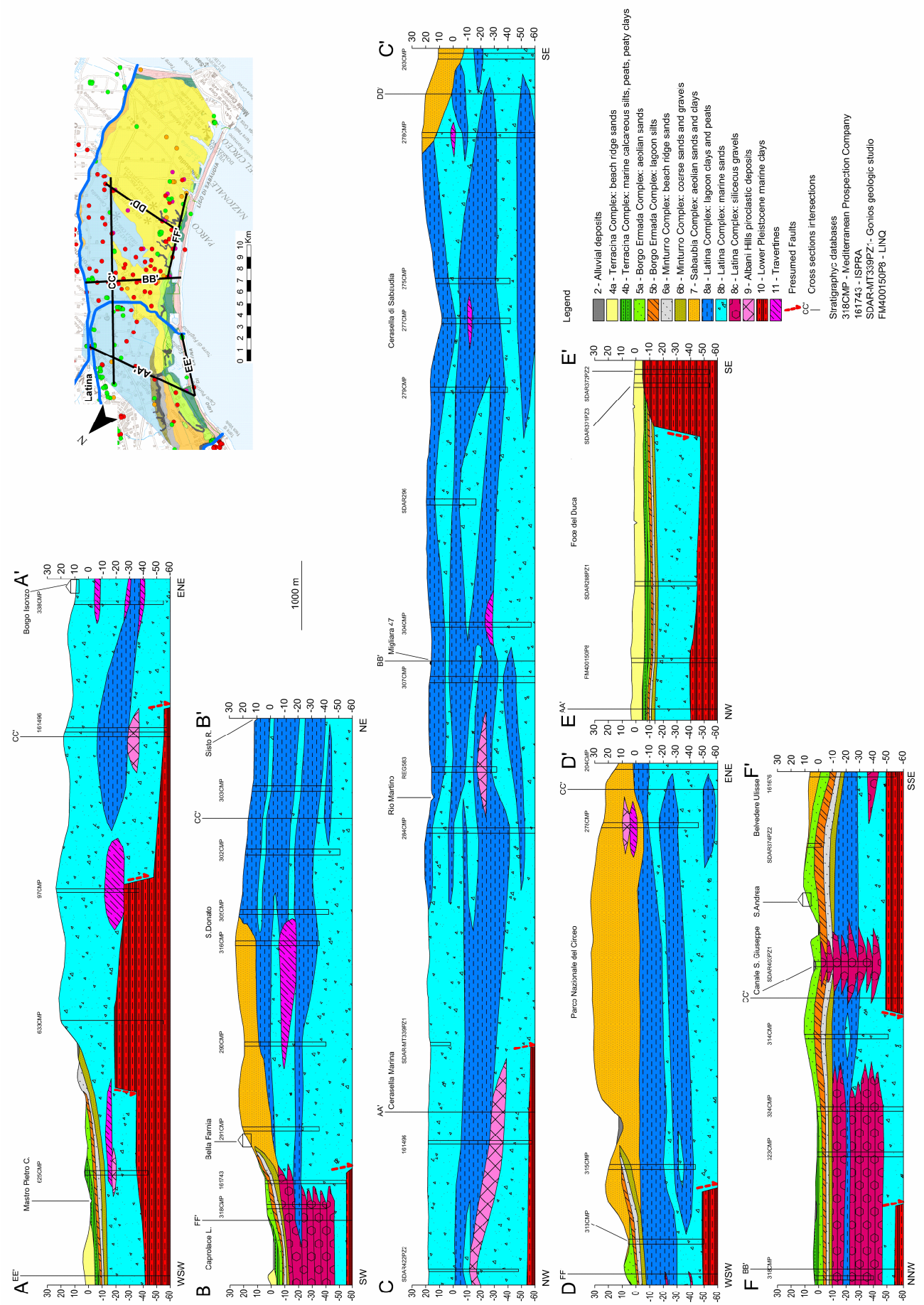

Fig. 4.4: the six detailed cross sections and the relative tracks. The area can be divided in two parts: the inner sector, with a high depth of the clayey basement and the coastal part, characterized by a shallow basement and a minor hydraulic potentiality

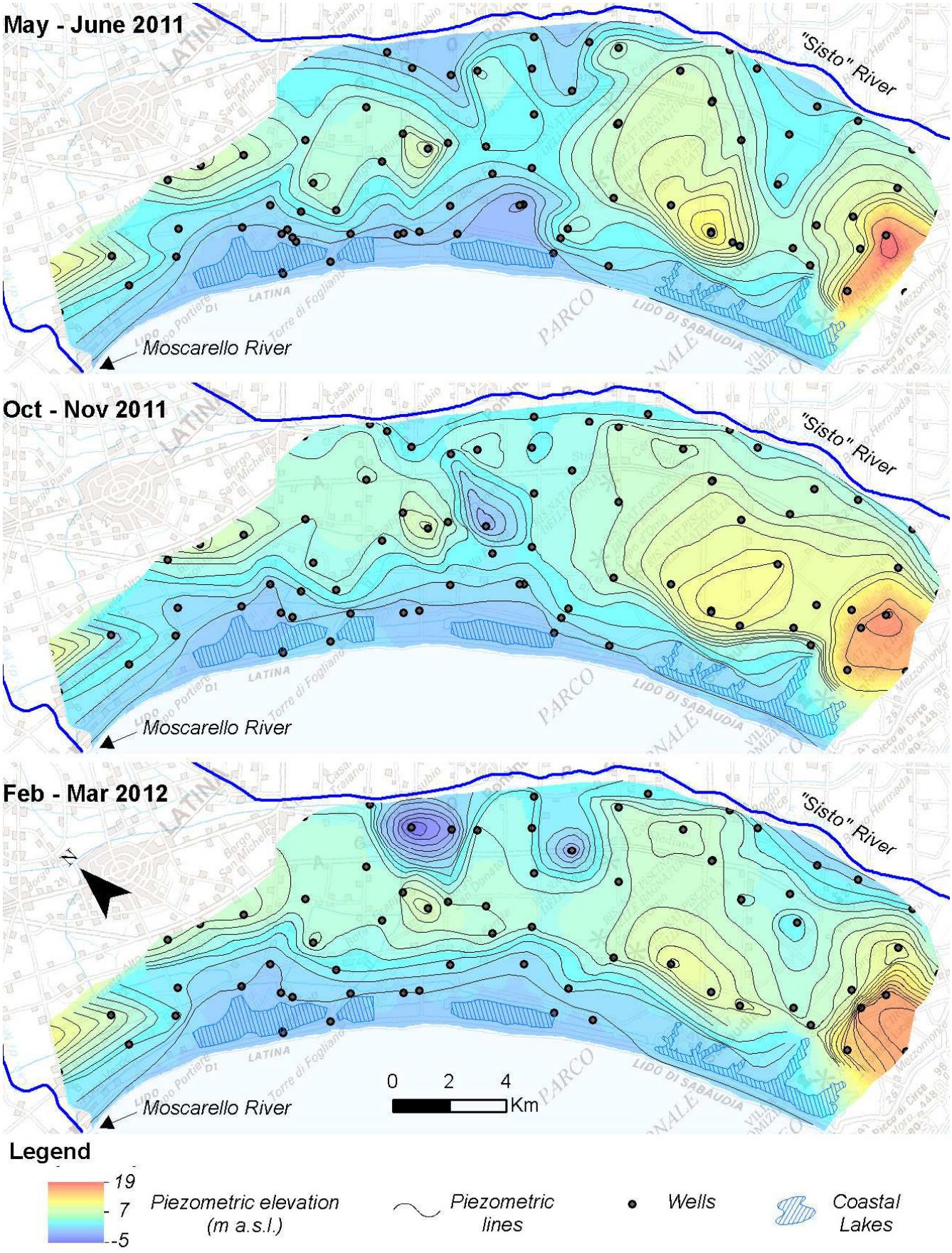

Fig. 4.5: groundwater patterns about the three surveys. The groundwater depressions were identified during all the survey periods, especially in the central sector. The positions of the survey points are indicated.

The monitoring network about the yearly seawater intrusion investigation is indicated in Fig.4.3. It was located along the coast line, between Fogliano and Caprolace Lakes.

Salinization in this area was strongly influenced by the presence of the coastal lakes. Coastal lakes hold a brackish composition and salinization can exceed seawater salinity in the summer (Noal and Bucci 2003).

Fogliano and Caprolace Lakes are salty because they are in direct communication with the sea by means of artificial mouths, dug during the reclamation works.

Data about salinity of Fogliano Lake are depicted in Fig.4.6. It shows how seawater is present during all the seasons and EC and Sal decrease during the rainy seasons and increase during the dry seasons.

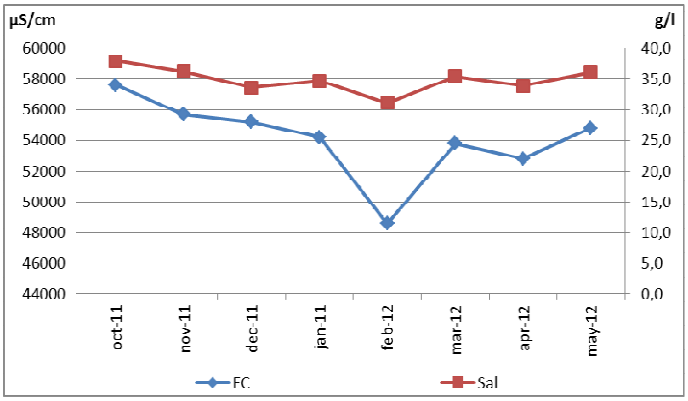

Fig. 4.6: data about EC and Sal about the Fogliano Lake. Data were collected nearby the P2 well, at the dock of Villa Fogliano. The graphic shows high values both of EC and Sal at the end of the summer (October), decreasing going to the rainy seasons.

Fig.4.7 shows the level data about Fogliano and Monaci Lakes (Hydrodata and DHI-Italia 2012) Fogliano Lake level fluctuation at the mouth (in green, located nearby P6 and P7 in Fig.4.3) and at the dock (in black, located nearby P2 in Fig.4.3) show a strict connection with the tide fluctuation because the Lake is in hydraulic connection with the sea. Otherwise the Monaci Lake level fluctuation (in blue) does not show strong connections with the tide fluctuation because it is occasionally in hydraulic communication with the sea, due to the presence of sluice gates. Furthermore the lake level is strictly related to a drainage pump, which inputs seawater in the lake when the level is too low and to the rainfall rate. For the Caprolace Lake the same trend of Fogliano Lake is supposed, due to the presence of artificial mouths in communication with the sea.

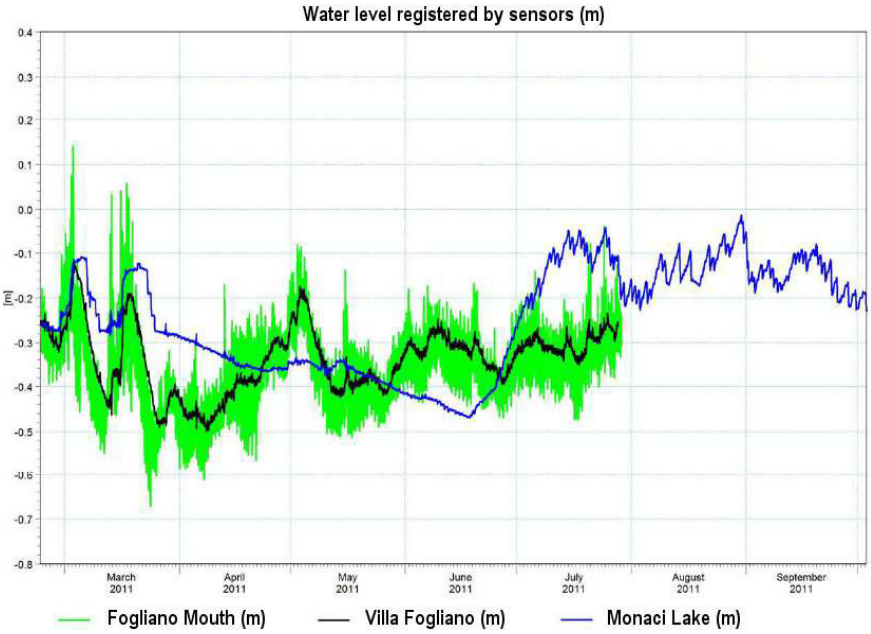

Fig. 4.7: data about the Fogliano and Monaci Lakes. The green line (Fogliano Mouth) shows a parallelism with the black one (Fogliano Lake at the dock) related to the sea level fluctuation. The blue line (Monaci Lake) shows an independent trend, due to the seawater inflow of a draining pump and to the rainfall rate (Hydrodata and DHI-Italia 2012)

Water table level data about the well network are shown in Fig.4.8a. The minimum and maximum values were for the P3 and P9 wells respectively, and they are related to the topographic height.

Data about the EC values of the nine wells at a specified depth are illustrated in the boxplot of Fig.4.8b. The wells can be divided in two groups:

- wells which showed a low dispersion and low values of EC (P3,P4,P5, P7, P8 and P9);
- wells which showed great dispersion and high values of EC (P1,P2 and P6).

The second group is about the wells affected by seawater intrusion. They can be divided in turn in two groups because P1 and P6, even if they exhibit different ranges of EC, show a similar behavior in terms of EC variability, while P2 shows the greatest variability of EC.

The different behavior depends on the closeness to different salinized water bodies. In fact P1 is located between Rio Martino River and Monaci Lake. Because of the salt-wedge in the river (see next paragraph) and seawater in the lake, P1 showed high values of EC with an average value of 44930 µS/cm and a yearly variability of 1746 µS/cm (1 g/l). P6 is located next the Fogliano Lake mouth and is surrounded by seawater on three sides. Its average EC value was about 9670 µS/cm and the yearly variability was 3870 µS/cm (1.6 g/l).

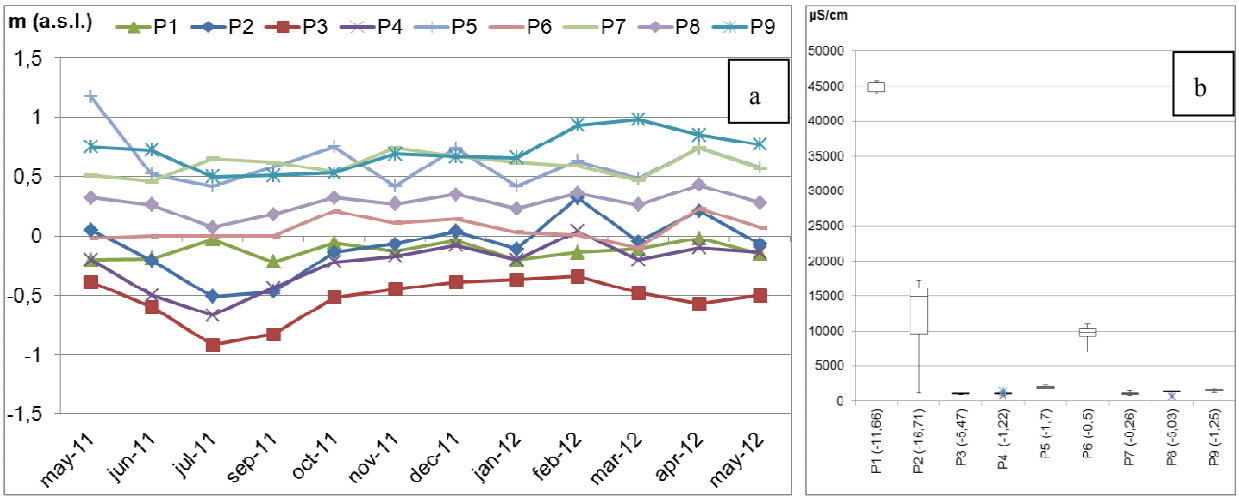

Fig. 4.8: a) data about the water table level of the monitoring wells. The minimum values is about P3, whose topographic height is below sea level. b) Boxplot about the EC values of the nine wells: P1,P2 and P6 showed high values of EC and a high variability. Their behavior depends on the closeness to the salinized water bodies

P2 is located about 300 meters from the Fogliano Lake shores and it allowed to collect data about the interface zone. Data showed an average EC value of 12640 µS/cm and exhibited the highest variability all over the study area, of about 16120 µS/cm (9.9 g/l). The vertical logs illustrate the fluctuation about the depth of transition zone, related to water table variability (Fig.4.9a and Fig.4.9b respectivey). In the month of December 2011 the transition zone is located lower than -8 m b.s.l. (Fig.4.9a) and the water table is slightly positive (Fig.4.9b). In February 2012 water table level increases strongly, reaching a water table elevation of more than 0.3 meters a.s.l. and, as a consequence, the interface zone disappears from the graphic because of the Ghyben-Herzberg principle. In April 2012 the water table level starts to drop and the transition zone appears again at the well bottom. In June 2012 the transition zone setup toward the surface occurs, as a consequence of the negative value of the water table (-0.3 meters b.s.l.).

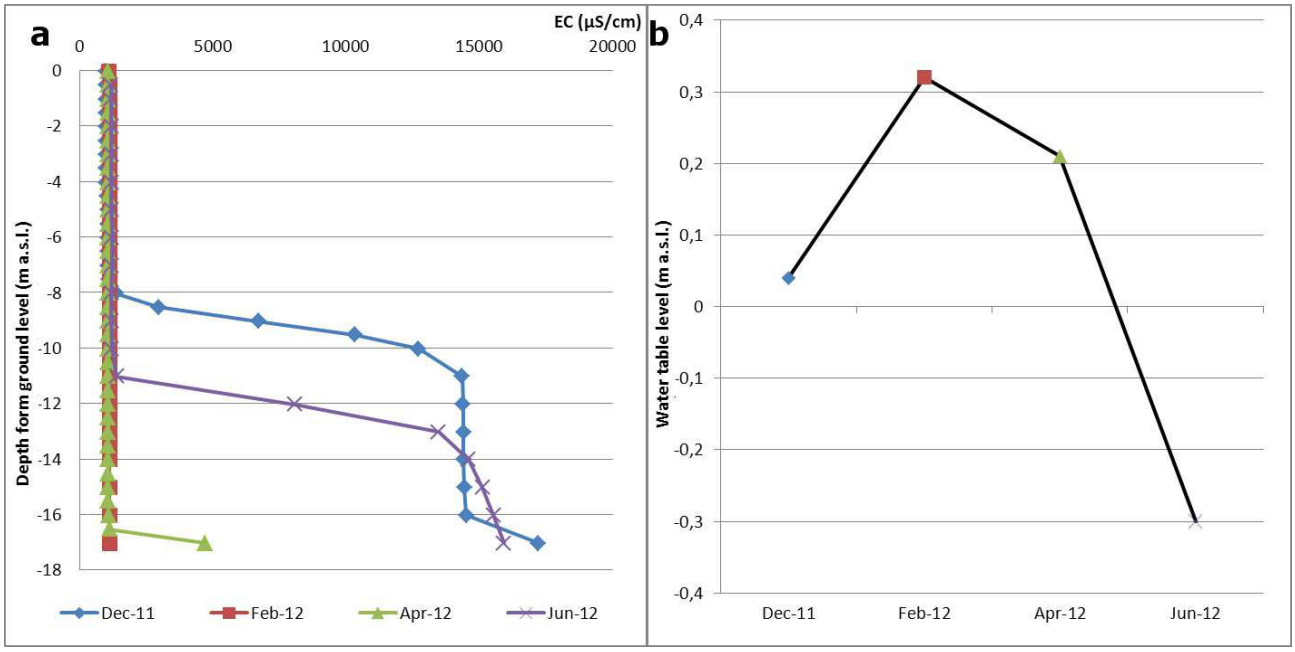

Fig. 4.9: a) four vertical measurements about the EC values of the P2 well; b) water table levels of the same period. It can be observed the close connection between the depth of the interface zone and the water table level.

Inside the well a multi-parameter sensor was installed to analyze the modification of the water table level, EC and Temp values.

As shown in Fig.4.7, the Fogliano Lake shows a strict connection with the tide fluctuation. To approximate the lake fluctuation, hourly data about sea level fluctuation were collected from the Anzio tide gauge (ISPRA 2012a), located on the coast line about 24 km North-westward with respect to the study area. Fig.4.10 shows the trends between the tide and water table fluctuations, demonstrating a lack of hydraulic connection between the lake and groundwater, although the well is very close to the lake (300 meters).

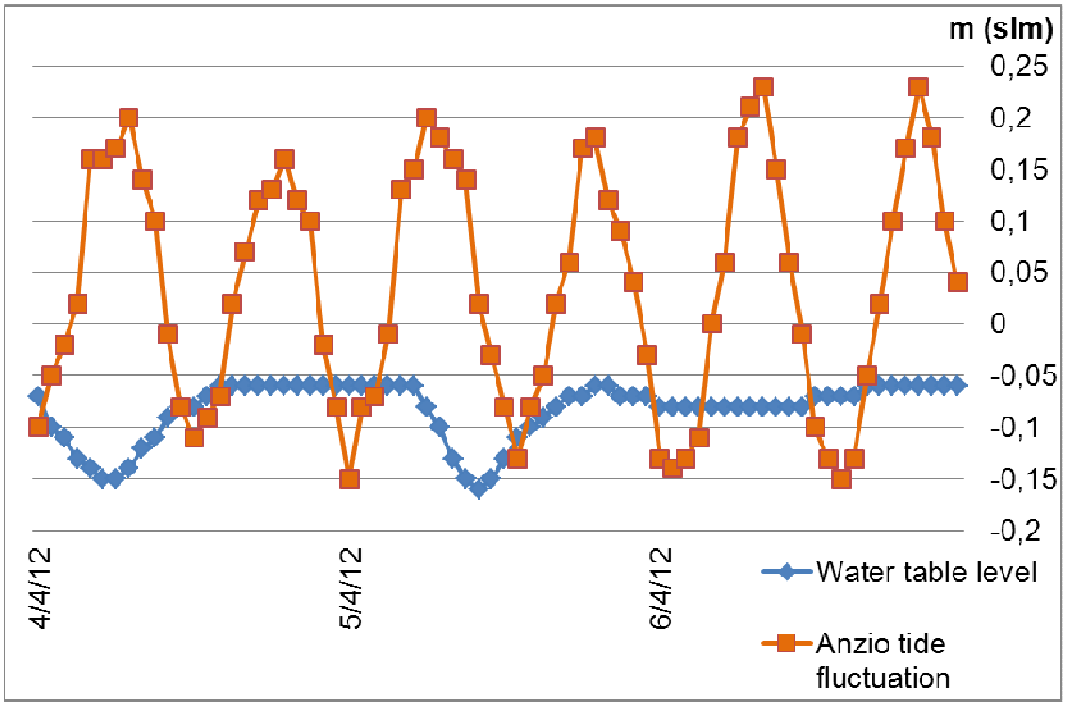

Fig. 4.10: lack of connections between the sea level (at Anzio tide gauge) and water table fluctuation. The water table drops indicate withdrawals

Another important issue provided from the multi-parameter sensor was about the seawater intrusion: in fact it was possible to identify two main man-induced processes of groundwater salinization. The first one was the lateral intrusion, induced by the water table drop as a consequence of groundwater pumping.

In Fig.4.11 it is possible to observe how the groundwater exploitation, proved by several water table depressions, leads to a general decrease of the water table level and an increase of the EC values is recorded in the well. This process was noticed at the end of April 2013, when the recharge rate started to decrease and water pumping started to be more intensive. As a consequence, from the 27th of April a rapid increase of EC values was noticed (from about 800 µS/cm up to about 17000 µS/cm) and a quick decrease of the water table level was recorded. Some of the EC values inflections are probably related to rainy events.

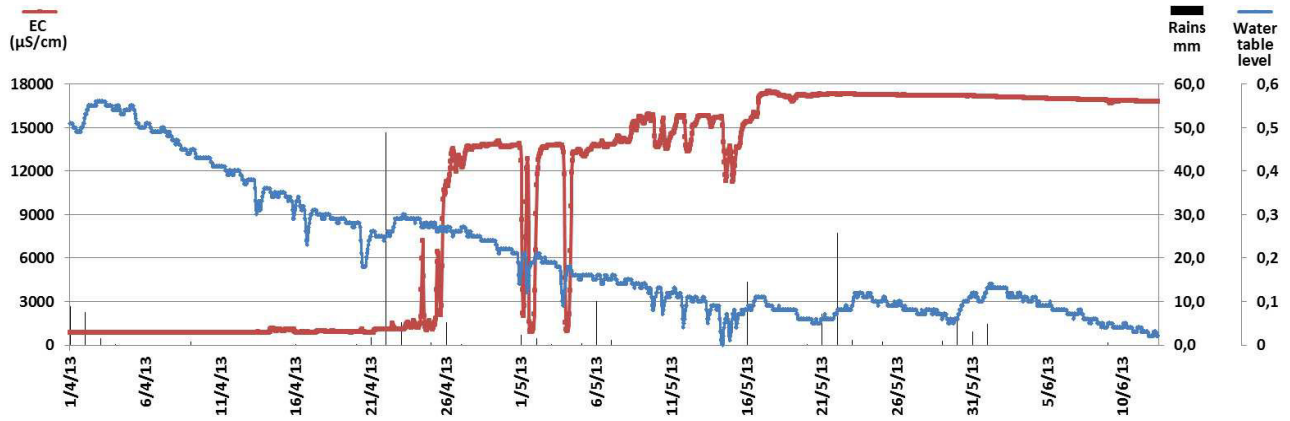

Fig. 4.11: lateral intrusion noticed in the P2 well. It can be observed how the water table level inflection determines an increase of EC values. Water table fluctuation depends on the recharge rate and the withdrawals

Another peculiarity recognized in the well was the difference of Temp values about groundwater and brackish water. Fig.4.12 shows how in January 2013, after a rainy period, water table level increase pushed down the interface zone and freshwater was noticed at the well bottom. In this case also the Temp was distinctive to identify seawater intrusion, because freshwater holds an average Temp of 15.93 °C, while the brackish water had an average Temp of 16.19 °C.

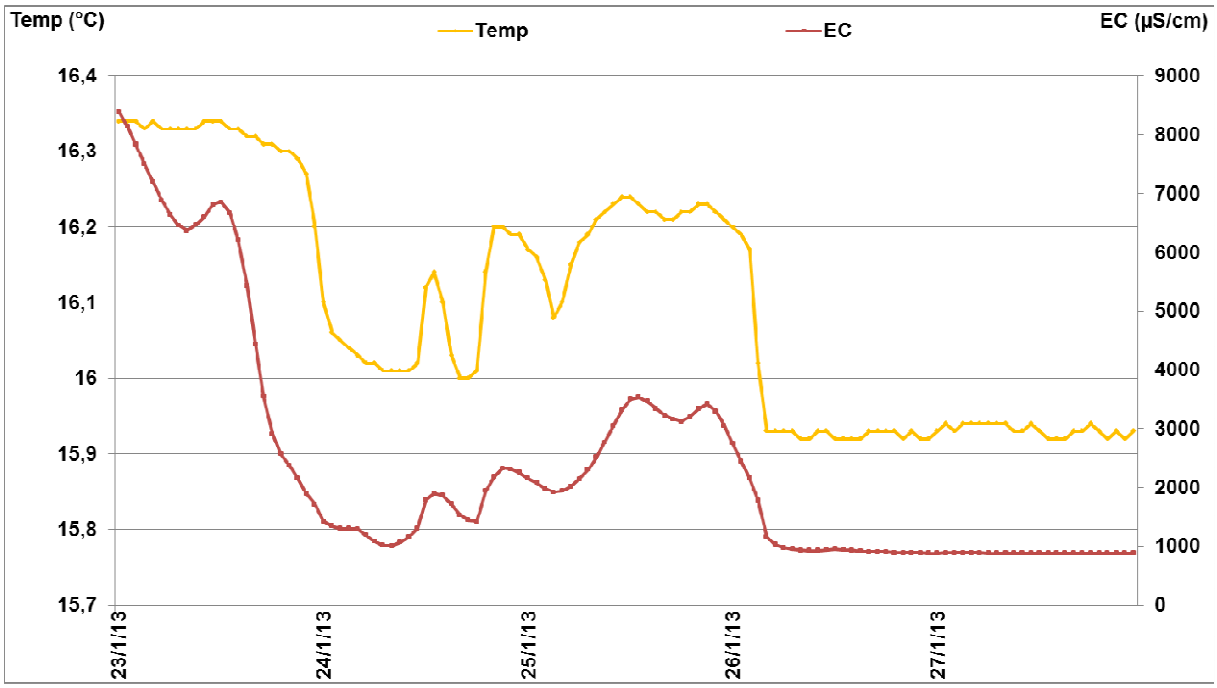

Fig. 4.12: identification of seawater intrusion using a thermal approach: freshwater in the well after the 26th of January (about 1000 µS/cm) holds a lower Temp with respect to that of the previous days

The upconing was the second process noticed by the multi-parameter sensor. It is mainly induced by pumping occurring around the P2 well. Fig.4.13 shows the presence of water table drops in the month of June 2012. In fact in the spring time agricultural activities are very strong and a lot of groundwater pumping occurs. Withdrawals determine a lot of water table depressions and, as a consequence, the interface zone comes to the surface, producing punctual raisings in the values of EC. This is proved by the phase opposition trend of the two values.

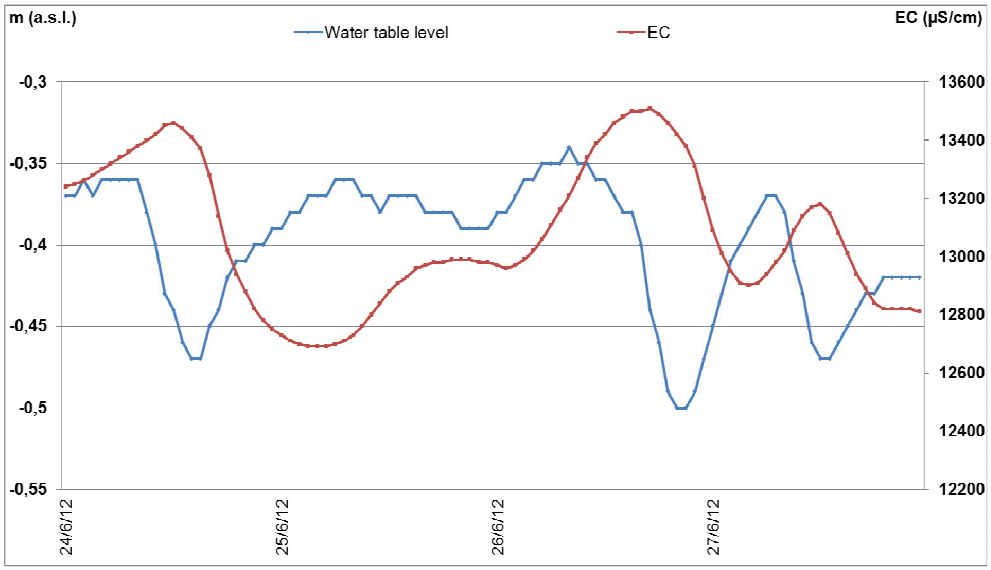

Fig. 4.13: trend in phase opposition of the EC and water level values, due to the process of upconing, created by groundwater pumping

In conclusion, the variability of EC values about the monitoring network showed a trend related to the rains, with an increase of EC values during the summer and a reduction during the Autumn and Springs, due to the dilution effect of the rains.

4.4.3 HYDROLOGICAL PATTERN

The location of the measurements collected during the hydrographical survey is represented in Fig.4.14, where the water-type distribution about the river and artificial canal bottoms is represented too. It shows the salinity distribution about the perennial hydrographical network due to the salt-wedge intrusion.

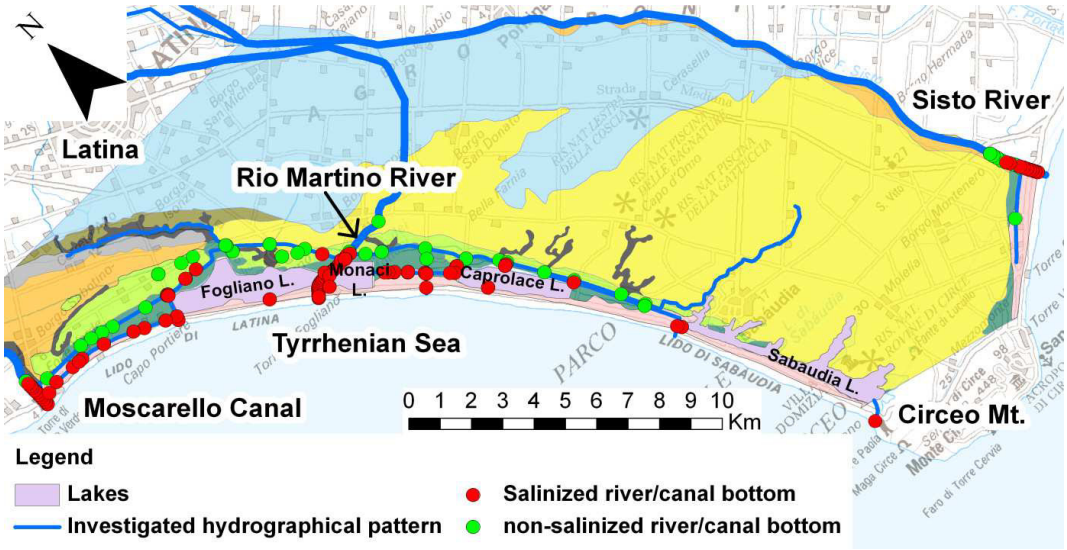

Fig. 4.14: Location of the surveyed point in the perennial hydrographical pattern. A differentiation for the salinized measurements was effectuated. For the legend of the geologic map see Fig.4.2

Hydrographical sections were realized to show the salinization pattern of the investigated rivers and canals. Sal range division was realized according to the Freeze and Cherry (1979) classification, which considers waters with Sal≤1 g/l as freshwater; 1<Sal<30 as brackish water; Sal ≥30 g/l as seawater. All the base maps were supported by ArcGisMapService (2013).

- The Moscarello Canal (Fig.4.15) is very important for the drainage of the Pontina Plain reclamation. It intercepts all the minor streams coming from Lepini and Colli Albani Mounts (Fig.0.2), flowing into the sea on the border of the study area. It is also known as the "High Waters Canal" because it drains the hydrographical network, whose river bottom is above sea level. It was navigated for about 1000 meters and its maximum depth was 1.3 meters. The salt-wedge intrusion was noticed up to 900 meters from the mouth and it is prevented by the discharge of a purification plant, which flows constantly into the river.
- Mastropietro and Colmata Canals run in parallel to the coast line (Fig.4.16). They flow both to the Moscarello Canal toward the Fogliano Lake, where the Capoportiere draining pump discharge the water into the sea. Mastropietro Canal drains an area below sea level, holds a maximum depth of 0.5 meters and appeared completely salty. Colmata Canal was dug in terrains above sea level, it showed a maximum depth of 0.25 meters and exhibited freshwater in all the bridge measurements.
- The Allacciante Canal (Fig.4.17), with a maximum depth of 0.5 meters, was dug around the Fogliano Lake, after the rectification of the lake shores. It drains an area where the ground level is below the sea level and it aims to direct the flows toward the Capoportiere drainage pump.
- Rio Martino River also known as "Medium Waters Canal" (Fig.4.18) collects water from reclamation canals, whose bottom is above sea level and could not flow naturally into the sea because of the coastal dunes presence. For this reason the river mouth was strongly affected during the reclamation works and a dam was built to allow water to flow into the sea. The boat navigation covered about 1850 meters and the salt-wedge presence was identified along the whole river bottom. The presence of the dam impedes the propagation of the salt-wedge inland. The maximum river bottom depth was of 2.7 meters.
- The Cicerchia Canal (Fig.4.19) receives water both from artificial canal network and natural ditches, located between the Fogliano Lake and from the sloping seaward side of the "*Duna Antica*" and it finally flows into the Rio Martino River. The bridge measurements covered a distance of about 3750 meters from the Sisto River connection and showed a maximum depth of 1.5 meters. The salinization, coming from the Rio Martino River, was documented up to 700 meters from the connection. The freshwater lens at the Ccic3 station is due to a freshwater input coming from a reclamation canal on the left bank.
- Nocchia and Caterattino Canals run in parallel to the coast line and they were investigated through bridge measurements (Fig.4.20). Nocchia Canal flows northeastward to the Sisto River and it starts nearby the CNP forest, on the "*Duna Antica*" ridge. It receives also waters from trenches on the left and right bank. It was investigated for about 9750 meters and its maximum depth is 1 meter, right at the connection with the Sisto River, where seawater can be detected. Caterattino Canal flows southeastward and it was surveyed for 6000 meters, with a maximum depth of 1 meter. It receives salinization both from the Caprolace Lake and the sea. In the central part, at the Divn3 station, it appeared composed completely by freshwater and this is likely due to a an inflow coming from the Nocchia Canal.
- Lavorazione and Papale Canals lie between Monaci and Caprolace Lakes. Papale Canal is in hydraulic communication with Monaci Lake and for this reason it presents a major salinization in the northernmost part (Fig.4.21). On the southern part it receives salinization from Caprolace Lake, although it is not in hydraulic communication with the lake. It holds a maximum depth of 0.6 meters. Both the northern and southern branches of the canal flow into the Lavorazione Canal, which leads the water to the Lavorazione Drainage Pump. It shows a complete salinization with the exception of the furthest measurement point from the see. The maximum canal depth is 0.8 meters.
- The Sisto River (Fig.4.22) is set along the northeastern border of the study area and it represents a potential hydrogeological boundary. It originates in a spring area located in a piedmont area of the Lepini Mounts. It

receives water from a carbonate aquifer and flowing to the sea, it drains the complexes of the "*Duna Antica*" aquifer. The boat navigation was about 1900 meters in length from the river mouth and the maximum observed depth was of 2.9 meters. The salt-wedge intrusion was recognized up to 900 meters from the mouth. From the measurement station Sis05 to Sis07 a brackish water plume was noticed up to the surface and it was probably caused to the riverbed lengthen, due to the presence of a dock. From the measurements points Sis10 to Sis12 a lens of brackish water was noticed in a bathymetric depression on the river bottom. To better understand this pattern anomaly, thermohaline graphics about three measurement stations Sal and T are shown in Fig.4.23. Sis1 represents data of Sal and Temperature about the closest station to the mouth. The trend between the two lines converge and move toward the right part of the graphic: it means that both salinity and temperature increase; Sis10 intercepts the brackish water lens and in this case only the Sal values increase (moving rightward), whereas the T values keep constant; Sis15 is about a vertical measurement in a freshwater column and the trend between the two lines is parallel. Since Sis10 shows a vertical constant T value, but the salinity increases with the depth, it means that the brackish water lens on the river bottom is evidence about an older salt-wedge intrusion, which reached the thermal equilibrium with freshwater.

The Moscarello Canal, Rio Martino River and Sisto River can be classified as strongly stratified estuaries (Cameron and Pritchard 1963; Pritchard 1955), characterized by moderate river discharge and weak tidal forcing (Dyer 1997). Salt-wedge pattern of the other canals cannot be classified because they host waters in a semi-stagnant environment.

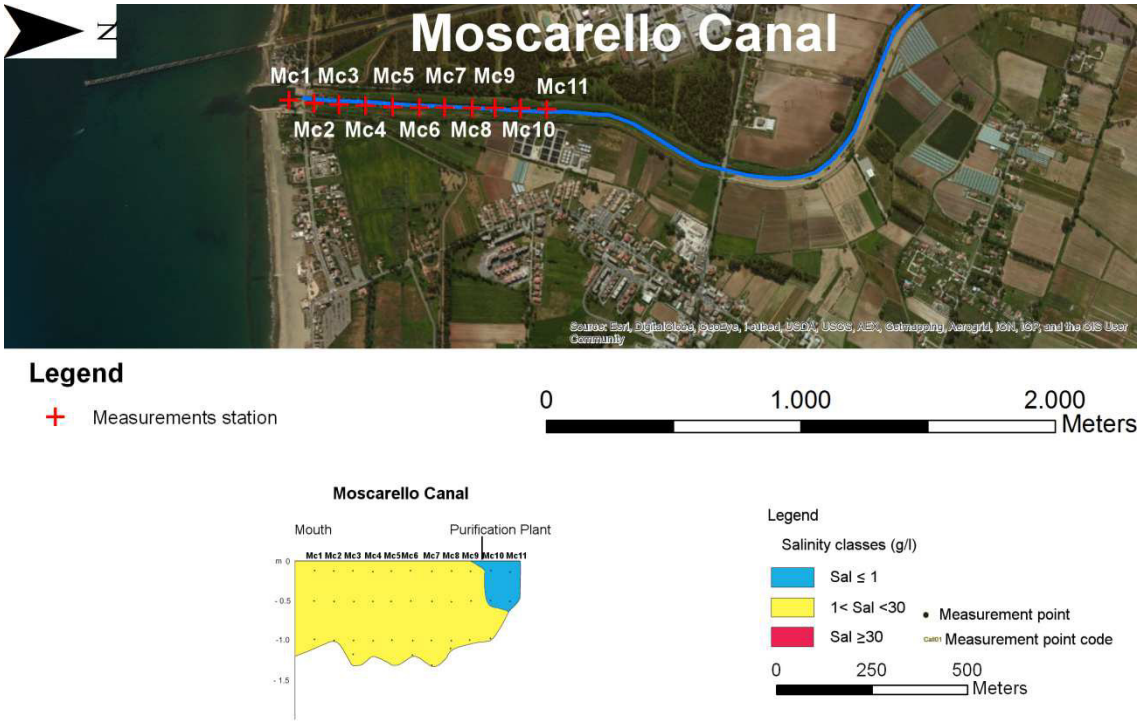

Fig. 4.15: Salinization pattern and location of the measurement points about Moscarello Canal

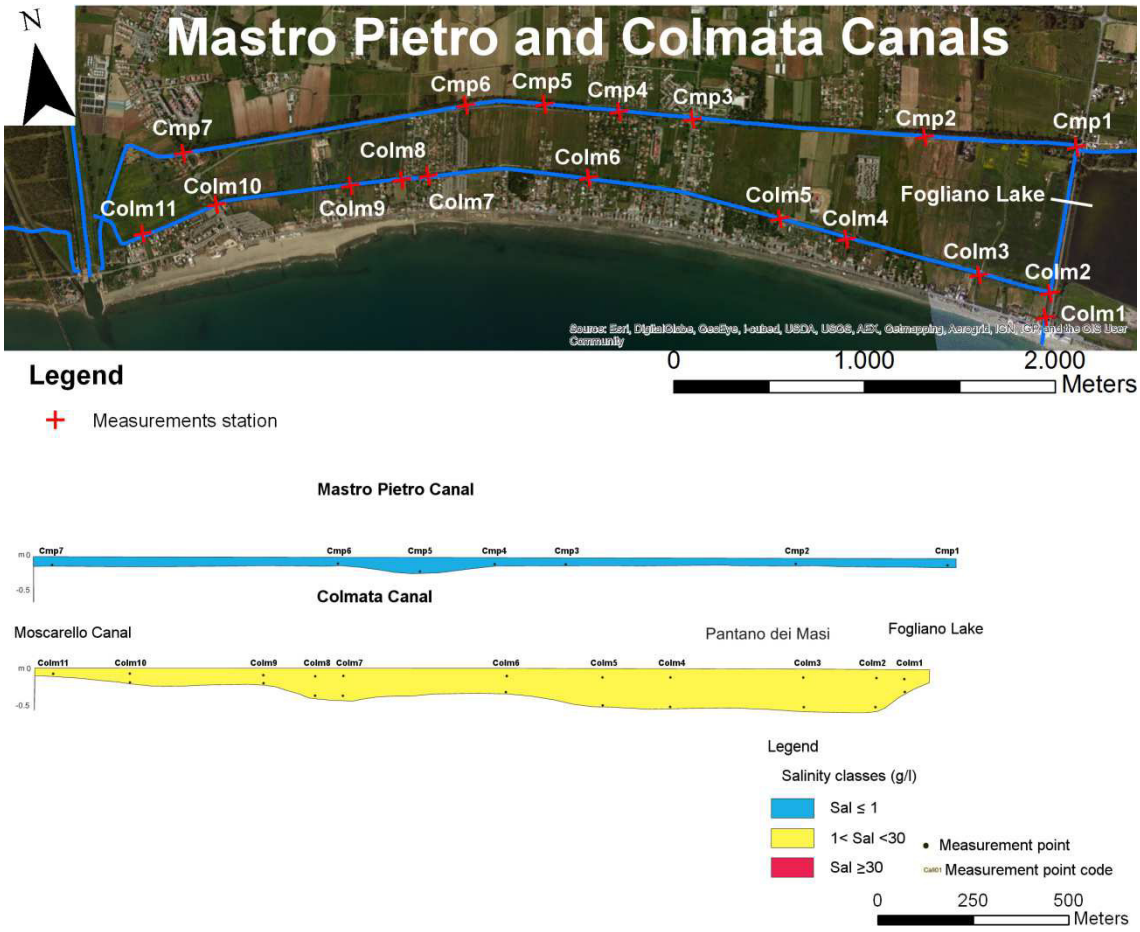

Fig. 4.16: Salinization pattern and location of the measurement points about Mastropietro and Colmata Canals

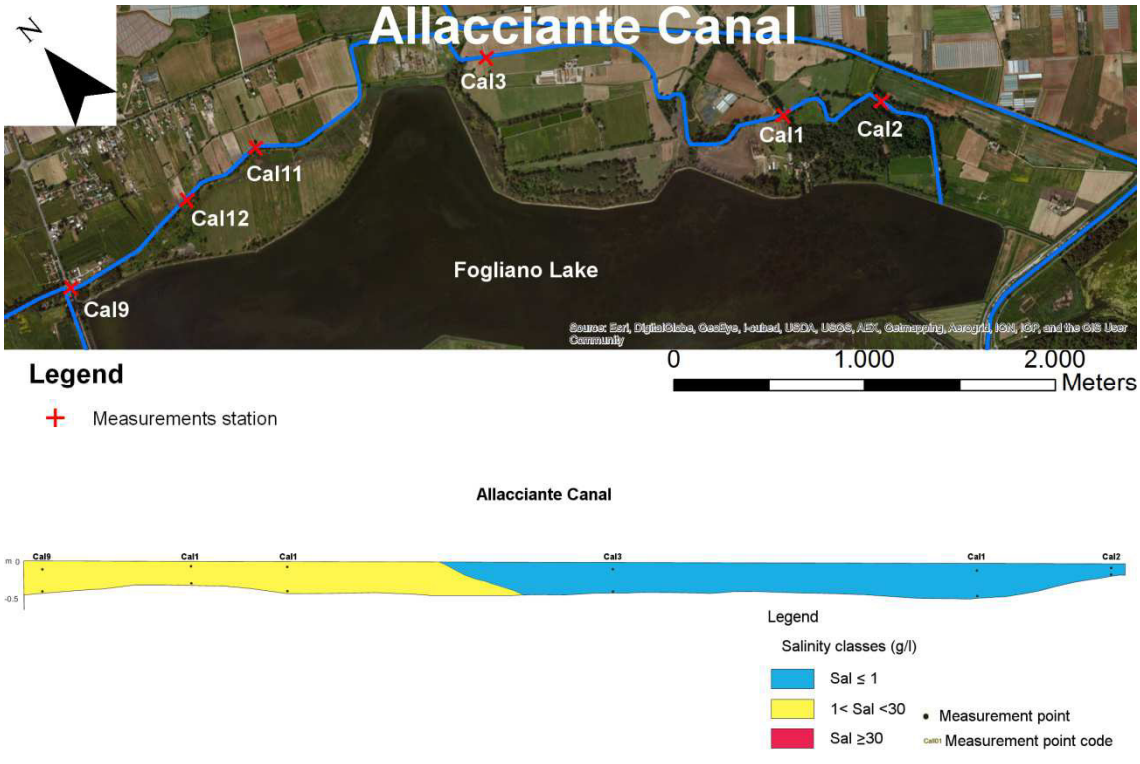

Fig. 4.17: Salinization pattern and location of the measurement points about the Allacciante Canal

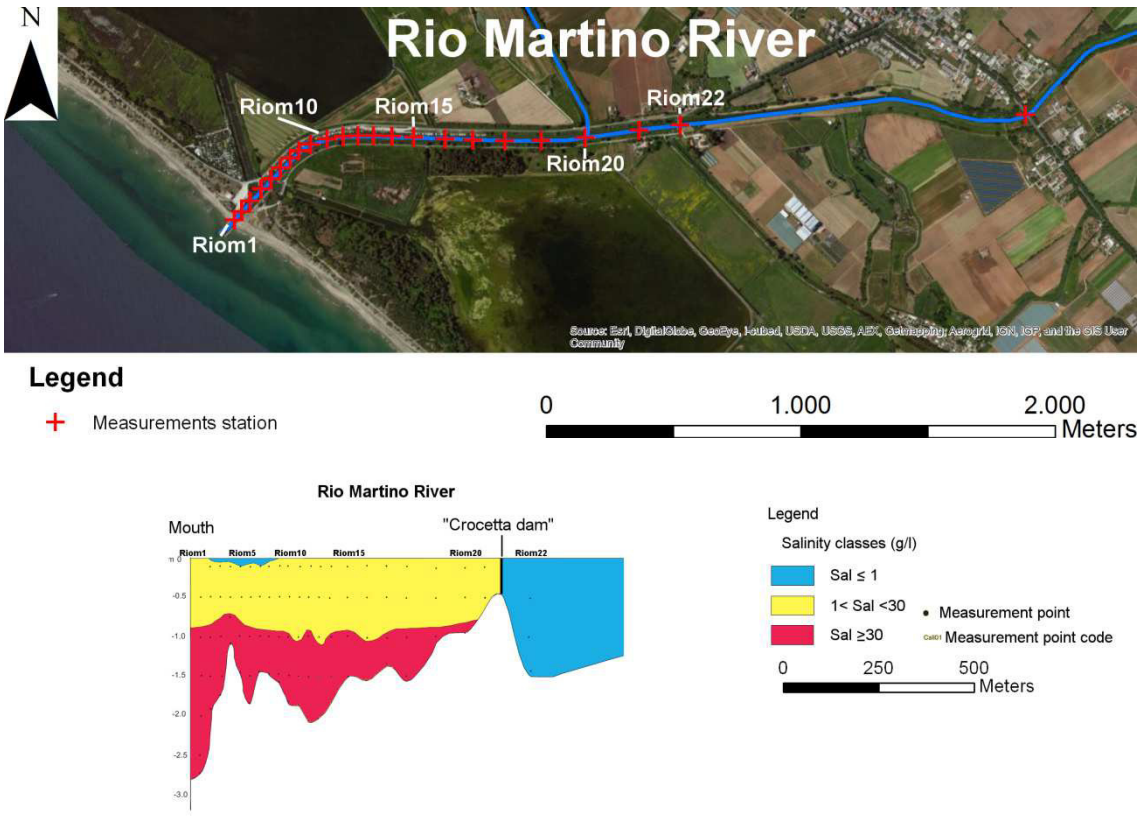

Fig. 4.18: Salinization pattern and location of the measurement points about Rio Martino River

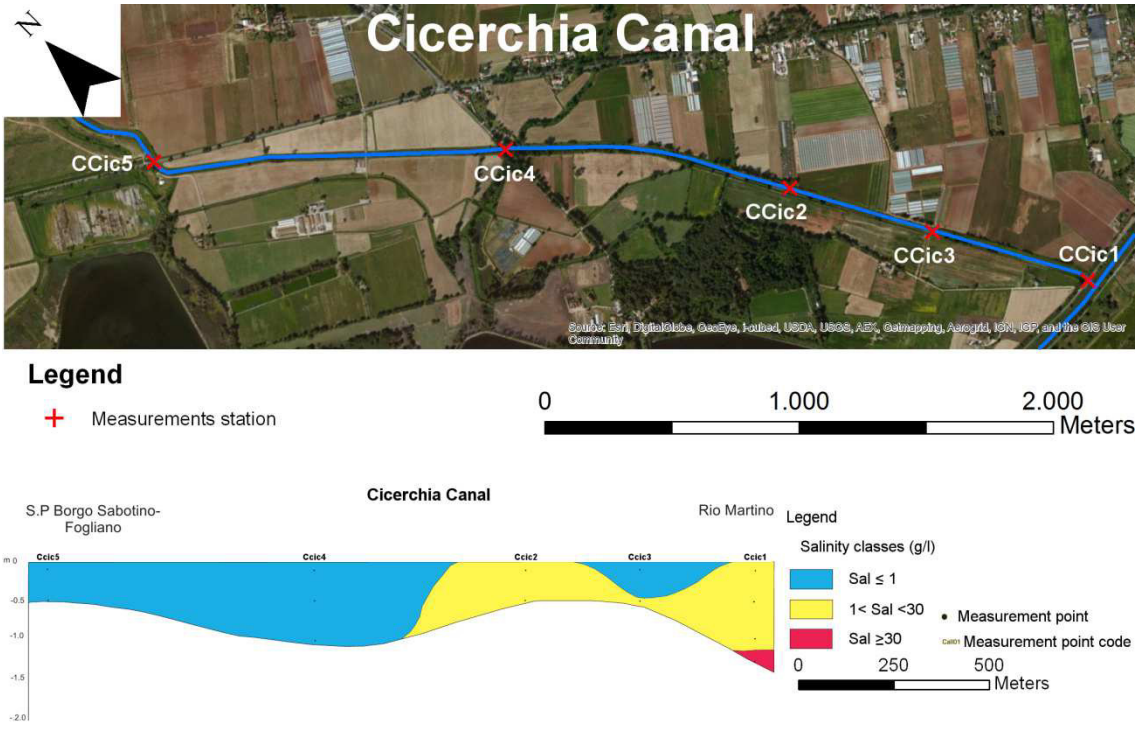

Fig. 4.19: Salinization pattern and location of the measurement points about the Cicerchia Canal

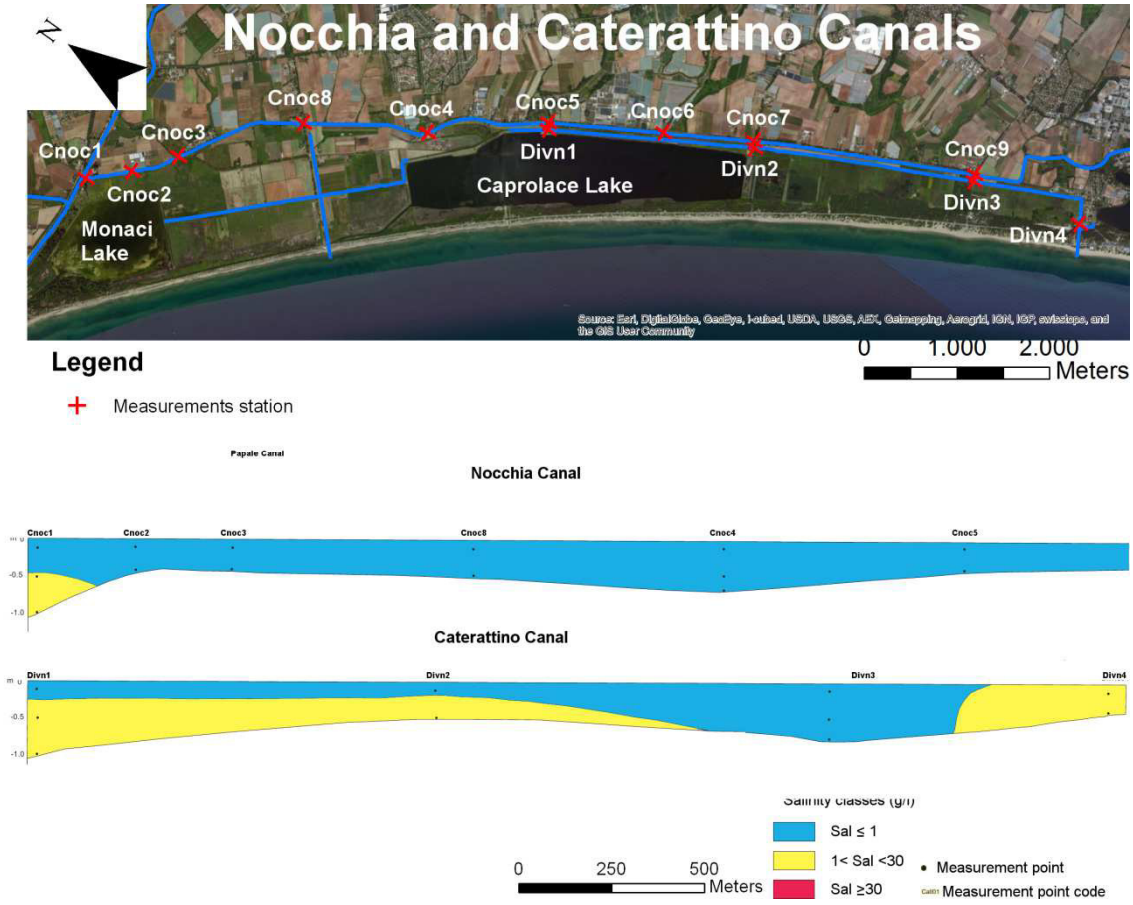

Fig. 4.20: Salinization pattern and location of the measurement points about Nocchia and Caterattino Canals

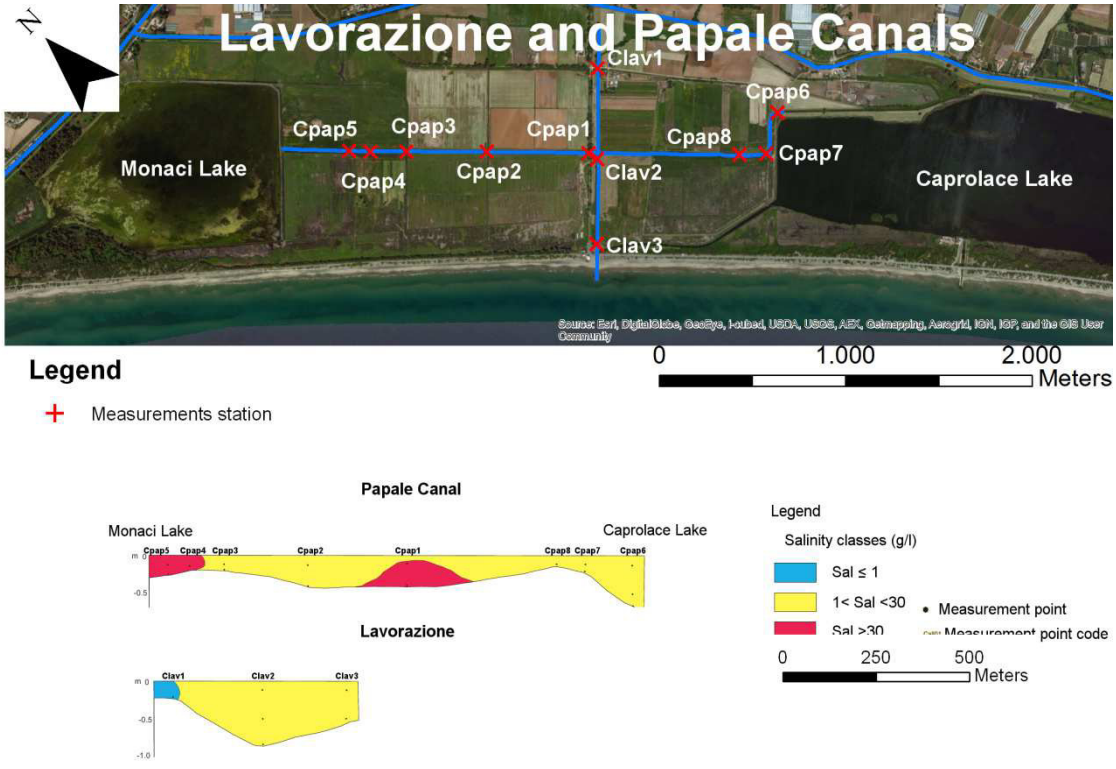

Fig. 4.21: Salinization pattern and location of the measurement points about Papale and Lavorazione Canals

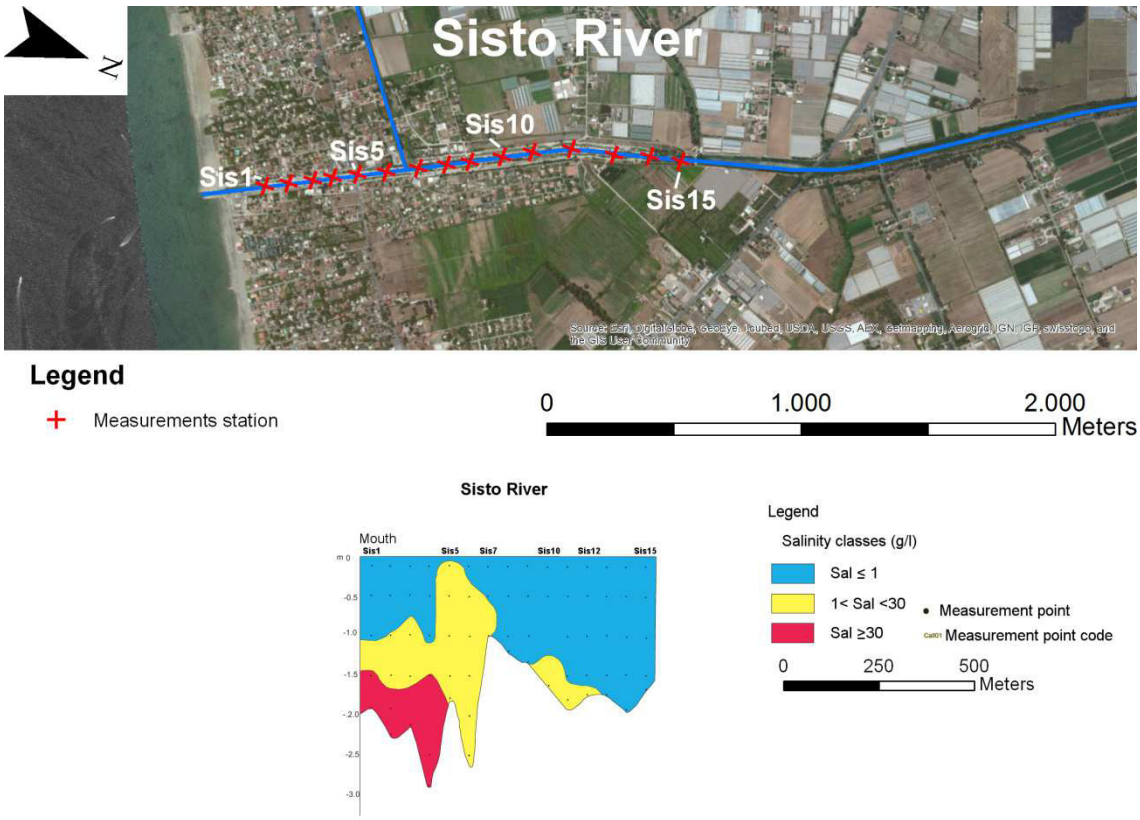

Fig. 4.22 Salinization pattern and location of the measurement points about the Sisto River

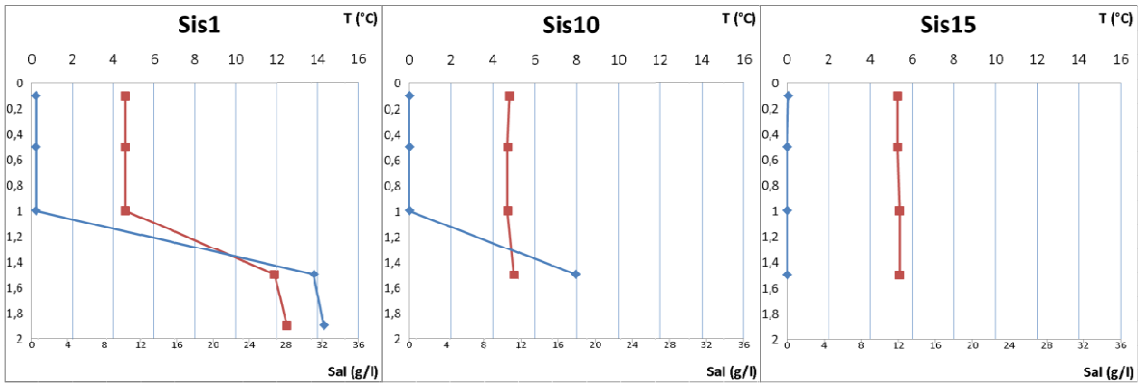

Fig. 4.23: thermohalines about three measurement points in the Sisto River. Red lines are about Temp while blue lines are about Sal. Sis1 represents data of Sal and Temperature about the closest station to the mouth The trend between the two lines converge and move toward the right part of the graphic: it means that both salinity and temperature increase; Sis10 intercepts the brackish water lens and in this case only the Sal values increase (moving rightward), whereas the T values keep constant; Sis15 is about a vertical measurement in a freshwater column and the trend between the two lines is parallel. Since Sis10 shows a vertical constant T value, but the salinity increases with the depth, it means that the brackish water lens lying on the river bottom is evidence about an older salt-wedge intrusion, which reached the thermal equilibrium with freshwater.

4.4.4 MORPHOLOGICAL ANALYSIS

The results of the morphological analysis are shown in Fig.4.24. It shows the digitalized topography about the 1927 and 2006 maps (Fig.4.24a and Fig.4.24b respectively) and the computation about the earth moving acted by the land reclamation activities. The Fig.24c indicates, using different colors, the areas affected by loss or gain about earth volumes. Tab.1 shows the surfaces subject to the reclamation works and the corresponding moved volumes. Acting a simple subtraction between thee loss and the gain volumes it is possible to quantify a loss volume of about 244000 m^3. The disappeared volume was probably used as filling material for the areas located below the sea level. The analysis

allowed also to evaluate the coastal lines subject to erosion or deposition: for example at Moscarello Canal mouth, a moving back of about 40 meters happened, while from the area A to the area B a shore line progress of about 25 meters was noticed.

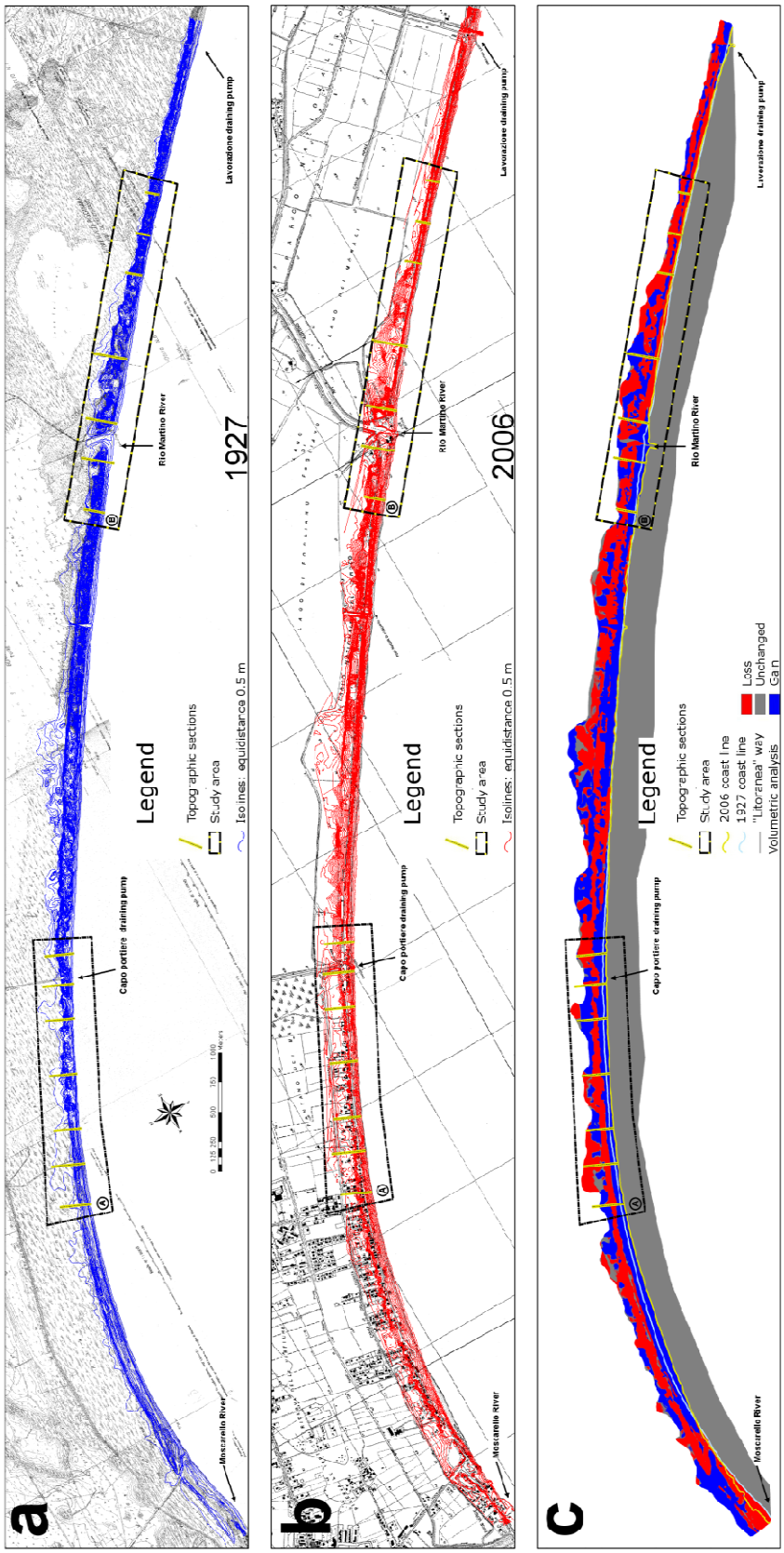

Fig. 4.24: topography about 1927 (a), 2006 (b) and morphological analysis acted by reclamation works (c) about the 13 km length coast line. The blue areas indicate a gain of volumes; the red areas indicate a loss of volumes and the grey area reveal the unchanged areas (Gragnanini 2009)

Total area: 616 hectares		
	ha	m^3
Loss	134	-1509421
Unchanged	352	0
Gain	129	1265440

Table 4.1: volumes loss and gain about the 13 km length area. The net loss volume was about 244000 m^3

4.5 DISCUSSIONS

Groundwater patterns showed a great variability during the three surveys due to the presence of several groundwater cones. Fig.4.25 shows data about the land use of Pontina Plain derived from satellite images (EEA 2006). The circles correspond to the water table depression identified during the three surveys (see Fig.4.5) and it can be observed how they lie in correspondence of the 211 legend category, which is about non-irrigated arable lands, greenhouses and nurseries. In Pontina Plain greenhouses are the main sources for agriculture and they don't allow a direct aquifer recharge. Therefore withdrawals are carried out during the whole year, especially during the summer. In this period the main crop types are eggplants, tomatoes, zucchinis and watermelons, that according to Doorenbos and Kassam (1979) classification, are high water requirement crops. For this reason a great volume of groundwater is pumped and the exploitation can happen even during the night. Fig.4.26 shows the water table level fluctuation about three spring days and it can be seen the presence of two cones of depression. Observing the cone of the 4th of April, it can be noticed how the decrease of level starts at midnight and the maximum depression is around 6 o'clock a.m.

The presence of several groundwater cones can determine, especially if they occur nearby the coast line, an inversion of the hydraulic gradient. It could induce a local inversion of the flow paths direction, determining a movement of seawater to the inner part of the coastal aquifer, behind the coastal lakes.

The data about the yearly survey show that the area most affected by seawater intrusion is that between the Fogliano and Monaci Lakes. In this area salinization is confined in the sandy and gravelly deposits below the terraced coastal deposits (see sections AA', BB' and DD' in Fig.4.4). The lakes are suspended on the Terracina Complex (calcareous silts, clays and peats), which isolates the lower aquifer from the lakes. It is demonstrated by the Fig.4.10, which shows a missing connection between the groundwater level and the lake fluctuation, expected in a well located about 300 meters from a salinized water body. Seawater movement is strictly dependent from the water table elevation: when it is above sea level the seawater lateral intrusion is contrasted by the freshwater lens thickness according to the Ghyben-Herzberg principle. When the water table is below sea level a movement of seawater is noticed inwards. In P2 well an upconing intrusion was noticed a well as demonstrated by the Fig.4.13, where an increase of EC is noticed in correspondence of an induced water table drop. The hydrographic network showed a salinization coming straight from sea and indirectly from the lakes. As a consequence the terraced complexes, in which they flow, resulted partially saturated by seawater. The most salinized area resulted to be Rio Martino River mouth, located between the Fogliano and Caprolace Lake, strongly affected by the reclamation activities. Fig.4.27 shows salinization about the rivers/canals bottom (about the January 2012 survey) and the EC values of groundwater in the wells (about the February-March 2012 survey). It can be observed how the two data layers superimpose as proof of the fact that the canals and the rivers operate as vehicle of salinization inland.

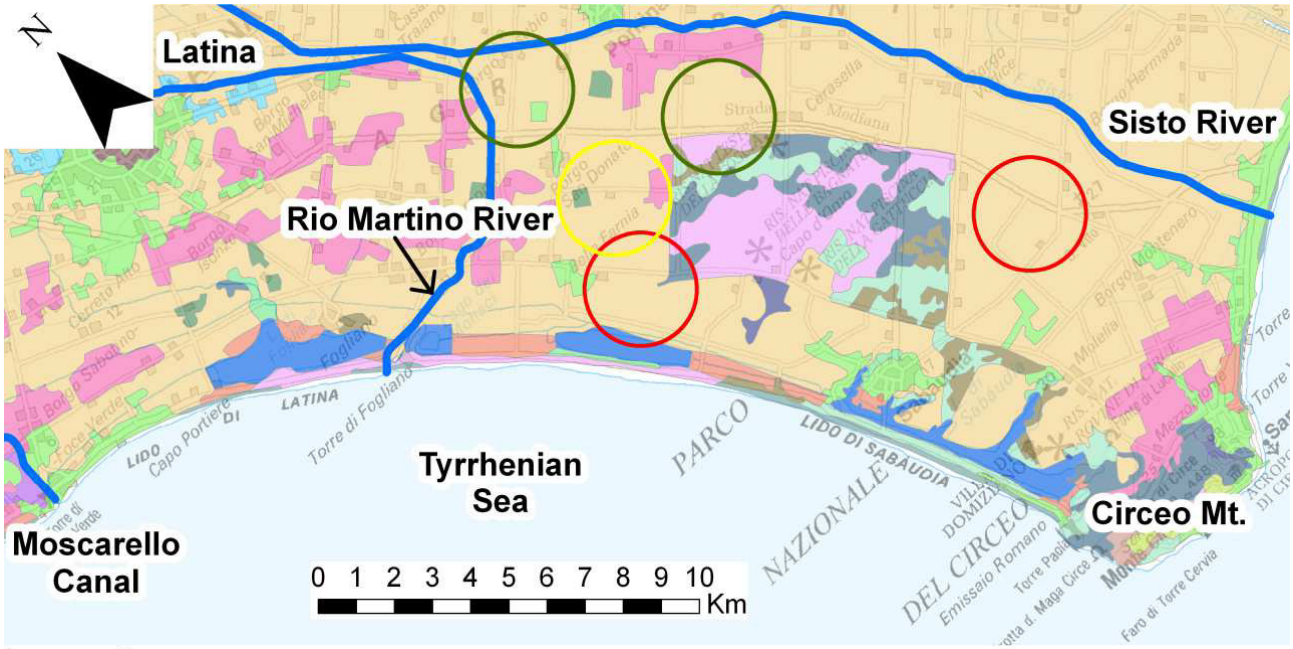

Legend

- 111 Continuous urban fabric
- 112 Discontinuous urban fabric
- 121 Industrial or commercial units
- 141 Green urban areas
- 211 Non-irrigated arable land, greenhouses and nurseries
- 221 Vineyards
- 222 Fruit trees and berry plantations
- 231 Pastures
- 242 Complex cultivation patterns
- 243 Land principally occupied by agriculture, with significant areas of natural vegetation
- 311 Broad-leaved forest
- 312 Coniferous forest
- 313 Mixed forest
- 321 Natural grasslands
- 322 Moors and heathland
- 323 Sclerophyllous vegetation
- 331 Beaches, dunes, sands
- 333 Sparsely vegetated areas
- 411 Inland marshes
- 512 Water bodies

Fig. 4.25: land use map derived from satellite images (EEA 2006). The circles correspond to the groundwater depressions identified during the three regional surveys (see Fig.4.5). In red the location of depressions identified in May-June 2011; in yellow the depressions identified in October-November 2011; in green the groundwater depressions identified during the February-March 2012 survey

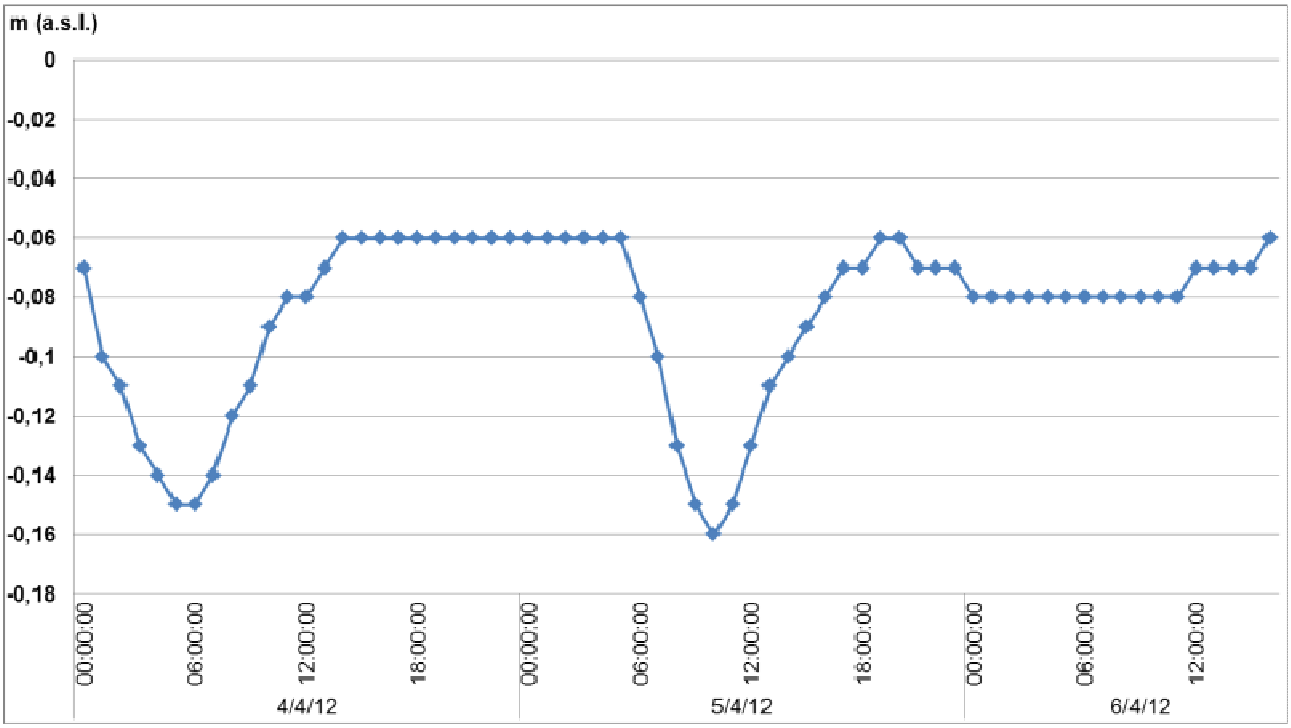

Fig. 4.26: water table depression cones due to groundwater pumping during three spring time days. Observing the cone of the 4th of April, it can be noticed how the decrease of level starts at midnight and the maximum depression is around 6 o'clock a.m. This graphic confirms that in Pontina plain withdrawals can occur even during the night

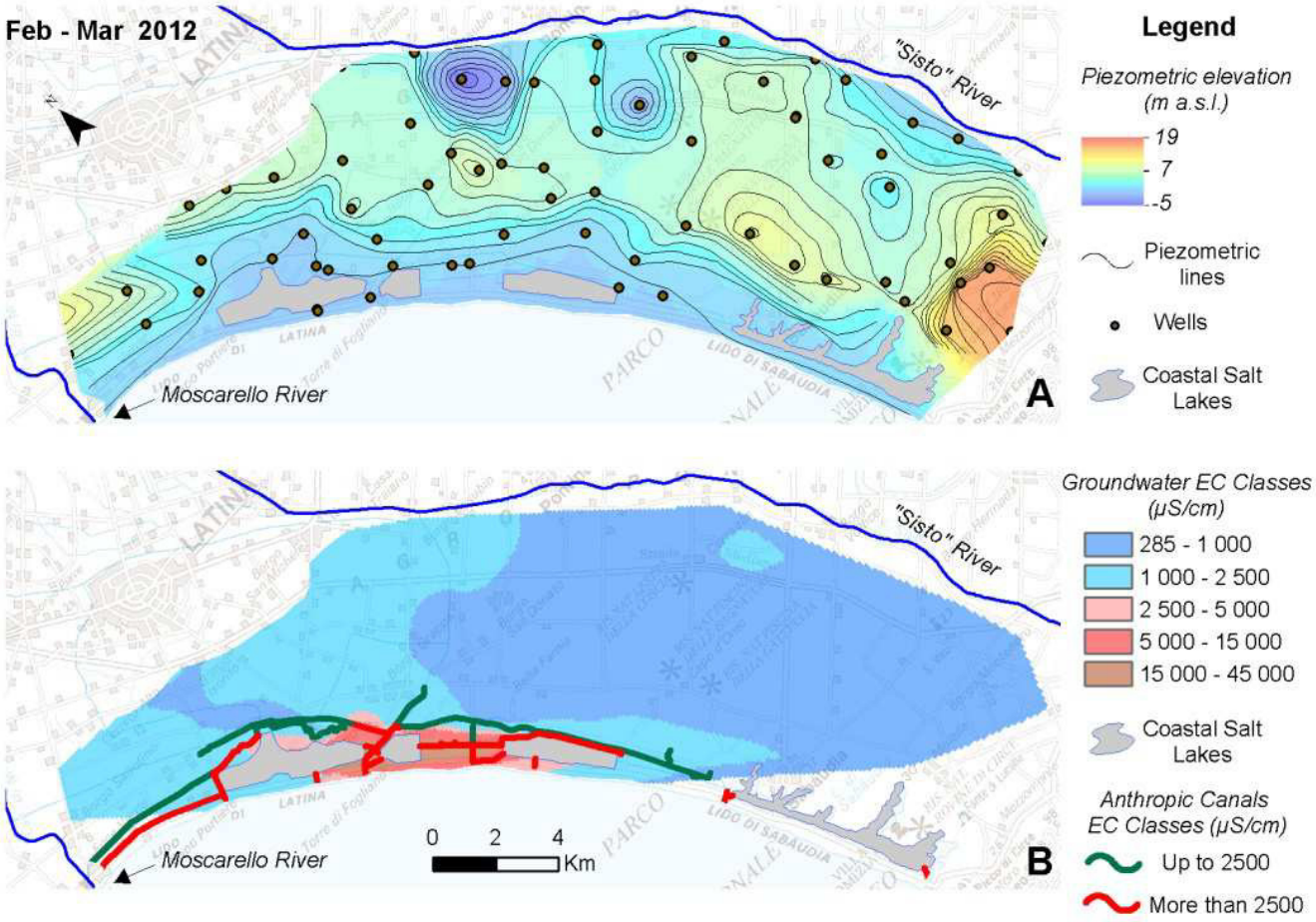

Fig. 4.27: correlation between groundwater salinization and salinity pattern of the drainage network

Analyzing the data about the dune removal at the Rio Martino River mouth it is possible to see how the natural barrier of the dune ridges has been strongly affected by reclamation works. Fig.4.28a shows the coast line position and the morphology about the 1927, when the Rio Martino was a natural river and about 2003, after the reclamation works. Fig.4.28b shows the topographic sections about the same periods. Observing the red line it is possible to evaluate how the reclamation works have strongly reduced the volume of the dune ridge and in particular in the B2 section, the morphology was completely leveled to best organize the river mouth. Therefore the demolition of the dune ridge determined the physical disappearance on ta natural barrier able to store freshwater lenses.

Effectuating the volumetric analysis through the GIS system (Fig.4.29) it was possible to quantify in this area a net loss of about 225000 m^3 of dune.

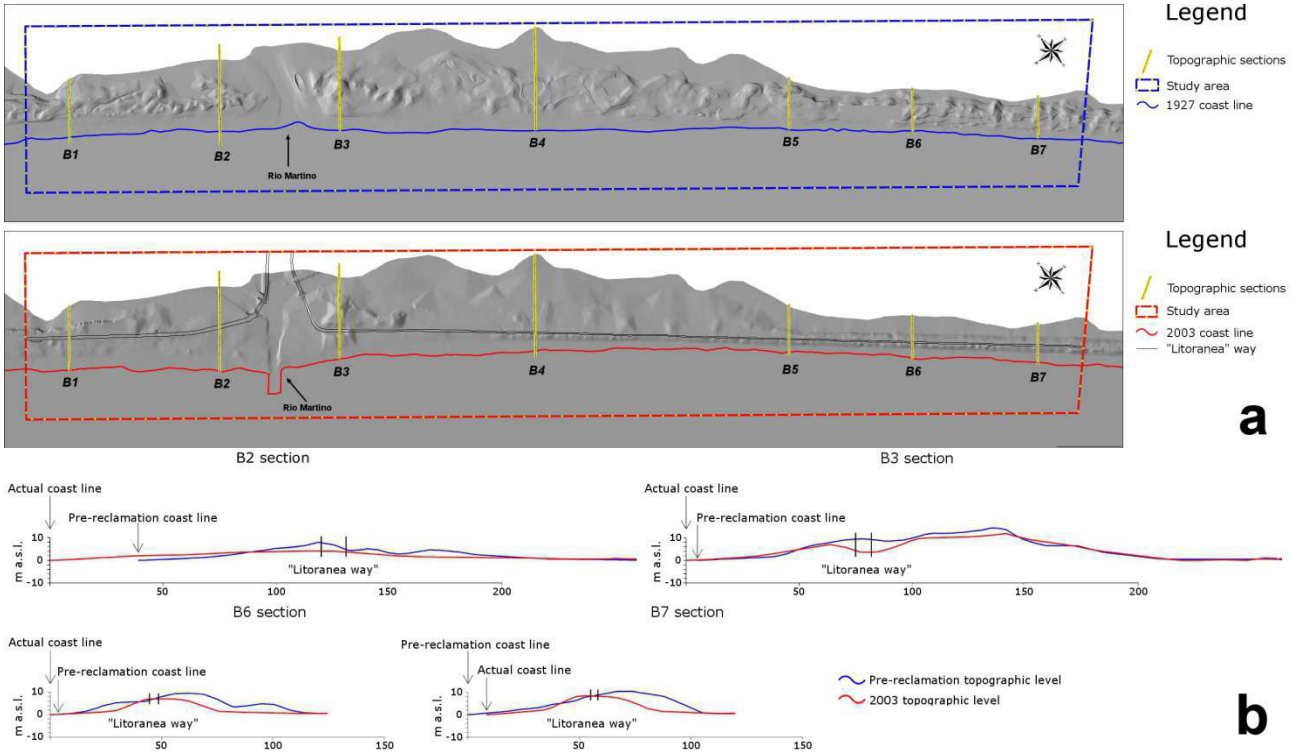

Fig. 4.28: a) morphology about 1927 and 2003; b) topographic section about the morphology of the two periods (Gragnanini 2009)

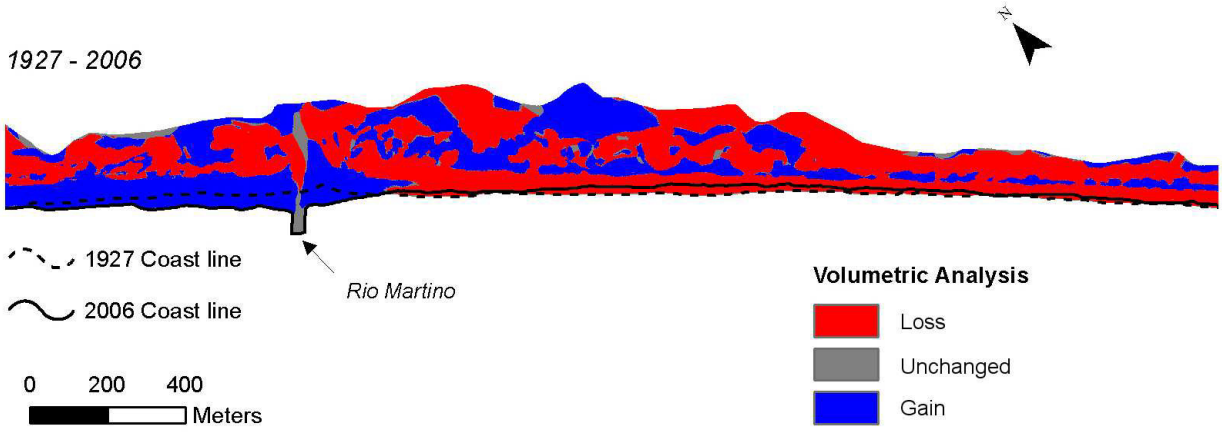

Fig. 4.29: Volumetric analysis about the Rio Martino area. A net loss of about 225000m^3 was evaluated by the Gis system (Gragnanini 2009)

4.6 CONCLUSIONS

This study allowed to analyze groundwater pattern modification during three surveys, realized in three different seasons. The constant presence of cones of depression proves that the groundwater system is exploited during the whole year and even during the night. The crop types cultivated in the greenhouses (eggplants, tomatoes, zucchinis and watermelons) could be the reason of the cone depressions, because of their great water needs. The hydrogeological pattern changed significantly during the surveys, but the hydraulic heads distribution kept quite unchanged. The stratigraphic reconstruction permitted to recognize where the multilayered aquifer is more or less productive: in fact in the inner sector, the depth of the clayey basement and the presence of several sandy layers, determine a great volumes of groundwater to store; in the coastal sector the local setup of the low permeability basement determine a reduction of the thickness of the aquifer, composed in this part by gravels and sands mainly. The aquifer productivity is therefore strictly conditioned by the tectonic history of the two sectors (Barbieri et al. 1999).

Particular anomalies of EC and Sal were not noticed in the innermost parts of the study area. Only an area between Fogliano Lake and Caprolace Lake was identified as subject to seawater intrusion. Two main processes of salinization about the costal aquifer were observed:

- lateral intrusion, depending on the modification of the recharge rate and the presence of intensive withdrawals;
- upconing, related to groundwater pumping.

The coastal area affected by seawater intrusion, identified during the survey, was different from that indicated in previous works. It is confined in an area included between the Fogliano and Caprolace Lake. Sappa & Rossi (2007) recognized as a seawater intruded area, the whole coastal area from the Monaci Lake to the northern part of Sabaudia Lake. This is likely due to the different network of surveyed wells: in fact in this study it was impossible to collect data about the surrounding area of the Sabaudia Lake because of a great presence of private houses.

Lakes resulted suspended with respect to the regional aquifer: the presence of the low hydraulic conductivity terraced complex of Terracina (4b in Fig.2) isolates the regional aquifer by downward intrusion from the coastal lakes. It is demonstrated by the lacking relationships between lake level and water table fluctuations.

The reclamation activities determined an increase of the drainage network, to allow freshwater to flow into the sea. This determined a spread of the coastal area subject to salinization because the drainages represent a preferential way of seawater intrusion (Giambastiani et al. 2007; UNESCO 1983; Xue et al. 2009). Reclamation works acted also on the dune ridges and a great volume of coastal dune disappeared. Especially in proximity to the coast line this reduction of dunes determined the disappearance of very porous sand bodies, able to store freshwater (Bakker 1990) and consequently to limit seawater intrusion.

In an agricultural context where regional water governance is missing, the uncontrolled withdrawals endanger the natural system. The presence of the Circeo National Park is helpful for the hydrogeological system: along the coast it prevents intensive agricultural activities from an overexploitation of groundwater; inland, it permits to preserve the morphological ridge of the Circeo National Park Forest, as an uncontaminated recharge area.

4.7 REFERENCES

Alimonti C, Raspa G, Gazzetti C, Sarandrea P (2005) Valutazione delle vulnerabilità degli acquiferi della pianura Pontina mediante tecniche di bilancio distribuito con metodi geostatistici. Paper presented at the Aquifer Vulnerability and Risk, Colorno-Italy,

Antonellini M, Mollema P, Giambastiani B, Bishop K, Caruso L, Minchio A, Pellegrini L, Sabia M, Ulazzi E, Gabbianelli G (2008) Salt water intrusion in the coastal aquifer of the southern Po Plain, Italy. Hydrogeology Journal 16 (8):1541-1556. doi:10.1007/s10040-008-0319-9

Aquater (1988) Redazione di un piano di gestione per il Parco Nazionale del Circeo, Censimento pozzi e sorgenti

ArcGisMapService (2013) http://server.arcgisonline.com/arcgis/services/World_Imagery/MapServer.

Autodesk (2004) Manuale introduttivo. http://docs.autodesk.com/MAP/2011/ITA/AutoCAD%20Map%203D%202011%20Help/Map3D_2011_HTML_Help/indexUsersGuideHTML.html?url=./filesUsersGuideHTML/WS5165537708879B04B87A9641B207B799F.htm,topicNumber=UsersGuideHTMLd0e4635.

Bakker TWM (1990) The geohydrology of coastal dunes. In: Th.W. Bakker PDJ, amp, Klijn JA (eds) Dunes of the European Coasts. vol 18. Catena Supplement, Destedt-Cremlingen, pp 109-119

Barbieri A, Carrara C, Castorina F, Dai Pra G, Esu D, Gliozzi E, Paganin G, Sadori L (1999) Multidisciplinary study of Middle-Upper Pleistocene deposits in a core from the Piana Pontina (central Italy). Giornale di geologia 61:47-73

Barlow PM (2003) Salwater Intrusion from the Delaware River During Drought-Implications for the Effect of Sea-Level Rise on Coastal Aquifers. In: Ground Water in Freshwater-Saltwater Environments of the Atlantic Coast. U.S. Geological Survey, Reston, Virginia, USA, pp 46-48

Bear J, Cheng AH-D, Sorek S, Ouzer D, Herrera I (1999) Geophysical investigations. In: Jacob Bear AHDCSSDO, Ismael H (eds) Seawater Intrusion in Coastal Aquifers - Concepts, Methods and Practises. Kluwer Academic Publishers, Dordrecht, The Nederlands, pp 9-50

Boni C, Bono P, Calderoni G, Lombardi S, Turi B (1980) Indagine idrogeologica e geochimica sui rapporti tra ciclo carsico e circuito idrotermale nella Pianura Pontina (Lazio meridionale). Geologia applicata e idrogeologia 15:203-247

Boni C, Bono P, Capelli G (1988) Carta Geologica del Lazio. Scala 1:250.000. Studio Marinelli, Roma

Bono P, Gliozzi E, Malatesta A, Zarlenga F (1985) Progetto Laghi Costieri.

Brunamonte F, Serangeli S (1996) Evoluzione naturale ed intervento antropico nello sviluppo dei fenomeni di subsidenza nella Pianura Pontina. Memorie della Società Geologica Italiana 51:823-836

Cameron WM, Pritchard DW (1963) Estuaries. In: The Sea, vol 2. Wiley, New York, USA, pp 306-324

Capelli G, Mastrorillo L, Mazza R, Petitta M, Baldoni T, Banzato F, Cascone D, Di Salvo C, La Vigna F, Taviani S, Teoli P (2012) Carta Idrogeologica del Territorio della Regione Lazio. Scala 1:100.000 (4 Fogli). S.EL.CA., Firenze - Italy

Casa R-, Rossi M, Sappa G, Trotta A (2009) Assessing Crop Water Demand by Remote Sensing and GIS for the Pontina Plain, Central Italy. Water Resources Management 23:1685–1712. doi:10.1007/s11269-008-9347-4

Cavinato GP, Corrado S, Sirna M (1992) Dati preliminari sull'assetto geologico-strutturale del settore sud-occidentale della struttura simbruino-ernica. Studi Geologici Camerti speciale 1991/1992 CROP 11:33-42

CMP (1968) Compagnia Mediterranea Prospezioni, Prospezione geoelettrica nella Pianura Pontina. Cassa per il Mezzogiorno,

Conforto B, Di Ricco G, Sappa M (1962) Indagine sulle acque sotterranee dell'Agro Romano e Pontino. vol 2. Cassa per il Mezzoggiorno,

Cooper HH (1959) A Hypothesis Concerning the Dynamic Balance of Fresh Water and Salt Water in a Coastal Aquifer Journal of Geophysical Research 64 (4):461-467

Custodio E, Llamas MR (2005) Superfici piezometriche. In: Flaccovio D (ed) Idrologia sotterranea, vol 1. Palermo, pp 511-528

De Pippo T, Donadio C, Pennetta M (2001) Evoluzione morfologica della Laguna di Sabaudia (Mar Tirreno, Italia Centrale). Geologica Romana 32:1-12

Doorenbos J, Kassam AH (1979) Yield response to water. Irrigation and Drainage Paper, vol 33. FAO, Roma

Drabbe J, Badon Ghyben W (1889) Nota in verband met de voorgenomen puboring nabij Amsterdam. Amsterdam

Dyer KR (1997) Estuaries-a physical introduction 2nd Edition. Chichester

EEA (2006) European Environmental Agency, Corine land cover. http://www.eea.europa.eu/data-and-maps/data/corine-land-cover-2006-clc2006-100-m-version-12-2009#tab-additional-information.

ESRI (2008) ArcGIS – A Complete Integrated System. http://www.esri.com/software/arcgis.

Freeze RA, Cherry JA (1979) Groundwater. Englewood Cliffs, New Jersey

Fubelli G, Gliozzi E, Parotto M (2001) Carta Geologica e Carta Geomorfologica del Parco Nazionale del Circeo.

Funiciello R, Parotto M (1978) Il substrato sedimentario nell'area dei Colli Albani: considerazioni geodinamiche e paleogeografiche sul margine tirrenico dell'Appennino Centrale. Geologica Romana 17:233-287

Giambastiani BMS, Antonellini M, Essink GHPO, Stuurman RJ (2007) Saltwater intrusion in the unconfined coastal aquifer of Ravenna (Italy): A numerical model. Journal of Hydrology 340 (1-2):91-104. doi:10.1016/j.jhydrol.2007.04.001

Gisotti G, Scarpelli F (1977) Un esempio di protezione delle acque sotterranee in una zona a Parco Nazionale (Circeo). Collana progetto finalizzato promozione della qualità dell'ambiente, vol AQ/2/7. CNR, Roma

Gonios (2012) Banca dati delle perforazioni.

Gowda K (1996) Land reclamation and its impact on environment: a case study of Victoria Harbour. University of Hong Kong, Hong Kong

Gragnanini V (2009) Intrusione salina nell'acquifero costiero compreso tra Foce Verde e Rio Martino (Pianura Pontina). Roma Tre, Rome

Herzberg B (1901) Die wasserversorgundeinigerNordseebâder. Journal gasbeleuchtung und Wasserversorgung 44:815-819, 824-844

Hubbert MK (1940) The theory of ground-water motion. Journal of Geology 47:785-944

Hydrodata, DHI-Italia (2012) Progetto Life Rewetland - Analisi del bilancio idrologico del sistema Lago di Fogliano-Lago dei Monaci e definizione di strategie di riduzione dei fenomeni di eutrofizzazione e salinizzazione.

IGM (1927) Istituto Geografico Militare, Carta della Bonificazione Pontina e della bonifica di Piscinara.

ISPRA (2012a) Dati del mareografo di Anzio di maggio 2012. http://www.mareografico.it/?session=0S40109837687072L74877081O&syslng=ita&sysmen=-1&sysind=-1&syssub=-1&sysfnt=0&code=STAZ&idst=2C.

ISPRA (2012b) Istituto Superiore per la Prevenzione e Ricerca Ambientale, Archivio nazionale delle indagini nel sottosuolo (L.464/84) http://sgi.isprambiente.it/GMV2/index.html.

ISPRA (2013) GeoMapViewer, Servizio Geologico d'Italia. http://sgi.isprambiente.it/GMV2/index.html.

Jiao JJ, Nandy S, Li HL (2001) Analytical studies on the impact of land reclamation on ground water flow. Ground Water 39 (6):912-920. doi:10.1111/j.1745-6584.2001.tb02479.x

Jiao JJ, Wang XS, Nandy S (2006) Preliminary assessment of the impacts of deep foundations and land reclamation on groundwater flow in a coastal area in Hong Kong, China. Hydrogeology Journal 14 (1-2):100-114. doi:10.1007/s10040-004-0393-6

Kamermans H (1991) Faulted land: the geology of the Agro Pontino. In: A. Voorrips SHLHK (ed) The Agro Pontino survey project, methods and preliminary results. Amsterdam, p 131

La Monica GB, Raffi R (1996) Morfologia e sedimentologia della spiaggia e della piattaforma continentale interna. Il Mare del Lazio.

LINQ (2012) Laboratorio di Idrogeologia dell'Università di Roma Tre, Banca dati dei punti di osservazione. Roma

Michael M, Michelle S, Wrightsell J (2000) Using ArcMap. Redlands, California

Mouton J Contributo allo studio delle acque sotterranee dell'Agro Romano e Pontino. In: L'acqua per la Piana Pontina: situazioni e prospettive, Latina, 1977.
Noal A, Bucci M (2003) Progetto "Parchi in qualità".
Pritchard DW Estuarine circulation patterns. In: American Society of Civil Engineers, 1955. pp 1-11
RegioneLazio (2006) Carta Tecnica Regionale Numerica della Regione Lazio.
RegioneLazio (2007) Schemi Idrici del Lazio Meridionale. Studio delle risorse. Relazioni Monografiche delle unità idrogeologiche del Lazio Meridionale e relazione di sintesi.
Sappa G, Coviello MT (2011) Processi di salinizzazione degli acquiferi costieri della Pianura Pontina, vol 84. Quaderni di tecniche di protezione ambientale. Bologna-Italy
Sappa G, Coviello MT, Rossi M The groundwater overexploitation of a coastal aquifer: a multidisciplinary approach. In: Ellenic Hydrogeology Conference, Athens-Greece, 2005.
Sappa G, Rossi M (2007) Idrogeologia del Sistema Acquifero della Pianura Pontina. Studi propedeutici al Piano per l'uso compatibile della risorsa idrica per la Regione Lazio. Firenze-Italy
Serva L, Brunamonte F (2007) Subsidence in the Pontina Plain, Italy. Bulletin of Engineering Geology and the Environment 66 (2):125-134. doi:10.1007/s10064-006-0057-y
Sevink J, Duivenvoorden J, Kamermans H (1991) The soils of the Agro Pontino. In: A. Voorrips SHLHK (ed) The Agro Pontino survey project, methods and preliminary results. 31-47, Amsterdam,
Song S-H, Zemansky G (2012) Vulnerability of groundwater systems with sea level rise in coastal aquifers, South Korea. Environmental Earth Sciences 65 (6):1865-1876. doi:10.1007/s12665-011-1169-7
Stuyfzand PJ (1995) The impact of land reclamation on groundwater quality and future drinking-water supply in the netherlands. Water Science and Technology 31 (8):47-57. doi:10.1016/0273-1223(95)00356-r
UNESCO (1983) Algorithms for computation of fundamental properties of seawater.
UNESCO (1991) Guidelines on the study of seawater intrusion into rivers. United Nations Educational, Scientific and Cultural Organization, Paris
Xue P, Chen C, Ding P, Beardsley RC, Lin H, Ge J, Kong Y (2009) Saltwater intrusion into the Changjiang River: A model-guided mechanism study. Journal of Geophysical Research-Oceans 114. doi:10.1029/2008jc004831

5. INCREASING SALINITY PATTERN DURING THE FALLS IN AN UNCONFINED AQUIFER NEARBY A CANAL ESTUARY: ASSESSMENT OF THE PROCESSES USING NUMERICAL MODELING

ABSTRACT

Remote sensing, hydrogeological and chemo-physical data collected in an ex-industrial area were used to develop a numerical model. The numerical study was conducted to test the movement of a groundwater saline plume detected in a coastal aquifer. In particular, attention was focused on the increasing salinity pattern observed during the falls. The aquifer was located at an anthropic canal estuary, in which a salt-wedge intrusion was noticed. The aquifer was supposed to be influenced by the canal water level modification, due to the rains. A 2D transient transport-flow model normal to the canal banks was developed using FEFLOW 6.0, to assess whether the canal water level was able to generate a hydraulic gradient directed toward the aquifer. The simulation confirmed that whenever the canal water level was higher than groundwater level, an inflow from the river bottom to groundwater happened (canal-dominated hydraulic gradient). Vice versa when groundwater level was higher than the canal level, an outflow from the aquifer occurred (groundwater-dominated hydraulic gradient). Different salinization scenarios were tested in the simulation, to determine the influences of the canal water salinity on the saline plume concentration. The model confirmed that, excluding extreme salinity values for the river water, the increasing salinity pattern during the falls could be induced by the canal-dominated hydraulic gradient, which determined a landward migration of the saline plume.

5.1 INTRODUCTION

Seawater intrusion in coastal areas is an increasing problem for the human development because it is caused by a constant increase of groundwater withdrawals for human, industrial, livestock and agricultural uses. Numerical modeling is an important tool to plan and to predict the behavior of a coastal groundwater systems (Barazzuoli et al. 2008; Qahman and Larabi 2006; Giambastiani et al. 2007) or to assess the origin of seawater intrusion (Akouvi et al. 2008). Numerical modeling is also an important tool to elaborate theories about processes affecting groundwater in coastal areas. Li and Barry (1999) for example developed a theoretical model for the submarine groundwater discharge and the associated chemical transfer to the ocean. Xin et al. (2010) analyzed the effect of wave forcing on a subterranean estuary. Lenkopane et al. (2009) investigated the groundwater transport under varying estuarine salinity (Sal) conditions. Despite this, relatively little work about numerical modeling have been validated with experimental data. An attempt was made by Brovelli et al. (2007), who implemented a numerical model that reproduced data from a laboratory experiment, designed to investigate the impact of tides on conservative contaminant transport in a coastal aquifer. Mao et al. (2006) investigated the effects of the beach slope near a low-relief estuary using numerical modeling, finding close connections between experimental and simulated data.

These approaches were developed by means of two-dimensional numerical models, that can allow an accurate exploration about the influence of factors, such as aquifer and soil materials, tidal amplitudes and regional groundwater hydraulic gradients (Werner and Lockington 2006).

The aim of this study was to validate experimental data using numerical modeling. A 2D numerical model was implemented to try to explain the salinity pattern coming from data collected in a piezometer drilled in an unconfined aquifer. The piezometer is located in the nearby of an anthropic canal estuary, the Moscarello Canal, in which a salt-wedge intrusion was noticed in previous surveys (see chapter 4). Groundwater data collected in the borehole showed a brackish water composition during all the surveys, suggesting the presence of a seawater plume in the aquifer. Furthermore the salinity trend showed an enhancement during the falls, although the recharge rate was very high. For this reason a dilution of brackish groundwater was expected. As a consequence the most likely source of aquifer salinization was supposed to be seawater penetrating the canal from the estuary. The 2D numerical model was setup along a W-E transect, normal to the Moscarello Canal. This 2D model aimed to identify the possible processes affecting

the salinization of the Lat12 borehole, related to the hydraulic gradient generated by the flood events of the Moscarello Canal. The alternation between a normal hydraulic gradient (flow paths directed toward the canal) and a canal-dominated one (seawater intrusion through the canal bed, determining an inflow of water into the aquifer), was supposed to be the driving force of the migration of a saline plume occurring in the aquifer.

5.2 GEOLOGICAL, HYDROGEOLOGICAL AND HYDROGRAPHICAL SETTING

The study area is located in Pontina Plain, in Central Italy along the Tyrrhenian coast line, about 10 km southwest of Latina city. This area was strongly affected by reclamation activities, started about 2000 years ago and finished in the late 30's of the past century (Brunamonte and Serangeli 1996; Serva and Brunamonte 2007). Reclamation works changed the hydrographical and the morphological pattern substantially, by means of drainages digging and filling activities. From a climatic point of view Pontina Plain can be classified as a meso-mediterrinian thermo-type, characterized by precipitations between 842 mm and 966 mm, with a few rain summer episodes (Barbieri et al. 1999). The mean annual temperature is fairly high, the dry summer period is pronounced and protracted for four months (May-August). The cold winter period occurs between November and April, with a mean low temperature of the coldest month between 3.6°C and 5.5°C (Barbieri et al. 1999).
The study area is set in an ex industrial area belonging to Società Gestione Impianti Nucleari (SOGIN). It is limited eastward by the Moscarello Canal and southward by the Tyrrhenian Sea. Groundwater data collection was performed in a new monitoring network (Fig.5.1), drilled by SOGIN from April to September 2012

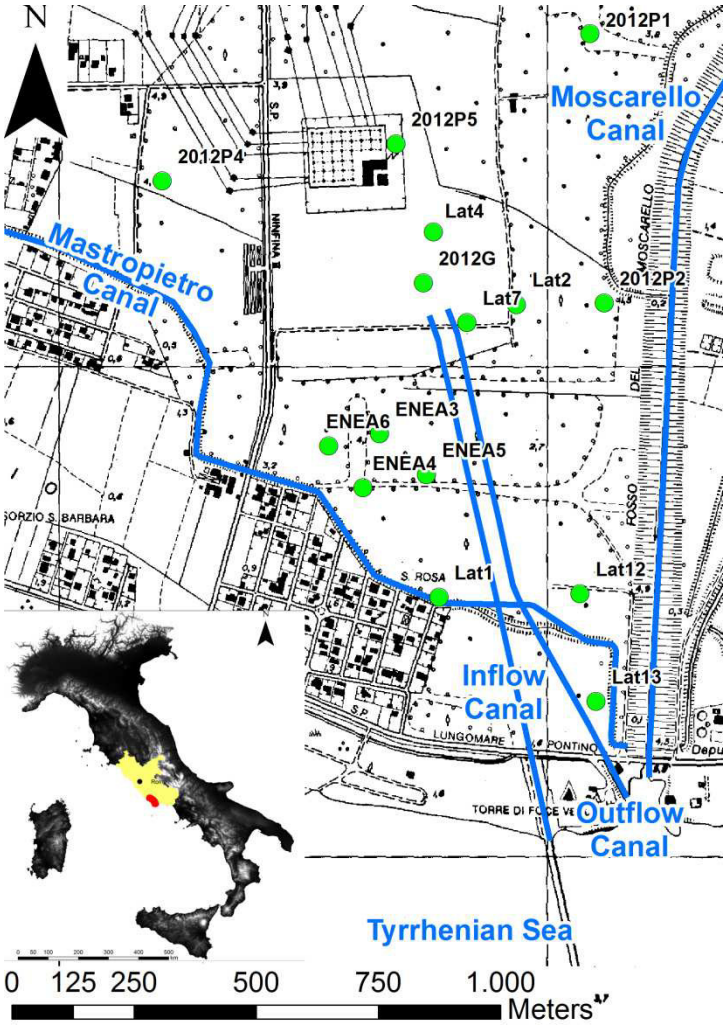

Fig. 5.1: location of the study area and the position of the new-drilled monitoring network.

Pontina Plain is made up of clastic sediments, aged from the Medium Pleistocene to Holocene, of marine, alluvial, marsh, lagoon and beach ridge environment (Conforto et al. 1962). The main lithologies recognized in the boreholes of the study area were: sands, silts, clays and volcanic deposits from the Colli Albani Volcanic Complex (Funiciello and Parotto 1978). The Medium Pleistocene-Holocene deposits overlie a low permeability Lower Pleistocene clayey basement. This aquiclude, in turn, covers Cretaceous-Jurassic carbonate rocks and was affected by normal faulting during the Pliocene and Pleistocene (Cavinato et al. 1992). The area is located on a structural high and it explains the reason of the shallowness of the Lower Pleistocene clays, that in the study area are about 25 m below the ground level. Generally the clastic aquifer is unconfined and it holds a medium-high permeability (Capelli et al. 2012). Fig.5.2 shows the stratigraphy about one of the boreholes drilled in the 2013. A clayey-sily horizon, with a changeable thickness ranging from 1 to 5 meters and a very low hydraulic conductivity [estimated in10^{-7} m/s (Casadio and Elmi 1995)], divides the groundwater system in two aquifers:

- the first one, shallow and mainly composed by sands, calcarenites and thin volcanic layers;
- the second one, deep and mostly composed by silty sands and a thick volcanic unit.

Therefore the geology of the study area can be simplified as depicted in Fig.5.3, where the horizon D represents the shallow aquifer and the underlying clayey-silt layer, whereas horizon C and horizon B represent the deep aquifer. The two aquifers can be in hydraulic communication because of the local lack of the clayey-silt deposit.

The two aquifers water levels, monitored during the field activity, are displayed in Fig.5.4. Both of them respond very quickly to the zenithal recharge, are subject to tidal fluctuation and the similar fluctuation trend let suppose that they are in hydraulic communication.

The hydrology of the study area is depicted in Fig.5.1 and it is mostly represented by reclaim and industrial canals:

- two concrete anthropic canals for the intake and outtake of seawater are present in the middle of the study area and they hold maximum depths of -4.70 m and -0.80 m b.s.l. respectively (SOGIN 2012).
- the Mastropietro reclaim canal is an irrigation canal that runs from the Astura Canal (2 km westward with respect the study area) to the Moscarello Canal. It runs over the intake canal on a bridge and passes under the outlet canal in a tunnel. Its bottom lies about 0.5 m a.s.l. and during the summer it is filled opening the sluice gate at Fosso Astura. During the winter the gate is closed and it only contains rainwater (D'Appolonia 1984);
- Moscarello Canal is an anthropic reclamation canal dug during the 30's of the past century. It collects water from the Albani Hills and the Lepini Mounts (see Fig.0.2 in the General Introduction) and it can be subject to great discharge, especially during the falls with a maximum flood of 5.3 m a.s.l. (SOGIN 2012). In Fig.5.5 two pictures about a low flow and a flood period are depicted. Salt-wedge intrusion processes occur at the Moscarello Canal mouth (see chapter 4).

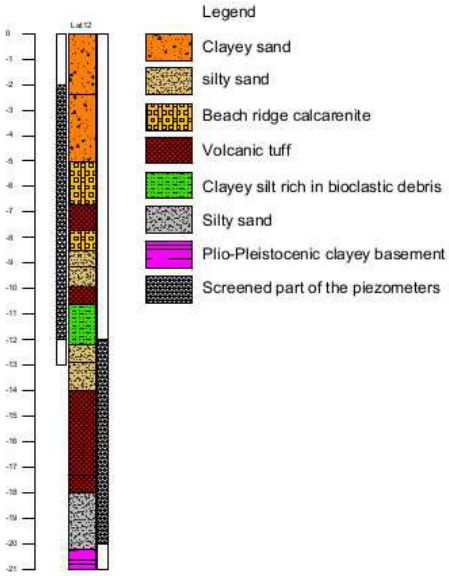

Fig. 5.2: stratigraphy of the Lat12 borehole. At about 11 meters from the ground level it can be observed the clayey-silt layer, which divide the aquifer in two parts

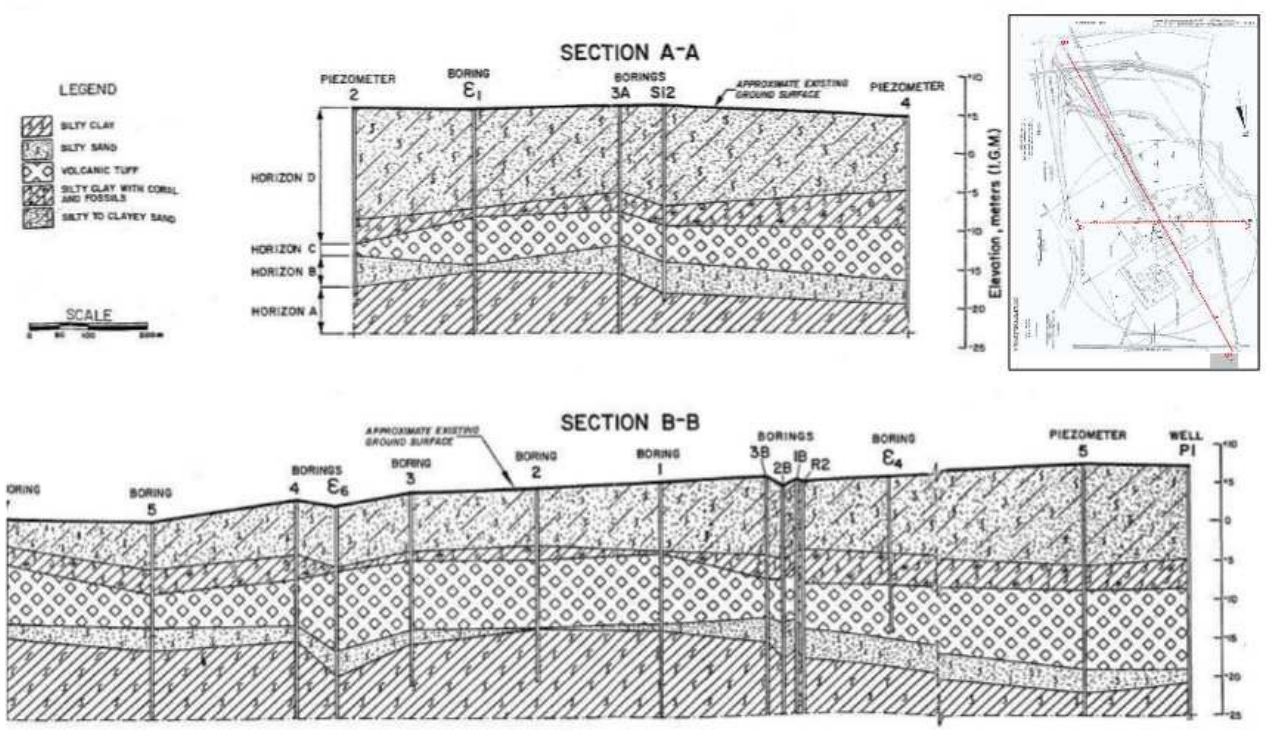

Fig. 5.3: geological cross-section about the study area; the horizon D represents the shallow aquifer and the underlying clayey-silt, whereas horizon C and horizon B represent the deep aquifer (D'Appolonia 1984)

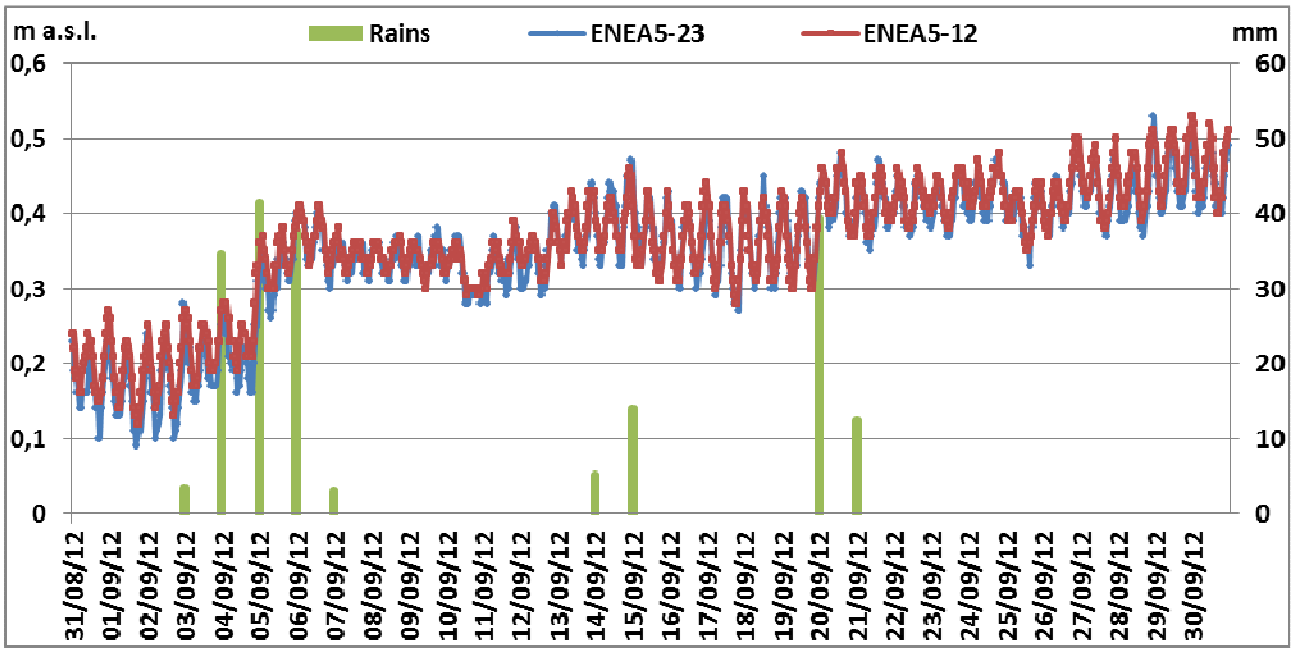

Fig. 5.4: water table level collected hourly at the ENEA5 station about the shallow aquifer (ENEA5-12) and the deep aquifer (ENEA5-23) (see Fig.5.1 for the location).

Fig. 5.5: Moscarello Canal water discharge: on the left is visible a low flow period, while on the right during a flood event

Groundwater pattern shows relationships with the morphology: higher water table levels are located next to the topographic reliefs and flow paths are directed eastward to the Moscarello Canal, southward to the sea and toward the intake and outlet canals in the central part of the study area (Fig.5.6). The recharge of the clastic aquifer mainly consists in the rainfalls.

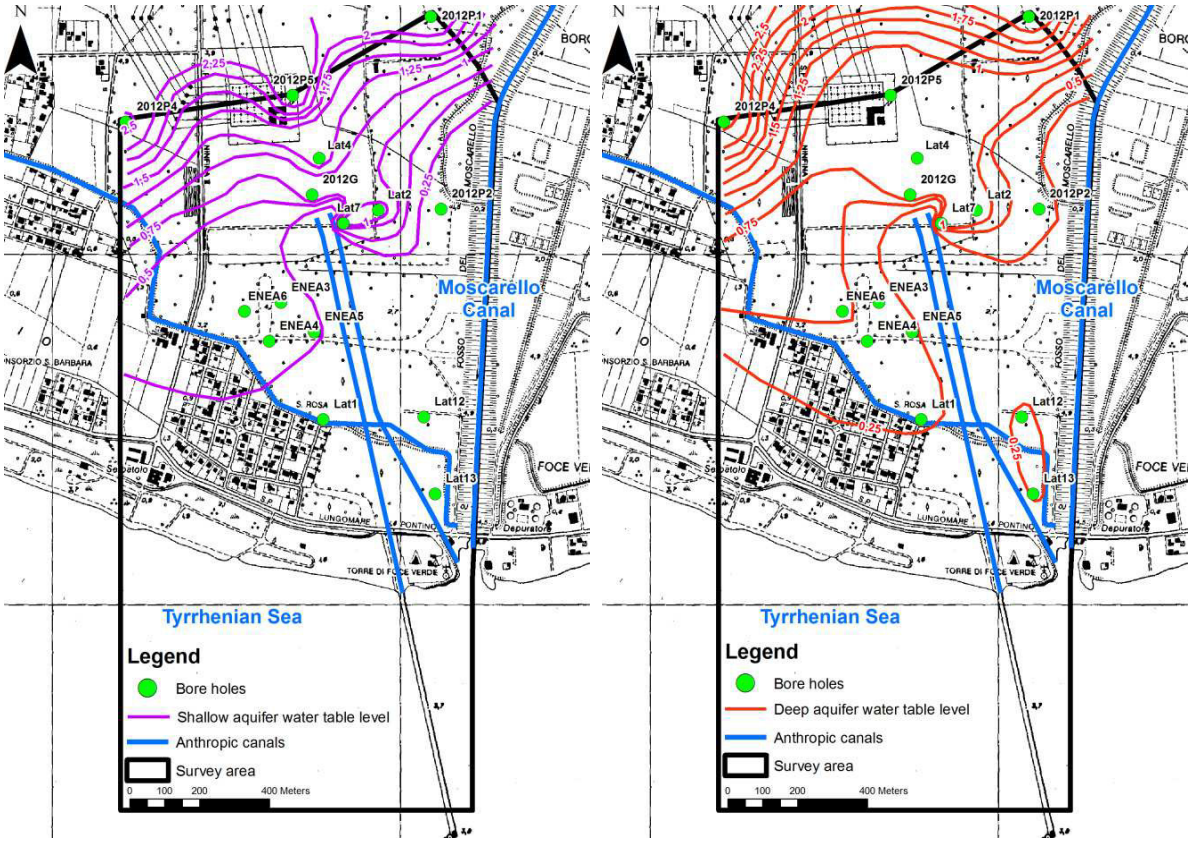

Fig. 5.6: groundwater pattern about the shallow (on the left) and deep aquifer (on the right) . Water levels were collected in October 2012

5.3 METHODS

5.3.1 SURVEY DATA METHODS

Hydrogeological surveys were carried out from June 2012 to June 2013, collecting data about water table level, Electrical Conductivity (EC, in µS/cm ± 0.5%, normalized at 25°C), Temperature (Temp ± 0.1, in °C), pH (pH, ± 0.01)

and Reduction Potential (Eh, in mV ± 0.5%), using a 100 m cable length multi-parameter probe. EC data were converted to Sal according to UNESCO (1983). The probe was used to collect data from the surface to the bottom of the borehole every 1 m, whenever the measurement values reached the stabilization. Data were collected in each of the measurement stations in in Fig.5.1, where two 220 mm diameter piezometers were installed to intercept the two aquifers. They reached maximum depths of 13 m and 30 m respectively for the shallow and deep aquifer piezometers. A scheme about the position of the screened part about one of the piezometers is depicted in Fig.5.2. The monitoring network consists in 15 measurement stations and data were collected with a time step of two months. Since the boreholes drilling concerned the landward piezometers firstly, only five surveys instead of six, were effectuated at the measurement stations Lat12 and Lat13.
At the ENEA5 station two sensors for water level and water level-EC measurements were installed, respectively for the shallow and deep aquifer, with the aim of collecting data hourly.

5.3.2 FEFLOW

As stated above, the aim of this study was to validate experimental data using numerical modeling.
FEFLOW 6.0 numerical modeling software (Finite Element Subsurface Flow System; Diersch, 2009) was chosen because it allows ti implement flow and transport simulations. FEFLOW is a finite-element simulation system for modeling 3D and 2D flow, mass and heat transport processes in groundwater and vadose zone, in steady or transient state (Fig.5.7). The finite element method was adopted for its flexibility and capacity to refine the nodal grid around points and/or single lines (inland boundary conditions, river boundary conditions) and to represent accurately the geographical layout of the aquifer. The user-friendly graphical interface provides easy access to the extensive modeling options and allows to analyze the simulation results in real time. The mathematical equations of flow and solute transport solved by FEFLOW in this study (after discretization in a finite-element grid) are given as follows:
Groundwater flow equation (Langevin and Guo 2006; Diersch 2009; Loaiciga et al. 2012):

$$\nabla \cdot \left[\rho \frac{\mu_f}{\mu} K \left(\nabla h + \frac{\rho - \rho_f}{\rho_f} \nabla z\right)\right] = \rho S_f \frac{\partial h}{\partial t} + \varphi \frac{\partial \rho}{\partial C} \frac{\partial C}{\partial t} \qquad \text{Eq.1}$$

In which ρ = density of salt groundwater; ρ_f = the density of fresh groundwater (≈1000 kg/m^3); μ = dynamic viscosity of salt groundwater; μ_f = dynamic viscosity of fresh groundwater; z = elevation head; φ = porosity; S_f = specific storage of fresh groundwater; C = the concentration of dissolved salts (or salinity) in groundwater; h = freshwater equivalent hydraulic head; t = time variable; ∇ = the gradient operator in three dimensional Cartesian coordinates; Kf = hydraulic conductivity of fresh groundwater, where $Kf = k\rho fg/\mu f$, k = permeability, g = acceleration of gravity.
Solute transport equation (Langevin and Guo 2006; Diersch 2009; Loaiciga et al. 2012):

$$\frac{\partial \varphi C}{\partial t} = \nabla \cdot (\varphi D \cdot \nabla C) - \nabla \cdot (qC) \qquad \text{Eq.2}$$

in which D = hydrodynamic dispersion tensor, q = vector of Darcian fluxes of groundwater and all other variables are defined in the above Eq.1.
In addition, there is the empirical equation relating the density ρ to salt concentration:

$$\rho = \rho_0 \left[1 + \frac{\alpha}{(C_s - C_0)} (C_s - C_0)\right] \qquad \text{Eq.3}$$

Where ρ is the generic water density, ρ_0 is the density of freshwater, C is the relative salt concentration, C_0 is the concentration of freshwater, C_s is the concentration of seawater at 35 g/l and α is the density ratio obtained by:
$\alpha = (\rho_{max} - \rho_0)/ \rho_0$ con ρ_{max} = 1.030 g/l and ρ_0 = 1.000 g/l

Equations 1,2 together with the empirical equation 3 for density, are discretized via the finite element method and solved simultaneously in FEFLOW (Diersch 2009).

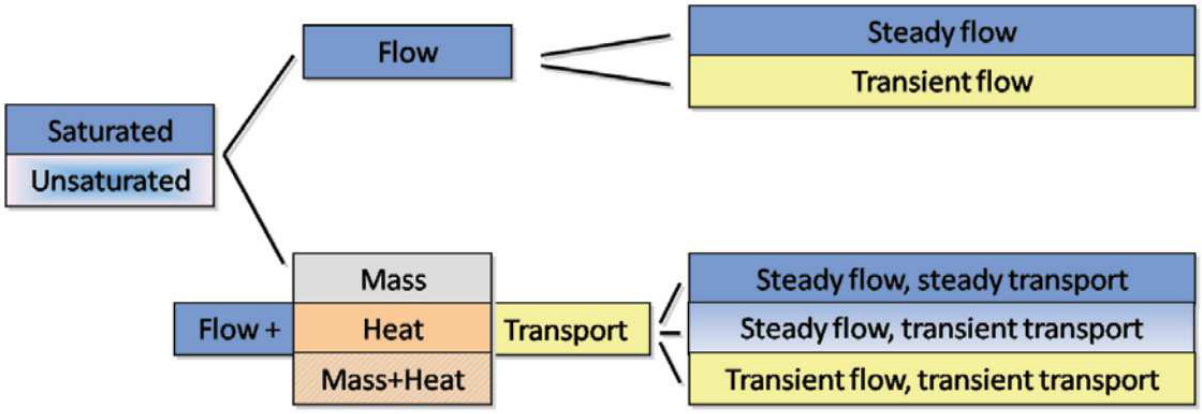

Fig. 5.7: simulation types of FEFLOW (Diersch 2009)

5.3.3 NUMERICAL MODELING METHODS

Sal Data about the study area showed a great variability during the survey period both for the deep and the shallow aquifer. Fig.5.8a and Fig.5.8b represent EC variability respectively for the shallow and deep aquifer.

Since some aspects about Sal enhancement were not deeply understood, the use of numerical modeling was supposed to be helpful for understanding the processes affecting Sal modifications in the study area. Nevertheless the implementation of a 3D numerical model was supposed to be excessively time needy and the possibility of reaching a good comprehension of the hydrogeological system was presumed to be improbable. For this reason, a 2D numerical model was supposed to be more appropriate to explain the shallow aquifer Sal variability, especially for the data collected in the Lat12 piezometer. In fact, it showed the highest Sal values and the largest variability among the data collected in the shallow aquifer.

Lat12 is located very close to the Moscarello Canal, whose flow variability is very high throughout the year as above mentioned (Fig.5.5).

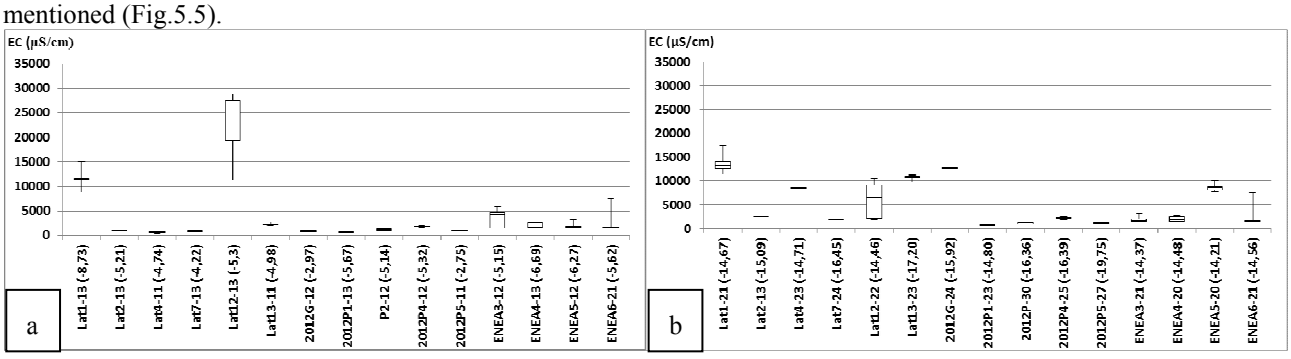

Fig. 5.8: boxplot about the EC values surveyed in the monitoring network in 2012-13 surveys. a) data about the shallow piezometers b) data about the deep aquifer. Number in brackets represent the depth of data sampling

Fig.5.9 shows the groundwater Sal values collected at the aquifer bottom and the water table level, about the Lat12 piezometer. At the moment of the first measurement, that was a post-summer period, a saline plume composed by brackish water was detected in the aquifer. Since the period from October to April is usually very rainy, a reduction of Sal was expected after the first measurement, due to dilution processes acted by fresher rainwater. A reduction of salinity related to a water table setup was expected as well, due to the Ghyben-Herzberg principle (Drabbe and Badon Ghyben 1889; Herzberg 1901). Therefore the increasing Sal trend suggested that another process was affecting groundwater Sal, likely related to the canal level fluctuation and involving the existing groundwater saline plume. The

model was setup to assess if the canal level rise induced by flood could generate a hydraulic gradient, able to push the existing saline plume in the piezometer direction. More in detail the model aimed to explain the Sal values variability observed during the 5 data collections in the Lat12 piezometer.

A 2D transient flow and mass transport numerical model was developed, assuming that the canal bottom was in hydraulic communication with the groundwater system.

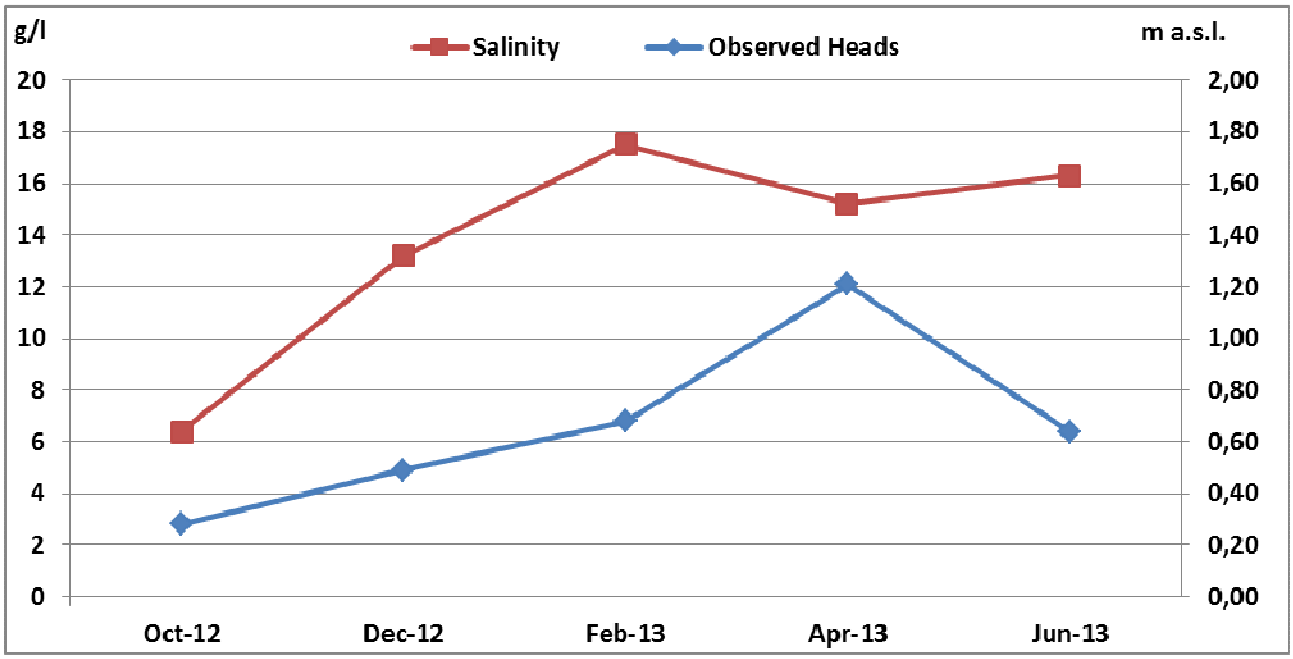

Fig. 5.9: Sal and water table level about the Lat12 piezometer. The values collected during the falls, instead of showing a Sal decreasing trend, showed increasing Sal values

The 2D vertical section was realized in parallel to the coast line with an W-E orientation (Fig.5.10a). The section is normal to the Moscarello Canal, whose orientation in the final part is N-S. The Sal conditions in the Canal are influenced by tidal effect and freshwater flushes induced by rainfalls, occurring moslty during Autumn and Spring. The model geometry is depicted in Fig.5.10b and represents a 2D vertical section of the unconfined shallow aquifer. It was realized according to the geological scheme of D'Appolona (1984), that presumes that the shallow aquifer composed by sands, calcarenites and thin volcanic layers, is sustained by the low permeability clayey-silt horizon (Fig.5.3).

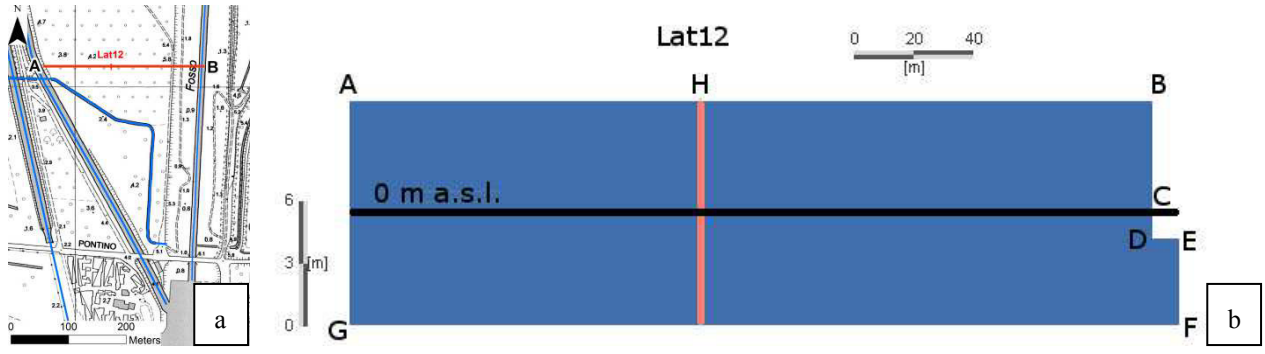

Fig. 5.10: a) location of the 2D vertical section; b) 2D vertical model geometry: the model describes an unconfined aquifer and it is assumed that a clayey-silt horizon lies at the bottom of the model. The Model Geometry is not in scale. AH=119 m; BH=153 m; BC=5.5 m; CD=1.3 m; DE=8 m; EF=4.2m; FG=280 m; AG= 11 m.

The model represents the canal-aquifer system as a vertical section. Longitudinal variations of the hydraulic gradient were neglected because the hydraulic gradient induced by canal level variations, was supposed to be higher than the groundwater one.

The aquifer was supposed to be in hydraulic communication with the canal bottom. Therefore the same hydraulic conductivity of the aquifer was supposed for the canal bottom.
The model was represented with a vertical bank, although it holds a different topographic section. In fact the Moscarello Canal banks are covered by concrete sheets and a seepage effect was supposed to not take place. Lenkopane et al. (2009) showed that vertical banks do not affect seepage effect significantly. In this way it was possible to neglect the seepage bank effect, not increasing model run times through seepage face dynamics addiction. The model was tested and confirmed this statement.
The influence of the outflow canal lying near the inland boundary (point A in Fig.5.10a) was not considered because its bed is concrete and a lack of hydraulic communication was supposed. The influence of Mastropietro canal was neglected because it is down-gradient with respect to the 2D model orientation.
The horizontal extent of the domain is 280 m (the inland boundary is 272 m from the canal bank and 8 m of canal width was simulated). The inland boundary is located 119 m from the Lat12 borehole, where Sal values were collected. Other model implementations showed that inland boundary conditions located at minor distances resulted to influence too much the model results.
The distance between Lat12 borehole and the canal bank was 153 m. The vertical extent of the model was 11 m (see stratigraphy about Lat12 in (Fig.5.2). Lenkopane et al. (2009) noticed that under similar conditions, the tide effect doesn't influence the salt propagation at more than 40 m from the canal bank and for this reason the tidal effect was neglected.
Usually 2D vertical models are used for the simulation of flow and saltwater intrusion but they are assumed to be completely confined. Modeling of unconfined conditions requires a simulation in unsaturated/variably saturated model. (Diersch 2009; Lenkopane et al. 2009).
In FEFLOW the groundwater flow and transport equations are coupled through the water density term and are solved jointly. Fluid density variations were assumed to be function of salt concentration and independent of temperature (assumed constant at 25°C) and viscosity (Werner and Lockington 2006; Lenkopane et al. 2009; Boufadel 2000).
In all the simulations the Obereck-Boussinesq assumption was used whereby the density is only considered in the buoyancy term of the Darcy equation. The time discretization was performed using the automatic time-step control and the forward Euler-backward Euler predictor–corrector time-stepping schemes were adopted, because they proved to be the most robust for the types of simulations performed (Lenkopane et al. 2009). The error norm used in the model was of the type Maximum Error Norm instead of the Euclidian L2 integral (RMS). This choice was taken because different values of Sal were used for the simulations and the Maximum Error Norm allowed a further time discretization, facilitating to reach the convergence without errors, but increasing model run times.
To smoothen steep concentration gradients the Galerkin finite element was used using a Lumped Mass computing mass matrix.
The model grid used for the simulations had 49100 nodes and 94861 triangular elements (Fig.5.11). Although the model area was similar to the one modeled by Lenkopane et al. (2009), a higher grid density of 31.35 triangular elements/m^2 was chosen [Lenkopane et al. (2009) used a grid density of about 12.88 triangular elements/m^2]. In fact it was supposed to be more appropriate, due to the great variability in terms of mass concentration and hydraulic heads used in the model.
The spacing of the grid was thickened along the model borders with a special resolution of 0,04 m. This nodal spacing resulted in grid Peclet numbers of less than two within the model area occupied by concentration fronts, which is within the suggested range of recommended values (Huyakorn and Pinder 1983; Lenkopane et al. 2009). After creating the model grid, the *"x"* axis of the local coordinate system was set on the 0 m a.s.l. line (black line in Fig.5.10). In this way FEFLOW used the local *"y"* coordinate as a reference for elevation dependent parameters, as the hydraulic head (Diersch 2009). In 2D models gravity direction is assumed to be the negative *"y"* axis.

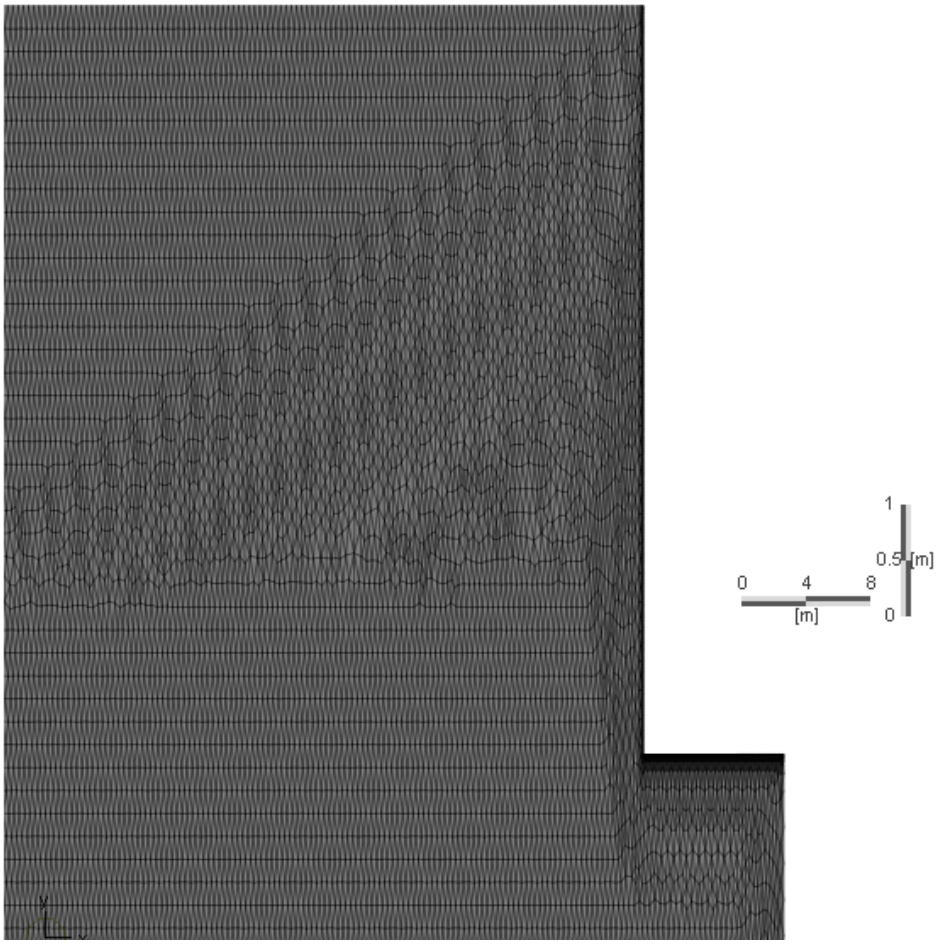

Fig. 5.11: particular of the model at the river bank with a grid density of 31.35 triangular elements/m^2; at the river bottom it is possible to see a thickening of the grid

The values used for the model parameters are listed in Tab.5.1. The hydraulic conductivity value of the aquifer ranged between $2.7 \cdot 10^{-3}$ and $1.25 \cdot 10^{-5}$ m/s (PERFOR 2013; SOGIN 2012; D'Appolonia 1984). The value of $3 \cdot 10^{-3}$ m/s was chosen during the calibration because better fitting the experimental data.
Recharge was neglected because it was considered in the water table fluctuation. Concentration dilution acted by rainwater was neglected too. A systematical analysis of all the parameters of the problem listed below was not undertaken.

Parameter	value
Hydraulic conductivity (PERFOR 2013)	0.003 m/s
Porosity (ε) (PERFOR 2013)	0.36
Residual saturation (θ_r) (Diersch 2009)	0.12
Maximum saturation (θ_s) (Diersch 2009)	0.42
Longitudinal dispersion coefficient (α_L) (Lenkopane et al. 2009; Gelhar et al. 1992)	2 m
Transverse dispersion coefficient (α_L) (Lenkopane et al. 2009; Gelhar et al. 1992)	0.4 m

Table 5.1: values of the model parameters

Simulations were tested for their convergence towards transient conditions. Convergence was always reached,
Boundary conditions were applied along the tract AG, BD and DE in Fig.5.10b, both for the hydraulic head and the mass concentration.

Hydraulic boundary conditions were about the Fixed hydraulic head type (1st kind/Dirichlet boundary condition) because of the well-known groundwater level at boundary and the surface water body was supposed to be perfectly connected to the aquifer.

Mass Transport Boundary Conditions were about the Fixed solute concentration (1st kind/Dirichlet boundary condition) and they are used when the background concentration at inflowing boundary is well-known.

The initial conditions to setup the model were obtained running the model as a transient flow-transient mass transport model. Since the initial conditions had to simulate a post-summer period, in which a salt-wedge shaped plume developed, a "passive seawater intrusion" was simulated. It was creating applying a very low hydraulic gradient toward the canal.

The assigned hydraulic boundary conditions were:

- 0.34 m a.s.l. at the canal bank and canal bottom boundary (BD and DE segments in Fig.5.10b);
- 0.38 m a.s.l. at the inland boundary (AG segment in Fig.5.10b).

The value 0.34 m a.s.l. at the canal bank-canal bottom boundary, was chosen assuming a 1‰ slope of the Moscarello Canal (D'Appolonia 1984; SOGIN 2012). Since the point B (Fig.5.10a) is located about 340 m from the canal estuary, a level of 0.34 m a.s.l. was supposed to be noticed there. The value of 0.38 at the inland boundary was chosen to create a low hydraulic gradient and simulate a "passive seawater intrusion" (groundwater hydraulic gradient toward the canal).

Boundary conditions about the mass concentrations were:

- 35 g/l of Sal at the canal bank-canal bottom boundary (BD and DE segments in Fig.5.10b);
- 6.4 g/l at the inland boundary (AG segment in Fig.5.10b).

The value of 6.4 g/l was chosen because it corresponds to the first measurement in the Lat12 piezometer. 35 g/l was chosen to simulate a seawater intrusion in the canal estuary during a low-flow period, that is a summer seawater intrusion. The model ran for 1000 days until it reached the steady-state conditions (Fig.5.12a). This initial conditions were assumed to be appropriate for the model because a salt-wedge can be obtained under the canal in just 90 days of simulation, that corresponds to the summer time period (Fig.5.12b).

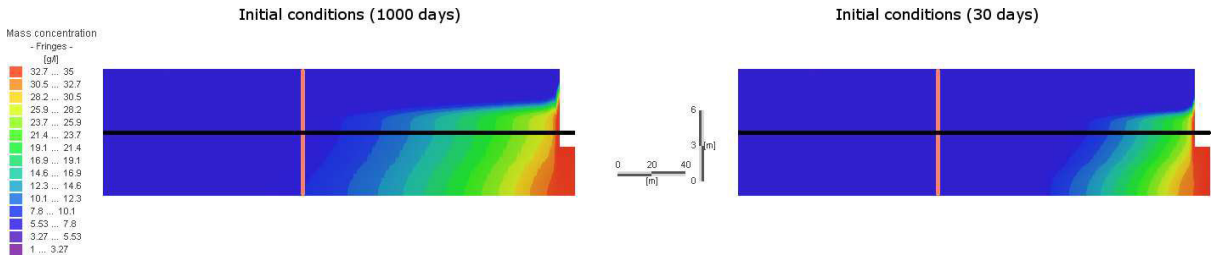

Fig. 5.12 (a) a simulation of 1000 days determined a salt-wedge shaped plume in steady-state conditions, necessary for the model implementation; (b) also a 30 days simulation can determine a salt-wedge shaped plume but it cannot be used for the model initial conditions. The pink line indicates the Lat12 piezometer position and the black line represents the 0 m a.s.l. line

For the transient flow and mass transport simulations, boundary conditions were represented in daily time series. Since the first day of survey was October 25th 2012 and the last day was June 14th 2013, from the beginning of Autumn to the beginning of the Summer, time-series were composed of 233 days, representing the whole period in which the surveys occurred.

The inland boundary conditions about the hydraulic head were represented by translating the average daily water table levels about the ENEA5 piezometer (Fig.5.1), where a remote sensing sensor was installed. The average difference about the Lat12 and ENEA5 water table levels, calculated on the basis of the average absolute value, was quantified in about 0.14 m. Therefore such value was subtracted from the average daily water table level of ENEA5 and used to create the water table level at the inland boundary conditions. The inland boundary conditions are 118 m distant from the Lat12, but the same water level was assumed to be at the boundary condition. The canal boundary conditions were derived from the hourly time levels collected at the Borgo Santa Maria water gauge (IdrograficoLazio 2013b). Since its location is about 4 km northward with respect to the point B location (Fig.5.10a), an operation of data translation was effectuated too. Since The point B is located at 0.34 m a.s.l. for the above mentioned reasons, the data time series were

normalized with respect to the zero and the average data levels were summed to this reference level, assuming that the canal section keeps constant.
The mass transport boundaries were specified along the same locations of the hydraulic head boundary conditions. Along all the other model boundaries no flux or mass were specified. In this way FEFLOW assumed them as impermeable.
The inland boundary was supposed to have a constant concentration of 6.4 g/l. The canal bank boundary was represented using time-series.
Both the mass and flow transport boundary conditions were represented in time-series using a linear interpolation to obtain a more realistic simulation.
A variable Sal scenario was simulated and after initial simulation, other salinity scenarios were texted to assess the influence of the Sal variation in the canal on one observation point.

5.4 Results and discussion

Fig.5.13 shows a graphic about the daily average water table level and daily average canal level related to the rains, collected at the Borgo Santa Maria meteorological station (IdrograficoLazio 2013a). Red line indicates the translated canal water level, whereas the blue line the translated water table level. It can be observed how the canal level is frequently higher than water table level because of flood events induced by rainfalls. Therefore an inversion of the hydraulic gradient can be hypothesized during a high discharge period.

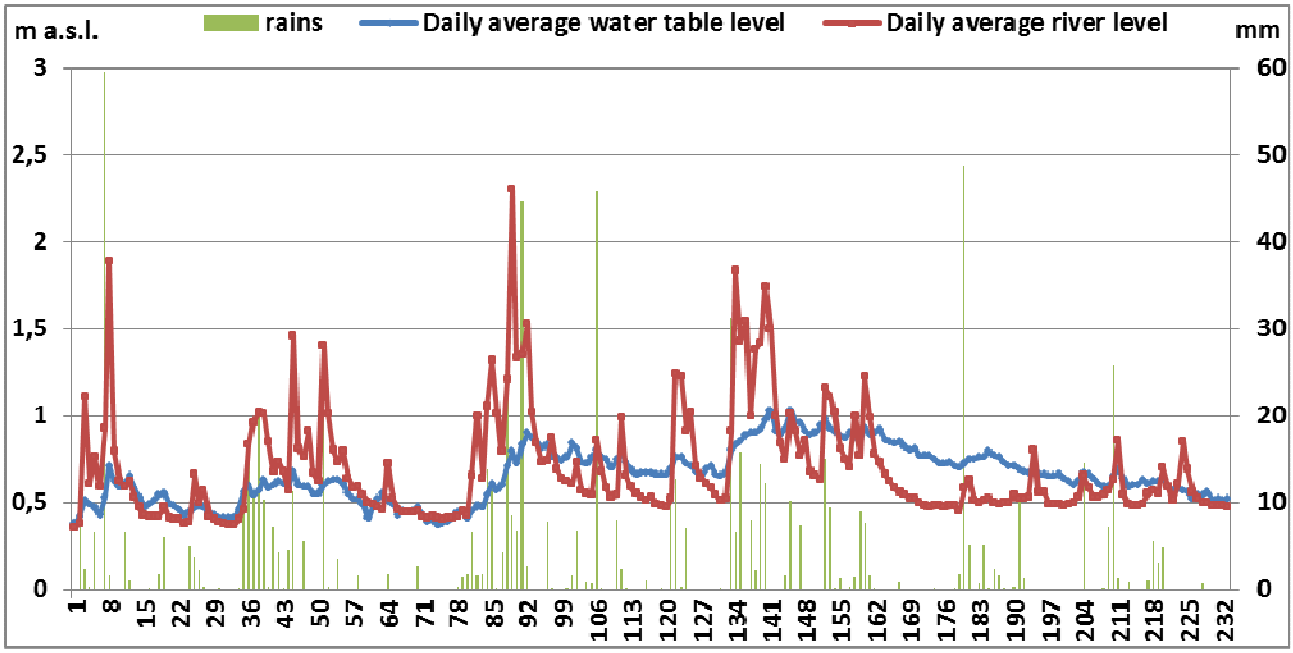

Fig. 5.13: translated water table and canal daily average levels. It can be observed how the canal level is frequently higher than water table level, mainly due to the rainfall effect

The graphic in Fig.5.14 was realized to visualize the direction of the hydraulic gradient. It was produced acting a subtraction between the canal level and water table level. Therefore when the value is positive the canal level is higher than water table level and an inflow of water from the canal bed to the aquifer is expected (above the red line in Fig.5.14). This flow path orientations was called canal-dominated hydraulic gradient. Vice versa when the hydraulic gradient is negative, a normal outflow of water from the aquifer to the canal is supposed (below the red line in Fig.5.14). In this case it was called groundwater-dominated hydraulic gradient.
Therefore this graph shows synthetically how the flow paths direction changed in time, going toward the inland boundary and the canal banks alternatively. The hydraulic gradient can be divided in four main phases, alternated during the simulation time:

1. 1st stage, canal-dominated hydraulic gradient, from day 1 to 93;
2. 2nd stage, groundwater-dominated hydraulic gradient, from day 94 to 121;
3. 3rd stage, a minor event of canal-dominated hydraulic gradient, from day 122 to 141;
4. 4th stage, the final groundwater-dominated hydraulic gradient from day 142 to 233.

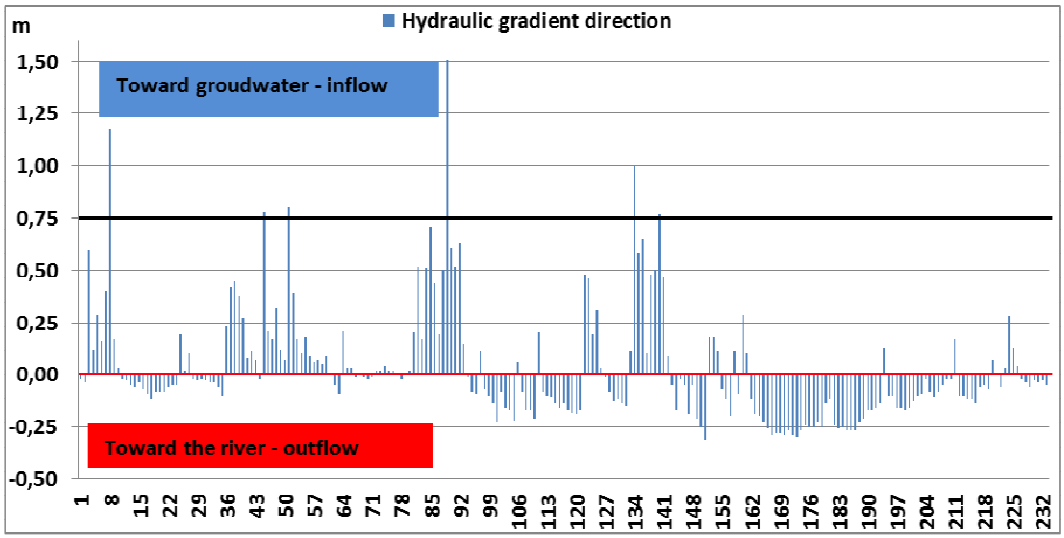

Fig. 5.14: hydraulic gradient direction obtained subtracting the canal level to groundwater level. Positive values (above the red line) indicate a higher canal water level, while the negative ones (below the red line) indicate a higher water table level. When the values are positive the hydraulic gradient is directed toward groundwater, vice versa when they are negative an outflow from the aquifer to the canal is expected

Before starting the simulations, mass boundary conditions were applied along the model borders. For the inland boundary condition a fixed Sal concentration of 6.4 g/l was used. For the canal boundary conditions a different Sal patterns were used, depending on the relative position of the canal level with respect to the water table level.
Sal Scenario1, based on the graphic in Fig.5.14, simulated a variable salinity pattern:

1. 35 g/l, when a low level of the canal occurred (below the red line in Fig.5.14). In this case an intrusion of seawater from the canal mouth was supposed, due to the relative low canal discharge;
2. 12 g/l, for the values ranging from 0 and 0.75 m (between the red and black line in Fig.5.14). The value of 12 g/l was used because it was collected in January 2012, during a medium discharge period. A mixing between freshwater and seawater in the canal was presumed to determine this Sal value of brackish water;
3. 1 g/l, for the values higher than 0.75 (above the black line in Fig.5.14). It simulated a complete freshwater flush happening in the canal during a flood event. This threshold value was chosen because it represents more than the double of the canal level in a low discharge period at the point B in in Fig.5.10a (0.34 m a.s.l.).

Therefore the data about the translated levels and the variable concentration were inserted at the boundary conditions of the model to start the simulation (Tab.5.2 in annex 2).
Simulation snapshots are depicted below to visualize the groundwater processes. They show the movement of the saline plume in the aquifer. The initial conditions of the simulation consisted in the groundwater mass concentration pattern constituted by a seawater plume (Fig.5.12a) obtained using the methodology described in the previous paragraph.
As stated above, the hydraulic gradient in the 2D vertical section can be divided in four periods, dominated by different hydraulic gradients. The 1st stage (day 1- 93) was characterized by a general high stand of the canal level determining a brackish water inflow into the aquifer. Whereby the threshold of 0.75 m (black line in Fig.5.14) was exceeded, a complete flush of freshwater occurred in the canal, with a resulting freshwater inflow in the groundwater system. This period determined a saline plume migration toward the inland boundary increasing the Sal values at the Lat12 piezometer position. Fig.5.15 shows four moments of the migration and at day 90 the salt-wedge completely disappeared under the canal bottom and a dome shaped saline dome isolated in the aquifer.

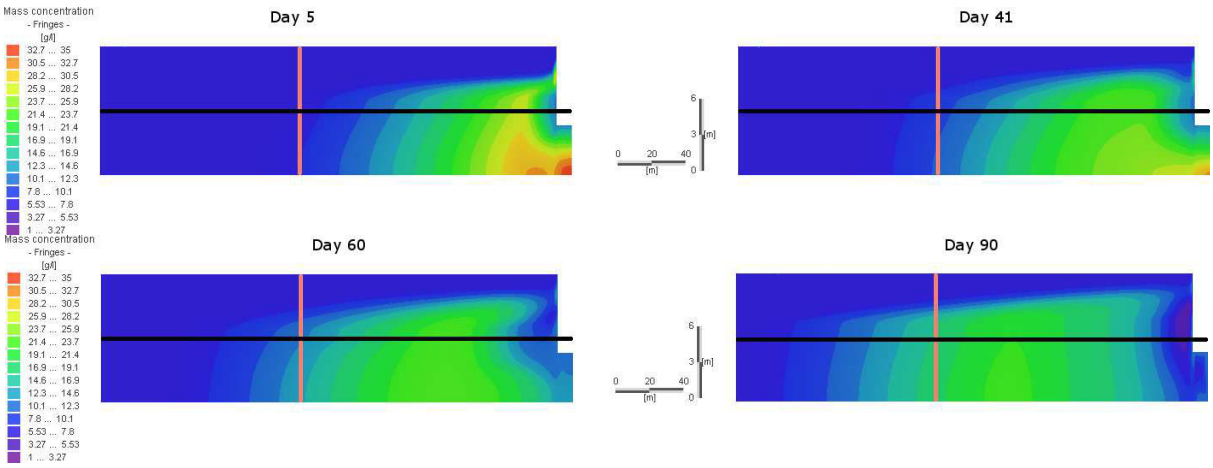

Fig. 5.15: 1st stage about the salt-wedge movement, dominated by a canal-dominated hydraulic gradient. In this stage the salt-wedge shaped plume moves toward the inland boundary condition and at its final stage it changes in a salt-dome shaped plume. The pink line indicates the Lat12 piezometer position and the black line represents the 0 m a.s.l. line

Fig.5.16 is about the 2nd stage (day 94-121) of the saline plume migration. In this period the rainfall rate decreased and consequently flood events. The hydraulic gradient turned toward the canal and another small salt-wedge shaped plume developed. At the end of this stage a saline dome and a salt-wedge shaped plumes lied on the aquifer bottom

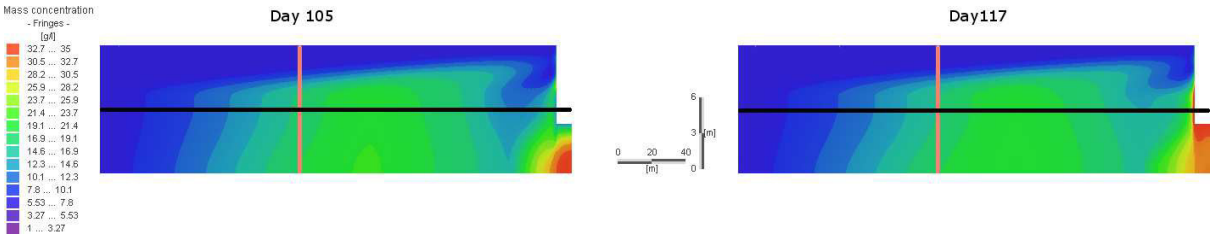

Fig. 5.16: 2nd stage of the plume migration, dominated by a canal ward hydraulic gradient. At this stage another salt-wedge developed. The pink line indicates the Lat12 piezometer position and the black line represents the 0 m a.s.l. line

In the 3rd stage (day 122-141) a new high discharge period of about 20 days occurred. A new canal-dominated hydraulic gradient determined a plume movement toward the inland boundary (Fig.5.17). The snapshot about the day 139 shows a fresher water-wedge developing below the canal bottom and pushing away the second saline plume. This canal flushing event determined the arrival of the first saline plume core at the Lat12 piezometer position. At the end of this stage two saline dome shaped plumes lied on the aquifer bottom.

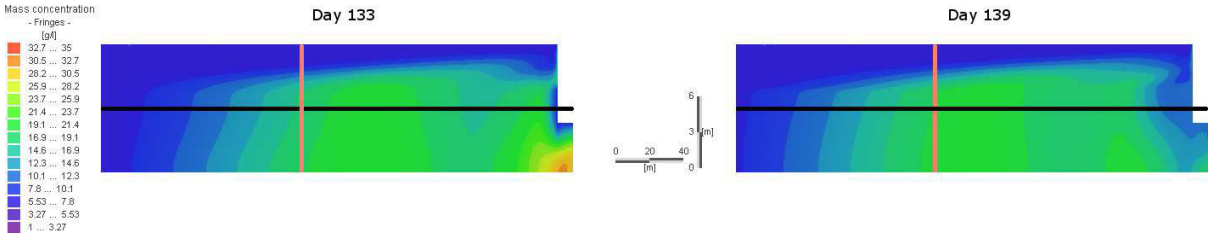

Fig. 5.17: 3rd stage of the saline plumes migration. At this stage a new canal-dominated hydraulic gradient determined a plume movement toward the inland boundary. A new salt-dome was generated. The pink line indicates the Lat12 piezometer position and the black line represents the 0 m a.s.l. line

Fig.5.18 is about the last stage (142-233), in which a summer hydraulic gradient toward the canal established again, because of the of flood events lack related to a rainfall reduction. Seawater started again to penetrate the canal bed and at day 159 the second saline dome completely disappeared. The saline dome shaped plume that had previously reached Lat12 piezometer, started to move backward to the canal direction and a new salt-wedge below the canal bed started to develop.

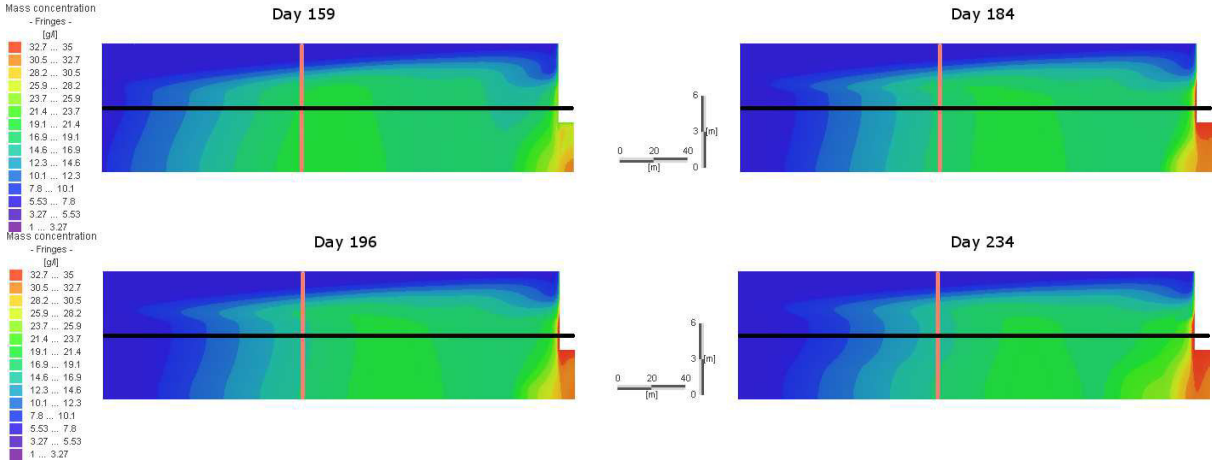

Fig. 5.18: last stage of the model simulation: a new groundwater-dominated hydraulic gradient moved back the salt-dome shaped plume to the canal, where another salt-wedge is developing. The pink line indicates the Lat12 piezometer position and the black line represents the 0 m a.s.l. line

The results of the simulation were compared with the concentration values collected by the software at an observation point (OP1) located at the bottom of the aquifer, in correspondence of the Lat12 piezometer (Fig.5.19). It allowed to analyze the movement of the plume at the aquifer bottom for every single modeling time-step.

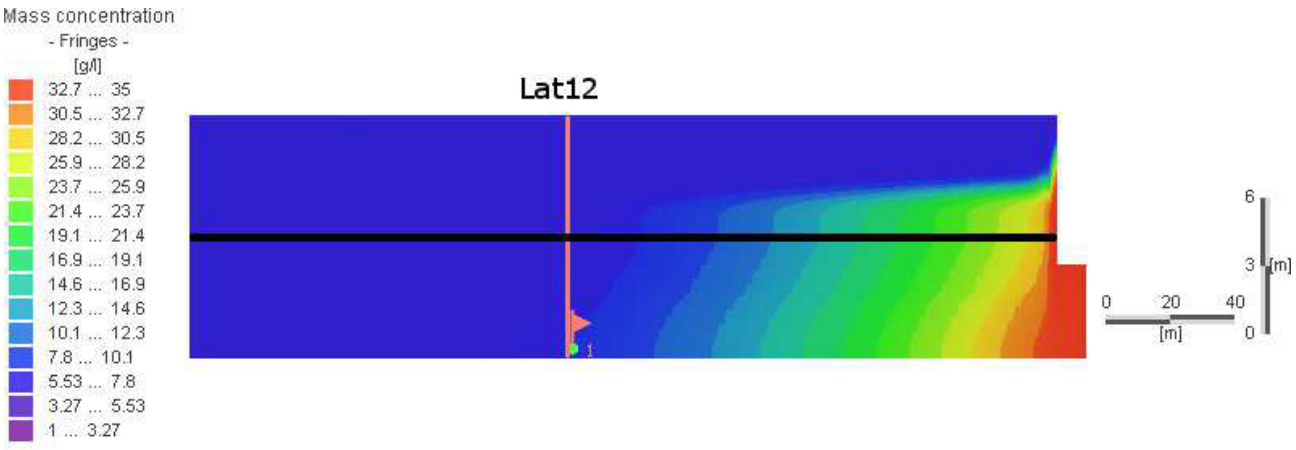

Fig. 5.19: location of the observation point 1 (OP1) located at the aquifer bottom (pink flag). The pink line indicates the Lat12 piezometer position and the black line represents the 0 m a.s.l. line

The model accuracy was assessed comparing observed data at Lat12 and simulated data at OP1. Fig.5.20 shows the observed and simulated water table data, whereas Fig.5.21 shows observed and simulated concentration data. Both the water table and concentration data rather follow the same trend with the exception of those about April 2013. Water table data show an anomalous setup, whereas concentration values a sudden reduction. The reason of this anomaly could originate from an inflow of freshwater from the Mastropietro Canal. In fact it is filled opening the sluice gate located at the junction with a major drainage canal. Fig.5.9 shows water table level and concentrations data collected at Lat12 and it can be observed how in the month of April 2013, a sudden setup of water table and a drop of Sal values took place. This process could be induced by an inflow of fresher water, acting a dilution of the brackish groundwater in the aquifer. This presumed process was not considered in the model implementation and produces some uncertainties on the model results. Nevertheless Fig.5.21, with the exception of the April 2013 data, allows to identify an increasing groundwater salinity pattern during the falls. For this reason the simulation results were considered to be satisfactory.

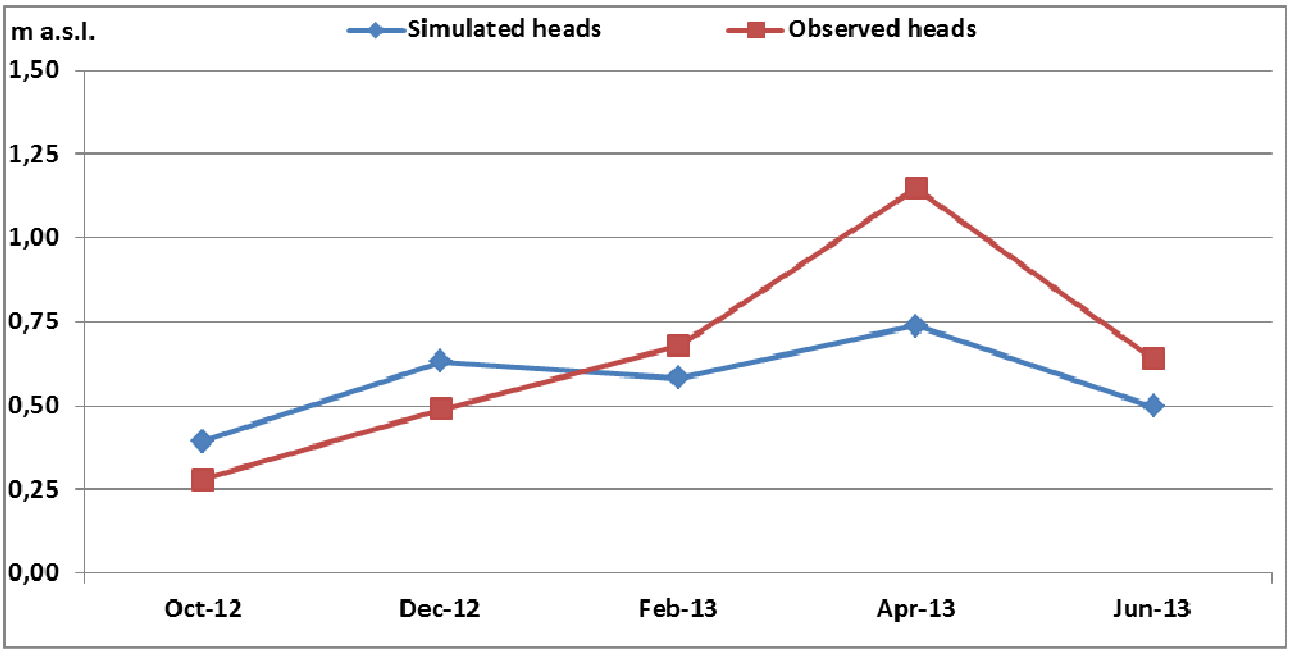

Fig. 5.20: graph showing simulated and observed groundwater-level altitudes (a) and concentrations (b) for the transient model

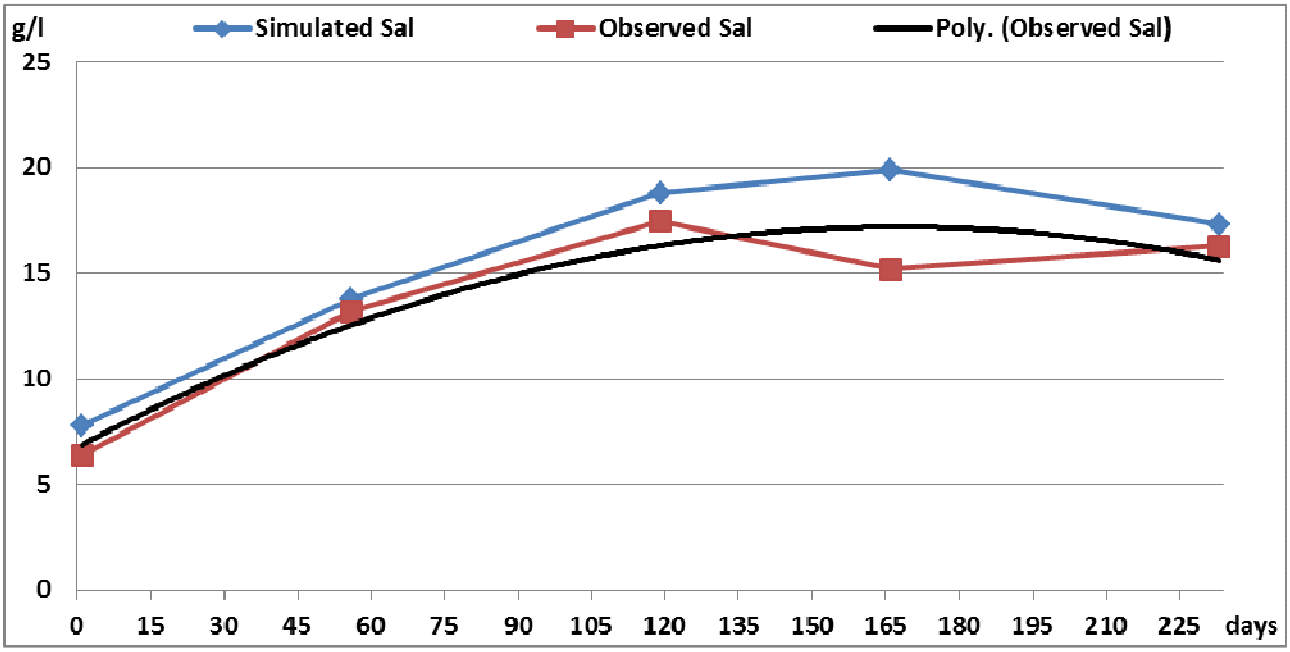

Fig. 5.21: trend line about the experimental and simulated data, that show an increase of the Sal values during the falls

5.4.1 HYDRAULIC GRADIENT EFFECT ON SALINE PLUME PROPAGATION

A better evaluation of the hydraulic gradient effect on the saline plume propagation is depicted in Fig.5.22. It shows the concentration monitored in the model at the OP1 and the direction of the hydraulic gradient. The four stages of the hydraulic gradient were marked and delimited by black lines. It can be seen how at the 1st stage (days 1-93), with a the canal-dominated hydraulic gradient, an increasing Sal trend occurs at the OP1. At the beginning of the 2nd stage (days 94-121) during the groundwater-dominated hydraulic gradient, a slight inflection of the Sal values was noticed at OP1. This trend finished with the new canal-dominated hydraulic gradient of the 3rd stage (days 122-141), when the concentration values arrive at the maximum value (the saline plume core reached OP1 position, see Fig.5.17). A reduction of flood events related to the beginning of the summer determined another groundwater-dominated hydraulic gradient. It was characterized by a decreasing trend, that can be observed at the 4th stage (days 142-233). Therefore it

can be concluded that canal dominated hydraulic gradients determined a saline plume migration toward the OP1 with an increase of Sal values, whereas groundwater-dominated hydraulic gradients determined a backward movement of the saline plume with a reduction of Sal values at OP1.

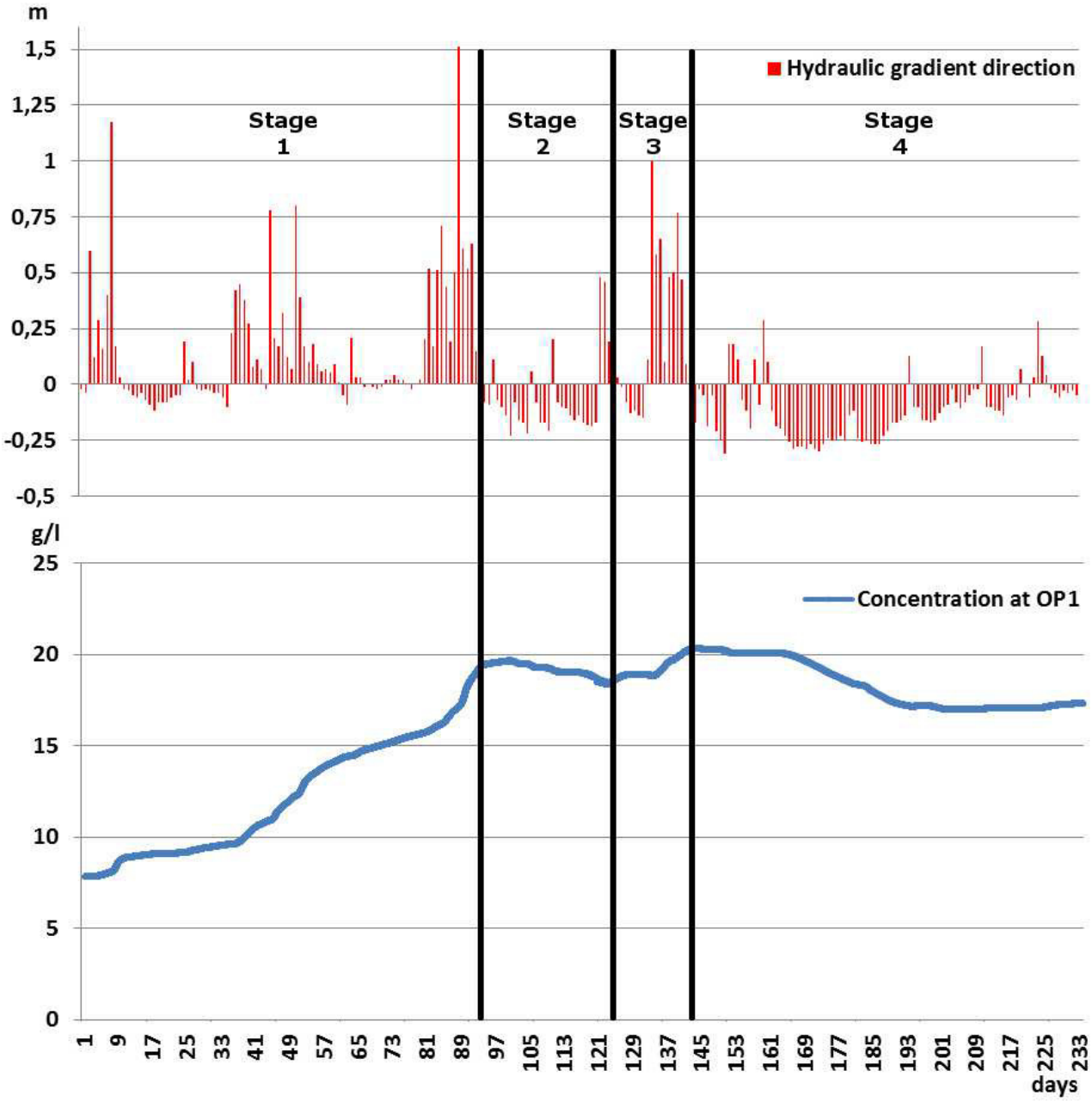

Fig. 5.22: simulated Sal values collected at the OP1 located at the Lat12 piezometer. It can be seen a strict dependence of Sal trend on the hydraulic gradient stages

5.4.2 RIVER CONCENTRATIONS SENSITIVITY ANALYSIS

The sensitivity analysis aimed to assess the influences determined by the canal Sal on seawater plume concentration and consequently on the Sal detected at OP1. Five different Sal scenarios were simulated at the canal mass boundary conditions, characterized by the following Sal values (Tab.5.2 in annex 2):

1. Scenario2 - constant salinity of 35 g/l;
2. Scenario3 - constant salinity of 1 g/l;
3. Scenario4 - constant salinity of 15 g/l;

4. Scenario5 - ranging salinity between 12-35 g/l; this scenario was created applying the same methodology of Scenario1 but neglecting the freshwater flushes.

Scenario2 e Scenario3 were texted to assess the influence of extreme concentrations on the saline plume salinity. Scenario4 was simulated to analyze the effect on an average Sal on the saline plume dynamics. Scenario 5 was simulated to analyze the absence of freshwater flushes into the canal system. Fig.5.23 shows how the influence on saline plume Sal was very high for extreme concentrations, determining a strong reduction (for values of 1 g/l) and increase (for values of 35 g/l) on the saline plume concentration and consequently on Sal values at OP1. Scenario4 showed a slight reduction of Sal concentration at OP1with respect to Scenario1, but the trend kept quiet similar. Scenario5 showed how the flushing events used in the Scenario1 simulation didn't determine a substantial variation in the saline plume concentration. It is evident observing the trend line about Scenario1 and Scenario5, that hold a very small Sal difference.

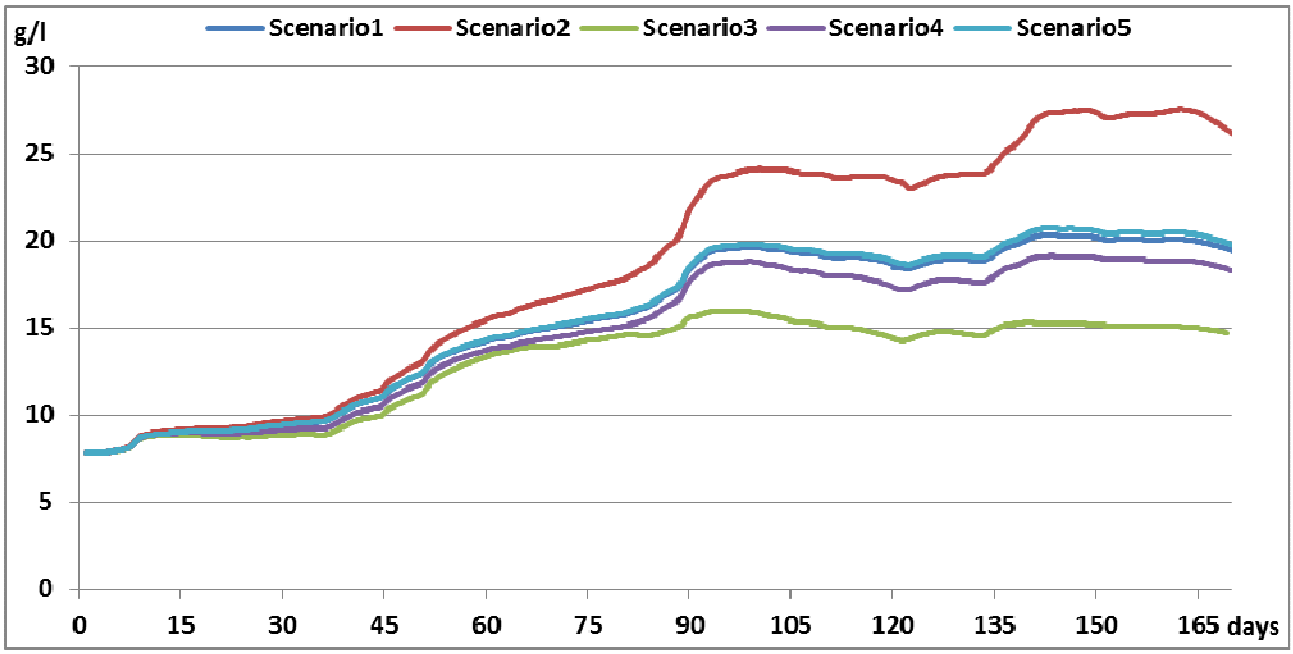

Fig. 5.23: results of simulation of different Sal scenarios on the concentrations at OP1 from day 1 to day 170. Sceanario1 - variable Sal of 1 g/l, 12 g/l and 35 g/l; Scenario2 - constant salinity of 35 g/l; Scenario3 - constant salinity of 1 g/l; Scenario4 - constant salinity of 15 g/l; Scenario5 - ranging salinity between 12-35 without flushing events

5.5 CONCLUSIONS

This study allowed to find the reasons of an increasing Sal pattern of a piezometer located in an unconfined sandy aquifer, sustained by a low permeability clayey-silt horizon. The piezometer was set at 272 m from an anthropic canal banks, in proximity to its mouth. A process of salt-wedge intrusion was noticed in the canal (see chapter 4) especially when the discharge is low. The canal was subject to tide fluctuation and level fluctuations induced by flood events related to the rains. Since Sal values in the piezometer showed an increasing trend during the falls, a relationship between canal level fluctuation and Sal variation in the aquifer was supposed. A 2D model in a transient flow-transient transport state was setup using FEFLOW 6.0, to simulate the canal-aquifer system. Since the piezometer is far from the canal banks, the effect of tide fluctuation on mass transport was neglected. The aquifer, provided of a high hydraulic conductivity, was supposed to be in hydraulic communication with the canal bottom. The effect of the canal banks on mass and flow transport was neglected. Since piezometer data showed a brackish water composition, a saline plume was supposed to be present in the aquifer. The initial conditions of the model were created running the model until it reached the steady-state conditions, after a simulation time of 1000 days. A “passive seawater intrusion” pattern was simulated to create the saline plume in the aquifer.

After simulating initial conditions, the simulation started. The hydraulic head boundary conditions were used at the model boundary and they were expressed in time series. They were obtained translating data about canal and groundwater levels, coming from other measurement stations. Mass concentrations boundary conditions were expressed in time series as well. For the inland boundary a constant mass concentration of 6.4 g/l was used, while for the canal boundary conditions, a variable Sal scenario was used. It was assumed to depend on the relative groundwater-canal levels, therefore freshwater, brackish water and seawater concentration were used (1 g/l, 12 g/l and 35g/l). Model results showed that the saline plume movement was strictly dependent on the hydraulic gradient. Hydraulic gradient can be divided in two main types: canal-dominated (canal level higher than groundwater level) and groundwater-dominated (groundwater level higher than canal level). Canal-dominated hydraulic gradients produced an inflow from the canal bed to groundwater, determining the saline plume migration toward the inland boundary. Consequently an enhancement of salinity at the piezometer happened. Vice versa groundwater-dominated hydraulic gradients determined a normal outflow from the groundwater system to the canal. Groundwater-dominated hydraulic gradients determined a reduction of Sal at the piezometer.

After the simulation, the model results and the experimental data were compared and they were considered consistent, with the exception of the data collected in April 2013. They are likely conditioned by other processes, not considered in the numerical model implementation. The sensitivity analysis was developed to assess the influence of different canal concentrations on the saline plume concentration. It was observed that except for extreme values of Sal, an average Sal concentration could be used for further numerical modeling investigations. Results showed that freshwater flushes used in the Scenario1 simulation didn't affect saline plume concentration substantially, especially if compared with the simulation results about Sal Scenario5, where freshwater flushes were neglected. Finally the model showed a great dependence on the hydraulic gradient generated by the river boundary conditions and the saline plume movement resulted to be strongly related to the river level.

5.6 REFERENCES

Akouvi A, Dray M, Violette S, de Marsily G, Zuppi GM (2008) The sedimentary coastal basin of Togo: example of a multilayered aquifer still influenced by a palaeo-seawater intrusion. Hydrogeology Journal 16:419–436. doi:10.1007/s10040-007-0246-1

Barazzuoli P, Nocchi M, Rigati R, Salleolini M (2008) A conceptual and numerical model for groundwater management: a case study on a coastal aquifer in southern Tuscany, Italy. Hydrogeology Journal 16:1557–1576. doi:10.1007/s10040-008-0324-z

Barbieri A, Carrara C, Castorina F, Dai Pra G, Esu D, Gliozzi E, Paganin G, Sadori L (1999) Multidisciplinary study of Middle-Upper Pleistocene deposits in a core from the Piana Pontina (central Italy). Giornale di geologia 61:47-73

Boufadel MC (2000) A mechanistic study of nonlinear solute transport in a groundwater-surface water under steady state and transient hydraulic conditions. Water Resources Research 36 (9):2549-2565. doi:10.1029/2000WR900159

Brovelli A, Mao X, Barry DA (2007) Numerical modeling of tidal influence on density-dependent contaminant transport. Water Resources Research 43 (W10426):1-15. doi:10.1029/2006WR005173

Brunamonte F, Serangeli S (1996) Evoluzione naturale ed intervento antropico nello sviluppo dei fenomeni di subsidenza nella Pianura Pontina. Memorie della Società Geologica Italiana 51:823-836

Capelli G, Mastrorillo L, Mazza R, Petitta M, Baldoni T, Banzato F, Cascone D, Di Salvo C, La Vigna F, Taviani S, Teoli P (2012) Carta Idrogeologica del Territorio della Regione Lazio. Scala 1:100.000 (4 Fogli). S.EL.CA., Firenze - Italy

Casadio M, Elmi C (1995) Il manuale del geologo.

Cavinato GP, Corrado S, Sirna M (1992) Dati preliminari sull'assetto geologico-strutturale del settore sud-occidentale della struttura simbruino-ernica. Studi Geologici Camerti speciale 1991/1992 CROP 11:33-42

Conforto B, Di Ricco G, Sappa M (1962) Indagine sulle acque sotterranee dell'Agro Romano e Pontino. vol 2. Cassa per il Mezzoggiorno,

D'Appolonia (1984) Impianto Prototipo Cirene - Preliminary study of hydrogeologic regime and groundwater flow.

Diersch HJG (2009) FEFLOW Reference Manual. DHI-WASY GmbH, Berlin

Drabbe J, Badon Ghyben W (1889) Nota in verband met de voorgenomen puboring nabij Amsterdam. Amsterdam

Funiciello R, Parotto M (1978) Il substrato sedimentario nell'area dei Colli Albani: considerazioni geodinamiche e paleogeografiche sul margine tirrenico dell'Appennino Centrale. Geologica Romana 17:233-287

Gelhar LW, Welty C, Rehfeldt KR (1992) A critical review of data on field-scale dispersion in aquifer. Water Resources Research 28 (7):1955-1974. doi:10.1029/92WR00607

Giambastiani BMS, Antonellini M, Essink GHPO, Stuurman RJ (2007) Saltwater intrusion in the unconfined coastal aquifer of Ravenna (Italy): A numerical model. Journal of Hydrology 340 (1-2):91-104. doi:10.1016/j.jhydrol.2007.04.001

Herzberg B (1901) Die wasserversorgundeinigerNordseebâder. Journal gasbeleuchtung und Wasserversorgung 44:815-819, 824-844

Huyakorn PS, Pinder GF (1983) Computational Methods in Subsurface Flow. Academic Press, New York

IdrograficoLazio (2013a) Dati del Pluviometro di Borgo Santa Maria relativi agli anni 2012-2013.

IdrograficoLazio (2013b) Dati orari dell'Idrometro di Borgo Santa Maria sul Canale Moscarello pel il periodo 1/3/2012-31/07/2013.

Langevin CD, Guo W (2006) MODFLOW/MT3DMSbased simulation of variable-density groundwater flow and transport. Ground Water 44 (3):339-351. doi:10.1111/j.1745-6584.2005.00156.x

Lenkopane M, Werner AD, Lockington DA, Li L (2009) Influence of variable salinity conditions in a tidal creek on riparian groundwater flow and salinity dynamics. Journal of Hydrology 375 (3-4):536-545. doi:10.1016/j.jhydrol.2009.07.004

Li L, Barry D (1999) Submarine groundwater discharge and associated chemical input to a coastal sea. Water Resources Research 35 (11):3253-3259. doi:1999WR900189.0043-1397/99/1999WR900189509.00

Loaiciga HA, Pingel TJ, Garca ES (2012) Sea Water Intrusion by Sea-Level Rise: Scenarios for the 21st Century. Ground Water 50 (1):37-47. doi:10.1111/j.1745-6584.2011.00800.x

Mao X, Enot P, Barry DA, Li L, Binley A, Jeng DS (2006) Tidal influence on behaviour of a coastal aquifer adjacent to a low-relief estuary. Journal of Hydrology 327 (1-2):110-127. doi:10.1016/j.jhydrol.2005.11.030

PERFOR (2013) Lavori per la realizzazione di nuovi piezometri per l'adeguamento della rete di monitoraggio idrogeologico presso la centrale di Latina.320

Qahman K, Larabi A (2006) Evaluation and numerical modeling of seawater intrusion in the Gaza aquifer (Palestine). Hydrogeology Journal 14:713–728. doi:10.1007/s10040-005-003-2

Serva L, Brunamonte F (2007) Subsidence in the Pontina Plain, Italy. Bulletin of Engineering Geology and the Environment 66 (2):125-134. doi:10.1007/s10064-006-0057-y

SOGIN (2012) Modello del flusso delle acque sotterranee.

UNESCO (1983) Algorithms for computation of fundamental properties of seawater.

Werner AD, Lockington DA (2006) Tidal impacts on riparian salinities near estuaries. Journal of Hydrology 328 (3-4):511-522. doi:10.1016/j.jhydrolog.2005.12.001

Xin P, Robinson C, Li L, Barry DA, Bakhtyar R (2010) Effects of wave forcing on a subterranean estuary. Water Resources Research 46. doi:10.1029/2010wr009632

GENERAL CONCLUSIONS

The present PhD thesis studied two areas located along the Tyrrhenian edge of the Latium Region: the Tiber Delta area and the Pontina Plain area, with an overall survey area of about 300 km^2. The two areas show many geological and anthropic similar characteristics: in fact they are constituted by multi-layered sedimentary aquifers and they were reclaimed in the past centuries. Both hydrographic network and morphology were strongly affected by anthropic works. Furthermore the richness of groundwater resources determines a great water demand for agricultural, industrial and domestic use.

The surveys aimed to analyze the groundwater salinization induced by rivers and anthropic canals, due to wind effect and river discharge modification in time. Furthermore the study of the river discharge effect on coastal aquifer salinization was performed with the help of the most innovative techniques of numerical modeling.

Firstly, multi-temporal regional surveys were conducted in both of the areas (two for the Tiber Delta area and three for the Pontina Plain area) to assess the hydrogeological patterns, flow paths direction and to update the knowledge about the groundwater morphology. The two study areas showed different levels of stress: Pontina Plain resulted to be strongly affected by withdrawals during the whole year, with a great frequency of cones of depressions, whereas Tiber Delta area showed a reduction of water table depressions. The difference could derive from the great presence of green houses in Pontina Plain, which determines a whole year groundwater pumping.

Secondly, hydrographical surveys were performed to assess the salinization presence in surficial water bodies. Surveys showed presence of salt-wedge intrusions in the rivers/canals of both the study areas. Rivers/canals of the study areas can be classified as strongly stratified estuaries characterized by moderate river discharge and weak tidal forcing. The only exception is represented by Fiumara Grande branch of the Tiber River, that can be classified as a salt-wedge stratified estuary, characterized by high river discharge and weak inflow of seawater in the near-bottom layer. The coastal lakes of Pontina Plain resulted completed salinized.

Groundwater salinization showed a strict dependence with the hydrographical network: in the Tiber Delta the main seawater intrusion source is represented by the Tiber River: the salt-wedge intrusion, noticed up to 8.8 km from the river mouth, is the main vehicle of seawater transport inland. The different hydraulic head between the Tiber level (above the mean sea level) and the Ostia Antica area (ground and groundwater levels below the mean sea level), could determine a lateral inflow of seawater from the river bottom to the multi-layered aquifer, likely accelerated by withdrawals. In the Ostia Antica area other salinization processes were identified by means of hydrogeochemical analyses, likely related to the presence of historical solar salt works deposits and to the the presence of connate saline waters.
In the Pontina Plain area a strict correlation between rivers/canals and groundwater salinization was noticed, as proved by salinization maps realized during the work. In this area the anthropic coastal hydrographic network determines a seawater intrusion in the sandy deposits belonging to the multi-layered aquifer of the terraced coastal complexes.

The assessment of the salt-wedge intrusion processes was performed using a multi-disciplinary approach. In the Tiber River, the wind effect was recognized as the main salinization mechanism. In fact, a statistical analysis based on wind speed higher than 4 m/s, allowed to identify the monthly wind patterns in the Tiber Delta area. Westerly winds, blowing in springtime, are able to induce a sea level setup and consequently a salt-wedge intrusion. Salt-wedge intrusion was detected at the mouths of both the Tiber branches mouths with thermohaline measurements. The salt-wedge intrusion took place despite of the high discharge of the river during the falls. Cross Correlation permitted to quantify fluctuation time-lags occurring on three water gauges located along the Tiber River course. Time-lags and standard deviations showed an enhancement moving upstream: it means that the river fluctuation is more conditioned by discharge

variations far from the mouth, whereas it is more influenced by tides nearby the mouth. Therefore the sea level fluctuation at a river mouth can hold a higher influence with respect to the river discharge and it can be able to determine a salt-wedge intrusion.

Westerly winds can determine a further groundwater salinization process, induced by the SSA deposition on coastal tree foliage, as noticed in the Litorale Romano Natural Reserve.

The importance of a canal discharge on an aquifer salinization was noticed in the SOGIN study area, with the help of the numerical modeling software FEFLOW 6.0. Data collected in a piezometer drilled in an unconfined sandy aquifer showed the presence of a seawater plume. Data showed an unexpected increasing salinity pattern during the falls.
The process responsible of affecting the seawater plume movement and consequently the salinity variability, was presumed to be the Moscarello Canal discharge variability.
The canal, in which a salt-wedge intrusion was noticed, was subject to a great flow variability, which determined a water level rise up. The 2D vertical flow and mass transient model showed that a level increase was able to determine a hydraulic gradient toward the aquifer and a consequent inflow of seawater.
During the simulations two types of hydraulic gradient alternated, depending on the relative height of the water table with respect to canal water lever:

- river-dominated hydraulic gradient (canal level higher than water table level), in which an inflow water in the aquifer was noticed with a consequent increase of salinity;
- groundwater-dominated hydraulic gradient (water table level higher than canal level), combined with an outflow of water from the aquifer and a reduction of salinity.

Simulations showed an increase of salinity values during the falls and a decrease at the beginning of the summer, confirming the experimental data trend.

Data collection and the numerical modeling allowed to analyze several processes concerning salt-wedge intrusion in river mouths and consequently seawater intrusion in coastal aquifers.
Therefore a specific hydrological investigation is essential to comprehend salinization processes that sometimes seem complex at first.
Finally, the assessment of salt-wedge intrusion processes into rivers must focus on the interaction of all the natural phenomena occurring simultaneously, such as the river morphology, the discharge rate, the wind influence and the tide effect.

ANNEX 1

Wind-induced salt-wedge intrusion in the Tiber river mouth (Rome–Central Italy)

Fabio Manca, Giuseppe Capelli, Francesco La Vigna, Roberto Mazza & Annalisa Pascarella

Environmental Earth Sciences

ISSN 1866-6280

Environ Earth Sci
DOI 10.1007/s12665-013-3024-5

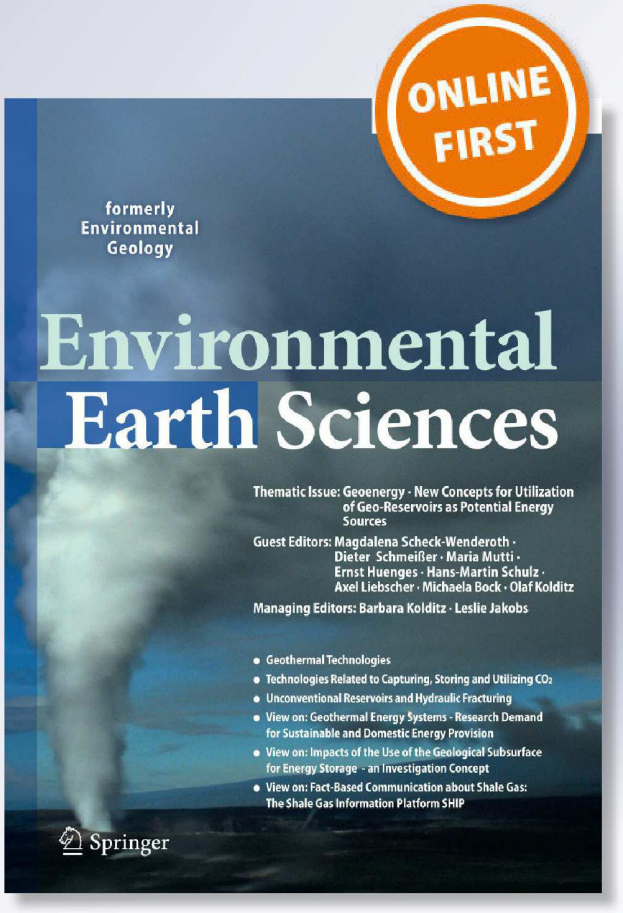

Springer

Environ Earth Sci
DOI 10.1007/s12665-013-3024-5

ORIGINAL ARTICLE

Wind-induced salt-wedge intrusion in the Tiber river mouth (Rome–Central Italy)

Fabio Manca · Giuseppe Capelli · Francesco La Vigna · Roberto Mazza · Annalisa Pascarella

Received: 11 June 2013 / Accepted: 17 December 2013

Abstract The wind effect on river water quality was illustrated by means of thermohaline measurements carried out in the Tiber River in May 2012. The survey was carried out using a boat, in stations located in the two Tiber branches: Fiumara Grande and Traiano Canal. Thermohaline variables (salinity and temperature) were used to describe the water-type patterns and to define the salt-wedge position. Although the river flow rate was rather high, saltwater intrusion happened. Wind data suggested that the more probable cause of salt-wedge intrusion was the wind action. Especially wind speeds higher than 4 m/s are able to dominate the sea current at surface layers, determining an increase in the sea level. Therefore, westerly winds determined a seawater inflow in the river mouths.

Keywords Tiber River · Salt wedge · Seawater intrusion · Wind influence · Thermohaline

F. Manca (✉) · G. Capelli · R. Mazza
LinQ - Numerical and Quantitative Hydrogeology Laboratory, Roma Tre University, Largo S. Leonardo Murialdo, 1, 00146 Rome, Italy
e-mail: fabio.manca@uniroma3.it

F. La Vigna
ROMA CAPITALE (Municipality of Rome), Environmental and Civil Protection Dept. - Environmental Geology and Hydrogeology Office, Circonvallazione Ostiense 191, 00154 Rome, Italy

A. Pascarella
Istituto delle Applicazioni del Calcolo - Italian National Research Council (IAC-CNR), Via dei Taurini 19, 00185 Rome, Italy

Introduction

Coastal areas are the most important environments for the human development due to the great water resources availability and climatic quality. The increasing urbanization, industrialization and agricultural requirements lead to various problems such as depletion of groundwater, deterioration of water quality, land subsidence and salinization (Capaccioni et al. 2005; Park et al. 2012). Really salinization became a very important issue in water management problems all over the world (Barlow and Reichard 2010; Trabelsi et al. 2012) and it is mainly caused by:

Evaporite dissolution (Ahmed et al. 2013)
Fossil seawater (Farid et al. 2013)
Seawater intrusion (Tran et al. 2012).

Seawater intrusion is defined as the mass transport of saline waters into zones previously occupied by fresher waters (Bear et al. 1999). In coastal areas, rivers are preferential way to lead seawater inland, through salt-wedge intrusion (Custodio and Llamas 2005). Salt-wedge intrusion happens when a water course carrying freshwater reaches a basin with saline water (sea, ocean or inland sea) and the saline water tends to propagate into the river mouth, affecting the quality of water (UNESCO 1991). Whereby the salt's front position moves upstream in close proximity to pumping areas, the direction of flow between the aquifer system and the river can be reversed, determining seawater intrusion in groundwater (Barlow 2003). In the last decades, several authors (Eagling et al. 2012; Pezzetta et al. 2011; Teien et al. 2006; Wong 1994; Wong et al. 2013) are pointing attention on estuarine environments to understand the problem of mobilization of metals and trace elements, connected to seawater intrusion. For this reason, understanding how the salt-wedge intrusion occurs can help researchers to understand water chemistry

Published online: 01 January 2014

ANNEX 2

Table 5.2: values about the hydraulic boundary conditions and salinity scenarios used in the 2D model

Date	day	Water table level (m a.s.l.)	Canal Level (m a.s.l.)	Scenario1	Scenario2	Scenario3	Scenario4	Scenario5
25/10/12	1	0,38	0,36	35000	35000	1000	15000	35000
26/10/12	2	0,42	0,38	35000	35000	1000	15000	35000
27/10/12	3	0,51	1,11	12000	35000	1000	15000	12000
28/10/12	4	0,49	0,61	12000	35000	1000	15000	12000
29/10/12	5	0,47	0,76	12000	35000	1000	15000	12000
30/10/12	6	0,43	0,59	12000	35000	1000	15000	12000
31/10/12	7	0,53	0,93	12000	35000	1000	15000	12000
01/11/12	8	0,71	1,89	1000	35000	1000	15000	12000
02/11/12	9	0,62	0,79	12000	35000	1000	15000	12000
03/11/12	10	0,59	0,62	12000	35000	1000	15000	12000
04/11/12	11	0,61	0,59	35000	35000	1000	15000	35000
05/11/12	12	0,65	0,62	35000	35000	1000	15000	35000
06/11/12	13	0,58	0,53	35000	35000	1000	15000	35000
07/11/12	14	0,53	0,47	35000	35000	1000	15000	35000
08/11/12	15	0,47	0,43	35000	35000	1000	15000	35000
09/11/12	16	0,49	0,42	35000	35000	1000	15000	35000
10/11/12	17	0,51	0,42	35000	35000	1000	15000	35000
11/11/12	18	0,54	0,42	35000	35000	1000	15000	35000
12/11/12	19	0,55	0,47	35000	35000	1000	15000	35000
13/11/12	20	0,49	0,41	35000	35000	1000	15000	35000
14/11/12	21	0,48	0,40	35000	35000	1000	15000	35000
15/11/12	22	0,46	0,40	35000	35000	1000	15000	35000
16/11/12	23	0,43	0,38	35000	35000	1000	15000	35000
17/11/12	24	0,44	0,39	35000	35000	1000	15000	35000
18/11/12	25	0,47	0,66	12000	35000	1000	15000	12000
19/11/12	26	0,48	0,50	12000	35000	1000	15000	12000
20/11/12	27	0,47	0,57	12000	35000	1000	15000	12000
21/11/12	28	0,44	0,42	35000	35000	1000	15000	35000
22/11/12	29	0,43	0,40	35000	35000	1000	15000	35000
23/11/12	30	0,41	0,39	35000	35000	1000	15000	35000
24/11/12	31	0,41	0,38	35000	35000	1000	15000	35000
25/11/12	32	0,41	0,37	35000	35000	1000	15000	35000
26/11/12	33	0,41	0,37	35000	35000	1000	15000	35000
27/11/12	34	0,46	0,40	35000	35000	1000	15000	35000
28/11/12	35	0,56	0,46	35000	35000	1000	15000	35000
29/11/12	36	0,6	0,83	12000	35000	1000	15000	12000
30/11/12	37	0,54	0,96	12000	35000	1000	15000	12000

01/12/12	38	0,57	1,02	12000	35000	1000	15000	12000
02/12/12	39	0,63	1,01	12000	35000	1000	15000	12000
03/12/12	40	0,58	0,85	12000	35000	1000	15000	12000
04/12/12	41	0,6	0,68	12000	35000	1000	15000	12000
05/12/12	42	0,62	0,73	12000	35000	1000	15000	12000
06/12/12	43	0,61	0,68	12000	35000	1000	15000	12000
07/12/12	44	0,59	0,57	35000	35000	1000	15000	35000
08/12/12	45	0,68	1,46	1000	35000	1000	15000	12000
09/12/12	46	0,6	0,81	12000	35000	1000	15000	12000
10/12/12	47	0,59	0,76	12000	35000	1000	15000	12000
11/12/12	48	0,59	0,91	12000	35000	1000	15000	12000
12/12/12	49	0,55	0,67	12000	35000	1000	15000	12000
13/12/12	50	0,55	0,62	12000	35000	1000	15000	12000
14/12/12	51	0,6	1,40	1000	35000	1000	15000	12000
15/12/12	52	0,62	1,01	12000	35000	1000	15000	12000
16/12/12	53	0,63	0,80	12000	35000	1000	15000	12000
17/12/12	54	0,63	0,73	12000	35000	1000	15000	12000
18/12/12	55	0,61	0,79	12000	35000	1000	15000	12000
19/12/12	56	0,55	0,64	12000	35000	1000	15000	12000
20/12/12	57	0,52	0,58	12000	35000	1000	15000	12000
21/12/12	58	0,52	0,59	12000	35000	1000	15000	12000
22/12/12	59	0,49	0,54	12000	35000	1000	15000	12000
23/12/12	60	0,41	0,50	12000	35000	1000	15000	12000
24/12/12	61	0,48	0,49	12000	35000	1000	15000	12000
25/12/12	62	0,52	0,47	35000	35000	1000	15000	35000
26/12/12	63	0,55	0,46	35000	35000	1000	15000	35000
27/12/12	64	0,51	0,72	12000	35000	1000	15000	12000
28/12/12	65	0,49	0,52	12000	35000	1000	15000	12000
29/12/12	66	0,43	0,46	12000	35000	1000	15000	12000
30/12/12	67	0,45	0,44	35000	35000	1000	15000	35000
31/12/12	68	0,44	0,44	12000	35000	1000	15000	12000
01/01/13	69	0,45	0,44	35000	35000	1000	15000	35000
02/01/13	70	0,47	0,45	35000	35000	1000	15000	35000
03/01/13	71	0,43	0,42	35000	35000	1000	15000	35000
04/01/13	72	0,39	0,41	12000	35000	1000	15000	12000
05/01/13	73	0,4	0,42	12000	35000	1000	15000	12000
06/01/13	74	0,37	0,41	12000	35000	1000	15000	12000
07/01/13	75	0,38	0,40	12000	35000	1000	15000	12000
08/01/13	76	0,39	0,41	12000	35000	1000	15000	12000
09/01/13	77	0,41	0,41	12000	35000	1000	15000	12000
10/01/13	78	0,44	0,42	35000	35000	1000	15000	35000
11/01/13	79	0,45	0,45	12000	35000	1000	15000	12000
12/01/13	80	0,41	0,43	12000	35000	1000	15000	12000
13/01/13	81	0,45	0,65	12000	35000	1000	15000	12000

14/01/13	82	0,48	1,00	12000	35000	1000	15000	12000
15/01/13	83	0,47	0,64	12000	35000	1000	15000	12000
16/01/13	84	0,54	1,05	12000	35000	1000	15000	12000
17/01/13	85	0,61	1,32	12000	35000	1000	15000	12000
18/01/13	86	0,57	1,01	12000	35000	1000	15000	12000
19/01/13	87	0,6	0,79	12000	35000	1000	15000	12000
20/01/13	88	0,71	1,21	12000	35000	1000	15000	12000
21/01/13	89	0,79	2,30	1000	35000	1000	15000	12000
22/01/13	90	0,72	1,33	12000	35000	1000	15000	12000
23/01/13	91	0,83	1,35	12000	35000	1000	15000	12000
24/01/13	92	0,9	1,53	12000	35000	1000	15000	12000
25/01/13	93	0,87	1,02	12000	35000	1000	15000	12000
26/01/13	94	0,85	0,84	35000	35000	1000	15000	35000
27/01/13	95	0,81	0,73	35000	35000	1000	15000	35000
28/01/13	96	0,83	0,74	35000	35000	1000	15000	35000
29/01/13	97	0,76	0,87	12000	35000	1000	15000	12000
30/01/13	98	0,76	0,69	35000	35000	1000	15000	35000
31/01/13	99	0,74	0,64	35000	35000	1000	15000	35000
01/02/13	100	0,76	0,62	35000	35000	1000	15000	35000
02/02/13	101	0,84	0,61	35000	35000	1000	15000	35000
03/02/13	102	0,81	0,73	35000	35000	1000	15000	35000
04/02/13	103	0,73	0,57	35000	35000	1000	15000	35000
05/02/13	104	0,72	0,55	35000	35000	1000	15000	35000
06/02/13	105	0,76	0,54	35000	35000	1000	15000	35000
07/02/13	106	0,8	0,86	12000	35000	1000	15000	12000
08/02/13	107	0,76	0,68	35000	35000	1000	15000	35000
09/02/13	108	0,75	0,58	35000	35000	1000	15000	35000
10/02/13	109	0,7	0,53	35000	35000	1000	15000	35000
11/02/13	110	0,75	0,54	35000	35000	1000	15000	35000
12/02/13	111	0,79	0,99	12000	35000	1000	15000	12000
13/02/13	112	0,73	0,65	35000	35000	1000	15000	35000
14/02/13	113	0,69	0,59	35000	35000	1000	15000	35000
15/02/13	114	0,66	0,55	35000	35000	1000	15000	35000
16/02/13	115	0,67	0,53	35000	35000	1000	15000	35000
17/02/13	116	0,67	0,51	35000	35000	1000	15000	35000
18/02/13	117	0,67	0,53	35000	35000	1000	15000	35000
19/02/13	118	0,66	0,49	35000	35000	1000	15000	35000
20/02/13	119	0,66	0,48	35000	35000	1000	15000	35000
21/02/13	120	0,66	0,47	35000	35000	1000	15000	35000
22/02/13	121	0,69	0,52	35000	35000	1000	15000	35000
23/02/13	122	0,76	1,24	12000	35000	1000	15000	12000
24/02/13	123	0,76	1,22	12000	35000	1000	15000	12000
25/02/13	124	0,72	0,91	12000	35000	1000	15000	12000
26/02/13	125	0,71	1,02	12000	35000	1000	15000	12000

27/02/13	126	0,68	0,71	12000	35000	1000	15000	12000
28/02/13	127	0,65	0,64	35000	35000	1000	15000	35000
01/03/13	128	0,69	0,61	35000	35000	1000	15000	35000
02/03/13	129	0,71	0,58	35000	35000	1000	15000	35000
03/03/13	130	0,66	0,54	35000	35000	1000	15000	35000
04/03/13	131	0,65	0,51	35000	35000	1000	15000	35000
05/03/13	132	0,67	0,52	35000	35000	1000	15000	35000
06/03/13	133	0,8	0,91	12000	35000	1000	15000	12000
07/03/13	134	0,83	1,83	1000	35000	1000	15000	12000
08/03/13	135	0,85	1,43	12000	35000	1000	15000	12000
09/03/13	136	0,89	1,54	12000	35000	1000	15000	12000
10/03/13	137	0,9	1,00	12000	35000	1000	15000	12000
11/03/13	138	0,9	1,38	12000	35000	1000	15000	12000
12/03/13	139	0,92	1,42	12000	35000	1000	15000	12000
13/03/13	140	0,97	1,74	1000	35000	1000	15000	12000
14/03/13	141	1,03	1,50	12000	35000	1000	15000	12000
15/03/13	142	0,91	1,00	12000	35000	1000	15000	12000
16/03/13	143	0,89	0,84	35000	35000	1000	15000	35000
17/03/13	144	0,92	0,75	35000	35000	1000	15000	35000
18/03/13	145	1,03	1,01	35000	35000	1000	15000	35000
19/03/13	146	0,96	0,91	35000	35000	1000	15000	35000
20/03/13	147	0,96	0,77	35000	35000	1000	15000	35000
21/03/13	148	0,91	0,86	35000	35000	1000	15000	35000
22/03/13	149	0,89	0,68	35000	35000	1000	15000	35000
23/03/13	150	0,9	0,65	35000	35000	1000	15000	35000
24/03/13	151	0,94	0,63	35000	35000	1000	15000	35000
25/03/13	152	0,98	1,16	12000	35000	1000	15000	12000
26/03/13	153	0,93	1,11	12000	35000	1000	15000	12000
27/03/13	154	0,91	1,02	12000	35000	1000	15000	12000
28/03/13	155	0,88	0,81	35000	35000	1000	15000	35000
29/03/13	156	0,87	0,75	35000	35000	1000	15000	35000
30/03/13	157	0,9	0,70	35000	35000	1000	15000	35000
31/03/13	158	0,89	1,00	12000	35000	1000	15000	12000
01/04/13	159	0,86	0,77	35000	35000	1000	15000	35000
02/04/13	160	0,93	1,22	12000	35000	1000	15000	12000
03/04/13	161	0,89	0,99	12000	35000	1000	15000	12000
04/04/13	162	0,9	0,78	35000	35000	1000	15000	35000
05/04/13	163	0,92	0,73	35000	35000	1000	15000	35000
06/04/13	164	0,86	0,66	35000	35000	1000	15000	35000
07/04/13	165	0,85	0,62	35000	35000	1000	15000	35000
08/04/13	166	0,84	0,58	35000	35000	1000	15000	35000
09/04/13	167	0,85	0,56	35000	35000	1000	15000	35000
10/04/13	168	0,82	0,54	35000	35000	1000	15000	35000
11/04/13	169	0,8	0,52	35000	35000	1000	15000	35000

12/04/13	170	0,81	0,52	35000	35000	1000	15000	35000
13/04/13	171	0,77	0,50	35000	35000	1000	15000	35000
14/04/13	172	0,77	0,48	35000	35000	1000	15000	35000
15/04/13	173	0,77	0,47	35000	35000	1000	15000	35000
16/04/13	174	0,75	0,48	35000	35000	1000	15000	35000
17/04/13	175	0,72	0,48	35000	35000	1000	15000	35000
18/04/13	176	0,72	0,47	35000	35000	1000	15000	35000
19/04/13	177	0,73	0,48	35000	35000	1000	15000	35000
20/04/13	178	0,71	0,48	35000	35000	1000	15000	35000
21/04/13	179	0,7	0,45	35000	35000	1000	15000	35000
22/04/13	180	0,72	0,58	35000	35000	1000	15000	35000
23/04/13	181	0,75	0,63	35000	35000	1000	15000	35000
24/04/13	182	0,75	0,51	35000	35000	1000	15000	35000
25/04/13	183	0,76	0,50	35000	35000	1000	15000	35000
26/04/13	184	0,76	0,51	35000	35000	1000	15000	35000
27/04/13	185	0,79	0,52	35000	35000	1000	15000	35000
28/04/13	186	0,77	0,50	35000	35000	1000	15000	35000
29/04/13	187	0,76	0,49	35000	35000	1000	15000	35000
30/04/13	188	0,73	0,50	35000	35000	1000	15000	35000
01/05/13	189	0,71	0,50	35000	35000	1000	15000	35000
02/05/13	190	0,71	0,54	35000	35000	1000	15000	35000
03/05/13	191	0,69	0,52	35000	35000	1000	15000	35000
04/05/13	192	0,68	0,52	35000	35000	1000	15000	35000
05/05/13	193	0,67	0,53	35000	35000	1000	15000	35000
06/05/13	194	0,67	0,80	12000	35000	1000	15000	12000
07/05/13	195	0,66	0,56	35000	35000	1000	15000	35000
08/05/13	196	0,66	0,56	35000	35000	1000	15000	35000
09/05/13	197	0,65	0,49	35000	35000	1000	15000	35000
10/05/13	198	0,65	0,49	35000	35000	1000	15000	35000
11/05/13	199	0,66	0,49	35000	35000	1000	15000	35000
12/05/13	200	0,64	0,48	35000	35000	1000	15000	35000
13/05/13	201	0,62	0,49	35000	35000	1000	15000	35000
14/05/13	202	0,6	0,50	35000	35000	1000	15000	35000
15/05/13	203	0,62	0,53	35000	35000	1000	15000	35000
16/05/13	204	0,67	0,65	35000	35000	1000	15000	35000
17/05/13	205	0,66	0,58	35000	35000	1000	15000	35000
18/05/13	206	0,64	0,53	35000	35000	1000	15000	35000
19/05/13	207	0,61	0,53	35000	35000	1000	15000	35000
20/05/13	208	0,59	0,54	35000	35000	1000	15000	35000
21/05/13	209	0,59	0,57	35000	35000	1000	15000	35000
22/05/13	210	0,65	0,63	35000	35000	1000	15000	35000
23/05/13	211	0,69	0,86	12000	35000	1000	15000	12000
24/05/13	212	0,64	0,54	35000	35000	1000	15000	35000
25/05/13	213	0,59	0,49	35000	35000	1000	15000	35000

26/05/13	214	0,6	0,48	35000	35000	1000	15000	35000
27/05/13	215	0,6	0,48	35000	35000	1000	15000	35000
28/05/13	216	0,63	0,49	35000	35000	1000	15000	35000
29/05/13	217	0,61	0,55	35000	35000	1000	15000	35000
30/05/13	218	0,62	0,57	35000	35000	1000	15000	35000
31/05/13	219	0,62	0,55	35000	35000	1000	15000	35000
01/06/13	220	0,63	0,70	12000	35000	1000	15000	12000
02/06/13	221	0,59	0,59	12000	35000	1000	15000	12000
03/06/13	222	0,57	0,51	35000	35000	1000	15000	35000
04/06/13	223	0,58	0,61	12000	35000	1000	15000	12000
05/06/13	224	0,57	0,85	12000	35000	1000	15000	12000
06/06/13	225	0,56	0,69	12000	35000	1000	15000	12000
07/06/13	226	0,52	0,56	12000	35000	1000	15000	12000
08/06/13	227	0,54	0,52	35000	35000	1000	15000	35000
09/06/13	228	0,54	0,50	35000	35000	1000	15000	35000
10/06/13	229	0,56	0,50	35000	35000	1000	15000	35000
11/06/13	230	0,51	0,48	35000	35000	1000	15000	35000
12/06/13	231	0,52	0,48	35000	35000	1000	15000	35000
13/06/13	232	0,51	0,48	35000	35000	1000	15000	35000
14/06/13	233	0,52	0,47	35000	35000	1000	15000	35000